

Development of Geopolymer Concrete for Precast Pipe Application

by Sumita Dangol

Thesis submitted in fulfilment of the requirements for
the degree of

Doctor of Philosophy

under the supervision of Dr Jun Li

Prof Vute Sirivivatnanon

Dr Rijun Shrestha

Dr Nadarajah Gowripalan

Faculty of Engineering and Information Technology
University of Technology Sydney

March 2023

CERTIFICATE OF ORIGINAL AUTHORSHIP

I, Sumita Dangol, declare that this thesis, is submitted in fulfilment of the requirements for the award of Doctor of Philosophy, in the School of Civil and Environmental Engineering at the University of Technology Sydney.

This thesis is wholly my own work unless otherwise referenced or acknowledged. In addition, I certify that all information sources and literatures used are indicated in the thesis.

This document has not been submitted for qualifications at any other academic institution.

This research is supported by the Australian Government Research Training Program.

Signature:

Production Note:
Signature removed prior to publication.

Date: 21st March 2023

ACKNOWLEDGMENTS

I would first like to start by expressing my sincere gratitude to my principal supervisor Dr. Jun Li for guiding me at times when I needed some direction, pushing me when I was stuck and motivating me to achieve the required results. I am also extremely grateful to my co-supervisors Professor Vute Sirivivatnanon for being my constant source of support, Dr. Rijun Shrestha for providing me this opportunity and Dr. Nadarajah Gowripalan for his assistance throughout this endeavour. This research has been possible because of their guidance and valuable suggestions. I would also like to express my gratitude to Australian Research Council (ARC) Research Hub for Nanoscience Based Construction Materials Manufacturing (NANOCOMM) and Cement Australia Pty Ltd, Darra, Qld. for funding this research and supplying with raw materials required in this study. I also like to thank Humes, a member of the Holcim group, for supplying pipes used in this study. I am extremely grateful to UTS Tech lab staff, especially Muller Hailu, Ann Yan, Peter Brown and Charles Sharpe. This research would not be possible without their valuable supports, insights and cooperation. I would also like to acknowledge the School of Civil Engineering, the Graduate Research School and the University of Technology Sydney for the support provided in this research study. This endeavour would also not have been possible without the emotional support I received from my husband, my parents, my sisters and brother throughout the journey, more so during the course of writing this thesis and my life and engagement with this endeavour. Finally, I would like to thank all my peers who have helped me in this journey, directly or indirectly.

LIST OF PUBLICATIONS

1. Dangol, S., Li, J., Sirivivatnanon, V. and Kidd, P., “Numerical Simulation of Three Edge Bearing Test of Reinforced Geopolymer Concrete Pipes”, 7th International Symposium on Nanotechnology in Construction, 31 Oct -2 Nov 2022.
2. Dangol, S., Shrestha, R., Sirivivatnanon, V., Kidd, P. and Perry. B., ‘Application of Geopolymer Concrete for Precast Components: a review’, 29th Biennial National Conference of the Concrete Institute of Australia, 9 Sept -11 Sept 2019.
3. Dangol, S., Li, J., Sirivivatnanon, V. and Kidd, P., “Bond-Slip Model for Finite Element Analysis of Reinforced Geopolymer Concrete Pipes”, under review. (Chapter 3 and 4)
4. Dangol, S., Li, J., Sirivivatnanon, V. and Kidd, P., “Numerical Investigation on Performance of Reinforced Geopolymer Concrete Pipes: A Parametric Case Study”, under review. (Chapter 3 and 5)
5. Dangol, S., Li, J., Sirivivatnanon, V. and Kidd, P., “Structural Behaviour of Reinforced Concrete Pipes with Pre-existing cracks: Experimental and Numerical investigation”, under review. (Chapter 5 and 6)

LIST OF ABBREVIATIONS

ACI	American Concrete Institute
AES	Analysis of Evolutive Sections
AS	Australian Standard
A-S-H	Alumina-Silicate-Hydrate
CBIS	Constrained Beam In Solid
CDP	Concrete Damage Plasticity
CPAA	Concrete Pipe Association of Australasia
C-S-H	Calcium Silicate Hydrate
CTOD	Crack Tip Opening Displacement
DEM	Discrete Element Method
EFC	Earth Friendly Concrete
EFG	Element Free Galerkin
FA	Fly ash
FEA	Finite Element Analysis
FEM	Finite Element Method
GFRP	Glass Fibre Reinforced Polymer
GGBFS	Ground Granulated Blast Furnace Slag
HDPE	High Density Polyethylene
LVDT	Linear Variable Differential Transformer
MAP	Mechanical Analysis of Pipes
MIC	Microbes Induced Corrosion
NP	Non-Cracked Pipe
OJ	Ogee joint
OPC	Ordinary Portland Cement
PVC	Poly Vinyl Chloride
SENT	Single Edge Notch Tension
SFR	Steel Fibre Reinforced
SFRC	Steel Fibre Reinforced Concrete

SPJ	Spigot-Pocket Joint
SP-NP	Spigot-Pocket Pipe without any cracks
SRM	Sewerage Rehabilitation Manual
SSD	Saturated Surface Dry
TEB	Three-Edge Bearing Test
UTM	Universal Testing Machine
VAF	Vertical Arching Factor
WRC	Water Research Centre
XFEM	Extended Finite Element method

LIST OF NOTATIONS

c/d	concrete cover to bar diameter
d	reinforcement bar diameter
D	internal diameter of pipe
D- load	design load
$D_{0.3}$	load corresponding to 0.3 mm crack
D_{peak}	load before stiffness loss in concrete pipe
D_{ult}	ultimate load
Δ	deflection in mm
δ	deflection percentage in terms of pipe diameter
D_{δ}	load corresponding to deflection
E_c	modulus of elasticity
E	constant same as tangent modulus
F	force
FS	factor of safety
f'_c	characteristic compressive strength
f_{cm}	mean compressive strength
f'_{st}	characteristic indirect tensile strength
f_{st}	mean indirect tensile strength
f'_r	characteristic flexural strength
f_r	mean flexural strength
f_{ct}	uniaxial tensile strength
$f_{ct.sp}$	splitting tensile strength
I_1	first invariant stress tensor
J_2	second invariant deviatoric stress tensor

J_3	third invariant deviatoric stress tensor
l_d	embedment length of the reinforcement bar
l_r	distance between ribs of reinforcement
M	metal cation of potassium or sodium
M_{test}	maximum moment in TEB test
M_{field}	maximum moment in buried condition
n	poly- condensation degree
S_r	slip in μm
TEB load	vertical load in TEB test
V_p	loading rate in pull out test
w/b	water to binder ratio
W	vertical load corresponding to crack
Z and w	integer
τ	bond strength
τ_u	ultimate bond strength
τ_{fric}	frictional strength
τ_{max}	maximum bond stress
δ_{max}	maximum slip
δ_1 or S_1	Slip corresponding to maximum bond stress
λ	internal damage parameter
$\eta(\lambda)$	function of internal damage parameter
ϵ_o	strain at maximum stress f_o
ϵ_c	strain at stress f_c
ϵ_{cm}	strain at peak stress f_{cm}

LIST OF FIGURES

Figure 1-1 Joint type in concrete pipe (da Silva, El Debs & Kataoka 2018).....	5
Figure 2-1 Reinforcement configuration for concrete pipes (adopted from Ramadan et al. (2020b) and Wong & Nehdi (2018)).....	15
Figure 2-2 Three edge Bearing Test set up (Mohamed & Nehdi 2016)	17
Figure 2-3 Heger earth pressure distribution (ASCE 1998).....	23
Figure 2-4 (a) Standard trench installation (b) Standard embankment installation (ASCE 1998).....	23
Figure 2-5 Stress-strain curve of OPC and geopolymer concrete.....	41
Figure 2-6 Compressive strength degradation in geopolymer concrete & OPC concrete (Albitar et al. 2017a)	44
Figure 2-7 Direct pull-out test set up (based on (RILEM 1970))	47
Figure 2-8 Schematic set up of Beam pull-out test (Cui 2015).....	48
Figure 2-9 a) Anchorage bond b) Flexural bond (adopted from Boopalan & Rajamane (2017)).....	50
Figure 2-10 Bond-stress slip relation (Based on (Hong & Park 2012) and (CEB-FIB 2010)	51
Figure 2-11 Deterioration of reinforced concrete (Isgor 2001)	60
Figure 2-12 Collapse process in concrete sewer pipes (Davies et al. 2001).....	72
Figure 3-1 Source material and activator used for geopolymer binder: (a) Fly ash (b) Slag (c) Soda ash and (d) Sodium Silicate.....	86

Figure 3-2 Aggregates for concrete mixing (a) 20mm coarse aggregates (b) 10mm coarse aggregate and (c) river sand	87
Figure 3-3 Concrete cylinders and beam casting	91
Figure 3-4 Concrete cylinder sealed before heat curing	92
Figure 3-5 Measuring of slump value at two ends and centre during Slump test to get average slump value	93
Figure 3-6 Compressive strength development in Grade 50MPa OPC and geopolymer concrete	95
Figure 3-7 Strength development in (a) Geocem 1 and (b) Geocem 2	97
Figure 3-8 Failure of concrete cylinders (a) OPC (b) Geocem 2 (c) Type 1 failure of Geocem 1	99
Figure 3-9 (a) Indirect tensile test set up (b) split geopolymer sample.....	101
Figure 3-10 Indirect tensile strength against compressive strength for Geocem 1 and Geocem 2	104
Figure 3-11 Set up for modulus of rupture test.....	105
Figure 3-12 Flexural strength versus compressive strength plot for Geocem 1 and Geocem 2 with proposed model.....	108
Figure 3-13 Test set up to determine Modulus of Elasticity of concrete.....	109
Figure 3-14 Stress-strain curve of geopolymer concrete	113
Figure 3-15 Curve fitting of stress-strain curve for geopolymer concrete.....	115
Figure 4-1(a,b,c) different size reinforcement bars used for pull-out test (d) mould preparation (e) 100mm sample casting (f) 150mm sample casting	123

Figure 4-2 Direct pull out test set up.....	125
Figure 4-3 Failure of tested specimen (a) split failure of geocem1 sample with 12mm rebar (b) pull-out failure observed in geocem 1 for 10 mm rebar (c) comparison of geocem 1 and OPC sample for 16 mm rebar with 5d embedment length (d) commonly observed split pattern in pull-out test specimen.....	127
Figure 4-4 Bond-slip curve for geopolymer and OPC concrete for (a) 10 mm (b) 12 mm (c) 16 mm reinforcement bar with 5d embedment length.....	133
Figure 4-5 Influence of embedment length on bond stress development in Geocem 1	136
Figure 4-6 Influence of embedment length on bond stress development in Geocem 2	137
Figure 4-7 Analytical bond-slip relationship in CEB-FIB (2010)	139
Figure 4-8 Effect of concrete cover to bar diameter (c/d) ratio on ultimate bond strength	143
Figure 4-9 Effect of bond strength on S_1	144
Figure 4-10 Influence of maximum bond strength on frictional bond.....	145
Figure 4-11 Influence of bond strength on S_2	146
Figure 4-12 Bond stress-slip model validation for 10 mm, 12 mm and 16 mm reinforcement bar sample for geocem 1 and geocem 2.....	148
Figure 5-1 Stress zone in pipe and failure mode in reinforced concrete pipes	153
Figure 5-2 Test set up for pipe with LVDTs installed to measure load-deflection behaviour of pipe.....	156

Figure 5-3 Measured load-deflection curves for the reinforced concrete pipes.....	157
Figure 5-4 Crack development in Test pipe 1 at different loading phases.....	159
Figure 5-5 Three failure surface of K&C concrete model (Malvar et al. 1997)	161
Figure 5-6 Tensile stress-strain curve of steel reinforcement	165
Figure 5-7 Typical stress-strain curve of steel reinforcement representing (a) ideal elastic-perfectly plastic model (b) bilinear elastic-plastic model with linear strain hardening (Du & Jin 2021)	166
Figure 5-8 3D model of reinforced concrete pipe (a) solid element mesh for concrete material (b) single cage steel reinforcement bar in 825 mm diameter pipe.....	168
Figure 5-9 Uniaxial Compression test simulation.....	169
Figure 5-10 Sensitivity analysis of the model.....	170
Figure 5-11 Calculation of deflection percentage	171
Figure 5-12 Load-deflection plot of un-calibrated FEA model	172
Figure 5-13 Load-deflection plot of 825mm pipe after calibration	173
Figure 5-14 Experimental and FEA model results comparison for 450mm pipe	174
Figure 5-15 Stress distribution in 825mm OPC concrete pipe when load application is (a) 32% (b) 68% (c) 80% of total applied load	175
Figure 5-16 Coupling of beam in solid in CBIS (Hayashi, Chen & Hu 2017).....	176
Figure 5-17 Load-deflection comparison for Geocem 1 and Geocem 2 concrete pipes of different diameter with and without bond consideration.....	178
Figure 5-18 Load- deflection plot for (a) 450 mm pipe (b) 825 mm pipe (c) 1200 mm pipe.....	181

Figure 5-19 Effect on load-deflection behaviour of 450mm pipe due to change in reinforcement steel area	184
Figure 5-20 Effect on load-deflection behaviour of 825 mm pipe due to change in reinforcement steel area	187
Figure 5-21 Effect on load-deflection behaviour of 1200 mm pipe due to change in reinforcement steel area	189
Figure 5-22 Effect on load-deflection behaviour of 450mm and 825 mm pipe due to change in concrete cover.....	190
Figure 5-23 Effect on load-deflection behaviour of 1200mm pipe due to change in concrete cover	192
Figure 5-24 Effect on load-deflection behaviour of 450 mm and 825 mm pipe due to change in yield strength of steel.....	195
Figure 5-25 Effect on load-deflection behaviour of 1200mm pipe due to change in yield strength of steel	195
Figure 6-1 (a) Load-deflection curve for control pipe (b) crack development during TEB test in NP control pipe (c) Spigot pocket pipe under TEB test.....	204
Figure 6-2 (a) Effect on load-deflection behaviour due to 150mm and 300mm long crack at crown (b) Crack propagation along the radial direction from crack location for 300mm long crown cracked pipe	207
Figure 6-3(a) Load-deflection behaviour due to 150 mm and 300 mm long crack at springline (b) multiple longitudinal cracks formed in pipe with 150 mm long crack at springline.....	208

Figure 6-4 Effect on load-deflection behaviour due to 10 mm and 15 mm deep crack at crown.....	209
Figure 6-5 Load-deflection behaviour of pipe with cracks at different location	210
Figure 6-6 (a) Finely meshed geopolymer concrete pipe (b) crack introduced at the crown of pipe model.....	212
Figure 6-7 Maximum stress distribution in pipe with pre-existing crack of varying length crack	214
Figure 6-8 Load-displacement curve of geopolymer concrete pipe with pre-existing cracks of varying length on the crown	215
Figure 6-9 Stress development in the pipe with cracks of different depth for same loading condition.....	217
Figure 6-10 Influence on load capacity of geopolymer concrete pipe with crack of different depths.....	217
Figure 6-11 Maximum principal stress development in pipe with cracks at different location.....	219
Figure 6-12 Influence on load capacity of geopolymer concrete pipe with crack at different location	221

LIST OF TABLES

Table 2-1 Classification of reinforced concrete pipes.....	18
Table 2-2 List of proposed models for indirect-tensile strength and flexural strength	38
Table 3-1 Chemical composition of fly ash and GGBFS used for geocem 1 and geocem 2.....	83
Table 3-2 Mix design for geopolymer and OPC concrete (kg/m ³).....	89
Table 3-3 Mechanical properties of geocem 1 and geocem 2 at 7 and 28 days.....	106
Table 4-1 Pull-out test result for reinforced OPC and geopolymer concrete samples	129
Table 4-2 Pull-out test results for reinforcement bars with different embedment length in geopolymer concrete specimen.....	135
Table 5-1 OPC concrete pipe details.....	155
Table 5-2 Parameters used for material modelling	164
Table 5-3 Compressive strength of OPC concrete obtained from uniaxial compression test.....	170
Table 5-4 Pipe details.....	171
Table 5-5 Physical and Material properties of pipe model	180
Table 6-1 Pipe details.....	203
Table 6-2 Cracked pipe tests	205

Table 6-3 Bearing capacity of OPC concrete pipe at different stages of crack development during TEB test	207
Table 6-4 Numerical case study of cracked pipes.....	213

TABLE OF CONTENTS

CERTIFICATE OF ORIGINAL AUTHORSHIP	i
ACKNOWLEDGMENTS	ii
LIST OF ABBREVIATIONS	iv
LIST OF NOTATIONS	vi
LIST OF TABLES	xiv
ABSTRACT	xxi
1. Introduction	1
1.1 General	1
1.2 Research objectives	7
1.3 Research significance	9
1.4 Thesis outline	10
2. Literature review	14
2.1 Background	14
2.1.1 Concrete pipe production	14
2.1.2 Three-Edge Bearing test for precast concrete pipes.....	16
2.1.3 Design of precast concrete	20
2.1.4 OPC concrete as traditional binding material	25
2.2 Introduction to geopolymer binder	27
2.2.1 Components of geopolymer	27

2.2.2	Geopolymerisation process	28
2.2.3	Curing conditions	29
2.2.4	Application of geopolymer concrete	31
2.2.5	Limitations of liquid activated geopolymer	33
2.3	Investigations of geopolymer concrete properties.....	34
2.3.1	Mechanical properties	34
2.3.2	Durability properties	42
2.3.3	Bond between steel reinforcement and concrete.....	45
2.4	Long-term properties of geopolymer concrete	59
2.5	Performance study of reinforced concrete pipes under TEB test	62
2.6	Durability of concrete pipes	67
2.7	Failure of pipes due to crack	70
2.8	Case study on effect of pre-existing cracks on pipe performance....	72
2.9	Summary	76
3.	Investigation of mechanical properties	79
3.1	Experimental program.....	81
3.1.1	Concrete strength grade.....	87
3.1.2	Mix design and concrete mixing procedure	87
3.1.3	Concrete casting and curing of specimens	90
3.2	Investigation of material properties of concrete.....	92
3.2.1	Workability	93
3.2.2	Mechanical properties	94
3.2.3	Stress-strain curve	112

3.3	Summary	116
4.	Bond-slip analysis	118
4.1	Background	118
4.2	Experimental program	121
4.2.1	Design of test specimen	122
4.2.2	Compressive strength and tensile strength test	124
4.2.3	Direct pull-out test.....	124
4.2.4	Experimental results.....	126
4.3	Model for bond-slip behaviour of geopolymer concrete	138
4.3.1	Bond stress-slip model for geopolymer concrete.....	142
4.4	Summary	148
5.	Finite element modelling of reinforced concrete pipe	151
5.1	Background	151
5.2	Experimental program	155
5.3	Finite element modelling of Three-Edge Bearing test	160
5.3.1	Material modelling.....	160
5.3.2	Model components	166
5.4	Model validation.....	168
5.4.1	Material model verification.....	168
5.4.2	Validation of finite element model of reinforced concrete pipe	171
5.4.3	Stress development in concrete pipe	174
5.5	Numerical modelling of geopolymer concrete pipes considering bond-slip behaviour	176

5.5.1	Numerical analysis of geopolymer concrete pipes.....	177
5.5.2	Load-deflection behaviour of geopolymer concrete pipes.....	179
5.6	Parametric study of geopolymer concrete pipes.....	183
5.6.1	Effect of change in reinforcement area	183
5.6.2	Effect of change in concrete cover to inner cage	189
5.6.3	Effect of change in yield strength	193
5.7	Summary	196
6.	Structural performance of cracked concrete pipe.....	199
6.1	Introduction	199
6.2	Experimental program	202
6.3	Parametric study of concrete pipe with pre-existing cracks.....	205
6.3.1	Effect of change in crack length on pipe performance	205
6.3.2	Effect of change in crack depth on pipe performance.....	208
6.3.3	Effect of change in crack location on pipe performance.....	210
6.4	Numerical modelling for cracked geopolymer concrete pipe	212
6.4.1	Pipe model with crack.....	212
6.4.2	Effect of crack length on geopolymer concrete pipe	213
6.4.3	Effect of crack depth on geopolymer concrete pipe.....	216
6.4.4	Effect of crack location on geopolymer concrete pipe.....	219
6.5	Summary	222
7.	Conclusion and recommendations	224
7.1	Conclusions	224
7.2	Recommendations for future studies	228

References	231
Appendix A	263
Appendix B	264

ABSTRACT

Recent development in material science has introduced geopolymer as an appropriate alternative to Ordinary Portland cement (OPC) that uses industrial by-products as its source material. Past studies on geopolymer concrete have demonstrated remarkable gain in early age strength and resistance against chemical reactivity by geopolymer concrete in relation to OPC. These properties of geopolymer can be capitalised in precast concrete pipes production. However, the general use of geopolymer binder in infrastructure development is yet to be observed in the absence of proper design guidelines. This study recognizes the need to interpret structural response of geopolymer concrete pipes and therefore, investigate the load-deflection behaviour of geopolymer concrete pipes. In this study, material properties of two types of geopolymer concrete: general purpose and high strength geopolymer concrete alongside OPC concrete with a grade 50 MPa concrete mix has been examined, along with the bond-slip behaviour between the reinforcement bar and geopolymer concrete. A three-dimensional finite element model of reinforced concrete pipe was developed to analyse the load carrying capacity of reinforced and non-reinforced geopolymer concrete pipes under three-edge bearing test. Parametric study on load-deflection behaviour of geopolymer concrete pipe was carried out. The effect on loading capacity due to pre-existing crack of varying length, width and location was also explored to assist in damage assessment of pipe in construction and service practices. Based on the experimental investigation on mechanical properties and bond-slip behaviour, suitable relationship for flexural strength, tensile strength and modulus of elasticity for powder based geopolymer concrete is proposed. The bond-slip relation for powder based geopolymer concrete is proposed and used to further analyse the difference in

finite element model with and without bond consideration. The numerical analysis results indicated geopolymer concrete compared to same grade OPC concrete achieved greater loading capacity in pipe structure due to higher tensile performance. It was found that geopolymer concrete pipes could meet the specified strength requirement for OPC concrete with up to 20% reduction in reinforcement area and increased concrete cover. Further comparing pipes with pre-existing cracks of different length, depth and location, the load bearing capacity in pipe was found to be affected more by the crack depth compared to crack length, while crack along the loading axis was found susceptible to pipe damage compared to cracks at other locations. The results obtained from the study can be utilised as guidelines for geopolymer concrete pipes design for their application in the construction industry.

Chapter 1

1. Introduction

1.1 General

Concrete pipes are an integral part of civil infrastructure primarily used for sewage and storm water drainage. These structures have been in use for centuries demonstrating their efficacy in terms of durability and reliability. With the rise of new technology and development in material industry, other manufacturing materials like steel, thermoplastics such as Polyvinyl Chloride (PVC) and High-Density Polyethylene (HDPE) for pipes are also found to be used often, however, concrete remains the primary construction material for sewage pipes.

While reinforced concrete pipes are rigid pipes; pipes made from steel, PVC and HDPE are called flexible pipes. The simple difference between these two types is their ability to compress in comparison to the surrounding soil. In case of rigid pipes, the surrounding soil is more compressible than the pipe itself, due to which, a rigid pipe relies on its own resistance created due to its structure to support external load. On contrary, flexible pipe depends on the horizontal force exerted on it by the enveloping soil to resist external load without excessive deformation. Hence, rigid pipes such as concrete pipes can be used conveniently even in low quality bedding soils.

The concrete pipe though favourable due to its reliable history, also has adverse effect on the environment because of the use of Ordinary Portland Cement (OPC) for manufacture. Producing OPC is an energy-intensive process in which large quantity of CO₂ is produced due to fuel combustion while heating raw materials and de-

carbonation of limestone during calcination process (Li et al. 2011). Every 1 ton of OPC produced, generates nearly 0.85 to 1 ton of CO₂, thereby accounting for 7% of CO₂ emitted globally (Huntzinger & Eatmon 2009; Turner & Collins 2013). OPC production along with the emission of greenhouse gases, use non-renewable resources as its source material. This has fuelled arguments around the sustainability of OPC for green future and hence, increased interest towards alternative binding agents. With the focus to reduce the carbon footprint and find alternative concrete binders, numerous researches have been carried out. Based on these research, geopolymer binder has been suggested as a suitable substitute to OPC (Davidovits 1991, 2005; Hardjito et al. 2004a).

Geopolymer is a new kind of cement-less binder, produced by combining aluminosilicate compounds with alkali that result in a solid material similar to hardened OPC concrete but with minimal carbon-footprint (Davidovits 1991; Habert, De Lacaillerie & Roussel 2011; Provis & Deventer 2014). The aluminosilicate compounds, which are the source components for geopolymer binders are obtained from industrial waste like ground granulated blast furnace slag (GGBFS) and fly ash, besides using natural materials like clay and metakaolin. Estimation on CO₂ emission during OPC and geopolymer binder production have shown the values for production of geopolymer to be 80% lesser than OPC (Davidovits 2005; Duxson, Provis, et al. 2007).

Considering its potential as a sustainable construction material, several studies have been undertaken to investigate the manufacturing methods, curing conditions and the chemical and mechanical properties. Researches have revealed that geopolymer concrete has shown significant development in compressive strength, high flexural

strength and better bonding with steel in comparison to OPC concrete (Diaz-Loya, Allouche & Vaidya 2011; Hardjito & Rangan 2005; Sarker 2011; Wallah & Rangan 2006). In addition to these mechanical properties, geopolymer concrete has proved remarkable resistance against sulphate attack, chloride penetration and fire resistance (Albitar et al. 2017a; Kupwade-Patil & Allouche 2013; Roa-Rodríguez, Aperador & Delgado 2014). These properties of geopolymer concrete can be utilised in the design of precast concrete pipes assuring increased durability in aggressive environments. Studies have reported that heat curing accelerates the polymerization process in geopolymer, thereby resulting in development of higher early age compressive strength (Fernández-Jiménez, Palomo & Puertas 1999; Nath, Sarker & Rangan 2015; Sindhunata et al. 2006; Vora & Dave 2013). This early age strength development allows for quick removal of formwork in precast pipes and provides multiple use of it in a given day, thus reducing the requirement of numerous formwork and resulting in time saved in production.

However, much of the studies on different geopolymer concrete were undertaken by activating different types of alumina-silicate compounds using highly concentrated alkali solutions like sodium hydroxide and sodium silicates. This process required careful handling of liquid alkali activator during batching, thus presenting a level of difficulty in practical use of geopolymer. However, availability of fly ash/GGBFS based powder form geopolymer like geocem can be used to take advantage of the properties of geopolymer concrete over OPC concrete. The powder form of geopolymer (geocem) is easy to handle similar to OPC, as the alkali sodium silicates and sodium carbonates are premixed in powder form with the fly ash and GGBFS such that the concrete or mortar mix can be prepared similar to OPC by just adding water to it.

Current industry practice has seen the application of geopolymer in pavements, retaining walls, water tanks and boat ramps (Aldred & Day 2012; Andrews-Phaedonos 2014; Provis & Van Deventer 2009). The first case of use of geopolymer concrete for structural purpose was for building the Global Change Institute at the University of Queensland, where 33 geopolymer precast floor-beam slabs were used to make up the floors for 3 levels (Aldred & Day 2012; Bligh & Glasby 2013). Built in 2013, it is still considered one of the sustainable constructed buildings as the carbon emission life cycle analysis of the geopolymer used in construction showcased reduction in carbon emission by more than 80% compared to reference blended OPC binder (Aldred 2013; Islam et al. 2015; Sani & Muhamad 2020). Such reduction in carbon emission is mainly due to elimination of high-temperature calcination step required for OPC (Andrews-Phaedonos 2011; Davidovits 2015). In addition to the sustainability benefits of geopolymer used, the floor-beam panel subjected to load-deflection test recorded deflection of 2.85mm based on uncracked section analysis which was lesser than the predicted 3mm value (Bligh & Glasby 2013). Further testing showed that 80% of 28 day flexural strength in geopolymer concrete was obtained within 7 days under ambient curing, and was 30% higher than OPC concrete (Aldred 2013). Geopolymer used in this building has clearly demonstrated comparable or even better performance than OPC structures.

Numerous studies of reinforced concrete pipes have been conducted to closely examine the structural behaviour of concrete pipes under three-edge bearing (TEB) test, taking into account design parameters like different reinforcement configuration, pipe wall thickness, use of steel and synthetic fibers and joints in pipe. Ramadan et al. (2020a) pointed out the flexural capacity in pipe could get compromised for elliptical caged reinforced pipe due to the rotational misorientation of cage during casting. It

was observed in his study that the load capacity for elliptical caged reinforced pipe was 20% - 40% less than the reinforced pipe with similar reinforcing steel. When steel fibers of dosage 25 kg/m^3 - 30 kg/m^3 were used for the study, 6% increase in load bearing capacity was noticed when compared to reinforced concrete pipes, while the crack size decreased by 15% for the same (Haktanir et al. 2007; Mohamed, Soliman & Nehdi 2014). Peyvandi, Soroushian & Jahangirnejad (2013) on their study also concluded pipe wall thickness can be reduced in response to the increase in flexural performance of reinforced concrete pipe with the use of PVA fibers. Similarly, from the study of different joint types of the pipes (Figure 1-1), it was noted that the presence of pocket in joints increases stiffness in pipe thereby influencing the load cracking in pipe (da Silva, El Debs & Kataoka 2018; Kataoka et al. 2017). Equivalent number of numerical study on reinforced concrete pipes, synthetic fibre reinforced concrete pipes and steel pipes have been carried out (Ferrado, Escalante & Rougier 2016; Kataoka et al. 2017; Mohamed & Nehdi 2016; Ramadan et al. 2020b). However, sufficient attention has not been paid towards the same for geopolymer concrete pipes.

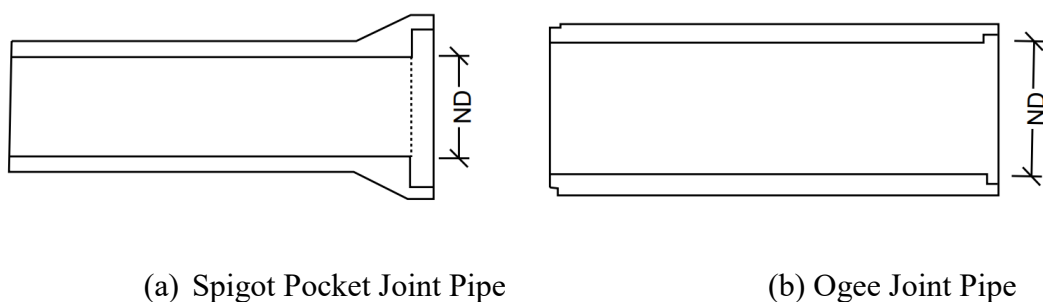


Figure 1-1 Joint type in concrete pipe (da Silva, El Debs & Kataoka 2018)

In addition, study concerning bond properties of geopolymer concrete has been conducted in limited number that focuses on the bond strength between the geopolymer concrete and reinforcement bars in comparison to OPC concrete and for

different cases of embedment length. The bond between reinforcement bars and concrete in reinforced concrete is a main characteristic that helps transfer the stress from concrete to reinforcement bars, thus affecting its structural performance. It is important to comprehend the bond-slip behaviour to characterize the loading capacity, deformation, crack pattern, anchorage capacity and lap splice length in structures (Hong & Park 2012; Kabir, Islam & Chowdhury 2015). Studies carried out on bond strength behaviour of geopolymer concrete for increasing compressive strength showed corresponding increase in bond strength (Boopalan & Rajamane 2017). Such bond strength increase was further noted for decrease in embedment length of reinforcement bars (Kathirvel et al. 2017; Kim & Park 2014; Vinothini et al. 2015). These researches have concluded that the bond strength of geopolymer concrete is higher by about 10% compared to OPC concrete, thus suggesting that the existing bond-slip equations for OPC can conservatively calculate the bond-slip relation for geopolymer (Castel & Foster 2015; Sarker 2011). Though the bond strength in geopolymer concrete is being explored, a reliable bond-slip equation for geopolymer concrete is yet to be determined which can contribute towards analytical study of structural responses of geopolymer concrete structures.

Further, concrete pipes are subjected to microbes induced corrosion resulting from H_2SO_4 reaction with OPC concrete. The H_2SO_4 in sewage pipes are formed after the release of H_2S gas from sewage water, which reacts to moisture present in pipe forming H_2SO_4 acid (Zhuge et al. 2021). This reaction of H_2SO_4 with CaOH component of OPC concrete causes loss of mass and strength in concrete and study have presented remarkable resistance to such reactivity and loss of strength by geopolymer in compared to OPC concrete (Hassan, Arif & Shariq 2019; Imtiaz et al. 2020; Valencia-Saavedra, de Gutiérrez & Puertas 2020). However, attempts to study

the impact on loading capacity of geopolymer concrete pipe subjected to such harsh environment has never been made.

Moreover, considering the external load, surrounding environment, substandard material or even faulty production process, concrete pipes are susceptible to damage due to cracks and corrosion either during the production process or after some use (Wong & Nehdi 2018; Zhang et al. 2020). This compromises the service performance of the concrete pipe. Hence, several studies evaluating the effect of the pre-existing cracks have been carried out. Buda-Ozog, Skrzypczak & Kujda (2017) analysed cracking due to tensile stress in reinforced concrete pipes and recommended that for optimum design of pipe it is crucial to specify the concrete tensile strength at failure considering the curvature of pipes. Similarly, the crack tip opening displacement (CTOD) of pipe with outer circumferential crack was studied under tensile loading and tension due to internal pressure by Jayadevan, Østby & Thaulow (2004). The effect of crack length on CTOD due to shallow and deep cracks were reported and it was deduced that for low strain hardening materials, the effect of crack length is considerable. On a study considering the strength of the buried pipe against corrosion depth, length and width, stated that corrosion depth is the main factor to affect the bearing capacity in pipe, while width has least effect on the bearing capacity (Li et al. 2021; Zhang et al. 2020). Albeit, study on ultimate load carrying capacity with pre-existing cracks on geopolymer concrete structures are yet to be carried out.

1.2 Research objectives

The primary goal of this study is to examine the load-deflection response of precast pipes utilizing the properties of the two powder form geopolymer binder

(geocem 1 and geocem 2) comprising of different ratio of fly ash and GGBFS in their composition. This research focuses on studying the ultimate failure load capacity of geopolymer pipes considering the bond-slip relation between geopolymer concrete and reinforcement bars and to determine the reinforcement requirement for the geopolymer pipes. In addition, the effect of crack dimension on bearing capacity of geopolymer pipes with pre-existing cracks is also highlighted, subsequently, adding value by formulating recommendations for pipes design using geopolymer binder. The specific research goals are:

- i) To explore the mechanical properties of geopolymer concrete, such as tensile strength, compressive strength and modulus of elasticity to verify previously stated characteristics of geopolymer concrete.
- ii) To conduct pull-out test for reinforced geopolymer to understand the bond-slip behaviour of geopolymer binder and to obtain bond-slip relationship for geopolymer binder to be used in finite element model.
- iii) To develop a three-dimensional finite element model of reinforced concrete pipes to simulate Three-Edge Bearing (TEB) test and investigate the load-deflection behaviour for geopolymer precast pipes on a validated model.
- iv) To carry out numerical analysis of geopolymer concrete to determine displacements, stresses and strains developed in pipe crown, inverts and spring-line under TEB test taking into account the bond-slip behaviour.
- v) To carry out parametric study in order to evaluate the load-deformation behaviour for different cases of pipe diameter, reinforcement details and concrete cover.

- vi) To evaluate the load bearing capacity in pipes with pre-existing cracks at different locations and different crack depth and length under test load in TEB test compared to undamaged concrete pipes.

1.3 Research significance

Several research carried out on geopolymer concrete have demonstrated its equivalent or somewhat outstanding engineering properties in comparison to OPC concrete, recommending its use as a viable alternative to OPC concrete. However, the application of geopolymer concrete by concrete industry is not that prevalent, especially in precast components where its early age strength gain can be utilised. This limitation in use of geopolymer for practical purpose is mostly due to the risk posed by the requirement in using liquid sodium hydroxide for the formation of the binder. This study uses a powder form of geopolymer concrete (geocem) developed by Cement Australia which is similar in appearance to conventional OPC and evaluates its structural performance in geopolymer concrete pipes against OPC concrete pipes. The significance of this study lies in addressing this issue by providing following contributions:

1. This thesis presents an experimental study of mechanical properties of grade 50 MPa geopolymer and OPC concrete to explore their suitability for precast concrete structures. Based on RILEM pull-out test, experimental study is also carried out to investigate the bond stress and slip relationship in reinforced geopolymer concrete. The experimental data are summarised to be used as input parameters for FE analysis.

2. This thesis reviews the finite element model of concrete pipes for TEB test and assesses the load-deflection behaviour of geopolymer concrete pipes. The numerical analysis results are compared against OPC concrete pipes results. Based on this analysis, detailed discussion of the ultimate failure load for geopolymer concrete pipes compared to OPC concrete pipes during the TEB test are presented.
3. This thesis analyses the bond-slip relationship test data for geopolymer concrete and establishes empirical equations that can be used in further studies.
4. The effect of bond-slip relation is also considered to analyse the non-linear behaviour of reinforced geopolymer concrete pipes in TEB test, which contributes to the analysis of structural responses of geopolymer concrete.
5. This study conducts parametric study for different reinforcement conditions to facilitate in producing more economical geopolymer pipes. The findings of this study will present a rational basis for the design of geopolymer concrete pipes which will be helpful in developing guidelines for precast pipe.
6. The thesis carries out the analysis of bearing capacity of geopolymer pipes affected by cracks of different depth, length and at different locations, hence providing a basis for service load performance of geopolymer pipes.
7. Finally, this thesis will provide a numerical tool that will be helpful in designing geopolymer concrete pipes, therefore limiting the need for conducting actual TEB test.

1.4 Thesis outline

This thesis delves into the load-deflection behaviour of geopolymer concrete pipes, accounting the bond-slip relation for different sized reinforcement bars and

evaluates the response of the geopolymer concrete pipe due to pre-existing cracks of different size and on different locations. The thesis is structured into 7 chapters.

In Chapter 2, the existing literature on the development of geopolymer concrete is reviewed and the relevance of geopolymer concrete in sewage pipe development is explored. It discusses about the prevalent industrial practice for OPC concrete pipe design, production and properties required in concrete material to achieve those design criteria. It includes a comparative review of the mechanical properties, durability properties along with the bond-slip behaviour of geopolymer concrete against OPC concrete. Current bond mechanism of OPC concrete and need for bond-slip relationship for geopolymer concrete to simulate accurate behaviour in pipe design is also discussed. Finally, it gives an overview of the impact on load bearing capacity of pipe with cracks developed in pipe either due to overloading, material defect or during production or installation phase. It explores the experimental and numerical studies carried out considering different variables affecting the performance of pre-cracked concrete pipes and the need to understand the effect on loading capacity of pipe due to such cracks as concrete pipes are always susceptible to crack development.

Chapter 3 describes the experimental work conducted in this study in relation to the mechanical behaviour of two types of geopolymer concrete, namely geocem1 (general purpose geopolymer) and geocem 2 (high early strength geopolymer), along with OPC concrete is described. Study of these two geopolymer concrete provides understanding for appropriate geopolymer formulation for use in precast components, depending on the prerequisite condition. The mechanical properties of grade 50 MPa geocem 1 and 2 cured at accelerated temperature and same grade OPC concrete cured at ambient temperature will be compared as per the relevant Australian Standards to

get an understanding of compressive strength, flexural strength, indirect tensile strength development at 7, 14 and 28 days and 28 days modulus of elasticity. The stress-strain curve for these three concretes will also be discussed.

Chapter 4 covers the pull-out test carried out to explore the bond-slip behaviour for geopolymer concrete against OPC concrete. The development of bond strength in geopolymer concrete is analysed for various cases of reinforcement bars with varying embedment length. The failure mode for both type of geopolymer concrete along with that for OPC concrete is discussed along with the influence of varying reinforcement bar diameter and embedment length on ultimate bond strength development. Based on the regression analysis carried out on experimental results, suitable equation to define the bond-slip behaviour between reinforcement bar and geopolymer concrete is suggested, thus providing numerical base for simulating bond-slip behaviour for FEA model.

In Chapter 5, development and evaluation of 3D finite element model for 450 mm, 825 mm and 1200 mm pipes simulating the TEB test in ANSYS LS-DYNA. The results for OPC concrete pipe are validated against experimental data presented in literature. The validated model is then used to generate FEA results for geopolymer concrete pipes. The numerical analysis of geopolymer pipe with the incorporation of bond-slip behaviour is also discussed. The load-deflection behaviour of reinforced geopolymer pipe is modelled with the bond-slip effects and compared against the FE results for geopolymer concrete pipes without adopting bond-slip behaviour in order to differentiate the effect of bond behaviour on load bearing capacity of the geopolymer pipes. Further, a parametric study is conducted to investigate the influence of variable reinforcement condition (30%, 50% and 80% of areas of steel

reinforcement), different concrete cover and varying yield strength of reinforcing steel on load-deflection behaviour of geopolymer concrete pipes. Results from the parametric study on geopolymer pipes are then compared with OPC pipes.

In Chapter 6, effect of cracks on geopolymer concrete pipes are shown. This chapter looks into the effect on geopolymer concrete pipe due to development of plastic cracks during production phase or cracks developed due to excessive load and surrounding environment. Since development of cracks in crown and invert greatly compromise the load bearing capacity of the pipe, numerical study is carried out to analyse the load bearing capacity of geopolymer pipeline and stress development in different sections of the pipe due to pre-existing cracks of various size and at different locations. The change in loading capacity of cracked pipe along with the stress concentration at different sections is then compared with intact pipes numerical results.

Chapter 7 concludes the thesis by presenting the primary conclusions of the research, along with the constraints in the work and providing suggestions to further explore the geopolymer concrete pipes behaviour.

Chapter 2

2. Literature review

2.1 Background

Archaeological evidences indicate the existence of sewer systems very early throughout the history of civilisation (ACPA 1981). Wong & Nehdi (2018) outlines that the construction of storm water and sewage pipes using bricks and concrete started back in the 1800s. It is evident that the building material for such sewer system progressed gradually from natural materials such as stone and clay to concrete over time. Concrete and reinforced concrete pipes are extensively used, not only as sewage pipes, but also as low-head pressure conduits for irrigation (Haktanir et al. 2007). Nowadays, precast concrete pipes industry is a well-established industry providing effective solutions for drainage and sewage around the globe.

2.1.1 Concrete pipe production

Precast concrete pipes are manufactured in various diameter with or without using single, elliptical, double or even triple cage reinforcement for different wall thickness and as per the required pipe strength. Figure 2-1 demonstrates different reinforcement type used for concrete pipes.

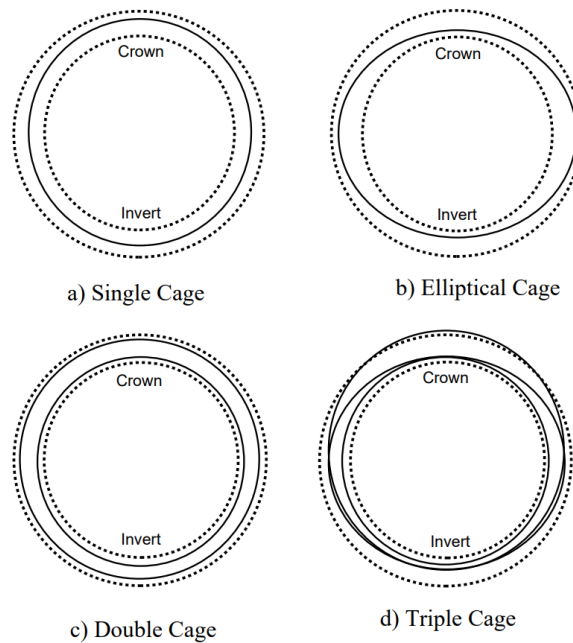


Figure 2-1 Reinforcement configuration for concrete pipes (adopted from Ramadan et al. (2020b) and Wong & Nehdi (2018))

The general method adopted for precast concrete pipes manufacture includes dry cast and wet cast (Shrestha 2014). Though the production process for both methods is similar, Shrestha (2014) adds that with wet cast concrete pipes, the water-cement ratio for the mix is 0.4 or higher and for dry cast, it is 0.3 to 0.36. Wet cast method is used for manufacturing pipes of larger diameter while dry cast is mostly used for mass production of common size concrete pipes. For precast concrete, concrete mix needs to be especially designed. A no-slump concrete needs to be prepared, which refers to concrete with slump value ranging from 0 mm to 25 mm (ACI211.3R-02 2009). Such mix favours concrete to consolidate quickly so the mould can be stripped off shortly. Mohamed (2015) indicates the cohesiveness in the fresh concrete mix for precast concrete pipe is achieved by adding just the right amount of water required to maintain the shape of the pipe (without cracking or slumping) after demoulding, so that the

mould can be removed shortly. Hence, contributing for rapid production of precast structures in a well monitored environment.

During the production process of precast pipes, the concrete mix is casted in a mould, consisting of two concentric cylindrical moulds. The reinforcement cage is fixed in place inside the mould with spacers. The concrete mix casted in mould is compacted either by centrifugal process, vertical vibration, packer head or vertical pressing. Consequently, the compacted concrete mix holds its shape when the mould is removed, which is then cured and left for setting. After a resting period of 6 hours at room temperature, curing of precast concrete pipe is done in three phases (Haktanir et al. 2007). In the first phase, the temperature of the curing room is increased gradually by 12°C per hour till it reaches 60°C. Steam curing is then started at a temperature of 60°C for 12 hours for phase two. And finally, the temperature is reduced at the rate of 12°C per hour to bring it to room temperature. For the purpose of handling, storing and transportation, the precast concrete pipes are provided with lifting holes in the top of the centre of mass of the pipe (AS/NZS4058 2007) which are then filled with plug of concrete or other appropriate materials. The finished products are then transported to site and assembled.

2.1.2 Three-Edge Bearing test for precast concrete pipes

The manufacturing process of concrete pipes and their compliance requirements are regulated by various standard specifications depending on the country of production. Three-Edge Bearing (TEB) test is the standard test used to evaluate the strength of concrete pipe. This test requires the application of uniform load using hydraulic jack along the crown of the concrete pipe through a wooden beam

placed above it, while two symmetrically placed bearing strips support the pipe along the invert as shown in Figure 2-2.

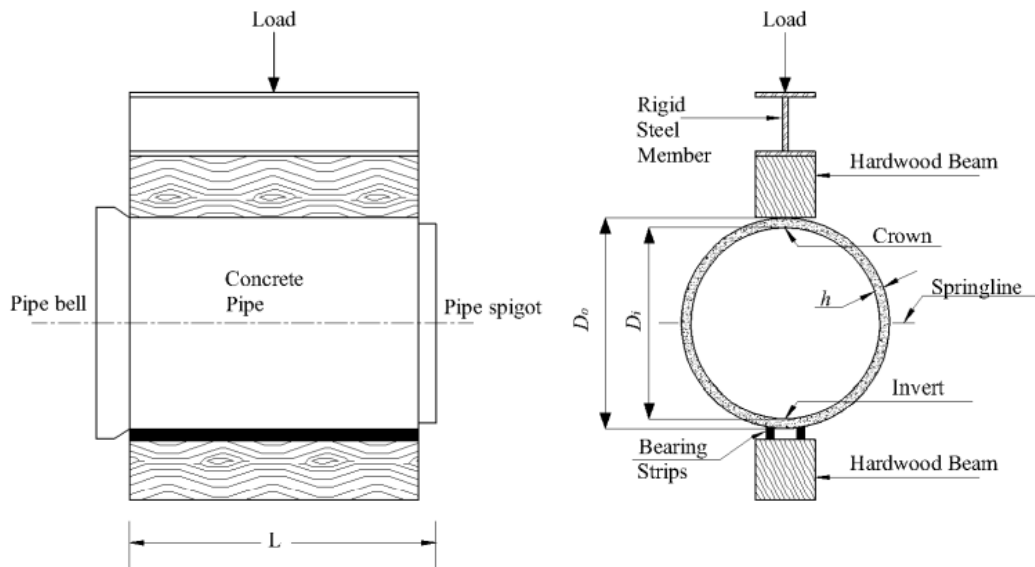


Figure 2-2 Three edge Bearing Test set up (Mohamed & Nehdi 2016)

The load is applied gradually until visible cracks appear on the pipe and to the point where the pipe is crushed. The performance of the pipe is then categorised in two type of test load: i) design load, corresponding to the load without the appearance of appropriate test crack and ii) ultimate load, load sustained by pipe without loss of load. The criteria mentioned for design load in unreinforced concrete pipe is not greater than 0.05 mm in crack width and not more than half the length of pipe, while for reinforced concrete pipe it is categorised as crack width not greater than 0.3 mm and length over 300 mm (AS/NZS4058 2007; ASTM C76M 2022). This method is based on observations of numerous destructive tests (ACPA 2011).

Based on the TEB test, the current practice in ASTM C76 classifies pipes with same design and ultimate strength into same class irrespective of its diameter. Thus,

providing guidelines for pipe design with specified wall thickness and required area of steel for particular diameter pipe to meet the designated strength class. AS/NZS 4058, however, classifies the certain diameter pipe to a particular load class depending on the proof load and ultimate load. For the pipe diameters ranging from 100 mm to 4200 mm, the proof load specified in the load class differs from diameter to diameter. Table 2-1 shows the classification of reinforced concrete pipe as per ASTM standard and Australian standard. Even though the class division is different in the two standards, the design method followed by both the standards is same. ASTM C76 class I to IV and AS/NZS 4058 class 2 to 4 uses 1.5 as factor for ultimate load, while ASTM C76 class V and AS/NZS 4058 class 6 to 10 uses a factor of 1.25.

Table 2-1 Classification of reinforced concrete pipes

ASTM C76 classification	Design Strength (N/m/mm)	Ultimate Strength (N/m/mm)	AS/NZS 4058 classification	Ultimate Load (kN/m)
I	40	60	2	1.5 X proof load
II	50	75	3	
III	65	100	4	
IV	100	150	6	1.25 X proof load
V	140	175	8	
-	-	-	10	

However, Spangler (1967) states that the crack width criteria of 0.3 mm approved to determine the design load from TEB test in ASTM standard is an arbitrarily selected

value to create uniformity regarding first visible crack during TEB test. Following the ASTM C76M (2022) and CSA-A257 (2014) standards for experimental analysis of reinforced concrete pipe under TEB test, Younis (2020) pointed out that the 0.3 mm crack width criteria though, provides a standard for crack load measurement, it might not accurately define the load capacity of pipe, since capturing the occurrence of 0.3 mm wide crack using crack-gauge depends on skill and experience of operator conducting the test. Likewise, analysing different international reinforced concrete pipe standards in terms of structural load testing, Wong & Nehdi (2018) stated that the test set up, load application and crack width limit criteria differed between standards. When different test such as two-edge bearing test and four-edge bearing test are used in China and UK respectively, the crack width limit varied from 0.15 mm to 0.3 mm when subjected to crack load. Similarly, since the concrete pipe is supported by surrounding soil under in-situ condition, the in-situ condition of pipe varies compared to the TEB test condition. Erdogmus, Skourup & Tadros (2010) stated that the concrete pipe under TEB test subjected to concentrated load and is more severe than the expected loading in the installed condition which is distributed over the pipe surface, hence the loading capacity of pipe in TEB test does not accurately represent the loading capacity of pipe in field condition. Though various set up of load testing and loading criteria is adopted, Peckworth & Hendrickson (1964) and Erdogmus, Skourup & Tadros (2010) stated that the TEB test is still widely used as an easy and inexpensive way to evaluate the minimum load carrying capacity of concrete pipes.

2.1.3 Design of precast concrete

For the structural design of concrete pipes, all the forces acting on the pipe due to earth load, pipe-soil interaction for transmission of surface loads to the pipe, and supporting reaction forces are to be considered. In an effort to develop a reliable design method, numerous studies have been conducted to determine the strength of pipes. The two available methods for design of reinforced concrete pipe have been discussed below.

2.1.3.1 Indirect design method

Reinforced concrete pipe development started with an indirect design method, an empirical method developed by Marston in early 1910. This primary design method was based on earth load calculation for buried rigid pipes considering the soil mechanics. Marston's theory was further developed by Spangler (1933), where the earth pressure distribution for buried pipe in an embankment installation was defined to calculate the supporting strength of the pipe. The Marston-Spangler theory states that load acting on the installed pipe is equivalent to the weight of soil prism on the pipe which could increase or decrease due to the influence of frictional shear force acting on the soil over the pipe by the trench wall side or the exterior soil prism (Spangler 1933). Hence, the theory of bedding factor was established in the study by Spangler (1933), where it is defined as a ratio of maximum moment in TEB test to the maximum moment in field condition (American Concrete Pipe Association (ACPA) 1993). The bedding factor expression by Spangler has been expressed in simpler form by Erdogmus, Skourup & Tadros (2010) as given in equation 2-1 as:

$$B_f = \frac{W}{\text{TEB load}} = \frac{M_{\text{test}}}{M_{\text{field}}} \quad (2-1)$$

where, W= vertical load corresponding to crack, TEB load= vertical load in TEB test, M_{test} = maximum moment in TEB test and M_{field} = maximum moment in buried condition.

The required strength of the pipe in indirect design method (D-load) is calculated based on the total load, bedding factor and a factor of safety and is expressed as equation 2-2.

$$\text{D-load} = \frac{W}{B_f} \times \frac{FS}{D} \quad (2-2)$$

where, FS= factor of safety and D = internal diameter of pipe

Combining equation (2-1) and (2-2) gives:

$$\text{D-load} = \text{TEB load} \times \frac{FS}{D} \quad (2-3)$$

Thus, indirect design method assumes the load computed from TEB test to be equal to the load developed when maximum settlement of the pipe has occurred in situ condition.

Until the 1970s, the Marston and Spangler's design theory was the only method available for concrete pipe design to determine the supporting strength of pipe for trench and embankment installations with different bedding conditions by converting pipe strength obtained from TEB test and factoring the effect of bedding type. This indirect design method is adopted when designing reinforced concrete pipes following ASTM C76, CSA A-257 and AS/NZS 4058, based on which required concrete strength, reinforcement requirements and pipe wall thickness are determined. It is a generally accepted design method.

American Concrete Pipe Association (ACPA) (1993), however, states that indirect design method is not a flexible method as it cannot account for the change in material properties like improved concrete strength, yield strength and other variables. It further points out the limit state condition of pipe during TEB test could be different from the buried condition of the pipe, as such the bedding factor relation based on the equivalent load in test and installed condition can sometimes be invalid.

2.1.3.2 Direct design method

The indirect method, while it considered the moment development due to lateral earth pressure on pipe wall, it missed out on considering the effect of axial thrust on the pipe wall where maximum moment occurs. For an arch structure, consideration of the axial thrust is important as the axial thrust creates compressive stress in the pipe cross section, reducing the flexural tensile stress in the section and allowing the material to span longer distances without major deformation (Erdogmus, Skourup & Tadros 2010). In the 1970s, American Concrete Pipe Association (ACPA), with an objective of evaluating the structural behaviour of concrete pipes and pipe-soil interaction conducted a research. Heger (1982), based on his study of the structural response of reinforced concrete pipe under TEB test, concluded that a new method for precast concrete pipe design was required such that it evaluates ultimate flexural strength and crack-control behaviour of the pipe, in account to the force, axial thrust and moment acting on the pipe. The direct design method for pipe design is a rational semi-empirical approach to determine the strength of the pipe based on the effects of force, thrust and bending moments acting on pipe wall.

Heger (1982) also developed single accurate earth pressure distribution (Figure 2-3) based on four standard installation methods for both trench and embankment type. A computer program called SPIDA was used to develop these four standard installation types that could determine the pressure distributions on pipe based on user-defined installation characteristics (Figure 2-4) (Hodges & Enyart 1993).

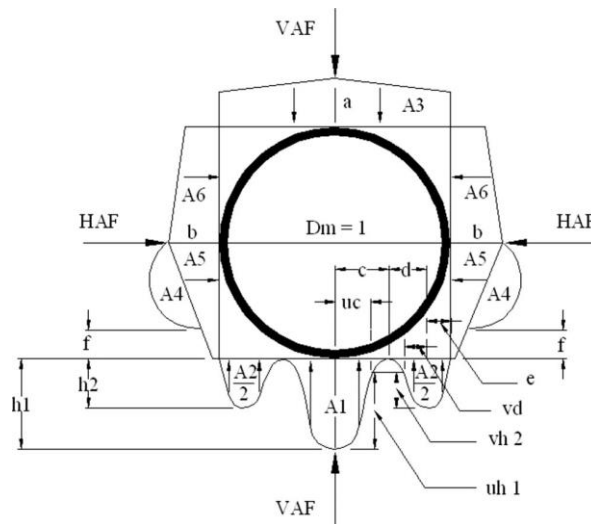


Figure 2-3 Heger earth pressure distribution (ASCE 1998)

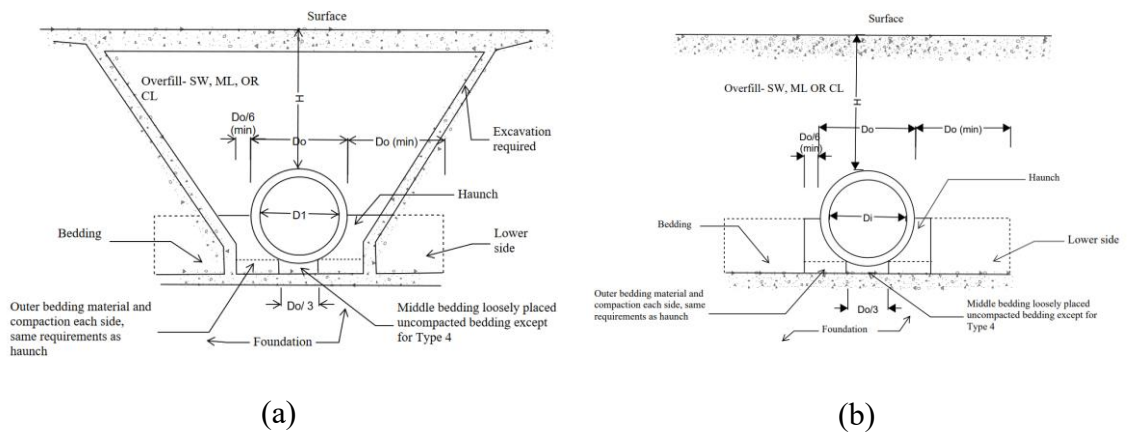


Figure 2-4 (a) Standard trench installation (b) Standard embankment installation (ASCE 1998)

As the concrete pipes form a composite system with the surrounding soil when buried in soil, the pipe-soil interaction also contributes to the strength and structural

behaviour of the pipe (ASCE 1998). Hence, in 1993 “ASCE Standard Practice for direct design of buried precast concrete pipe using standard installations (SIDDD)” was formulated which incorporated the direct design method for precast concrete pipe, four standard installation type and Heger earth pressure distribution (Erdogmus, Skourup & Tadros 2010).

The direct design method is a flexible method, as it accounts for the five limit states: i) concrete compression, ii) reinforcement tension, iii) radial tension, iv) diagonal tension, and v) crack control for the design of concrete pipes (Erdogmus & Tadros 2006; Mohamed 2015). Based on these five limit states, reinforcement area, concrete strength and wall thickness is determined. This method provides unique solution for specific pipe installation, as such it is considered efficient in terms of use of reinforcement.

Even though these methods are different in terms of the design factor like consideration of bedding factor and D-load as opposed to consideration of moments, force and thrust; both methods follow similar approach in load calculation. Both design methods consider earth load, live load and standard installation type. In addition, these methods have been adjusted over time. The new standard installations which were developed mainly for direct design method to eliminate the constraints of the installations type used in direct design method, has also been adopted in indirect design method (Erdogmus, Skourup & Tadros 2010). Indirect design method, where the earth load is calculated by multiplying the prism load with the vertical arching factor (VAF), is described in Heger earth pressure distribution, as shown in Figure 2-3. Conversely, the crack width limit that was primarily conceptualised in indirect design method to predict the strength of reinforced concrete pipe based on the results of TEB test is also

considered in the direct design method. Both these methods are equally used by designers and with the use of new advanced materials, studies recommending design methodologies are also being carried out (Erdogmus, Skourup & Tadros 2010; Peyvandi, Soroushian & Jahangirnejad 2014; Wong & Nehdi 2018).

2.1.4 OPC concrete as traditional binding material

OPC Concrete is a commonly used material to manufacture sewer infrastructures (Shook & Bell 1998). The calcium silicate hydrate (C-S-H) gel formed during the reaction of OPC with water is responsible to bind the concrete constituents together and to provide required strength in OPC concrete. However, as the reaction is an exothermic process, heat of hydration causes concrete structure to crack if curing is not done properly. Hence, OPC concrete is used for precast pipes as quality control can be achieved better in a factory setting. Furthermore, to achieve high quality and precision such as: uniform pipe wall thickness, appropriate angle for bends and rings for joint section for the components used in sewer construction, prefabrication of concrete pipes are preferred. Hence, precast applications of OPC concrete have been much valued in construction industry, mainly because it helps in speedy construction under well monitored environment, thereby allowing good quality control as well as being economical in nature.

The process of concrete pipe construction has seen the use of OPC for a long time, but it has certain limitation too. OPC is used in concrete pipe for its high compressive strength, but the tensile strength of OPC concrete is relatively low, which is why steel reinforcements are needed to meet the structural performance requirement of the pipe. And, since concrete is a permeable material, the reinforcement bar used is

susceptible to corrosion. This affects the service life of concrete-based pipes which can lead to structural failure like collapse, causing public hazard. A study conducted by Wu, Hu & Liu (2018) found the service life of concrete tunnel segment constructed in 2001 in Edmonton, Canada reduced from 100 years to less than 20 years because of biologically induced corrosion of concrete. With OPC concrete structures, network of fine cracks on the surface (craze cracks) and hairline cracks at the surface is common and is considered structurally safe (AS/NZS4058 2007). However, presence of CO₂, H₂S and H₂SO₄ in the pipelines and other reactive component present in the surrounding soil, generally present risk of sulfate attack, alkali silica reaction, carbonation and corrosion due to seepage in concrete pipes with time (Bowker et al. 1991; Wong & Nehdi 2018; Wu, Hu & Liu 2018). Such reaction of chemical and acidic components with concrete causes decomposition of concrete and loss in compressive strength (Attal et al. 1992). As such concerns regarding durability and serviceability of OPC concrete has been an issue.

OPC is a primary choice of material for pipeline construction but raising concerns for sustainability of OPC production process, durability of concrete pipes against chemical attack and to achieve its service life span seeks for new construction technology to deal with it. Studies conducted to mitigate the serviceability and durability issue of OPC concrete pipes have explored new material types. The use of fibre reinforcement system in concrete pipes for effective structural performance, while reducing the reinforcement requirement for the pipe and increasing the cover thickness over reinforcement has been advocated in many studies (de la Fuente et al. 2011; Haktanir et al. 2007; Peyvandi, Soroushian & Jahangirnejad 2013). Similarly, research carried out by Gibbons (1997), Swamy (2002), Al-Chaar, Alkadi & Asteris (2013) and Binici et al. (2012) demonstrated that addition of supplementary

cementitious materials such as pozzolans, ground granulated blast furnace slag (GGBFS), metakaolin, fly ash to OPC under control proportion can boost specific properties such as resistance to alkali silica reactivity and sulphate reactivity, depending on environmental conditions where the concrete components are being used.

2.2 Introduction to geopolymer binder

Davidovits used the term “geopolymer” for the first time in 1978 to categorize a group of synthetic alumina-silicates that had chemical composition similar to naturally formed zeolites (Davidovits 1989). Simply put, geopolymer is a binding material, similar to OPC, created by the polymeric reaction between alumina-silicate materials with alkaline solution (Davidovits 1991). As an addition to inorganic polymer material, industrial interest on geopolymer has surged as a future binder material in concrete industry.

2.2.1 Components of geopolymer

Geopolymer is a binder produced by polymeric reaction of aluminium silicate compounds with alkaline solution, its two main components are: alumina-silicate compound as source material and alkali solution as activator.

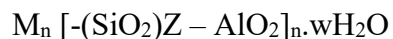
The source material initially used for geopolymer investigation were mostly of geological origin like metakaolin, clays, kaolinite (Provis & Van Deventer 2009). Subsequent studies focused on utilizing industrial by-products like ground granulated blast furnace slag (GGBFS), rice husk ash, fly ash and red mud as source materials for geopolymer (Palomo, Grutzeck & Blanco 1999; Puertas, Martínez-Ramírez, Alonso

& Vazquez 2000; Purdon 1940; Roy 1999). Study also confirmed source materials such as metakaolin, fly ash and GGBFS demonstrated better geopolymerisation reaction than kaolin and clay (Barbosa, MacKenzie & Thaumaturgo 2000; Van Jaarsveld, Van Deventer & Lukey 2003).

To activate the source material, high alkaline liquids are used for geopolymer formulation. The alkaline activator generally used are either concentrated solutions of sodium silicates (Na_2SiO_3) or sodium hydroxide (NaOH) or potassium silicates (K_2SiO_3) or potassium hydroxide (KOH) or combination of two (Davidovits 1991; Provis & Deventer 2014; Provis & Van Deventer 2009; Van Jaarsveld, Van Deventer & Lukey 2003).

2.2.2 Geopolymerisation process

The molecular structure of geopolymer consists of poly-sialate, where SiO_4 and AlO_4 form tetrahedral chain by alternatively sharing oxygen atom. The empirical formulation of poly-sialate is shown below (Davidovits 1991):



where,

‘M’ is a metal cation of potassium or sodium,

‘n’ is a poly-condensation degree and

‘Z’ and ‘w’ are integer 1, 2, 3

This poly-sialate with alkali forms a paste that has similar binding properties to calcium-silicate hydrate gel present in OPC concrete. This reaction sets and hardens

the polymer which is termed as geopolymerisation process. Davidovits (1991) explains geopolymerisation as a condensation process of silicate and aluminate monomers to formulate geopolymer chain. It comprises of 3 steps:

- i) Dissolution- where silica and alumina compounds dissolve in alkaline solution (pH level around 14) to release Si^+ and Al^+ ions.
- ii) Gelation (reorganisation) - where aluminate monomers and silicate monomers undergo condensation to form three dimensional polymer structure.
- iii) Transformation (hardening) – where hardening of the geopolymer gel occurs.

During the geopolymerisation process, water is also released as an end product as opposed to the hydration process in OPC (Bakria et al. 2011; Rovnaník 2010; Sindhunata et al. 2006), which affects the curing methodology for geopolymer.

2.2.3 Curing conditions

Since the geopolymerisation process in geopolymer binder is different than the hydration process in OPC concrete, numerous studies have been undertaken to study the influence of different curing conditions on geopolymer binder. As the curing methods have significant impact on strength development, different curing methods like heat/oven curing, steam curing and ambient curing have been studied for geopolymer binder.

For complete geopolymerisation process, Duxson, Fernández-Jiménez, et al. (2007) states that geopolymer require heat ranging from 60°C to 90°C. On a study carried out by curing alkali activated fly ash at 65°C and 85°C temperatures, higher strength development in geopolymer cured at 85°C for 24 h was observed in

comparison to geopolymer cured at 65°C (Palomo, Grutzeck & Blanco 1999). While for geopolymer cured beyond 24hrs, the rise in strength was reported to be negligible. Prolonged heat curing alters the geopolymer matrix due to thermolysis of poly-sialate bond causing strength deterioration after 28 days (Singh et al. 2015). Rovnaník (2010) and Heah et al. (2011) reported that the strength development at early age for metakaolin based geopolymer was accelerated when cured at temperature of 40 °C to 80 °C, while the samples cured at ambient conditions were not feasible for early age strength gain. But the overall grade and property of ambient cured geopolymer at 28 days age were however not affected by ambient curing. However, study by Rovnaník (2010) on the mechanical properties of heat cured geopolymer stated that the mechanical properties deteriorated over time compared to ambient cured sample. Similarly, on an experimental study by Vijai, Kumutha & Vishnuram (2010), it was presented that for ambient cured geopolymer concrete, development of compressive strength was better than heat cured sample with the age of curing, however the overall strength gain was higher for heat cured geopolymer sample.

An exploratory study for heat curing at temperature from 40°C to 140°C gradually increased by 20°C for 24 hrs, ambient curing, steam curing at 60°C to 110°C for 18hrs and water bath, revealed that the gain in strength was higher for fly ash based geopolymer concrete which was cured at high temperature, concluding 60°C to be an optimum temperature for heat curing and 80°C for steam curing, whereas samples cured at ambient temperature and water bath were reported to have lower strength development (Yewale, Shirsath & Hake 2016). For geopolymer concrete, exposed to steam curing at 60°C in two stages: firstly for 4hr before removing the mould and secondly for 21 hrs after removing the mould, reported no change in strength development due to two stage curing (Hardjito & Rangan 2005).

Based on the study of curing of geopolymer concrete, heat curing at temperature of 40°C to 80°C was reported to be an effective curing method for geopolymer binder resulting in high early age strength gain (Nurrudin et al. 2018; Rangan 2008).

2.2.4 Application of geopolymer concrete

The practical implementation of geopolymer in construction industry is still in its infancy. Geopolymer concrete was primarily used for minor concrete works such as pavements, retaining walls and water tanks (Aldred & Day 2012; Andrews-Phaedonos 2014; Provis & Van Deventer 2009).

Initial effort of using geopolymer concrete for structural purpose was made for building an eco-friendly building at the University of Queensland called the Global Change Institute, where Grade 40MPa Earth Friendly Concrete (EFC) formulated by using GGBFS and fly ash geopolymer concrete was used to construct 33 geopolymer precast floor-beam slabs to make up the floors for 3 levels (Aldred & Day 2012; Bligh & Glasby 2013; Gourley 2014). The geopolymer concrete when compared with same grade OPC concrete was reported to exhibit higher mechanical strength and complied to AS3600 (2018) requirements (Aldred 2013; Bligh & Glasby 2013). The same geopolymer material was also used to construct 435mm thick unreinforced pavement for Brisbane West Wellcamp Airport, which has been fully operational with commercial flights since 2014 (Glasby et al. 2015). The requirement of flexural strength of 4.8 MPa at 28 days by AS1012.11 (2000) was surpassed by the geopolymer showcasing 5.8 MPa strength at 28 days. Based on this result, the reason behind usage

of geopolymer concrete in runway pavement was reported to be this higher flexural strength in geopolymer (Glasby et al. 2015).

Research on the performance of geopolymer concrete as structural members such as beam and column structure have also been carried out. Based on the analytical study undertaken to define the strength of the column, it was reported that the design provisions specified in AS3600 (2018) and ACI318 (2019) can be followed for geopolymer concrete column design as the test failure load for the columns were comparable to those calculated load from the standards (Rangan 1990; Sarker 2009; Sumajouw et al. 2007). Likewise, the load-deflection behaviour and the load bearing capacity of geopolymer concrete beam were noted to be comparable to that of OPC concrete beams, though the ratio of test to calculated flexural strength for geopolymer concrete were high (Sumajouw & Rangan 2006) .

In a recent study published on specification and use of geopolymer concrete by Andrews-Phaedonos (2014) for VicRoads, use of geopolymer concrete for concrete pipes has been recommended. Due to the resistance property of geopolymer concrete, its applicability is more prominent in pipelines that are exposed to aggressive chemicals through soil and water. The degradation in compressive strength and mass loss reported for geopolymer concrete subjected to sulphate attack was remarkably lower in compared to OPC, making it a suitable material for sewage pipe exposed to microbial induced sulfuric attack (Albitar et al. 2017a; Hassan, Arif & Shariq 2019; Zhuge et al. 2021). Furthermore, the high early age strength gained by geopolymer, from high temperature curing allows, it to be used more profitably in precast pipe production.

2.2.5 Limitations of liquid activated geopolymer

Studies on geopolymer concrete have demonstrated outstanding performance with regards to its mechanical properties and chemical resistance (Hardjito & Rangan 2005; Neupane et al. 2016; Sofi et al. 2007b; Wallah & Rangan 2006). However, there is a huge gap between the findings of the research studies and practical application of geopolymer, as the geopolymer used for studies were mostly liquid activated geopolymer using sodium silicate and sodium hydroxide as its main component, with no standard formulation (Collins & Sanjayan 1999a; Fernández-Jiménez, García-Lodeiro & Palomo 2007; Hardjito & Rangan 2005; Rovnaník 2010). As such, the possibility of unsafe handling of concentrated alkali solution is high and poses serious health risk, thus, it is not preferred for general use. Skilled workers are required to mix this two part geopolymer to ensure the amount of chemical used is controlled when batching since the engineering properties of liquid activated geopolymer depends largely on the concentration of the liquid activator used. As such, liquid activated two-part geopolymer binder imposes limitations for general use in concrete industry even though it exhibits better performance than OPC in terms of mechanical strength and durability properties.

For practical application of geopolymer in concrete industry, powder form geopolymer has been developed recently which uses a combination of type F fly ash (low CaO content) and ground granulated blast furnace slag (high calcium and silicon content) as its precursor, hence appearing similar to OPC and the concrete mix can also be prepared in a similar manner (Kidd 2009). An experimental analysis conducted by Hajimohammadi, Provis & Van Deventer (2008) testified that desired workability of powder form geopolymer can be attained by adding water similar to OPC concrete

mix and found the workability to be better than liquid activated geopolymer and OPC concrete with similar water to binder ratio. This approach of developing powder activated geopolymer has concentrated on the feasibility of geopolymer concrete for general usage. Duxson & Provis (2008) mentioned the probabilities of powder form geopolymer, being used as one part “just add water” geopolymer, is higher than the traditional two-part liquid activated geopolymer, thus creating new opportunities for use of geopolymer concrete in construction industry.

2.3 Investigations of geopolymer concrete properties

With the promising environmental benefits by using industrial by-products (Heath et al. 2013; Heath, Paine & McManus 2014), many research have been undertaken to examine the engineering and chemical properties of geopolymer binder.

2.3.1 Mechanical properties

Mechanical properties of geopolymer binder has been explored for various geopolymer types. Its compressive strength, flexural strength, indirect-tensile strength and modulus of elasticity have been explored through numerous studies.

1) Compressive strength

The material characteristics in concrete is mostly defined by the compressive strength of the binder. The development of compressive strength at early age is greatly affected by the curing temperature, time period and alkaline activator (Bakria et al. 2011; Palomo, Grutzeck & Blanco 1999; Sindhunata et al. 2006), hence to explore development of compressive strength in geopolymer, investigative study has been

carried out in both accelerated temperature and ambient temperature for different time period and for different components.

The initial compressive strength development in fly ash based geopolymer concrete cured at room temperature is reported to be lower in comparison to same grade OPC concrete, even though the compressive strength of geopolymer concrete was greater than OPC concrete in latter stage (Puertas, Martínez-Ramírez, Alonso & Vázquez 2000; Wallah & Rangan 2006). Sofi et al. (2007b) explains this latter increase in strength is because the polymerisation reaction continues beyond the 28 days. While for GGBFS based geopolymer, significant gain in compressive strength in relation to OPC concrete was reported, strongly suggesting to substitute fly ash by GGBFS in geopolymer for optimum results (Collins & Sanjayan 1999b; Douglas, Bilodeau & Malhotra 1992; Nath & Sarker 2012). On an experimental study carried out by Lee & Lee (2013) suggested that the proper slag content is 15% to 20% of total binder by weight for alkali activated fly ash/GGBFS based geopolymer concrete, which produced optimum compressive strength in geopolymer concrete cured at room temperature. Neupane (2016) reported for ambient cured powder based geopolymer concrete, the gain in compressive strength was significantly low at 1-3 days, while the gain was much higher than OPC concrete at 28 to 90 days. Such development in compressive strength at latter stage was also reported for ambient cured metakaolin based geopolymer concrete (Rovnaník 2010; Sindhunata et al. 2006).

Similarly, studies conducted for fly ash based geopolymer concrete subjected to accelerated temperature curing showed that most geopolymer attains 30% of the 28 day strength during the first 4 hours of curing at 60°C (Hardjito & Rangan 2005; van Jaarsveld & Van Deventer 1999), while Rovnaník (2010) reported it to be 50% of the

28 day strength during the first 4 hours of curing at 80°C. This rapid increase in strength during accelerated heat curing is explained due to increase in solubility of alumina-silicate compound during geopolymerisation process (Sindhunata et al. 2006). Nuruddin et al. (2011) also described gain in compressive strength for rice husk ash and fly ash based geopolymer compared to ambient curing. The experimental study carried out by Atiş et al. (2015) at different range of heat curing performed on Class F fly ash based geopolymer cured for 24 hr suggested on average, temperature of 65°C - 75°C is a more ideal curing temperature for geopolymer mortar. Similar temperatures were advocated in other studies for accelerated heat curing of geopolymer, however, prolonged heating of more than 24 hours was advised to avoid (Hardjito et al. 2004a; Rovnaník 2010; Vora & Dave 2013). This was because prolonged heat curing can result in changed geopolymer matrix due to loss of moisture causing decrease in compressive strength (Van Jaarsveld, Van Deventer & Lukey 2003).

As heat curing can be achieved more easily for precast components, thus the property of geopolymer in gaining early age strength can be more suitable for use in precast construction.

2) Indirect tensile and flexural strength

As per AS3600 (2018), the uniaxial tensile strength in concrete is assumed to be equivalent to 90% of indirect tensile strength or 60% of flexural strength (Aldred 2013). Results of the studies conducted to investigate indirect tensile strength and flexural strength of geopolymer have also showed higher indirect tensile strength and flexural strength in comparison to same strength OPC concrete (Collins & Sanjayan 1999a; Hardjito & Rangan 2005; Neupane 2015; Ramujee & PothaRaju 2017; Sofi et al. 2007b). An investigative study undertaken by Atiş et al. (2009) to study the effect

of activator on strength development in alkali-activated slag mortar, found that between sodium silicate, sodium carbonate and sodium hydroxide, use of sodium silicate developed maximum tensile strength. It was further added that optimum ratio of sodium silicate offer high tensile strength development. However, it was observed that the geopolymer possessed 1.4 times higher value for indirect tensile strength while for flexural strength it was recorded to be 1.6 times than OPC concrete (Raijiwala & Patil 2011). Contrarily, Sofi et al. (2007b) reported the tensile strength of GGBFS and fly ash based geopolymer concrete with high compressive strength to be considerably low in comparison to normal strength and high strength OPC concrete, while Lee & Lee (2013) discovered that for alkali-activated GGBFS and fly ash concrete, the tensile strength was 20% lesser than OPC concrete.

In the absence of standard relationship for the calculation of the tensile strength value for geopolymer, various studies have proposed different equations in relation to the experimental results (Lavanya & Jegan 2015; Lee & Lee 2013). Research carried out by Nguyen et al. (2016) to examine the behaviour of fly ash based geopolymer concrete beam under flexural test, reported that for geopolymer concrete, the tensile strength value calculated using the equation for normal concrete was lesser than the actual value obtained for geopolymer concrete from the indirect tensile strength test. Table 2-2 list out few different models proposed in previous studies to determine the flexural strength and indirect tensile strength geopolymer concrete. It has been reported that the proposed relationship model estimates higher value for indirect tensile strength and flexural strength for geopolymer compared to estimated value based on ACI318 (2019) and AS3600 (2018) (Albitar et al. 2015; Nath & Sarker 2017).

Table 2-2 List of proposed models for indirect-tensile strength and flexural strength

Binder Type	Source	Proposed models	
		Indirect Tensile Strength	Flexural Strength
OPC	ACI318 (2019)	$f_{st} = 0.56\sqrt{f_c'}$	$f_r = 0.62\sqrt{f_c'}$
	AS3600 (2018)	$f_{st} = 0.4\sqrt{f_c'}$	$f_r = 0.6\sqrt{f_c'}$
Geopolymer (Fly ash+ Slag)	Sofi et al. (2007b)	$f_{st} = 0.5\sqrt{f_c'}$	$f_r = 0.6\sqrt{f_c'}$
	Lee & Lee (2013)	$f_{st} = 0.45\sqrt{f_c'}$	-
	Nath & Sarker (2017)	-	$f_r = 0.93\sqrt{f_{cm}}$
	Neupane, Chalmers & Kidd (2018)	$f_{st} = 0.7\sqrt{f_c'}$	$f_r = 0.89\sqrt{f_c'}$
Geopolymer (Fly ash)	Tempest (2010)	$f_{st} = 0.616\sqrt{f_c'}$	-
	Diaz-Loya, Allouche & Vaidya (2011)	-	$f_r = 0.69\sqrt{f_{cm}}$
	Ryu et al. (2013)	$f_{st} = 0.17(f_{cm})^{3/4}$	-
	(Albitar et al. 2015)	$f_{st} = 0.6\sqrt{f_c'}$	$f_r = 0.75\sqrt{f_c'}$
	Ramujee & PothaRaju (2017)	$f_{st} = 0.08(f_{cm})^{0.92}$	-

where, f_{st} and f_{st}^* stands for mean and characteristic indirect tensile strength, f_r and f_r^* stands for mean and characteristic flexural strength and f_{cm} and f_{cm}^* stands for mean and characteristic compressive strength.

3) Modulus of elasticity and poisson's ratio

Modulus of elasticity dictates the displacement of structure under stress, hence to understand the stress-strain distribution for geopolymer concrete, studies have been undertaken to determine the modulus of elasticity of geopolymer concrete. GGBFS and fly ash based geopolymer concrete that was treated at room temperature demonstrated modulus of elasticity similar to OPC concrete (Douglas, Bilodeau & Malhotra 1992; Sofi et al. 2007b), indicating the feasibility of using existing model for OPC concrete based on AS3600 (2018) and ACI318 (2019) for the calculation of modulus of elasticity of geopolymer concrete. However, for geopolymer cured at accelerated temperature, the modulus of elasticity was recorded to be lesser than OPC concrete (Fernández-Jiménez, García-Lodeiro & Palomo 2007; Hardjito & Rangan 2005). Rovnaník (2010) and Sindhunata et al. (2006) based on their study on influence of curing on geopolymer concrete suggested that when geopolymer concretes are cured at high temperature, it causes increase in total pore volume as a consequence of losing moisture, thereby, compromising the density of geopolymer mortar. As such modulus of elasticity gets negatively impacted in concrete due to this decrease in density (Pauw 1960). Based on the curing method adopted for geopolymer concrete, its modulus of elasticity varies with regards to OPC concrete. Similar conclusion was also drawn by Duxson et al. (2005) based on the experimental result on alkali-activated geopolymer suggesting modulus of elasticity in geopolymer concrete is considerably affected by microstructural development rather than strength development.

Similarly, the Poisson's ratio measures the lateral strain with respect to longitudinal strain when compressive stress is applied to the concrete. Poisson's ratio for geopolymer concrete possessing different compressive strength that ranged from

16 MPa to 89 MPa reported value between 0.126 to 0.16 (Diaz-Loya, Allouche & Vaidya 2011; Hardjito & Rangan 2005). Further suggesting to consider the Poisson's ratio value of 0.2 as recommended in AS3600 (2018) for OPC concrete, since the difference was negligible.

4) Stress-strain behaviour

For OPC concrete, the stress-strain behaviour has been well documented and is depicted by perfectly linear curve in elastic phase till the concrete achieves ultimate strength, after which strain softening is observed (Popovics 1973). Concrete stress-strain curve is beneficial in determining parameters such as maximum stress, strain corresponding to maximum stress, maximum strain and even residual stress. Therefore, it is necessary to gain understanding of the stress-strain behaviour of new materials to fully characterize their performance for design purpose and its actual application (Noushini et al. 2016). Though studies to explore stress versus strain behaviour of geopolymer concrete have been undertaken, only few studies have attempted to develop a numerical model for geopolymer concrete that can predict its stress-strain curve (Chitrala, Jadaprolu & Chundupalli 2018; Farhan, Sheikh & Hadi 2019; Thomas & Peethamparan 2015; Venu & Rao 2018). The stress-strain curve of OPC and geopolymer concrete presented in existing literature by has been shown in Figure 2-5 (Bahraq et al. 2019; Farhan, Sheikh & Hadi 2019; Hardjito & Rangan 2005; Mohamad Ali, Farid & Al-Janabi 1990; Noushini et al. 2016; Strukar et al. 2018).

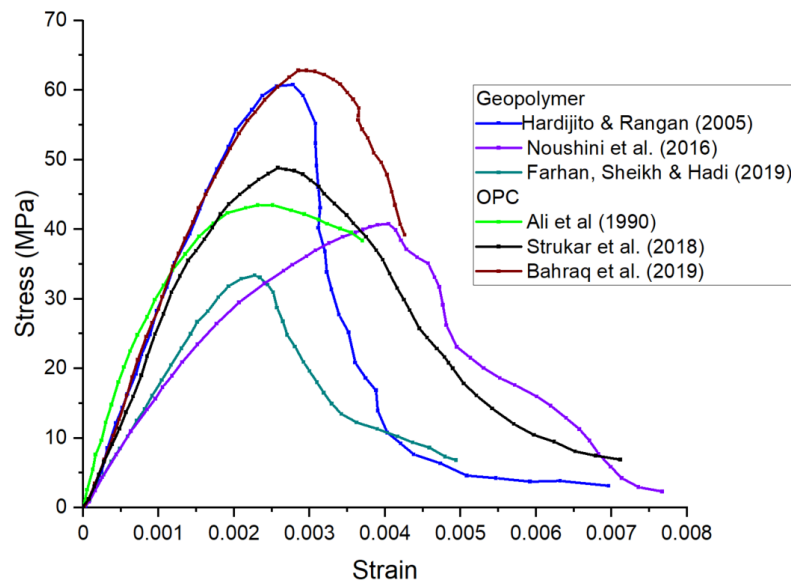


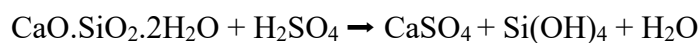
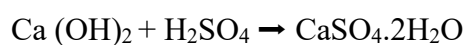
Figure 2-5 Stress-strain curve of OPC and geopolymer concrete

Study carried out by Farhan, Sheikh & Hadi (2019) to investigate the stress-strain behaviour for alkali activated slag concrete, fly ash based geopolymer concrete and OPC concrete under compression showed that the stress-strain behaviour is linear up to the peak stress for all concrete types, following which alkali activated slag concrete and fly ash based geopolymer concrete exhibited brittle failure with rapid decline post peak stress in the stress-strain curve. Such brittle reaction was credited to the high observation of micro-cracking in fly ash based geopolymer, It was further noted that for fly ash based geopolymer concrete with higher compressive strength, the stress-strain curve was observed to be more steeper with sudden and explosive failure rather than softening as in OPC concrete. Similar behaviour was also observed for alkali activated GGBFS based geopolymer concrete with rapid decline in stress in post-peak behaviour, while for alkali activated fly ash based concrete, the stress-strain behaviour closely resembled with OPC concrete (Thomas & Peethamparan 2015). Comparing the experimental stress-strain curve with analytical curve for geopolymer

concrete having compressive strength between 40 MPa to 66 MPa, Hardjito et al. (2005) suggested that the analytical model proposed by Collins, Mitchell & MacGregor (1993) for OPC concrete can accurately forecast the stress versus strain relationship for fly ash based geopolymer concrete. Likewise, comparative study on stress-strain behaviour for fly ash and GGBFS based geopolymer concrete cured at room temperature was carried out by Junaid, Karzad & Altoubat (2020) against the analytical model proposed by Collins, Mitchell & MacGregor (1993) and Talha Junaid, Kayali & Khennane (2017) with acceptable level of accuracy with analytical model. On the other hand, Chitrala, Jadaprolu & Chundupalli (2018) proposed new model to predict the stress-strain behaviour of geopolymer concrete based on the study carried out on geopolymer concrete with granite fines as partial substitute to fine aggregates.

2.3.2 Durability properties

The calcium hydroxide (Ca(OH)_2) present in OPC concrete makes it susceptible to react with aggressive components like sulphate and other acids, resulting in decomposition of concrete (Albitar et al. 2017a; Joorabchian 2010; Rostami, Shao & Boyd 2011). Calcium hydroxide in concrete reacts with sulphate to form calcium sulphate. Thus, formed calcium sulphate further reacts with calcium silicate hydrate causing severe structural damage to concrete (Min & Song 2018). Sulphuric acid corrosion reaction has been explained by Monteny et al. (2000) as below:



One of the most significant property of geopolymer that sparked interest for further research is its durability property. Geopolymer is non-OPC binder that does not depend on calcium compounds for its binding property (Davidovits 1991). Previous comparative studies conducted between geopolymer concrete and OPC concrete have reported that geopolymer concrete have high resistance capacity in acidic environment (Binici et al. 2012; Fernández-Jiménez, García-Lodeiro & Palomo 2007; Roa-Rodríguez, Aperador & Delgado 2014; Wallah & Rangan 2006).

Albitar et al. (2017a) while evaluating durability property for geopolymer concrete and OPC concrete found that class F fly ash based geopolymer concrete performed exceptionally well than OPC concrete when immersed in sulphuric solution for 9 months. It was reported that the coarse aggregates in OPC concrete was visible with yellow layer of sulphur on it, which can attribute to form sulphur dioxide, while the influence of sulphuric acid was noticed to be minimal on fly ash based geopolymer concrete. Figure 2-6 showcase the modification in compressive strength reported for these concrete samples compared to the samples placed at ambient condition over a period of 9 months.

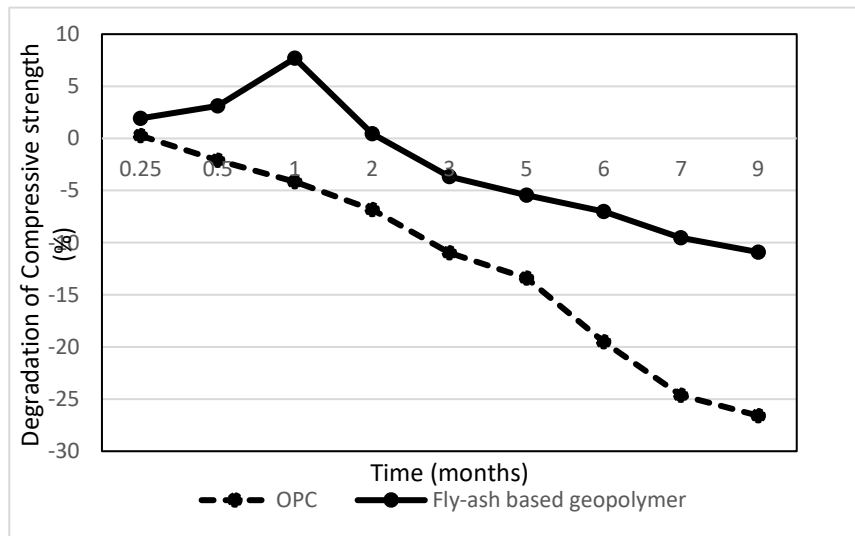


Figure 2-6 Compressive strength degradation in geopolymer concrete & OPC concrete (Albitar et al. 2017a)

The compressive strength of OPC concrete decreased significantly when immersed to sulphuric acid solution while geopolymer concrete showcased higher resistance residual compressive strength and resistance to volume loss (Hardjito et al. 2004a; Palomo et al. 1999; Thokchom, Ghosh & Ghosh 2009). Studies based on fly ash and GGBFS based geopolymer concrete exposed to magnesium sulphate, sulphuric acid, chloride and sea water have also reported higher resistance of geopolymer concrete against these chemicals (Fernández-Jiménez, García-Lodeiro & Palomo 2007; Kupwade-Patil & Allouche 2013; Kurtoglu et al. 2018).

The rust formed due to the chemical reactivity of steel reinforcement in concrete, also causes bond loss between the reinforcement bar and the concrete, thereby affecting the tensile strength of the concrete structure (Shook & Bell 1998). Thus, the chemical resistance property exhibited by geopolymer makes geopolymer

concrete structure less susceptible to steel reinforcement corrosion in comparison to OPC concrete.

Based on these comparative studies of geopolymer concrete and OPC concrete, not only did geopolymer concrete achieve higher compressive strength, flexural strength and indirect tensile, but the residual compressive strength and resistance to acidic substance demonstrated by these geopolymer concrete specimens were also remarkable. Fahim Huseien et al. (2017) marked geopolymer concrete as a suitable construction material with low carbon emission, minimal maintenance requirement and longer service life, while utilising industrial waste for production.

2.3.3 Bond between steel reinforcement and concrete

Bond denotes the connection which makes the steel reinforcement and concrete act as a single unit. The structural performance of reinforced concrete structure relies on the bond mechanism which transfers force through the interface between steel reinforcement bar and concrete, thus, preventing slip of reinforcement bar. The bond behaviour influences the embedded length of steel reinforcement, subsequently the load-bearing capacity of structural members, its deflections and crack development (Mo, Alengaram & Jumaat 2016; Pop et al. 2013). ACI408R-03 (2003) states bond strength as a structural property of reinforced concrete and thus understanding bond mechanism is critical for structural member design. The bond in reinforced concrete is contributed mainly due to i) chemical adhesion ii) friction and iii) mechanical interaction of reinforcement bars with concrete (Lutz & Gergely 1967; Tepfers 1979). Chemical adhesion and friction plays major role in bond strength for plain reinforcement bars and onto friction after slip, due to the small dislodged

concrete particles between the reinforcement bar and the surrounding concrete. For deformed bars, interlocking action between the reinforcement ribs with concrete largely contributes to its bond strength, while adhesion and friction are secondary contributors. The bond performance is assessed by bond-slip relationship deduced from bond tests.

2.3.3.1 Bond tests

The bond strength in reinforced concrete structure is commonly determined through two experimental methods: i) direct pull-out test (RILEM 1970) and ii) beam pull-out test (ASTM-A944 2022).

In direct pull-out test, a cube or cylinder sample is prepared with a reinforcement bar cast in uniaxial direction, such that half the length of reinforcement bar within the concrete cube is in contact with the concrete while the other half within the concrete is encased such that no bond is formed (RILEM 1970). The reinforcement bar incorporated in the concrete cube sample is pulled out from one side by tensile force while the other end remains stress free. The tensile force applied up to the failure of bond and relative displacement between the reinforcement bar and concrete is measured, based on which bond-slip relationship is deduced.

The set up for the direct pull-out test is shown in Figure 2-7, where the concrete cube is supported on a steel plate while pull-out force is exerted on the reinforcement bar and the linear variable differential transformer (LVDT) attached collects the slip data.

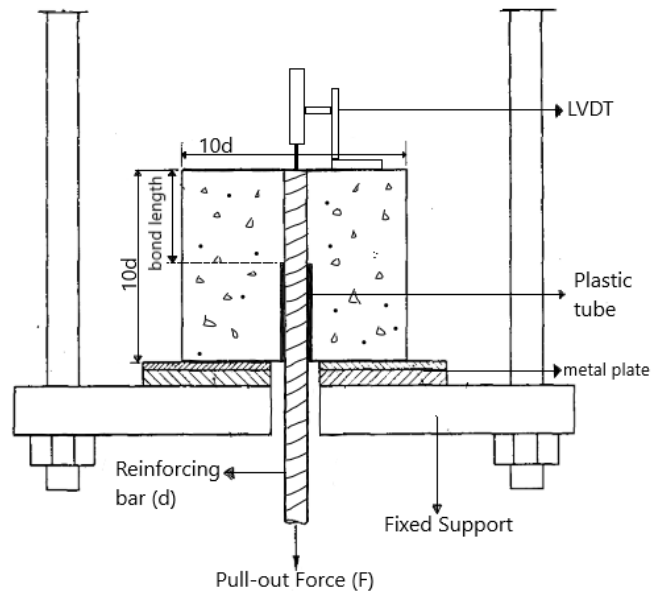


Figure 2-7 Direct pull-out test set up (based on (RILEM 1970))

This method has been preferred in numerous research carried out to determine the bond strength of the reinforced concrete sample and factors influencing the bond-slip relationship because of its simplicity and cost effectiveness. Even though it is believed the test results from direct pull-out test is not fully accurate ((FIB) 2000). Xing et al. (2015) further added that the bond strength of the deformed bars in direct pull-out test is overestimated, as the concrete sample during the test is under compression, while the tensile stress is acting on reinforcement bar.

The beam pull-out test is considered as a more accurate method as the stress condition is more rational in this method, thus representing more realistic bond strength. For this test method, a beam sample is prepared with the longitudinal test bar encased in polyvinyl chloride (PVC) pipes on two ends from the beam end to control the embedment length (ASTM-A944 2022). This sample preparation allows the sample to experience flexural tension during the test. Figure 2-8 demonstrates a

schematic set up for beam pull-out test. The tension force is applied to the longer end of reinforcement, while slip is measured from shorter free end of the reinforcement bar.

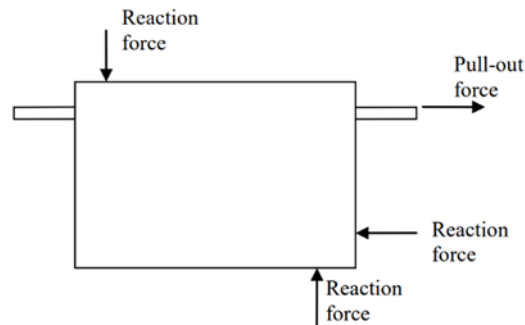


Figure 2-8 Schematic set up of Beam pull-out test (Cui 2015)

The process for deriving a bond-slip relationship based on experimental data is not univocally defined (Xing et al. 2015), hence both methods are equally preferred to obtain the bond response such as failure modes, bond strength, bond stress versus slip curve and different factors influencing the bond mechanism.

2.3.3.2 Failure modes

The failure of bond test samples are recorded under two failure modes, namely: splitting failure and pull-out failure.

For reinforced concrete with deformed bars, when pull-out force is applied, the ribs transfers the tensile stress generated in reinforcement bar onto the surrounding concrete. When the tensile stress acting on concrete exceeds the ultimate tensile stress, radial splitting force is developed which radiates out to the surrounding concrete from the bonded surface causing splitting failure of bond (Tepfers 1979). Most of the deformed bar samples fail by splitting failure (Gambarova & Rosati 1996). The pull-

out failure can also occur on reinforced concrete with deformed bars, if transverse reinforcement is provided to confine the splitting force, resulting in rupture of concrete around the ribs thus triggering pull out failure of ribbed bars (Lutz & Gergely 1967).

In case of reinforced concrete with plain bars, as there are no ribs in bar to transfer the tensile stress to the concrete, radial splitting force in concrete is not generated. The plain rebar reinforced concrete sample fails when the resistance due to chemical adhesion and friction is lesser than the applied pull-out force, resulting in pull-out failure (Xing et al. 2015). Yifei (2015) states the failure load for bond strength recorded from pull-out failure is much higher compared to splitting failure for same reinforcement details, as bond strength is fully developed in pull-out failure.

2.3.3.3 Bond stress and bond strength

The bond stress developed at the interface arises based on two conditions: i) anchorage bond, developed where bars are terminated and subjected to tensile or compression force due to pulling out or pushing in of the bars respectively, ii) flexural bond, developed due to variation in tensile force throughout a bar due to a change in bending moment (Ferguson 1966; Singh et al. 2015). These two bond conditions for the reinforcement bars along a short length is shown in Figure 2-9.

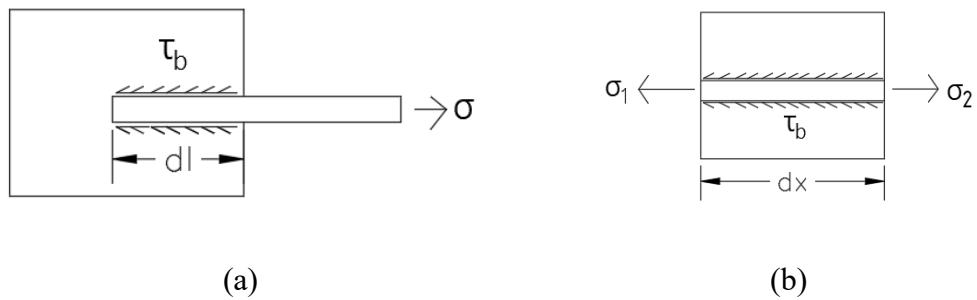


Figure 2-9 a) Anchorage bond b) Flexural bond (adopted from Boopalan & Rajamane (2017))

When the development of bond stress is considered to be consistent throughout the entire bonded length, bond strength of the reinforced concrete can be calculated based on the bond stress per unit length divided by the lateral surface area of the bar (Shen et al. 2016) as shown in equation 2-4. This is extensively used to calculate bond strength for the reinforced sample subjected to pull-out test.

$$\tau_u = \frac{F}{\pi \cdot d \cdot L_d} \quad (2-4)$$

where, τ_u = bond strength, F = failure load for the reinforced concrete section, d = reinforcement bar diameter, l_d = embedment length of the reinforcement bar.

2.3.3.4 Bond- slip curve

Bond stress versus slip curve is an actual representation of the slip conforming to bond stress developed between concrete and reinforcement bar during bond test. Bond-slip curve is an important aspect of bond behaviour that helps determine ultimate bond strength of the reinforced concrete (equation 2-4) and define the mode of failure of concrete. Moreover, it is significant in outlining a reasonable bond-slip relationship

which can predict the bond strength and slip value based on other variables (Long, Tan & Lee 2014; Lowes, Moehle & Govindjee 2004).

A number of researches have been undertaken in the past to gain an understanding of the bond stress-slip relationship adopting different test methods, like milling the steel bar to observe the distribution of stress in steel (Mirza & Houde 1979; Nilson 1972), injecting ink around the bar to monitor the inner crack development (Goto 1971) and hence, different bond-slip models based on those test curve have been proposed (Nilson 1971). But these models do not completely fit with the bond-slip mechanism (Lin et al. 2019). Eligehausen, Popov & Bertero (1982) challenged the limitations of the previous models and proposed three-piece BPE model. This model was later adopted by CEB-FIB (2010) considering the material non-linearity. Figure 2-10 represents the collective bond-slip curve for reinforced concrete with plain and deformed bar clearly illustrating the difference between the bond failures for different cases.

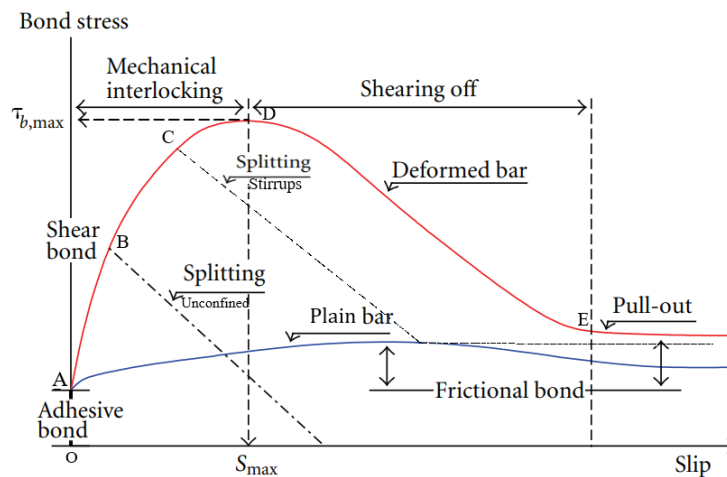


Figure 2-10 Bond-stress slip relation (Based on (Hong & Park 2012) and (CEB-FIB 2010))

The bond-slip curve representing the deformed bar shows an initial rise in bond strength against the adhesive bond (O-A) and as local crushing and micro cracking start to form at the interface, the curve softens. When the radial splitting force greater than the shear bond is developed, splitting of the reinforced concrete is observed if no confinement is provided (B) resulting in rapid decline of bond strength. For concrete with stirrups, the development of inner cracks is hindered by stirrups, thus increasing the bond capacity to the point (C) where it no longer resists the pull-out force, eventually resulting in splitting failure. In case of well confined reinforced concrete, the curve keeps increasing gradually up to maximum bond strength value after which the curve plateaus. This point onward mechanical interlocking fails and increase in slip is observed for constant bond strength. Bond strength starts to decrease (D-E) for increasing slip value, and a constant bond strength value is attained due to friction between cracked concrete and reinforcement bar, resulting in pull-out failure after the friction bond is lost (CEB-FIB 2010; Hong & Park 2012; Shen et al. 2016).

Conversely, for concrete with plain bar, the bond strength increases sharply assisted by adhesive bond, after which an increase in slip is observed for a constant value of bond strength obtained due to frictional bond. Finally, when the resistance due to friction fails, pull-out failure of the plain bar is observed.

Bond – slip curve provides detailed information on bond strength development and failure method of the concrete in bond test, thus numerous studies have been conducted to understand the bond mechanism for different material types considering different variables and using different methods.

2.3.3.5 Case studies of bond behaviour of geopolymer concrete

The bond behaviour of reinforced concrete has a significant influence on loading capacity of reinforced concrete member, crack development and failure. Hence to predict an accurate response of OPC concrete in conjunction with reinforcement bar numerous bond test studies have been undertaken for various situations, such that the bond-slip relationship could be defined. However, geopolymer concrete being a novel construction material, limited research has been conducted to understand the bond mechanism for geopolymer concrete and failure mode. Bond between the concrete and the reinforcement bars dictate the performance of reinforced concrete members, hence, in the absence of adequate reliable data in terms of bond performance, design development and application of geopolymer concrete for structural components is also constrained. This inadequate information on bond performance of geopolymer concrete is because the past research on geopolymer concrete were focused on micro-scale investigation like reaction process and evaluation of basic properties, complexity of bond mechanism and cost related to bond tests (Mo, Alengaram & Jumaat 2016; Yifei 2015).

1) Bond strength study

Many research study conducted on bond performance of geopolymer concrete is concentrated on exploring the bond strength development in geopolymer concrete considering concrete strength, bar diameters and embedment length as variables and further comparing it to OPC concrete. Fernandez-Jimenez, Palomo & Lopez-Hombrados (2006) carried out series of pull-out tests following RILEM (1970) and (CEB-FIB 1990) for fly ash based geopolymer concrete that incorporated NaOH and

combination of NaOH and sodium silicate solution as activators which demonstrated average compressive strength of 31.6 MPa and 41.5 MPa respectively. The bond strength of these two samples for 8mm rebar were comparable, while for 16mm rebar the bond strength of geopolymer with NaOH and sodium silicate solution as activator was approximately 1.5 times higher than the other sample. However, both the samples performed well in comparison to bond test result for OPC concrete.

Similarly, Sofi et al. (2007a) investigated the bond behaviour between reinforcement bar and fly ash based geopolymer by utilising both testing method and reported that on average the test result for bond strength recorded in pull-out test was higher than that from beam test, while the results of geopolymer and OPC concrete from pull-out tests were comparable and thus, stated pull-out method to be useful for bond strength comparison. The bond strength comparison for 12mm, 16mm and 20mm size reinforcement bar showed bond strength decrease with increasing rebar size. The bond strength gained by geopolymer concrete favoured comparably to bond strength requirement for OPC concrete on AS 3600. Based on the experimental results, Sofi et al. (2007a) concluded that recommendations for OPC concrete from AS3600 (2018) and ACI318 (2019) can be used to calculate the required development length for geopolymer concrete. Similar conclusion was reached by Castel & Foster (2015) based on their study for bond strength development in blended slag and fly ash based geopolymer concrete in pull out test. The report showed that the geopolymer concrete displayed approximately 10% higher bond strength than OPC concrete. Further relying on the bond-slip curve for geopolymer and OPC concrete, it was suggested that the existing bond models for OPC concrete can be utilised for geopolymer concrete with similar compressive strength.

Another study undertaken by Sarker (2010) and Sarker (2011), to examine the response of fly ash based geopolymer in terms of bond capacity and compared to OPC concrete, beam-end tests were conducted. The strength of concrete and cover to rebar diameter ratio for both the OPC and geopolymer concrete were kept constant. It was observed that both OPC and geopolymer samples failed by splitting, however, the bond strength for geopolymer was higher compared to OPC concrete, suggesting use of existing bond model for conservative prediction of geopolymer bond performance. Testifying the development of higher bond strength in geopolymer due to higher splitting tensile strength of geopolymer, Chang et al. (2009) stated that bond strength of geopolymer concrete is correlated to the tensile strength of geopolymer concrete subjected to beam-end test. The same was reported to be true for geopolymer concrete reinforced with sand coated glass fibre reinforced polymer bar (GFRP) (Maranan et al. 2015; Tekle, Khennane & Kayali 2016). Higher bond capacity in geopolymer concrete with regards to OPC concrete was noted which resulted in failure of GFRP bar reinforced geopolymer concrete sample by splitting while OPC concrete sample failed by pull-out. However, Songpiriyakij et al. (2011) reported similar bond strength obtained by both OPC concrete and geopolymer concrete including rice husk, fly ash and silica fume.

Moreover, bond study carried out on fly ash based geopolymer concrete against OPC concrete for plain and deformed reinforcement bar by Selby (2012) reported remarkable adhesive bond shown by geopolymer concrete with plain reinforcement bar in comparison to OPC concrete in pull-out test. The plain bar reinforced geopolymer concrete was observed to have double the bond strength of plain bar reinforced OPC concrete. Even for geopolymer concrete reinforced with deformed bar displayed high bond strength with respect to OPC concrete reinforced with deformed

bar having similar compressive strength. Meanwhile, Castel & Foster (2015) noted chemical adhesion of geopolymer concrete was comparable to the reference OPC concrete when plain reinforcement bars were used. This difference in frictional bond captured for plain reinforcement bar in geopolymer concrete is attributed to the use of different materials and curing condition, however, geopolymer concrete still exhibit comparable bond strength to that with OPC concrete.

Apart from these studies investigating the basic bonding properties of geopolymer concrete compared to OPC concrete, many study have also been conducted to explore the bond performance of geopolymer concrete for various influencing factors.

2) Parameters affecting bond-slip behaviour

The bond strength development in concrete is characterised by numerous factors like compressive strength of concrete, concrete cover, reinforcement bar diameter, and embedment length (Esfahani & Rangan 1998; Sarker 2011; Soroushian & Choi 1989). As such, there have been numerous studies conducted to understand efforts have been made to study the influence of different parameters on bond performance of geopolymer concrete.

For geopolymer concrete, the bond strength study with varying compressive strength for 12 mm and 16 mm reinforcement bar revealed that with increase in compressive strength of the geopolymer concrete, bond strength of geopolymer concrete also increases (Boopalan & Rajamane 2017; Kathirvel et al. 2017; Vinothini et al. 2015). Sofi et al. (2007a) carried out beam-end test on 12 mm, 16 mm and 20

mm reinforcement bar with varying compressive strength and presented that increase in concrete cover and compressive strength of the geopolymer concrete for all reinforcement type results in increase in bond strength value. In case of increasing diameter, Kim & Park (2014) and Kathirvel et al. (2017) reported decrease in bond strength for test samples with embedment length of 5 times the bar diameter, which aligns with the bond strength development in OPC concrete for different reinforcement bar (Soroushian & Choi 1989). Maranan et al. (2015) also stated that with the increase in GFRP bar diameter and bond length in geopolymer concrete, the bond strength decreased, while the test data reported by Fernandez-Jimenez, Palomo & Lopez-Hombrados (2006) for 12 and 16mm reinforcement bar varied.

3) Numerical analysis of geopolymer concrete bond

Apart from the experimental analysis for bond-slip behaviour in geopolymer concrete, few research have been undertaken to explore the behaviour of geopolymer concrete elements such as columns and beams using finite element modelling. The comparable load-deflection response for prestressed geopolymer concrete beam (Neupane, Hadigheh & Dias-da-Costa 2019), steel reinforced concrete beam (Pham et al. 2021) and column (Sarker 2009) obtained from numerical analysis of reinforced geopolymer concrete compared to OPC concrete, was based on the concept of perfect bond between geopolymer concrete and reinforcement bar modelled by embedding the steel bar into the geopolymer concrete domain. Though slipping behaviour occurs at the contact surface between the reinforcement bar and geopolymer concrete, such perfect bonding condition is adopted for numerical efficiency in terms of accuracy and computational cost (Nguyen et al. 2016; Uma, Anuradha & Venkatasubramani 2012;

Valliappan & Doolan 1972). However, Kumbar et al. (2013) state such assumption to be too idealistic and do not reflect the actual condition, creating differences between experimental results and numerical output.

An attempt to model the bond behaviour in concrete beam was initially carried out by Ngo & Scordelis (1967) by using a linear elastic model, where constant-strain triangular element were used for concrete and steel bar and a special bond link element (with no material dimension) to represent the bond between concrete and steel bar. But the linear bond-slip relation used to represent the complex bond behaviour was unsuccessful. Following which, perfect bond condition was assumed for bond representation in reinforced concrete elements. Later, Nilson (1968) used nonlinear spring elements to describe the bond-slip relationship between the concrete and reinforcement bar. This bond link model, using spring elements, were defined in perpendicular direction and parallel to the embedded bars in order to simulate the bond-slip curves and the dowel effect of the ribs of the bar respectively. This spring element (COMBIN39) was also used by Hammaty, DeRoeck & Vandewalle (1991) and Wang & Wang (2006) in their 3D finite element modelling using ANSYS to simulate the bond-slip curve obtained from pull-out test. Concrete was represented by SOLID65 element while LINK8 element used to represent reinforcing steel bar in ANSYS. The spring element linked steel bar node with the corresponding concrete node at the same position. The spring element were added parallel to pull-out direction (Z-direction) to simulate the pull-out load and also in X- and Y- direction to simulate the influence of ribs. The stiffness in spring element was defined by a non-linear force-displacement curve. This defined stiffness for the spring element on the nodes for concrete and steel bar controlled the movement of those nodes, there by simulating more realistic bond-slip behaviour between concrete and steel bars. While this model

for finite element analysis was used for OPC concrete, Cui (2015) adopted this spring element model to define the link between geopolymer concrete and reinforcement bars and simulated the bond-slip behaviour of geopolymer concrete under beam pull-out test and for geopolymer concrete beam. Based on this finite element analysis result for geopolymer concrete beam, it was indicative that the use of spring model to simulate bond behaviour between geopolymer concrete and reinforcement bar generated consistent result to that of experimental result and further recommended use of spring model as a feasible means to model the bond behaviour for geopolymer concrete. However, many attempts to verify this bond-slip behaviour for geopolymer concrete in different structural elements have not been carried out. Therefore, this study aims to simulate the structural response of reinforced geopolymer concrete pipe by adopting appropriate bond-slip relation to define the bond-slip behaviour of steel reinforcement and geopolymer concrete.

2.4 Long-term properties of geopolymer concrete

During the service life span of concrete structures, it is exposed to several issues related to strength and durability. The compressive strength development in geopolymer concrete has been reported to be higher than OPC concrete while exceeding the strength requirement specified in AS3600 (2018) (Hardjito & Rangan 2005; Nath & Sarker 2012; Sofi et al. 2007b; Wallah & Rangan 2006). This indicates that the use of geopolymer concrete is a feasible alternative to OPC concrete from structural perspective.

Apart from this, the long-term properties of concrete is defined by durability of the concrete, which refers to the resistance of concrete to deterioration and decay.

Durability can be affected by many factors ranging from physical deterioration, chemical deterioration and reinforcement corrosion as shown in Figure 2-11. It is influenced by the materials constituents, design mix, curing method and mixing process for concrete preparation (Lingyu et al. 2021; Siddika et al. 2021). Permeability is one of the main factor affecting the durability that influences the capillary absorption and resistance to deleterious materials that leads to chemical and physical attacks (Amran et al. 2021; Castel 2016).

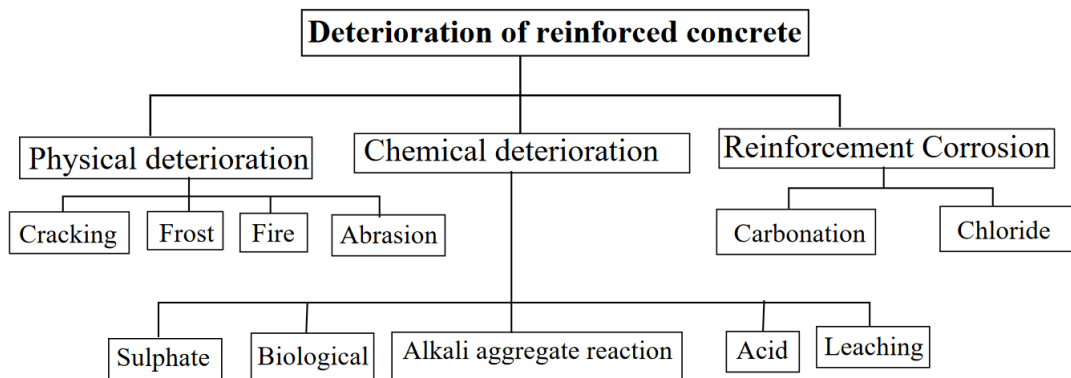


Figure 2-11 Deterioration of reinforced concrete (Isgor 2001)

Studying the permeability of fly ash based geopolymer concrete, Amran, Debbarma & Ozbakkaloglu (2021) stated that the fly ash based geopolymer concrete contributes to the refinement of aperture structure with lesser permeability and lesser chloride dispersal than OPC concrete. It is reported to be due to fly ash in geopolymer concrete which generates slow reactivity effect due to relatively lower surface area of fly ash, thus inducing lower permeability and porosity in geopolymer concrete and enhancing the long term performance of geopolymer concrete (Langan, Weng & Ward 2002; Nyale et al. 2013; Wongpa et al. 2010). Similarly, conducting the microstructure analysis of GGBFS and rice husk ash using SEM, EDS and XRD tests, Mehta &

Siddique (2018) stated that the higher compressive strength and lower permeability properties exhibited by geopolymer concrete is due to the compact and dense micrograph of geopolymer concrete. Such dense microstructure was reported to be due to coexistence of polymerization products (sodium alumina-sulphate (NASH)) with additional calcium based hydration products like calcium silicate hydrate (CSH). Liang & Ji (2021) also reported that the strength properties and the permeability of slag based geopolymer concrete was significantly better than OPC due to lower total porosity and better pore structure due to large amount of aluminosilicate reaction products formed from chemical bonds through dehydroxylation.

Similarly, the long- term durability of reinforced concrete structure also depends on the protection of the reinforcement bars in concrete provided by the passive layer formed on the steel surface due to high pH in OPC concrete (Broomfield 2007). As this layer starts to break down due to carbonation and chlorides, corrosion of reinforcement occurs affecting the service life of the reinforced concrete structure. However, the carbonation data collected for fly ash based geopolymer concrete by Law et al. (2015) suggested that the carbonation of geopolymer to be non-deleterious compared to carbonation of OPC as the pH remains at same level providing required protection to the steel bar. Similarly, for slag based geopolymer concrete it was reported that slag encourages formation of dense CASH gel leading to greater durability and strength under chloride contact (Albitar et al. 2017a; Amran, Debbarma & Ozbakkaloglu 2021; Liang & Ji 2021).

Though geopolymer concretes are relatively new material which have not been subjected to extensive field testing and lacks long-term study records and still in its early stages, the past studies on factor affecting the long-term durability of geopolymer

concrete have reported viability of geopolymer concrete as alternative to OPC concrete with better durability properties.

2.5 Performance study of reinforced concrete pipes under TEB test

Pertaining to the study of concrete pipe behaviour under external loading, the load-deflection curve obtained from TEB test is divided into 4 stages: i) elastic stage ii) concrete damage stage iii) steel yielding stage and iv) failure stage (Hu & Liu 2012). Numerous research have been carried out to define the anticipated load-deflection behaviour of concrete pipes considering different design parameters, such as change in pipe diameter, reinforcement area and positioning, concrete cover, use of fibre reinforcement and influence of pocket on pipe performance (da Silva, El Debs & Kataoka 2018; de la Fuente et al. 2011; Haktanir et al. 2007; Hendrickson Jr 1955; Kataoka et al. 2017; Mohamed, Soliman & Nehdi 2015).

The long history of use of reinforced concrete pipe has been backed up by numerous research exploring its load bearing capacity and performance under different circumstances. The use of reinforced concrete pipe started with small diameter ranging from 100mm to 1800mm diameter, Hendrickson Jr (1955) in his experimental based study to support use of large diameter reinforced concrete pipes greater than 1800mm indicated the large diameter pipe needs to be reinforced against shear failure by using hook tie bar such that pipe could develop full strength. Similarly, pertaining to the cost saving nature of single elliptical reinforcement in concrete pipe, Ramadan et al. (2020a) carried out a comparative study of single elliptical caged concrete pipe against traditional double caged reinforced concrete pipe to study the structural performance of concrete pipes, following the specification of ASTM C76M (2022) and CSA-A257

(2014). Based on the experimental test carried out on 1050 mm and 1200 mm size pipe, the study reported that single elliptical reinforced concrete pipe demonstrated 20%-45% reduction in strength along with brittle failure in comparison to double circular reinforced concrete pipe with similar area of reinforcing steel. The brittle failure of pipe accompanied by concrete scabbing was observed due to radial tension in pipe which happened because of the lack of second layer of reinforcement in single elliptical pipe. Ramadan et al. (2020a), hence concluded that the current provisions in ASTM C76M (2022) and CSA-A257 (2014) needs to be updated to accommodate the performance capacity of single elliptical reinforced pipes.

Analysing the current industry practice of pipe class division following ASTM C76M (2022) and CSA-A257 (2014) standards which relies on $D_{0.3}$ load, noted based on formation of 0.3 mm wide crack along 300 mm length during TEB test, an experimental study by Younis (2020) suggested determining $D_{0.3}$ load depends on human judgement and cannot be used to decide structural efficiency of concrete pipe. Instead, it was recommended to use D_{peak} load, which is an initial peak load attained at linear-elastic phase, before the sudden drop due to crack formation in single cage reinforced pipe, and $D_{0.3}$ can be calculated as 0.97 times D_{peak} . Similar peak load before crack was also observed in load-deflection curve by Abolmaali et al. (2012), Mohamed, Soliman & Nehdi (2014) and da Silva, El Debs & Kataoka (2018) on their study for single cage reinforced concrete pipe. So rather than depending on determining $D_{0.3}$ load for pipe classification, reliable D_{peak} load can be used. The same can be used for triple cage reinforced pipe too, however, for double cage reinforced pipe gradual transition between linear-elastic and non-linear plastic phase was observed without significant D_{peak} load, thus Younis (2020) suggested using deflection control criteria

D_{δ} , instead of $D_{0.3}$. The deflection percent of inside pipe diameter (δ) is set to a limit of 0.35% to 0.4% and corresponding load value D_{δ} is used instead of $D_{0.3}$ load.

Apart from circular pipe performance, a comparative study on influence of Spigot-pocket joint (SPJ) and Ogee joint (OJ) in pipe performance was studied by da Silva, El Debs & Kataoka (2018) for 800 mm and 1200 mm pipe with single cage reinforcement and double cage reinforcement respectively. Diametrical compression test defined by ABNT-NBR8890 (2007), similar to TEB test, was used to evaluate the load crack, for which load-displacement curve and load-strain curve were plotted. It was reported that the load bearing capacity of OJ pipe was 12% and 4% higher than SPJ point for 800 mm and 1200 mm diameter pipe, concluding that pipes behave as a circular ring. Furthermore, it was also reported that pocket increases the stiffness in pipe and hence, load cracking observed in SPJ pipe was higher than for OJ pipe. Finite element analysis of this case was also carried out by Kataoka et al. (2017) in which the numerical data for load-deflection was compared to experimental results from da Silva, El Debs & Kataoka (2018) stating 3D numerical models for pipe can simulate the behaviour of SPJ, as the cracking pattern in numerical simulation matched the experimental results, hence recommending the use of numerical models for future parametric study.

In addition to this, studies recommending steel fibre reinforcement usage in concrete pipes have been carried out (Campos 2010; de la Fuente et al. 2011; Haktanir et al. 2007; Mohamed, Soliman & Nehdi 2014; Peyvandi, Soroushian & Jahangirnejad 2013). Comparing the strength and crack development for different dosage for steel fibres on pipe with traditional reinforced concrete pipe, Haktanir et al. (2007) reported steel fibre reinforced concrete pipe performed better than traditional reinforced

concrete pipe on TEB test and was a better economical alternative to traditional concrete pipes. (de la Fuente et al. 2011) and Mohamed, Soliman & Nehdi (2015) and also reported similar behaviour from their test study and further added that behaviour of steel fibre reinforced concrete pipe can be tested under continuous loading in TEB test unlike an extra cycle of loading suggested in (EN-1916). Furthermore, realising the vulnerability of damage due to chemical reaction in steel fibre reinforced concrete pipe, Campos (2010), Peyvandi, Soroushian & Jahangirnejad (2013) and de la Fuente et al. (2013) used polypropylene fibre and macro-synthetic fibre in their study, which are resistant to chemical reaction to improve the durability and structural efficiency of the pipes. It was further noted that the pipe wall thickness can be reduced for fibre reinforced pipe, thus reducing its overall weight (Peyvandi, Soroushian & Jahangirnejad 2013). In a similar effort to develop new type of reinforced concrete pipe, El Naggar, Allouche & El Naggar (2007) evaluated the structural performance of “cellular” concrete pipes, where a concrete pipe with multiple conduits incorporated within its walls were developed and subjected to D-load. It was reported that the structural performance of such pipe, especially with four-conduit configuration was noted to be similar to traditional solid wall concrete pipes, and the conduits delayed the occurrence of major cracks, thereby increasing the D-load value.

Beside all these experimental studies, equivalent number of finite element analysis have been carried out for reinforced concrete pipes such that parametric study of pipes could be carried out without destructive TEB test. The main issue with finite element analysis of reinforced concrete members is the characterization of material properties such that realistic behaviour of reinforced concrete members could be predicted (Barbosa et al. 1998). de la Fuente et al. (2011) developed MAP model to simulate the crushing test for the steel fibre reinforced (SFR) concrete pipe. The non-

linear behaviour of material was represented by Analysis of Evolutive Sections (AES) model which discretized concrete into fibre type element and reinforcement bars into concentrated area element. Contrasting the experimental results with numerical simulation, it was concluded that numerical model could be used for optimal design of SFR pipe without conducting TEB test. de Figueiredo et al. (2012) and Peyvandi, Soroushian & Jahangirnejad (2013) also concluded the same from the numerical model simulation for fibre reinforced concrete pipe considering the relative difference between the numerical results and experimental being around within 10%. Mohamed & Nehdi (2016) also developed a three dimensional non-linear model using ABAQUS to simulate SFR pipe performance under TEB test to investigate the effect of six different variables: pipe diameter, wall thickness, fibre type and content, concrete compressive strength, and targeted pipe strength, and reported the ultimate load capacity of the pipe can be well predicted for all such variables with the average error of $\pm 6.5\%$ compared to experimental results.

Likewise, for single cage pipe, double cage pipe and triple cage reinforced concrete pipe, Younis et al. (2021) modelled 3D finite element model using ABAQUS, which was calibrated and validated against the experimental data. The model successfully imitated the elastic and inelastic phases of the concrete pipe in the load-deflection curve, and stress behaviour of concrete and steel reinforcement was also reported to be in good agreement with experimental observations. The developed model was further used for parametric study to understand the influence of reinforcement area, yield strength and reinforcement cover, concluding the reinforcement area and yielding strength as greatly impacting the post-crack behaviour of pipe, while the performance of pipe was greatly influenced by concrete cover to inner steel cage (Younis et al. 2021). Similar numerical modelling study conducted to

investigate the impact of single elliptical cage rotation in reinforced concrete pipe by Ramadan et al. (2020) stated that rotation of the elliptical cage has minimum effect on elastic behaviour and stiffness of pipe till 1mm deflection, however, remarkable difference is observed in plastic phase of the pipe where the steel reinforcement is fully engaged.

Though all these research efforts to contribute towards effective application of reinforced OPC concrete pipe is still going on, however, attention towards use of geopolymer concrete for reinforced concrete pipes has not been focused on yet. As an emerging alternative to conventional concrete, geopolymer concrete is finding its application in infrastructure constructions. It is important to study the structural performance of geopolymer concrete pipes, the load–deflection behaviour and its failure pattern to understand the design requirement for geopolymer concrete pipes. Thus, to construct geopolymer concrete pipes that can serve its life span with minimum serviceability issues, study of the structural behavior also needs to be done so that appropriate design methods for the pipes can be developed. Hence, one of the objectives is to carry out reliable finite element analysis of geopolymer concrete pipe to study its loading capacity, failure criteria and stress development in geopolymer concrete and steel reinforcement during TEB test simulation.

2.6 Durability of concrete pipes

In general, the design of concrete pipe focuses largely on structural analysis for loading capacity and hydraulic functions, while it is equally important to understand the service life performance or durability of pipe material (ACPA 2016). Many researches have been directed towards the durability of concrete pipe material and it

has been reported that concrete pipes are susceptible to physical, mechanical, chemical and biological damage. Physical and mechanical damage are initiated due to thermal change, weathering, impact or abrasion, while chemical and biological damage is associated with leaking of harmful chemical substances into concrete causing carbonation, chloride and sulfate attack and microbially induced corrosion (MIC) (Binici et al. 2012; Neville 2004; Wu, Hu & Liu 2018; Zhuge et al. 2021). The question of durability for concrete pipe is raised even more because of the biological damage caused in pipe. Fernández-Jiménez & Puertas (2002) stated that approximately 45% of damage in concrete pipes are due to microbe induced sulphuric acid attack. Explaining the biological mechanism of hydrogen sulphide (H_2S) formation in concrete sewer pipe Attal et al. (1992) noted that the aqueous H_2S in sewage water is converted to H_2S gas by the bacterial activities, dissolution of H_2S with the moisture in the pipe forms H_2SO_4 resulting in acidic corrosion of concrete due to decomposition of calcium aluminate and calcium silicate hydrate and ettringite. This acid corrosion causes loss of concrete cover and degradation in loading capacity of the pipe, hence significantly affecting the service life of the concrete pipe.

There have been efforts made to study alternate materials to overcome such durability issue of OPC concrete. Numerous studies conducted to explore the durability of geopolymer concrete in comparison to OPC concrete exposed to different acidic environment (Çevik et al. 2018; Hassan, Arif & Shariq 2019; Lingyu et al. 2021). An experimental evaluation for durability performance of fly ash based geopolymer concrete exposed to solutions of acetic and sulphuric acid of 1M for 360 days, revealed that mass loss in OPC concrete was 19% while, only 6% of mass loss was recorded for geopolymer (Valencia-Saavedra, de Gutiérrez & Puertas 2020). It was further highlighted that the loss in compressive strength for geopolymer was only

66% compared to 98% loss by OPC concrete. Similar results were reported for higher mass loss and compressive strength degradation in OPC concrete compared to geopolymer concrete by Hardjito et al. (2004b) for samples exposed to different concentration of H_2SO_4 and concluded the degradation of concrete matrix is main cause of strength loss rather than the degradation of aggregates. Pasupathy et al. (2017) also reported 47% loss of strength in OPC, while the loss of strength was 33% for geopolymer, when exposed to acetic acid solution for 12 months.

Çevik et al. (2018) also found outstanding performance of geopolymer concrete in relation to OPC concrete when subjected to 5% concentration of H_2SO_4 , 5% concentration of $MgSO_4$ and 3.5% concentration of seawater (NaCl) solution and realised that H_2SO_4 exposure presented the most hazardous condition for all concrete types. The weight loss for OPC concrete was reported to be three times the weight loss value for geopolymer concrete. It was also noted that despite the mechanical strength of geopolymer concrete being comparable to OPC concrete under ambient condition, the mechanical strength degradation of OPC concrete was higher than geopolymer concrete when exposed to acidic solution. The significant loss of mass and strength in OPC concrete is mainly because of the presence of alkali CaOH in OPC concrete, which easily reacts with acid solution causing change in concrete matrix and expansion in volume, creating voids that are filled by acidic components, thus resulting in acid corrosion of OPC concrete. However, in geopolymer, the poly-sialate bond structure formed between Si-O and Al-O is less reactive to acid at room temperature, hence, the acid corrosion in geopolymer concrete is comparatively low (Lingyu et al. 2021). Hence, the use of geopolymer is an optimum choice for sewage pipes, considering the inherent resistance to sulphuric acid and other acidic components. However, to design concrete pipes considering durability, it is necessary to understand the service

condition of the pipe, the degradation in strength and therefore, its impact on the design loading capacity. But there is still a gap in research with regards to performance load for geopolymer concrete pipe.

2.7 Failure of pipes due to crack

One important factor to consider for concrete pipe design is consideration of serviceability performance due to crack development. Cracks in concrete pipe is a common issue and can occur due to multiple reasons like external load, low quality materials, construction defect, thermal deformation, uneven supporting backfill and degradation due to environmental corrosion. Plastic cracks developed in wet concrete during production process are often unavoidable. However, cracks in the hardened concrete due to excessive load, thermal contraction and shrinkage are also expected and hence, rather than preventing the crack formation, limiting the crack width is considered during pipe design (Millar & Paull 2017). As such, rather than the development of crack, Millar & Paull (2017) highlighted the main concern was the consequence of crack formation, specifically the effect of its width and depth on durability and structural integrity throughout the service life of the structure. This damage concern is further added by structural overload and strength loss due to reinforcement corrosion. CPAA (2006) provided a general guide to assess the structural stability of pipes with cracks with a view to suggest solution for such crack development. It explains multiple longitudinal cracks developed at the top of the pipe are of less concern, as such the installation of such pipe could be accepted. However, appearance of single, wide longitudinal cracks on the inside of the crown and invert denotes serious condition of the pipe resulting from shear failure and hence, design for

such pipes need to be assessed. Such longitudinal cracks can also form at spring-line due to excessive crushing stress. Beside longitudinal cracks, circumferential cracks also occur in pipes due to uneven bedding and relative vertical movement due to settlement. It develops due to excessive shear or bending stress and occurs mostly near joints (Davies et al. 2001) and have insignificant effect on the load bearing capacity of the pipe (CPAA 2006).

The current design practice enforces design of pipe with service life of 100 years (AS/NZS4058 2007). However, unveiling the structural damage in concrete pipes, Cullen (1982) reported that around 5000 collapses of concrete pipes were estimated by Water Research Centre (WRC) in UK in 1984, which held true till 2001 as reported by Davies et al. (2001). Following the damage study three stage collapse process (Figure 2-12) of concrete sewer pipe was documented by WRC in sewerage rehabilitation manual (SRM) for the first time in 1983, described as:

Stage 1: The initial defect stage, where minor pipe cracking occurs due to poor construction system or loading condition exceeding the pipe load limit. Cracks are observed first on the interior surface of crown and invert and then on exterior surface of spring-line. However, the pipe can still function effectively as the pipe remains held by the surrounding soil.

Stage 2: The deterioration stage, where penetration of ground water and also breakout of harmful contents carried by pipeline occurs, thus deteriorating the mechanical properties of the pipe. The penetration of ground water carries acidic content which exacerbate the corrosion process of reinforcement bar. Fractures in the pipes develop along with slight deformation and loss of side support occurring in this stage.

Stage 3: The collapse stage, which initiates when the deformation exceeds 10% of its overall depth. Loss of side support causes the pipe to bulge further from spring line and the crown to drop, finally causing collapse of the pipe.

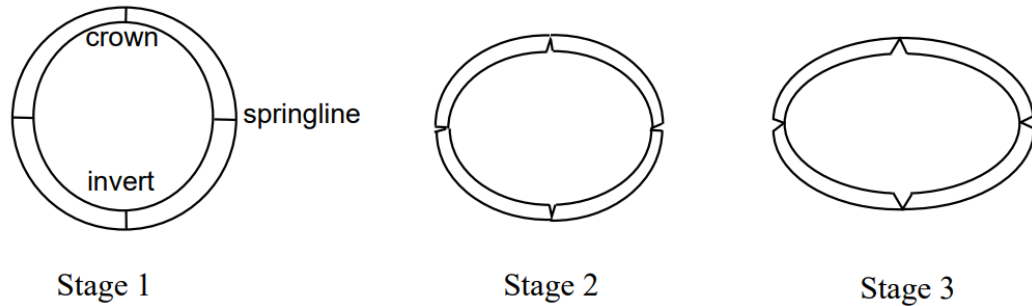


Figure 2-12 Collapse process in concrete sewer pipes (Davies et al. 2001)

Thus, development of cracks in concrete pipes create serious and costly problems (da Silva, El Debs & Kataoka 2018). It not only reduces the loading capacity of pipe, but leads to pipe leakage and ground collapse causing public hazard. It is, therefore, important to consider the effect on mechanical performance of concrete pipe due to pre-existing cracks while designing of the reinforced concrete pipes.

2.8 Case study on effect of pre-existing cracks on pipe performance

For the construction of concrete pipes, great deal of attention is focused on durability of pipe, as it defines the ability of pipe to maintain its characteristic strength and serviceability. Many researches have thus, been carried out to explore the problems due to cracked pipes. Buda-Ozog, Skrzypczak & Kujda (2017) state that the compliance of theories of concrete cracking with experimental results is less compatible compared to theory of strength limit. This is because cracking issue in

concrete pipe is a complex problem that is affected by several poorly controlled factors (Al-Saleem & Langdon 2014; Branco, Arruda & Correia 2013).

For the purpose of identification of the various parameters that influence the fracture response of pipe subjected to large deformation due to tension, Jayadevan, Østby & Thaulow (2004) carried out finite element analysis examining the effect of crack depth, length, radius to thickness ratio and material hardening on the evolution of crack tip opening displacement (CTOD) with deformation in surface cracked pipes under pure tensile loading. It was suggested that a linear relation exists between CTOD and strain for surface cracked pipes, and is a function of crack depth, crack length, radius-to-thickness ratio, strain hardening, and internal pressure. In a reliability analysis to evaluate the cracking opening limit state for reinforced concrete pipe as given by NBR-6118 (2003), Silva, El Debs & Beck (2008) identified concrete compressive strength, pipe section useful height and pipe wall thickness as the problem parameters that contribute the most towards failure probabilities of concrete pipe. It was further added that the design based on central safety factor for crack opening following NBR-6118 (2003) does not offer uniform reliability. Similarly, Buda-Ozog, Skrzypczak & Kujda (2017) compared the results of numerical analysis of cracks formation with experimental results and it was noted that the tensile strength of the concrete in pipe is 65% greater than the tensile strength of concrete for straight element due to the effect of curvature of pipe; hence higher tensile strength contributes towards greater resistance during cracking test. As such, for optimal design of concrete pipe, it was recommended to adopt suitable value for concrete tensile strength at failure.

Likewise, Nourpanah & Taheri (2011) studied the response of pipes with semi-circumferential cracks of various sizes, under the combined effect of internal pressure

and inelastic bending, during pipe installation and operating condition. The 3D model developed to study the critical curvature of pipe suggested increase in both crack depth and crack length decreases the critical curvature of pipe significantly. It was also advocated that the single edge notch tension (SENT) test specimens used to model the fracture in pipe can reveal fracture characteristics that are very similar to that of actual pipes. Tabiei & Zhang (2016) used different numerical models: Finite Element Method (FEM), Discrete Element Method (DEM), Element Free Galerkin (EFG) method and Extended Finite Element method (XFEM), to determine their abilities and limitations to model 3D crack propagation problems and concluded that all these methods can be used for 3D crack propagation study if proper criteria is used. Of these models, DEM, EFG and XFEM being relatively new, however, has some limitations for easy use. Valiente (2001) studied the damage in circumferential reinforcement that can reduce the safety margin of tensile stress in concrete and stated that the shallow cracking and corroded areas in concrete pipe, due to stress corrosion cracking process, aids in developing contact between the aggressive environment and wire causing brittle failure of wire. Thus, the combined effect of brittle fracture of wire and stress development in concrete up to tensile strength leads to bursting of pipeline.

Another study on damage in concrete pipes due to cracking during installation process, it was concluded that the compressive stress acting on pipe during normal jacking can produce tensile stress resulting in crack formation in the pipe (Li et al. 2018). It was further added such crack formation is intensified if there is a presence of pores in pipe due to poor material used, resulting in concrete tension fracture. Hu et al. (2010) carried out experimental and numerical study on influence of longitudinal cracks on bearing capacity degradation for super caliber prestressed concrete cylinder pipes (diameter greater than 4 m) in the presence of external pressure. Based on the

numerical result it was reported that while the tension damage in the prestressed concrete cylinder pipes was observed in the crown, invert and spring-line, the ultimate anti-crack load capacity (that is, the load corresponding to the crack of more than 300 mm length) due to crack in the core concrete was least affected. Zhang et al. (2020) studied the effects of length, depth, and location of cracks on the load bearing capacity of concrete pipes and reported that the load capacity of the pipe is inversely related to the length and depth of the crack while maximum circumferential strain can be observed at the location of the crack, such that when the pipe with pre-existing crack reaches its ultimate load capacity, pipe fails along the crack position. The experimental results were also compared with finite element model of pre-cracked concrete pipe and stress development in the pipe and failure load capacity were similar to the experimental results. The finite element model to simulate the fracture or crack in the concrete has been successfully studied in a number of researches and various methods like crack propagation following smeared crack approach or discrete crack propagation following nodal release method and delete-and-fill re-meshing method has been recommended (Koenke et al. 1998; Tabiei & Wu 2003). In a study by Bentz et al. (2013) and Lehner & Konečný (2017) the cracks in concrete has been applied as a reduced material parameter, similar to smeared crack approach where crack is not represented explicitly and is associated to stiffness loss in element. Tabiei & Wu (2003) states that for concrete materials that fails in diffuse manner smeared cracking method can be successfully applied. Hence, cracking in concrete has been modelled for finite element analysis of pre-cracked concrete pipes.

Numerous experimental and numerical attempts have been made to explore different cases of crack development in OPC concrete pipe, however, geopolymer being a new type of binder whose structural performance as precast pipes still have not

been studied, it is equally important to explore the effects on pre-existing cracks on performance of geopolymer concrete pipes. The study on pre-existing cracks on geopolymer concrete pipe helps to understand the crack width limit for serviceable geopolymer concrete pipe and can be further used in design of geopolymer pipes.

2.9 Summary

This chapter reviews the use of OPC concrete for precast pipe production and development of current standards based on the available design method, and explores the possibility of using new type of one-part, 'powder form' fly ash and GGBFS based geopolymer binder for precast concrete pipe production. Backed up by previous studies undertaken to understand the mechanical properties of geopolymer concrete, it was found that geopolymer concrete performs better than OPC concrete when cured at higher temperature resulting in early age strength development, making it an appropriate alternative to OPC for the production of precast concrete components. It further demonstrated higher flexural strength and indirect tensile strength in comparison to OPC concrete with same compressive strength grade and better resistance to sulphuric acid attack. These properties can possibly be utilised to reduce reinforcement requirement in reinforced concrete pipe or producing large diameter non-reinforced concrete pipes. However, use of geopolymer concrete in actual structural components have not been prevalent. Though few cases of use of geopolymer concrete have been reported, they were mostly based on liquid activated geopolymer concrete.

In addition, the limitations for use of geopolymer concrete in construction industry is also discussed, and it is also identified that much of the research carried out

for geopolymer concrete concluded that the relation for tensile strength and elastic modulus is justified by the standard specifications defined for OPC concrete. The same was suggested for bond-slip behaviour of geopolymer concrete (Boopalan & Rajamane 2017; Castel & Foster 2015; Kathirvel et al. 2017; Sarker 2011). Most of the research on bond behaviour of geopolymer concrete studies the basic bonding capacity for geopolymer concrete under pull-out test and suggested that the use of bond-slip relation for OPC can be used to define the same for geopolymer concrete, though the experimental results showed high bond strength. Limited study explored the bond-slip relation for geopolymer concrete and used bond-slip behaviour for numerical modelling of geopolymer concrete beam. Lack of sufficient literature to support the use of bond-slip behaviour in geopolymer concrete components also presents difficulty for accurate modelling of geopolymer concrete component.

It is further realised that research carried out for concrete pipes were all based on OPC concrete with steel reinforcement bar or fibre reinforced concrete for different cases of pipe diameter, reinforcement area, concrete cover, wall thickness and explored the load-deflection behaviour of concrete pipe under such varying conditions. Additionally, detailed study on failure mechanism for reinforced concrete pipe was also available, suggesting measures to follow for different failure cases (Al-Saleem & Langdon 2014; CPAA 2006). But for geopolymer concrete, there was a distinct lack of study of geopolymer concrete pipes with evidently higher tensile performances. In addition, loading capacity of pipe with pre-existing cracks from either curing or service load also requires further attention. Since crack development in concrete pipes have a significant effect on the ultimate load carrying capacity and serviceability of the pipe, understanding the response of geopolymer concrete pipes under such circumstances is

equally important to develop an understanding of crack width limit criteria for geopolymer concrete pipes.

Therefore, research aimed towards the exploration of the structural behaviour of one-part, powder form of fly ash and slag based geopolymer concrete pipe and the parametric study for different reinforcement area and concrete cover, is necessary to be undertaken. Beside this, adopting bond-slip model in simulating TEB test for pipe is also required to verify the test results with that of existing experimental results such that accurate behaviour can be characterised for geopolymer concrete and for industrial application of geopolymer concrete to be implemented. It is equally necessary to conduct investigation on the loading capacity and stress development in geopolymer concrete pipe with pre-existing cracks and crack width limit for serviceable performance of the geopolymer concrete pipe such that guidelines for pipe design can be recommended.

Chapter 3

3. Investigation of mechanical properties

OPC concrete is the preferred material choice for all sorts of construction work and has been extensively studied to develop standard equations defining the relationship for different mechanical properties such as tensile strength, flexural strength or modulus of elasticity, with respect to compressive strength of concrete. As such, the mechanical properties of OPC concrete required for design purpose can be reliably calculated based on the compressive strength. Thus, it is considered as one of the significant mechanical properties of concrete.

However, geopolymer concrete is a fairly new construction material, for which there are no standard formulation for geopolymer binder. Most of the studies in geopolymer concrete are based on liquid activated geopolymer, where liquid form of alkali activator like sodium hydroxide (NaOH) and sodium silicate (Na_2SiO_3) are used to activate source material (Fernández-Jiménez, Palomo & Puertas 1999; Motorwala et al. 2013; Nath, Sarker & Rangan 2015). The usage of caustic liquid activator in preparing geopolymer concrete pose safety hazard during the handling and mixing process, as a result, wide use of geopolymer concrete is still not practical in construction industry. However, numerous studies have been carried out to determine the mechanical properties of geopolymer concrete in comparison to OPC concrete focusing on the effect of mix proportion, activator solution and curing conditions (Diaz-Loya, Allouche & Vaidya 2011; Farhan, Sheikh & Hadi 2019; Gunasekera, Setunge & Law 2017). Study carried out by Deb, Nath & Sarker (2014) analysed the workability and strength properties of geopolymer concrete by varying the percentage of GGBFS (0%, 10% and 20% of the total binder) and by varying the sodium silicate

to sodium hydroxide ratio in the activator to 2.5 and 1.5. It was observed that with increase in GGBFS content and decrease in sodium silicate to sodium hydroxide ratio in alkali activator, workability in geopolymer concrete decreased while increase in compressive and tensile strength was observed for these ambient cured geopolymer concrete when compared to reference OPC concrete cured in water. Other studies by Xie & Xi (2001) and Wallah & Rangan (2006) have reported when water to binder ratio in geopolymer concrete is increased, impact on compressive strength development can be noticed to be inverse. Similarly, study carried out by Hardjito et al. (2004b), investigating the mechanical properties of fly-ash based geopolymer concrete reported that the increase in curing temperature accelerated the development of compressive strength in geopolymer concrete, although a substantial increase was not noticed for temperature beyond 60°C. Such significant gain in compressive and flexural strength for heat cured geopolymer concrete within 3 to 5 days of curing was also reported by Diaz-Loya, Allouche & Vaidya (2011). However, the 28 days mechanical behaviour was reported to be similar to OPC concrete, suggesting use of existing relationship for OPC concrete based on ACI318 (2019). While correlating the existing standard equations for OPC concrete with mechanical properties for a range of Class F fly ash based geopolymer concrete, Gunasekera, Setunge & Law (2017) reported that when compared with geopolymer concrete with similar compressive strength, the flexural strength in geopolymer concrete was higher compared to calculated values, and the tensile strength was comparable to the predicted value. Farhan, Sheikh & Hadi (2019) suggested that the existing equations on OPC can be utilised for conservative prediction of tensile strength and flexural strength for normal strength geopolymer concrete, however when compressive strength of 65 MPa is considered for study of high strength geopolymer concrete, these equations based on

OPC concrete fails to estimate appropriate value for the same. The data available for geopolymer concrete are mostly based on the liquid alkali activated geopolymer concrete, using different combinations of source materials, hence resulting in a variation in results.

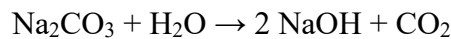
As the use of liquid activated ‘two-part’ geopolymer concrete are not user friendly and presents hindrance for commercial viability. This issue of using geopolymer concrete for bulk production can be resolved by using powder form ‘one-part’ geopolymer concrete that just needs water to be added, thereby replicating OPC concrete mixing process. Albeit, much research investigating the mechanical properties of powder form geopolymer concrete is still lacking and the empirical equations to derive the tensile strength, flexural strength and modulus of elasticity for powder based geopolymer concrete is still not well defined.

Therefore, this chapter is aimed providing comprehensive information mechanical properties of powder form geopolymer concrete. In this chapter, experimental study carried out to obtain the mechanical properties for a powder alkali activated geopolymer concrete has been discussed. The compressive strength, flexural strength, tensile strength and modulus of elasticity are evaluated and the results are compared with statistically meaningful geopolymer concrete database, in order to suggest suitable equations that captures the behaviour of ‘one-part’ powder form geopolymer concrete.

3.1 Experimental program

1) Binder materials

For geopolymer binder used in this study, fly ash and ground granulated blast furnace slag (GGBFS) were used as the source material, while powdered sodium silicate (Na_2SiO_3) and sodium carbonate (Na_2CO_3) were used as alkali activators. Silmaco (2018) and Redox (2017) classify sodium silicate and sodium carbonate as non-dangerous goods. Silmaco (2016) states that the sodium silicate has high concentration of active components in it, which makes it a suitable choice to formulate high concentrated products. Similarly, sodium carbonate is an (inorganic) alkaline salt, which indirectly contributes towards alkalinity required for geopolymer binder reaction. Both these activators get stimulated in the presence of water, thus presenting least risk during handling and mixing. As a result, the preparation of geopolymer concrete can be conducted in a way similar to that of OPC concrete. When the activators react with water as shown in the equation 3.1, the produced NaOH , CO_2 and SiO_2 react with GGBFS and fly ash to form geopolymer matrix.



The type of geopolymer binder utilised in this study was prepared by blending the source materials and activator in fixed proportion as specified by Cement Australia. For the purpose of this study, following two types of geopolymer binders have been used:

- i) General purpose binder (geocem 1) – composing of fly ash (50% by weight), GGBFS (30% by weight), alkali activator (16% by weight) and sodium based retarder.
- ii) High strength binder (geocem 2) – composing of fly ash (30% by weight), GGBFS (50% by weight), alkali activator (16% by weight) and sodium based retarder.

Using X-ray fluorescence, the chemical composition of GGBFS and fly was determined (Vu et al. 2019) and is presented in the Table 3-1 below:

Table 3-1 Chemical composition of fly ash and GGBFS used for geocem 1 and geocem

2

Oxide compositions wt. %	Fly Ash	GGBFS
Na ₂ O	0.47	0.32
MgO	1.28	6.84
Al ₂ O ₃	22.29	14.14
SiO ₂	58.15	33.89
P ₂ O ₅	0.77	0.01
SO ₃	0.15	1.59
K ₂ O	1.39	0.28
CaO	5.39	40.46
TiO ₂	1.03	0.58
V ₂ O ₅	0.02	0.01
Cr ₂ O ₃	< 0.01	0.01
Mn ₃ O ₄	0.07	0.21
Fe ₂ O ₃	6.95	0.45
ZrO ₂	0.01	0.02
BaO	0.03	0.05
LOI	1.09	-0.11
Total	99.09	98.74

Many research carried out to examine the engineering properties of fly ash and GGBFS based geopolymer concrete. The study carried out by Fernandez-Jimenez, Palomo & Lopez-Hombrados (2006) on heat cured fly ash based geopolymer concrete to determine the strength properties of geopolymer concrete have found that the indirect tensile strength and flexural strength of geopolymer concrete were higher than that of OPC concrete while the modulus of elasticity was lower. Hardjito & Rangan (2005) and Neupane et al. (2014) also suggested better performance of geopolymer concrete in terms of indirect tensile strength and flexural strength development, while compressive strength and modulus of elasticity of geopolymer concrete were essentially comparable to that of OPC concrete. Diaz-Loya, Allouche & Vaidya (2011), based on similar development of compressive strength in geopolymer concrete and OPC concrete, suggested that the existing design criteria for OPC concrete could be used for fly ash based geopolymer concrete.

Similarly, previous study by Bernal et al. (2011) on slag based geopolymer concrete cured at room temperature has also found higher flexural and indirect tensile strength development in geopolymer concrete, while compressive strength development was comparable in relation to OPC concrete. Chi (2012) suggested alkali activated slag concrete when cured at temperature of 60°C has superior performance compared to air cured slag based geopolymer concrete and the strength development is higher than reference OPC concrete.

Furthermore, addition of slag to fly ash based geopolymer concrete were reported to improve the mechanical properties of the geopolymer concrete due to simultaneous formation of alumina-silicate-hydrate (A-S-H) gel and calcium-silicate-hydrate (C-S-H) gel (Yip 2004; Yip et al. 2008). Lee & Lee (2013) carried out a study

to determine proper slag content for fly ash/slag based geopolymer concrete cured at room temperature and concluded 15-20% of total binder by weight resulted in appropriate setting time, workability and development of compressive strength. Similarly, Deb, Nath & Sarker (2014) varied the proportion of GGBFS from 0%, 10% and 20% in fly ash and GGBFS based geopolymer concrete and observed very notable increase in strength but decrease in workability with increase of GGBFS content.

Past studies have shown that increasing the slag content increases the compressive strength of geopolymer concrete, however studies on slag based geopolymer concrete was mostly based on ambient temperature curing. For this study, two geopolymer concretes with different proportion of fly ash and GGBFS have been used to study the mechanical properties development at accelerated heat curing. The purpose behind using the two types of binders was to check the difference in early strength development and bond development in the two types of geopolymer.

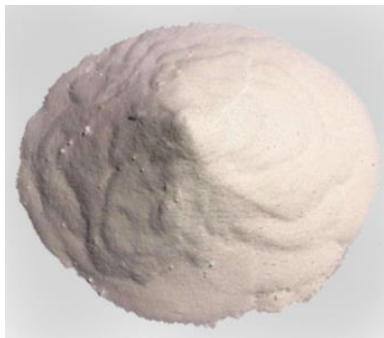
Besides using the two types of geopolymer, a general-purpose ordinary Portland cement conforming to AS3972 by Cement Australia was also utilised to develop control concrete to compare properties of geopolymer concrete with standard OPC concrete. The components used for geopolymer preparation are showcased in Figure 3-1. These components when mixed, were similar in appearance that of OPC and could be used similar to OPC by just adding water.



(a)



(b)



(c)



(d)

Figure 3-1 Source material and activator used for geopolymer binder: (a) Fly ash (b) Slag (c) Soda ash and (d) Sodium Silicate

2) Aggregates

For the preparation of concrete mix, well-graded coarse aggregates of size 20mm and 10mm and river sand as fine aggregates were used (Figure 3-2). Both 20mm and 10mm coarse aggregates were cleaned to get rid of dirt and clay. The cleaned aggregates were soaked for in clear water for 1 day, then dried to achieve saturated surface dry (SSD) condition.



(a)

(b)

(c)

Figure 3-2 Aggregates for concrete mixing (a) 20mm coarse aggregates (b) 10mm coarse aggregate and (c) river sand

3.1.1 Concrete strength grade

To investigate the mechanical properties of geopolymer concrete in comparison to OPC concrete, concrete strength of Grade 50 MPa was designed for both binder types. Concrete Pipe Association of Australasia (CPAA) states that for concrete pipe in Australia and New Zealand the common range of strength used is up to 60MPa or higher, even though, AS/NZS1597.1 (2010) recommends use of 40 MPa and 50 MPa concretes for precast structures. As such, aiming to explore the applicability of geopolymer concrete for common practice and study the structural response of geopolymer concrete pipe, design mix for grade 50 MPa concrete was followed.

3.1.2 Mix design and concrete mixing procedure

For geopolymer concrete, there is no standard process for mix design, as such the mix design process of OPC concrete was followed to attain the target strength at 28 days. The principle behind mix design for target strength, is to achieve required

compressive strength and workability, based on which precursors, activators, water and aggregate contents are determined. Such target strength method for mix design has been achieved either by using fixed water content, fixed binder content or fixed paste content (Li et al. 2019). The fixed water content method is based on workability while fixed binder content method considers strength of concrete and for fixed paste content, both workability and strength are considered.

The mix design for geocem 1 and geocem 2 in this study is based on fixed binder content. Such mix design method was utilised by Anuradha et al. (2012), Ferdous et al. (2015) and Patankar, Ghugal & Jamkar (2015). Anuradha et al. (2012) studied different mixes for different grades of fly ash based geopolymer concrete and concluded the fly ash (FA) content of 550 kg/m^3 was suitable grade 30 MPa geopolymer concrete. Similarly, Junaid et al. (2015) determined the suitable proportion of FA content to achieve strength ranging from 25-40 MPa, 40-55 MPa and 50-60 MPa to be $360\text{-}380 \text{ kg/m}^3$, $380\text{-}420 \text{ kg/m}^3$ and $420\text{-}440 \text{ kg/m}^3$ respectively. Hardjito & Rangan (2005) and Ferdous et al. (2015) also relied on the FA content of 400 kg/m^3 for preparation of geopolymer concrete. It should be noted that in fixed binder content method of mix design, the effect of aggregate is not considered.

The specifics of the mix design for geocem 1 (G1), geocem 2 (G2) and OPC adopted in this study are given in Table 3-2 below:

Table 3-2 Mix design for geopolymer and OPC concrete (kg/m³)

Binder type	Aggregates (kg/m ³)			Binder content (kg/m ³)			w/b ratio
	20mm aggregates	10mm aggregates	Fine Sand		FA	GGBFS	
OPC	788	523	833	411	-	-	0.5
Geocem 1	788	523	833	411	206	123	0.33
Geocem 2	788	523	833	411	123	206	0.35

From the Table 3-2 it can be noted that for the mix design of all three concrete type, equal amount of binder and aggregates were used, while the water to binder ratio was adjusted to achieve the required strength. This is also based on the findings that varying the water content in geopolymer concrete compensates the influence of different proportion of fly ash in achieving consistent result (Cui 2015). This mix design proportion was based on saturated surface condition of aggregates, such that better compressive, flexural and splitting tensile strength for both type of geopolymer concrete and OPC concrete could be achieved (Lee & Lee 2017). It is evident that the amount of water required for geopolymer is lesser than that for OPC to achieve similar strength.

For concrete mixing, rotating pan mixer with total capacity of 60 litres was used. All the materials required were weighed and set aside before the mixing process. The mixer was cleaned properly before adding 20 mm and 10 mm aggregates and river sand along with 10% of required water. After this, the sand and aggregates were then mixed properly for 1 minute and the mixer was stopped. All the components of binder were then added to the mixed aggregates and mixing was again started. At this time, approximately 80% of required water was added while the materials were mixing. The mixer was set to mix for 3 minutes and then was stopped for 3 minutes. The concrete

was again mixed for another 3 minutes, after which slump test was carried out. Water was then added if required based on the slump test result. The concrete from the slump test was poured back to the mixer and mixed again for 2 minutes. Before carrying out second slump test, the concrete was allowed to rest for 2 minutes. Once the slump value of 120 ± 10 mm was achieved, the concrete was then poured back for final mix for another 1 minute. Following this mixing process, concrete was prepared for concrete sample casting.

3.1.3 Concrete casting and curing of specimens

For concrete casting, standard plastic moulds of 100 mm x 200 mm (diameter x height) were used to cast cylinder samples, while aluminium rectangular mould with dimension 100 mm x 100 mm x 350 mm (width x depth x length) were used to cast concrete beams. The concrete cylinders and flexural beams were casted as per AS1012.8.1 (2014) and AS1012.8.2 (2014) guidelines respectively. For each test, at least three specimens were prepared. All these moulds were cleaned and oiled before casting. The concrete was casted into the mould in three stages. The moulds were filled by 1/3 of volume each time and compacted by vibration on a vibrating platform. The casted cylinders and beams were levelled and plastic film was used for sealing (Figure 3-3) to prevent excessive moisture loss.



Figure 3-3 Concrete cylinders and beam casting

Different curing methods are known to impact the mechanical and physical performance of geopolymer concrete, previous researches have suggested use of sealed curing at ambient temperature and heat curing to be effective curing methods (Hardjito & Rangan 2005; Nath, Sarker & Rangan 2015; Sakulich et al. 2010). The use of water curing for geopolymer concrete is not recommended due to the leaching of alkali activators from the geopolymer concrete into the water and thus, causing efflorescence issue on the surface of concrete cylinder (Zhang et al. 2013). As geopolymer binder is significantly different than OPC, the reaction involved in geopolymerisation process in geopolymer binder to achieve structural integrity is different to that of OPC, which depends on calcium-silicate-hydrate (C-S-H) gel formation to achieve structural integrity (Khale & Chaudhary 2007; Van Jaarsveld, Van Deventer & Lukey 2002). Hence, different curing method suitable to OPC and geopolymer concrete have been adopted to achieve optimum results. Accelerated heat curing was adopted for geopolymer concrete, where geopolymer concrete was cured at a temperature higher than the ambient temperature at an early stage. Accelerated heat curing was also adopted to explore the ways to apply geopolymer concrete for precast concrete pipes. For precast concrete structures, AS/NZS1597.1 (2010)

recommends steam curing of pipes with gradual heat increase at the rate of 24°C per hour up to a maximum temperature of 70°C.

As such for geopolymer concrete, the samples after casting were left to set at laboratory temperature for an hour and then sealed properly before heat curing (Figure 3-4). The samples were stored in an oven where the temperature was increased at 24°C per hour for 2 hours and then maintained at 60°C for 6 hours. The heat cured samples were left at room temperature to cool down. After 24 hours of casting, these heat cured samples were demoulded and sealed properly before leaving it at room temperature till the test day. Similarly, after 24 hours, all the OPC concrete samples were also demoulded and water cured at laboratory temperature of 23°C and 65 % relative humidity till the test day.



Figure 3-4 Concrete cylinder sealed before heat curing

3.2 Investigation of material properties of concrete

To explore the material properties of the prepared concrete samples; geocem 1, geocem 2 and OPC concrete, all samples were consigned for various experimental tests

defined for OPC concrete under the Australian Standard guidelines. To explore the mechanical performance of geopolymer concrete, their compressive strength, flexural strength and indirect tensile strength were evaluated. Alongside, the modulus of elasticity and Poisson's ratio as well as the fresh concrete workability were also explored. These properties of geopolymer concrete were compared with that of OPC concrete to understand the difference in mechanical properties.

3.2.1 Workability

The standard slump test was used to measure the workability of fresh concrete as shown in Figure 3-5.

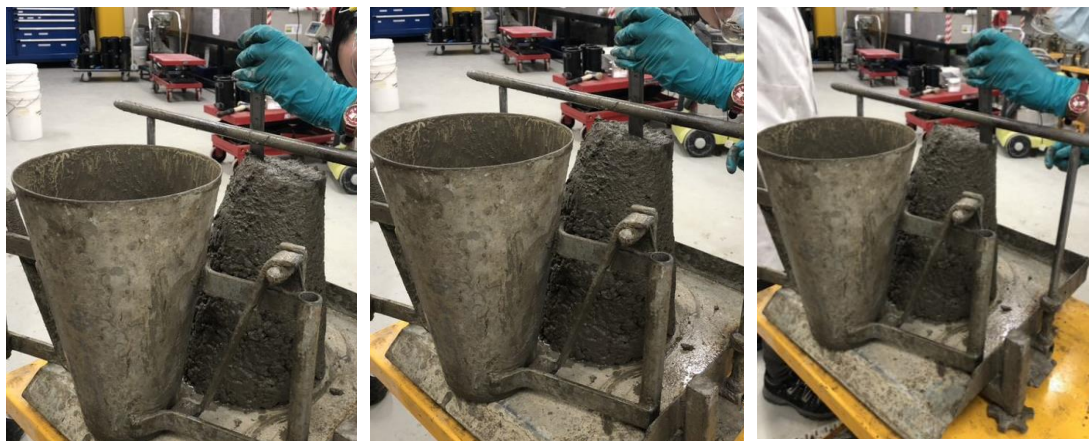


Figure 3-5 Measuring of slump value at two ends and centre during Slump test to get average slump value

The slump value obtained for geocem 1 and geocem 2 were approximately 120 ± 20 mm similar to that of OPC concrete, even with less amount of water. The nature of fly ash causes the geopolymer concrete mix to appear relatively dry when water was first added during the mixing process, but after it was allowed to rest for a

minute, it released water to the surface causing the concrete mix to flow easily. The water required for geopolymer concrete to achieve similar workability for same volume of mix was less than half the amount of water required for OPC.

3.2.2 Mechanical properties

The strength developed in hardened concrete defines the mechanical properties of concrete. The mean strength of the concrete is measured as per the tests carried out at 28 days. Concrete cylinders were used to test the compressive strength, indirect tensile (splitting) strength and modulus of elasticity of all types of concrete while the casted beams were used for flexural strength test.

3.2.2.1 Compressive strength

Compressive strength is a characteristic property of any concrete type as it defines its capacity to withstand load or compressive force. Compressive strength is also an important property because standards for OPC concrete such as AS3600 (2018) and ACI318 (2019), provide guidelines to calculate tensile strength and modulus of elasticity of concrete based on the compressive strength value when accurate data to define those properties values are not available. For geocem 1, geocem 2 and OPC concrete, tests for assessment of compressive strength were conducted on three samples following the guidelines from AS1012.8.1 (2014).

Before compression test, the samples were prepared to have plain smooth surface by grinding the rough surface in an automatic grinding machine. The samples were then measured for their exact height and diameter to calculate the area of cylinder

used. Using universal testing machine, compression load was then applied to the cylinder until the load decreased steadily, displaying a well-defined fracture pattern (ASTMC39M 2021).

To measure the early age compressive strength development in geopolymer concrete, samples were also tested after 6 hours of curing. The compressive strength development in geocem 1 and geocem 2 was found to be 27 MPa and 39 MPa. Around 50% and 60% of 28 days compressive strength development was developed in 6 hours of curing at 60°C for geocem 1 and geocem 2, which supports the applicability of geopolymer concrete for precast pipes. Further tests to determine the development of compressive strength in OPC, geocem 1 and geocem 2 concrete were carried out at 1 day, 7 days, 14 days, 28 days and 90 days. Figure 3-6 illustrates the development of compressive strength in geocem 1, geocem 2 and OPC concrete over a period of 90 days.

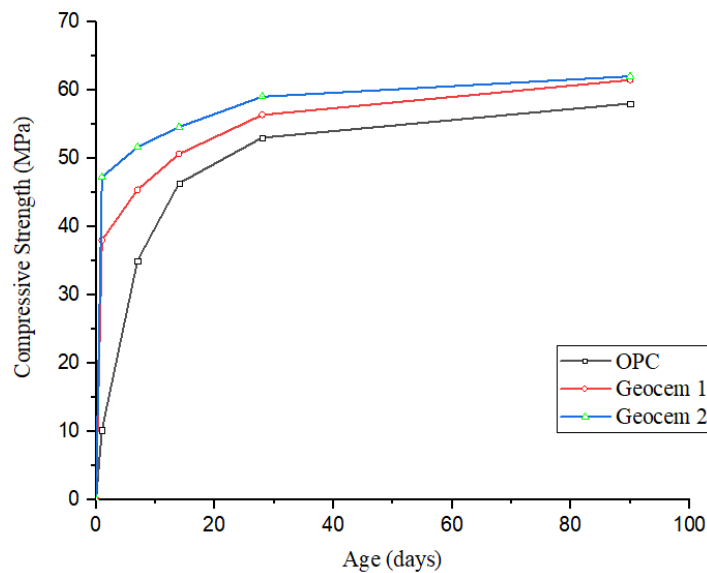
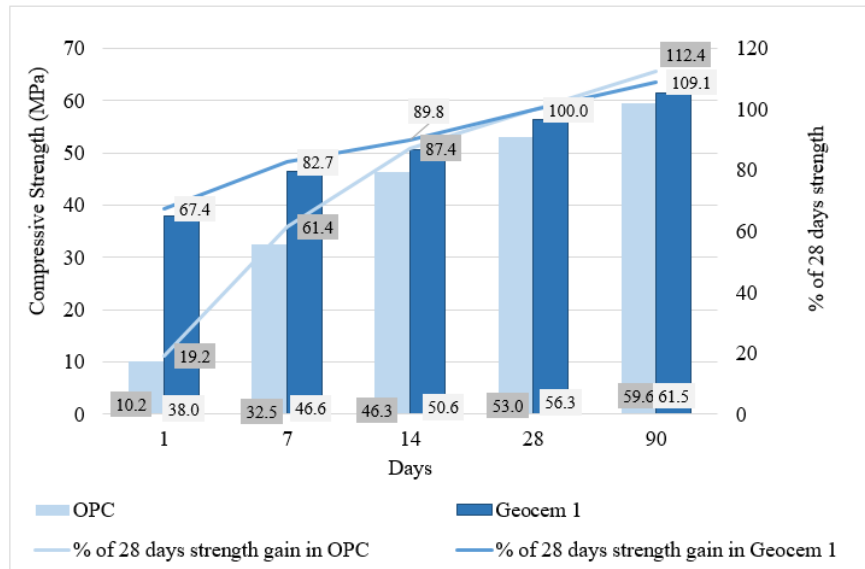
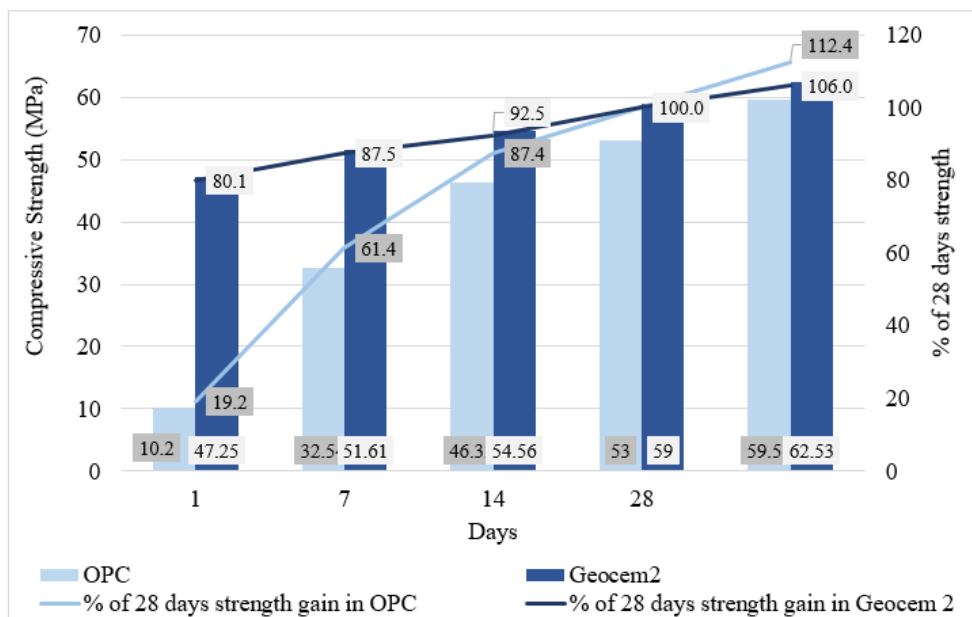


Figure 3-6 Compressive strength development in Grade 50MPa OPC and geopolymer concrete

Rapid growth of compressive strength was noticed for both geocem1 and geocem 2 concrete at 1 day, where the observed compressive strength was 38 MPa and 47 MPa respectively, while in OPC concrete the 1-day compressive strength was recorded to be 10 MPa. Such high early age strength gain can be attributed to accelerated heat curing resulting in increase in solubility of alumina-silicate compound during geopolymerisation process. Gomaa et al. (2020) reported gain in strength by geopolymer concrete at 1 day was 92% of the 28-day compressive strength compared to 29% gain by OPC concrete at early stage. Such gain in geopolymer concrete is also noted to be higher for geopolymer with increased content of GGBFS (Deb, Nath & Sarker 2014), as observed between geocem 1 and geocem 2. Kumar, Kumar & Mehrotra (2010) explained the improvement in compressive strength with increase in GGBFS content was due to the formation of calcium-silicate-hydrate (C-S-H) and alumina-silicate-hydrate (A-S-H) gel and compactness of microstructure. In 1 day, geocem 1 and geocem 2 gained 67% and 80% of 28-days compressive strength, while only 20% of 28-day strength was gained by OPC in 1 day. From 7 to 28 days, development of compressive strength was noticed to be gradual (Figure 3-7), while for OPC concrete, compressive strength development was observed to be significant at 7 days and progressed continuously till 28 days.



(a)



(b)

Figure 3-7 Strength development in (a) Geocem 1 and (b) Geocem 2

For geopolymer concrete, swift increase in early age strength due to curing at accelerated temperature has also been reported by Hardjito et al. (2004b), Wallah & Rangan (2006) and Bakria et al. (2011). The average compressive strength value of

geocem 1, geocem 2 and OPC concretes were 55 MPa, 59 MPa and 52 MPa respectively at 28 days. The increase in compressive strength after 28 days for geopolymer concrete were not significant when compared to the 90 days compressive strength value. From Figure 3-7, it can be observed that after rapid gain in strength within 7 days, the rate of increase in strength for both geopolymer concretes after 7 days were marginal until 90 days, while for the OPC concrete continuous increase in strength could be observed up until 90 days.

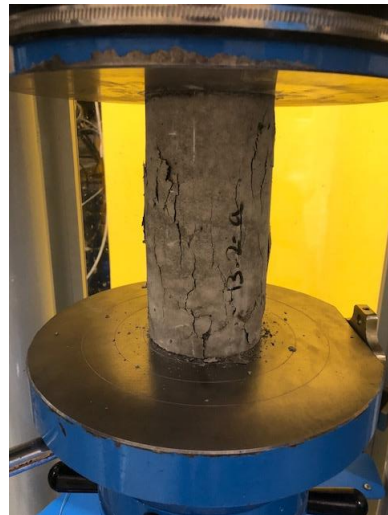
Furthermore, when the compressive strength value between geocem 1 and geocem 2 was compared, it was observed that geocem 2 showcased significant increase in strength at early age than geocem 1, though the compressive strength value at latter stage were almost similar. Such increase in strength at early age by geocem 2 was due to the presence of GGBFS in higher proportion (by 20%) than geocem 1. Nath & Sarker (2014) based on the study of effect of GGBFS on early strength development in fly ash based geopolymer cured at ambient temperature reported that the strength of the fly ash based geopolymer concrete increases as the percentage of GGBFS increases in the geopolymer binder. Parthiban et al. (2013) and Qiu et al. (2019) further reported that the GGBFS assists in long term strength gain in geopolymer concrete when cured at room temperature, suggesting the use of geopolymer for precast construction. However, the results obtained for geocem 1 and geocem 2 further suggests that the GGBFS assists in high strength gain at early age when cured at accelerated temperature. As such, both geocem 1 and geocem 2 are suitable for use in precast pipes, geocem 2 can be used in cases where high strength development is required at very early age.

During compressive strength test, the failure pattern for both geopolymer and OPC concrete cylinders were similar, and formation of cones at both ends or just on

one end (Type 1 and Type 2 failure) as defined in ASTM C39M (2021) was observed and can be seen in Figure 3-8. Figure 3-8a and b show the OPC and Geocem 2 concrete sample under failure load, while Figure 3-8c shows the Geocem 1 concrete sample past the failure load.



(a)



(b)



(c)

Figure 3-8 Failure of concrete cylinders (a) OPC (b) Geocem 2 (c) Type 1 failure of Geocem 1

3.2.2.2 Indirect tensile (Splitting tensile) strength

Tensile strength of the concrete is an important parameter in design of concrete structures. However, measuring the true tensile strength of the concrete using uniaxial tensile test is a complex process, requiring dog bone shaped samples which are pulled apart from two ends by applying uniaxial tensile stress. The uniaxial tensile test is hard to set up particularly due to its axial alignment requirement (Li 2011; Liao et al. 2020). As such indirect tensile testing is one of a common method adopted to measure the tensile strength of concrete. AS3600 (2018) specifies the relation between uniaxial tensile strength and splitting tensile strength as:

$$f_{ct} = 0.9 \times f_{ct,sp} \quad (3-2)$$

where, f_{ct} is the uniaxial tensile strength and $f_{ct,sp}$ is the splitting tensile strength obtained from test.

The indirect tensile test was carried out for three samples in accordance to AS1012.10 (2000). The concrete samples were horizontally laid and supported by metal frame with wooden strip at top and bottom. Force was then applied radially on to the cylinder, resulting in the splitting of the cylinder along its diameter (Figure 3-9b). The experimental setup of this test is shown in Figure 3-9a.



(a)



(b)

Figure 3-9 (a) Indirect tensile test set up (b) split geopolymer sample

The concrete samples were tested for indirect tensile strength at 7 days and 28 days. For geocem 1 and geocem 2, the 7 days indirect tensile strength were observed to be 2.45 MPa and 2.9 MPa respectively, while an indirect tensile strength of 1.56 MPa was observed for OPC. At 28 days, geocem 1 reported to gain 4.5 MPa strength and 4.8 MPa by geocem 2, while for OPC concrete the final strength gain at 28 days was 2.9 MPa. The 7 days samples of geopolymer concrete acquired 70% to 80% of 28 days indirect tensile strength. This remarkable gain of indirect tensile strength by geopolymer at 7 days has also been reported by Neupane, Chalmers & Kidd (2018), where gain in 90% of 28 days indirect tensile strength gain was reported. Similarly, Deb, Nath & Sarker (2014) indicated the increase in split tensile strength of up to 20% for fly ash based geopolymer concrete with the increases in GGBFS.

These values obtained for indirect tensile strength for geocem 1 and geocem 2 were higher than the suggested value for indirect tensile strength in AS3600 (2018) and ACI318 (2019) for 50 MPa concrete provided in Chapter 2. Based on the

compressive strength value for concrete, the indirect tensile strength suggested by AS3600 (2018) ($0.36\sqrt{f_c'}$) and ACI318 (2019) ($0.56\sqrt{f_c'}$) are 2.5 MPa and 3.9 MPa respectively. For OPC concrete, the indirect tensile value was closer to relation defined in AS3600 (2018). Sofi et al. (2007b) and Nguyen et al. (2016) also reported that geopolymer concrete achieved higher indirect tensile strength in comparison to same grade OPC concrete. Lee & Van Deventer (2004) explains the gain in indirect tensile strength demonstrated by geopolymer concrete as the effect of soluble silicates, where the soluble silicates first work to reduce the alkali saturation in the concrete pore and later contributes to greater inter-particle bonding between the geopolymer binder and the aggregates. This creates stronger aggregate- binder interface in geopolymer concrete, thus, making it hard to cut through the bonded interface.

AS3600 (2018) provides the relation between tensile strength and compressive strength for OPC, which has been expressed as:

$$f_{st} = 0.36 \sqrt{f_c'} \quad (3-3)$$

where, f_c' = characteristic compressive strength

f_{st} = indirect tensile strength

Many relations to calculate the indirect tensile strength for geopolymer concrete based on compressive strength have been proposed. However, due to the non-uniformity in the use of base materials and alkali activators used, variations in proposed relations for indirect tensile strength based on compressive strength have been observed.

Gunasekera, Setunge & Law (2017) proposed similar relationship for flexural strength (3-4), based on compressive strength of concrete as:

$$f_{st} = 0.45 \sqrt{f_{cm}} \quad (3-4)$$

where, f_{cm} = mean compressive strength

Mohammed, Ahmed & Mosavi (2021) and Lavanya & Jegan (2015) proposed similar indirect tensile strength models for geopolymer concrete as:

$$f_{st} = 0.222(f_c)^{0.7436} \quad (3-5)$$

$$\text{and } f_{st} = 0.249 (f_{cm})^{0.772} \quad (3-6)$$

Sofi et al. (2007b) proposed the following equation to determine the indirect tensile strength of geopolymer concrete:

$$f_{st} = 0.48 \sqrt{f_c} \quad (3-7)$$

Similarly, based on the test results, Hardjito & Rangan (2005) and Neupane, Chalmers & Kidd (2018) suggested a relation to determine the indirect tensile strength:

$$f_{st} = 0.7 \sqrt{f_{cm}} \quad (3-8)$$

The experimental data plot of indirect tensile strength in relation to compressive strength for geocem and against existing relations is demonstrated in Figure 3-10. Based on the test results, the relation suggested by AS3600 (2018) and ACI318 (2019) predicts conservative indirect tensile strength value while the relation proposed by Hardjito & Rangan (2005) overestimated the tensile strength value. Thus, a best fit curve to define the relationship between indirect tensile strength and compressive strength for geopolymer concrete can be proposed as equation 3.11 with R^2 value of 0.68.

$$f_{st} = 0.55 (f_{cm})^{0.53} \quad (3-9)$$

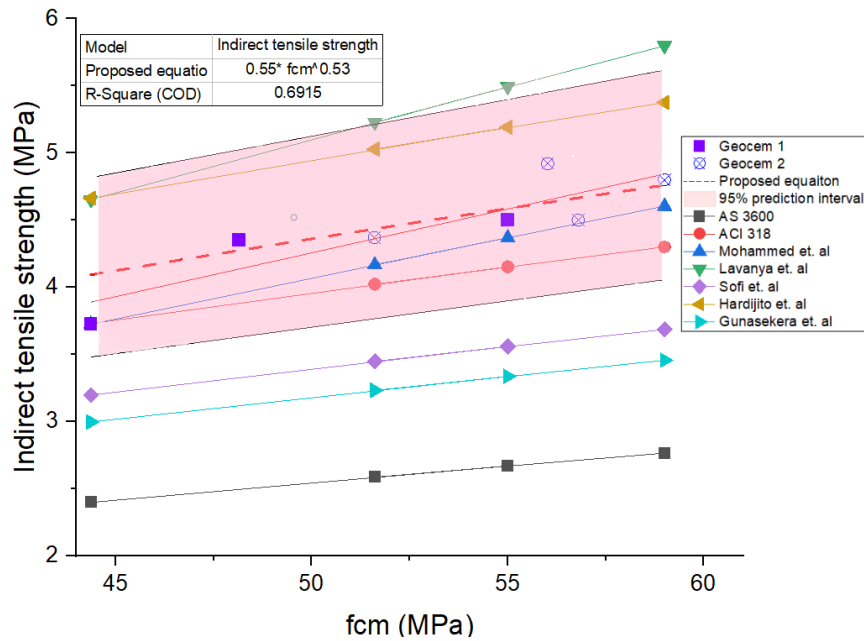


Figure 3-10 Indirect tensile strength against compressive strength for Geocem 1 and Geocem 2

Most of the indirect tensile strength value based on previous equations falls within the 95% prediction interval of the proposed equation, indicating the reliability of proposed equation.

3.2.2.3 Flexural strength

Flexural strength or modulus of rupture test is another indirect test, used to measure the tensile strength of the concrete. In general, the flexural strength of the concrete demonstrates higher value than the split tensile strength (Nath & Sarker 2017) and is considered to be 70 % greater than the actual tensile strength value of the concrete (Liao et al. 2020). Although flexural strength gives a measure of tensile strength, it is much higher than tensile strength as the inner layers of prism during the test have not reached their failure criterion (Li 2011).

As per AS1012.11 (2000), the flexural strength or modulus of rupture of the concrete samples for this study were obtained from four point bending test. The sample was placed such that the clear span between the supporting rollers for the beam was 3 times the loading span that is 100mm. The test set up for flexural strength test is displayed in Figure 3-11.



Figure 3-11 Set up for modulus of rupture test

The flexural strength of the two concrete samples were measured at 7 days and 28 days. At 7 days, the average flexural strength of geocem 1, geocem 2 and OPC concrete were measured to be 6.35 MPa, 6.46 MPa and 3.15 MPa respectively (Table 3-3). High gain in flexural strength at a period of 7 days was obvious in both geopolymers in comparison to OPC concrete. The 28 days flexural strength of geocem 1 and geocem 2 concrete were observed to be 6.54 MPa and 6.8 MPa respectively, which was almost 20 % higher compared to 5.41 MPa strength gain by OPC concrete at same age.

Table 3-3 Mechanical properties of geocem 1 and geocem 2 at 7 and 28 days

Sample	Compressive strength (MPa)		Tensile strength (MPa)		Flexural strength (MPa)	
	$f_{c,7}$	$f_{c,28}$	$f_{st,7}$	$f_{st,28}$	$f_{r,7}$	$f_{r,28}$
G1-S1	44.4	55.1	2.73	4.5	6.4	6.6
G1-S2	42.6	49.5	-	4.4	6.1	6.5
G1-S3	49.8	59	2.2	4.4	-	-
G2-S1	51.6	59	2.8	4.8	6.5	6.8
G2-S2	56.8	58.2	2.7	4.9	6.3	7
G2-S3	50	59.8	2.9	4.8	-	-
OPC-S1	30.6	52.4	1.4	2.2	2.8	4.9
OPC-S2	34.2	55.6	1.7	3.7	3.6	6.1
OPC-S3	31.3	52.4	1.6	2.9	-	-

Following the standard equation defined for traditional concrete in AS3600 (2018) ($0.6\sqrt{f_c}$) and ACI318 (2019) ($0.62\sqrt{f_c}$) the calculated value for flexural strength of geocem 1 and geocem 2 would be 4.24 MPa and 4.38 respectively, which is lesser than the obtained value. As such the standard equations for OPC concrete cannot be applied for geopolymer concrete.

Many relationships based on experimental analysis for geopolymer concrete has been suggested. Based on the regression model, Diaz-Loya, Allouche & Vaidya

(2011) proposed equation 3-10 similar to ACI318 (2019) to model the flexural strength and compressive strength relationship as:

$$f_r = 0.69 \sqrt{f_c'} \quad (3-10)$$

where, f_c' = characteristic compressive strength

f_r = flexural strength

Gunasekera, Setunge & Law (2017) proposed similar relationship for flexural strength (3-11), based on compressive strength of concrete as:

$$f_r = 0.7 \sqrt{f_{cm}} \quad (3-11)$$

Nath & Sarker (2017) also recommended an equation for flexural strength as:

$$f_r = 0.93 \sqrt{f_{cm}} \quad (3-12)$$

where, f_{cm} = mean compressive strength

Similarly, Albitar et al. (2015) suggested following relation for flexural strength:

$$f_r = 0.75 \sqrt{f_c'} \quad (3-13)$$

Figure 3-12 shows flexural strength versus compressive strength plot for geocem 1 and geocem 2 against the existing relationship based on liquid activated geopolymer concrete. Based on regression analysis, an equation representing the relationship between flexural strength and compressive strength is proposed in equation 3-14.

$$f_r = 0.88 \sqrt{f_{cm}} \quad (3-14)$$

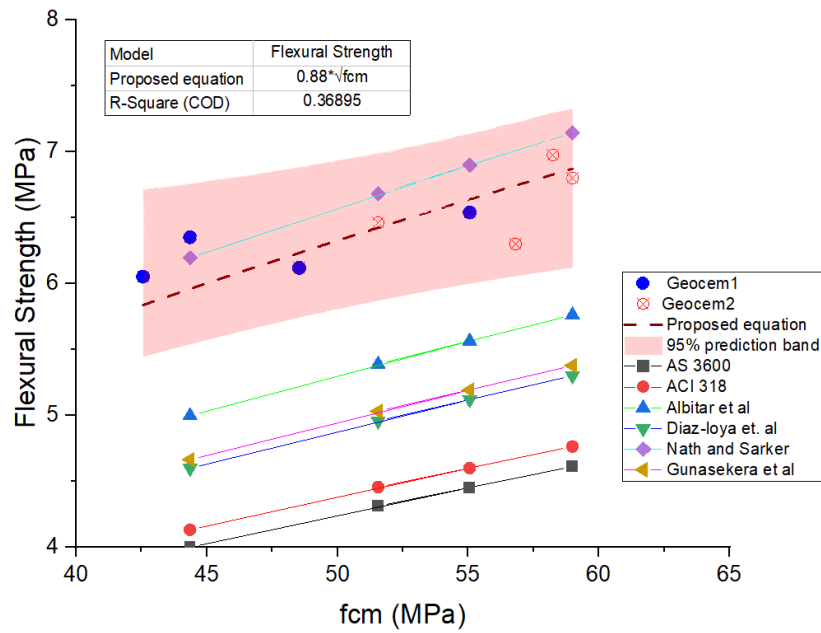


Figure 3-12 Flexural strength versus compressive strength plot for Geocem 1 and Geocem 2 with proposed model

The proposed model was found to best fit the derived data. It is noted that the proposed relationship for flexural strength by Nath & Sarker (2017) was a close match to the test data for flexural strength of powder based geopolymer concrete, while relationship suggested by AS3600 (2018) and ACI318 (2019) underestimates the flexural strength value for geopolymer concrete.

3.2.2.4 Modulus of elasticity

The modulus of elasticity or Young's modulus and Poisson's ratio measures the deformation characteristics of concrete. As per AS1012.17 (1997), the modulus of elasticity is a secant modulus that measures the stress up to 40% of the average compressive strength of the concrete. The elastic modulus is thus, calculated as the ratio of compressive stress to strain. The bending stiffness of flexural member is

dictated by the modulus of elasticity, thus higher modulus of elasticity means decrease in deflection.

For the test, two cylinder samples were tested to define the average compressive strength and three other samples to establish the value of modulus of elasticity and Poisson's ratio. A steel rig was used with LVDTs (Linear Voltage Differential Transducers) fixed in it; two LVDTs measured the axial deformation of the concrete cylinder and one LVDT placed horizontally measured the lateral deformation at the middle height of the test cylinder. The test set up to measure the modulus of elasticity and Poisson's ratio using compressometer is demonstrated in Figure 3-13.



Figure 3-13 Test set up to determine Modulus of Elasticity of concrete

The modulus of elasticity obtained at 28 days for geocem 1, geocem 2 and OPC concrete were 33.7 GPa, 34.6 GPa and 33.5 GPa respectively. Both type of geopolymer concretes and OPC concrete demonstrated similar modulus of elasticity. These obtained values matches closely with the Young's modulus value of 34.8 GPa defined

by AS3600 (2018) for 50 MPa concrete. There are many relations that are described to calculate modulus of elasticity based on compressive strength, however there is still no precise equation that defines this relationship (Neville 1995). The modulus of elasticity of concrete is determined by compressive strength and unit weight of concrete (Carreira & Chu 1985). The relationship for modulus of elasticity has, thus, been proposed considering either both density and compressive strength of concrete or only accounting the compressive strength of concrete.

For the calculation of the modulus of elasticity, ACI363R (1992) recommended equation 3-15 that relied on mean compressive strength (f_{cm}):

$$E_c = 3320 \sqrt{f_{cm}} + 6900 \text{ (MPa)} \quad (3-15)$$

Based on equation 3-15, the modulus of elasticity calculated to be 32.4 GPa for geopolymer concrete. Both the values suggested by AS and ACI closely matches with the observed value for both type of geopolymer concretes.

Noushini et al. (2016) presented equation for modulus of elasticity for geopolymer concrete based on mean compressive strength as:

$$E_c = -11400 + 4712 \sqrt{f_{cm}} \quad (3-16)$$

Diaz-Loya, Allouche & Vaidya (2011), based on their study suggested an equation to derive the modulus of elasticity for geopolymer concrete as:

$$E_c = 580 f_c' \quad (3-17)$$

Similarly, Yifei (2015) also proposed a relation for modulus of elasticity as:

$$E_c = 874.5 f_c'^{0.8452} \quad (3-18)$$

Hence, for 50 MPa geopolymer concrete, the modulus of elasticity obtained by following these equations by from Diaz-Loya, Allouche & Vaidya (2011) was 31 GPa

and from Yifei (2015) was 25 GPa. Hence, the relationship by Diaz-Loya, Allouche & Vaidya (2011) is more suitable to predict the value of modulus of elasticity in normal grade geopolymer concrete, thus, is proposed to be used for determining modulus of elasticity for geopolymer concrete. For geopolymer, the modulus of elasticity is reported to increase along with the increment in compressive strength; around 50 % increase in modulus of elasticity for change in compressive strength between 40 MPa and 60 MPa geopolymer concrete (Venu & Rao 2018).

Poisson's ratio is another deformational characteristic of concrete that measures the deformation in the concrete cylinder in a direction which is perpendicular to the direction of the force being applied. When load is applied to the cylinder, longitudinal strain develops due to axial deformation, while lateral strain develops in radial direction due to diametrical deformation. The ratio of lateral strain over longitudinal strain is calculated as Poisson's ratio.

The Poisson's ratio was observed to be 0.16 and 0.18 for geocem 1 and geocem 2 respectively. For OPC concrete, the observed Poisson's ratio was 0.18. Neville (1995) suggests the Poisson's value of OPC concrete generally falls within the range of 0.15 to 0.22. This range for Poisson's ratio of OPC concrete is similar to the measured value for geopolymer concrete.

Diaz-Loya, Allouche & Vaidya (2011) and Hardjito & Rangan (2005) also reported that for different grades geopolymer concrete, ranging from 10 MPa to 80 MPa, developed similar value for Poisson's ratio ranging between 0.08 to 0.22 and 0.13 to 0.16 respectively. As the value for Poisson's ratio for both geopolymer concrete fall between 0.16 and 0.18, it can be considered that the expected value range of OPC concrete can conservatively define the Poisson's ratio value of geopolymer concrete.

3.2.3 Stress-strain curve

Along with the compressive strength test, the stress-strain behaviour of geopolymer concrete were also tested. To obtain the stress-strain curve of geopolymer concrete cylinder in compression, 60 mm long strain gauges were used. Three strain gauge were attached symmetrically around each sample cylinder, which were connected to transducers to collect data digitally. The cylinders were loaded at constant displacement rate of 0.3 mm/min. In the absence of deformation-control testing machine, the stress-strain curve was measured by using strain gauge. However, using the strain gauge could only acquire the ascending part of the stress-strain behaviour because when the concrete cracked the strain gauge failed to collect the details for post-peak behaviour.

The concrete cylinder showed brittle failure once peak stress was reached. Figure 3-14 shows the stress-strain curve obtained for 50 MPa geocem 1 and geocem 2. From the stress-strain curve, it can be observed that the critical strain for both geopolymer is 0.003, and the critical strain for OPC concrete is also known to lie between 0.002 to 0.003 (ACI318 2019; Carreira & Chu 1985; Hognestad, Hanson & McHenry 1955). The modulus of elasticity obtained for geocem 1 (33.7 GPa) and geocem 2 (34.7 GPa) from the Young's modulus test in section 3.2.2.4 falls within the 10% variation of the modulus of elasticity calculated from the stress-strain curve of respective geopolymer concrete.

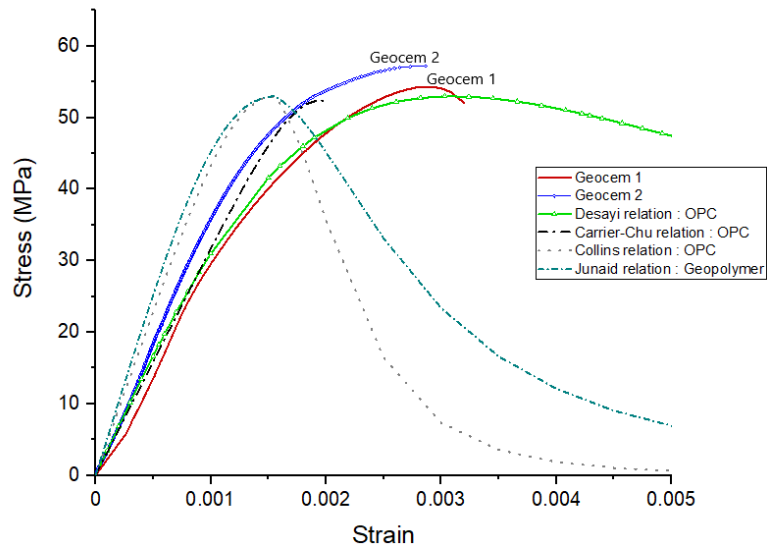


Figure 3-14 Stress-strain curve of geopolymer concrete

Similar brittle failure of heat cured fly ash and GGBFS geopolymer concrete during stress-strain behaviour study was also reported by Thomas & Peethamparan (2015). Popovics (1973) also reported that the results obtained for geopolymer matched well with the stress-strain behaviour of OPC concrete. The rapid decline in stress after the peak stress was observed and was more pronounced in slag based geopolymer concrete than in fly ash based geopolymer concrete. Diaz-Loya, Allouche & Vaidya (2011) were also unable to plot the post peak behaviour of the fly ash based geopolymer concrete because of the brittle nature of geopolymer, beside the unavailability of suitable device to measure post crack behaviour.

Figure 3-14 shows the stress-strain behaviour for geopolymer concrete obtained from this study which was further compared with the analytical stress-strain model proposed for OPC concrete using the proposed modulus of elasticity and strain value corresponding to maximum stress. Desayi & Krishnan (1964) has suggested a simple relation to depict the ascending and descending part of the stress-strain curve for OPC concrete through the following equation:

$$f_c = \frac{E \varepsilon_c}{1 + \left(\frac{\varepsilon_c}{\varepsilon_o}\right)^2} \quad (3-19)$$

where, E = a constant same as tangent modulus = $2 \frac{f_o}{\varepsilon_o}$

ε_o = strain at maximum stress f_o

ε_c = strain at stress f_c

Collins, Mitchell & MacGregor (1993) also proposed an equation to derive stress-strain curve for OPC concrete.

$$f_c = f_{cm} \frac{\varepsilon_c}{\varepsilon_{cm}} \frac{n}{n-1 + (\varepsilon_c/\varepsilon_{cm})^{nk}} \quad (3-20)$$

where, f_{cm} = peak compressive stress, ε_{cm} = strain at peak stress (f_{cm}),

$$n = 0.8 + (f_{cm}/17),$$

$$k = 0.67 + (f_{cm}/62) \text{ when } \varepsilon_c/\varepsilon_{cm} > 1$$

$$= 1 \text{ when } \varepsilon_c/\varepsilon_{cm} \leq 1$$

The equation proposed by Collins, Mitchell & MacGregor (1993) has been used in many other research to compare the stress-strain relationship for geopolymer concrete. Hardjito et al. (2005) used (Collins, Mitchell & MacGregor) model to compare the stress-strain behaviour for low calcium fly ash based geopolymer concrete and concluded that OPC concrete model for stress-strain curve can be used for geopolymer concrete, even though the descending part for geopolymer concrete were rather steep. Comparing the experimental data obtained from alkali activated low calcium fly ash based geopolymer concrete with the (Collins, Mitchell & MacGregor) model, Talha Junaid, Kayali & Khennane (2017) suggested the use of Collins model for geopolymer with suggestion for modification of n and k values as shown below:

$$n = 0.7 + (f_{cm} / 23),$$

$$k = 0.6 + (f_{cm} / 86) \text{ when } \varepsilon_c / \varepsilon_{cm} > 1$$

$$= 1 \text{ when } \varepsilon_c / \varepsilon_{cm} \leq 1$$

Noushini et al. (2016) when compared the experimental results for geopolymer concrete with Collins, Mitchell & MacGregor (1993) model reported that for heat cured geopolymer, the model showed lower stiffness and lower strain at peak stress and did not predict the stress-strain curve for geopolymer concrete accurately.

Based on the results obtained and curve fitting of the previously proposed models (as shown in Figure 3-15), the model proposed by Desayi & Krishnan (1964) closely matches with the powder form GGBFS and fly ash based geopolymer concrete.

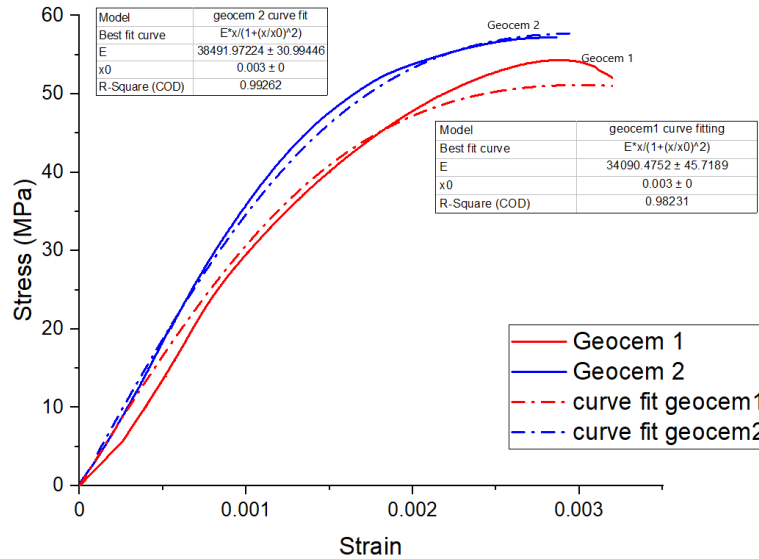


Figure 3-15 Curve fitting of stress-strain curve for geopolymer concrete

3.3 Summary

The material properties of powder form fly ash and GGBFS based geopolymer concrete of grade 50 MPa were prepared and explored in this study. Different proportion of fly ash and GGBFS were used for the development of general purpose geopolymer concrete (geocem 1) and high strength geopolymer concrete (geocem 2) along OPC concrete for comparison. Considering the geopolymerisation process in geopolymer concrete, sealed and accelerated heat curing for initial 6 hours was adopted to cure geopolymer concrete while standard ambient temperature water curing was adopted for OPC concrete. The prepared concrete specimens were tested for mechanical properties as per relevant Australian Standards. Following conclusions were derived based on the results obtained from the experiments conducted on geopolymer concrete.

- The use of powder form of alkali activator in geopolymer binder makes the geopolymer concrete able to be mixed and handled safely in a manner similar to that of the OPC concrete.
- The water/binder ratio for geopolymer concrete to achieve same strength grade concrete was less compared to OPC concrete requirement.
- Both type of geopolymer concretes demonstrated high strength gain in 1 day compared to OPC, though gradual increase in strength after 7 days were observed. Between geocem 1 and geocem 2, higher amount of GGBFS in geocem 2 resulted in high strength gain in geocem 2 compared to geocem 1.
- Heat cured geopolymer concrete developed around 30 % higher the indirect-tensile strength compared to ambient cured OPC concrete. Similarly, the flexural

strength developed by geopolymer concrete were 20% greater than OPC concrete.

- For both flexural strength and indirect tensile strength, the values obtained for geopolymer concrete were higher than the values obtained from relations suggested for OPC concrete in AS3600 (2018) and ACI318 (2019).
- Relation for indirect tensile strength and flexural strength was suggested based on the regression analysis to best fit the acquired experimental data. However, it is to be noted that the relationship is based on limited number of samples, therefore, further study to verify the proposed model for a wide range of sample size is recommended.
- The modulus of elasticity and Poisson's ratio of both geopolymer concrete were similar to that of OPC concrete which can be predicted using equations suggested in AS3600 (2018) and ACI318 (2019).
- Geopolymer concrete exhibited brittle failure during compressive stress-strain test resulting in rapid decline of stress following post peak stress. The ascending part of the stress-strain curve for the geopolymer closely matched with Desayi & Krishnan (1964) numerical model for the stress-strain behaviour of OPC concrete.
- It can be concluded that the ratio of indirect tensile strength to compressive strength and the ratio of flexural strength to compressive strength of both geocem 1 and geocem 2 was higher than that of OPC concrete of same grade, where as the modulus of elasticity and poisson's ratio were similar thus, the mechanical properties of geopolymer concrete can be beneficial in certain structural members such as pipes.

Chapter 4

4. Bond-slip analysis

4.1 Background

Reinforced concrete is a composite material which consists steel reinforcement and concrete. The properties of concrete such as ductility and its low tensile strength are compensated by the passive steel reinforcement with high tensile strength and ductility. Its structural performance relies on the mechanical properties of the concrete and reinforcement bar, along with the bond mechanism between these two components. When an external load is subjected to concrete structure, the load is directly applied to the concrete while the reinforcement bars receive part of the load transferred through the contact surface between the bonded concrete and reinforcement bar area (Shafaie, Hosseini & Marefat 2009). The force acting on the interface of the reinforcement bar and concrete is called bond-stress. The stress developed in reinforced concrete causes relative displacement between the reinforcement bar and surrounding concrete, along the rebar direction, which is termed as slip, and affects the structural response of the structure. Hence, knowledge of bond behaviour for reinforced concrete structure is crucial to understand the response of the reinforced concrete structure under structural load.

The bond behaviour of OPC concrete with steel rebar has been well researched, based on which many empirical equations to define the bond versus slip behaviour in OPC concrete structure have been developed, such that accurate response of reinforced OPC concrete member can be anticipated (CEB-FIB 1990; Lin et al. 2019; Nilson 1971; Rehm 1957). To examine the bond-slip behaviour in reinforced concrete member, two commonly used test methods are direct pull-out test and beam pull-out

test. The most commonly used test method to examine the bond behaviour of reinforced concrete member is direct pull-out test, mainly because of its simplicity and cost effectiveness (Gambarova & Rosati 1996; Kabir, Islam & Chowdhury 2015). Stating the bond stress distribution to be non-uniform when conducting pull-out test and due to absence of suitable theoretical method to determine bond strength of reinforcement steel in concrete, Abrishami & Mitchell (1996) suggested a combination of pull-out and push-in forces can simulate uniform bond stress distribution in reinforcement steel and concrete, providing clear understanding of bond behaviour. From the data collected for pull-out test, push-in test and combination of pull-out and push-in test, analytical model to estimate the bond-slip response and bond stress distribution was proposed. Lin et al. (2019) considered the bond-slip behaviour of deformed reinforcing bars based on beam-end specimen to determine the influence of lateral confinement provided by concrete cover and stirrups. Thereby, establishing the confining ability of concrete cover and stirrups as governing factor, the study presented the post peak bond stress behaviour to be linear before plateauing in pull-out failure, while non-linear behaviour was showcased during splitting failure, thus proposing bond stress versus slip model for deformed reinforcing bars which can be applicable for both pull-out and splitting failure modes. Besides reinforcing bars, research to understand the bond behaviour of fiber reinforced plastic (FRP) reinforcements have also been carried out. Cosenza, Manfredi & Realfonzo (1997) researched the influence of type of fiber, shape and type of matrix of the fiber, rebar type and concrete compressive strength on the bond behaviour. Further, the bond strength was noted to be influenced by fiber and resin properties rather than the concrete compressive strength. In addition, the test data was analysed against the proposed bond-slip model (CMR model) and the well-known relationships by Malvar (1994) and BPE model

(Eligehausen, Popov & Bertero 1982), where the BPE model was found to match well with the experimental results while the ascending branch of the bond-slip curve was best simulated by the CMR model. Similar studies on bond-slip behaviour of reinforcement bar in plain and steel fiber reinforced concrete was initiated by Harajli, Hamad & Karam (2002) where the impact of concrete cover to diameter ratio and volume fractions of fibers was explored, based on which local bond stress-slip model to predict response for plain concrete and fiber reinforced concrete with embedded reinforcement bars was proposed. Further, studies carried out by Gambarova & Rosati (1996) and Khaksefidi, Ghalehnovi & De Brito (2021) respectively explored the effect of varying diameter rebars and the influence of different strength type rebars on bond-splitting mechanism, concluding concrete cover to bar diameter ratio, rebar geometry, embedment length, concrete strength and yield strength significantly affects the failure mechanism.

Although a lot of work has been done to understand the bond-slip response of OPC concrete, the bond behaviour study carried out for geopolymer concrete on the other hand has been limited. Existing work mainly focuses on the development of bond strength in liquid-based geopolymer concrete considering varying compressive strength, cover to diameter (c/d) ratio and embedment length (Castel & Foster 2015; Sani & Muhamad 2020). Comprehensive study on bond-slip behaviour of geopolymer concrete with steel rebar has still not been carried out and therefore, the lack of reliable empirical equation to be used for analysis of geopolymer concrete structure can be realised.

To date, all the studies on the structural analysis of precast concrete pipes have been carried out assuming perfect bonding between concrete and reinforcement bar

(Mohamed & Nehdi 2016; Naggar, Allouche & Naggar 2007; Ramadan et al. 2020). Since the pipe test and analysis of pipe are focused on service load capacity of pipe, bond-slip mechanism is not significantly observed under such loading condition, hence perfect bonding condition is assumed. However, the bond–slip behaviour controls the ultimate flexural performance of reinforced concrete structure, thereby controlling deflection, crack formation and ultimate strength capacity in reinforced concrete structures (Alkhaldeh 2019; Capozucca 2013; Wight & Macgregor 2012). Thus, it is essential to incorporate bond-slip behaviour into the structural analysis of reinforced concrete structures in order to predict the structural performance of concrete structures under ultimate load capacity. As such, the purpose of this research is to investigate the change in bond strength development and bond-slip response for powder form geopolymer concrete and steel rebar.

In this chapter, experimental analysis is conducted to examine the bond-slip behaviour of steel reinforced geopolymer concrete. Powder form geopolymer concrete instead of liquid form geopolymer concrete is considered in the current study, impact from different reinforcement bar size and various embedment length is discussed. Based on the results of bond test, bond-slip relationship for powder form geopolymer concrete is proposed.

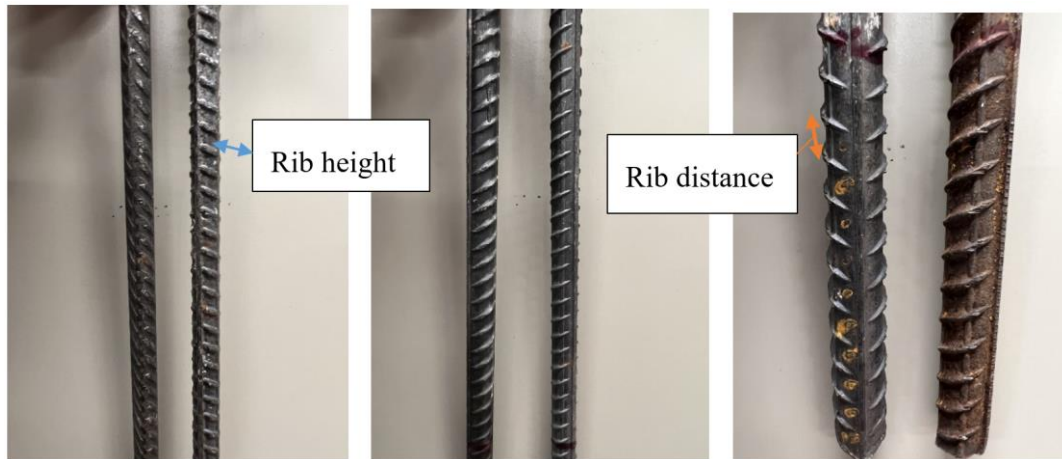
4.2 Experimental program

The direct pull-out test was used in the experimental investigation to examine the bond-slip behavior of geopolymer concrete and the development of bond strength in powder form geopolymer concrete.

4.2.1 Design of test specimen

The standard RILEM pull-out test was used to investigate the bond behaviour of geopolymer and OPC concrete. Following the RILEM (1970) pull-out test guide, concrete cube specimen for geocem 1, geocem 2 and OPC concrete were prepared. Their size are designed to be approximately 10 times of the diameter of rebar, as such 100 mm cubes were used for 10 mm and 12 mm reinforcement bars specimen while 150 mm cube was used for 16 mm reinforcement bar. The embedment length for each specimen were maintained at 5 times the reinforcement bar diameter ($5d$) such that constant bond stress is developed along the bonded length (Castel & Foster 2015; Desnerck, De Schutter & Taerwe 2010; RILEM 1970). To investigate the impact of embedment length on bond strength development in geopolymer concrete, additional samples were prepared with embedment length of $3d$ and $7d$ for reinforcement bars of diameter 10 mm, 12 mm and 16 mm. 2 specimens were prepared for each nominal reinforcement bars of 10 mm, 12 mm and 16 mm with embedment length of $3d$, $5d$ and $7d$. In total 42 specimens were tested. To control the embedment length of the reinforcement bar, PVC pipe was used to cover the reinforcement bar, where the bonded length was not required, and it was sealed using silicon. For specimen preparation, geopolymer and OPC concrete mix were prepared following grade 50 MPa design mix, while reinforcement bars of yield strength 500 MPa was used.

Figure 4-1(a,b,c) shows different rebars used in the study, Figure 4-1 (d) shows the mould preparation for 100 mm cube sample with 10 mm rebar and Figure 4-1(e) and (f) show the casted sample for 100 mm and 150 mm cube sample for pull-out test.



(a) 10 mm rebar

(b) 12 mm rebar

(c) 16 mm rebar



(d)



(e)



(f)

Figure 4-1(a,b,c) different size reinforcement bars used for pull-out test (d) mould preparation (e) 100mm sample casting (f) 150mm sample casting

OPC concrete, geocem 1 and geocem 2 concrete cube samples were prepared using grade 50 MPa concrete. The geopolymer concrete specimens after casting were left to set for an hour then sealed and cured at 40°C for 1 hour before elevating the temperature to 60°C for 6 hours. After 24 hours of curing, the heat cured samples were then demoulded, following which they were covered and cured under ambient temperature condition until the test. All the OPC concrete specimens were also

demoulded after 24 hours and were concealed by wet cloth to cure at a temperature of 23°C and 65% relative humidity till the test.

Along with the cube samples for bond test, 100 mm × 200 mm cylinders were also cast to evaluate compressive strength and splitting tensile strength development at 28 days. Heat curing was adopted for geopolymer concrete cylinders while curing of OPC concrete cylinders were prepared similar bond test samples by curing at room temperature.

4.2.2 Compressive strength and tensile strength test

The concrete cylinders were tested for compressive strength development and tensile strength as per AS1012.8.1 (2014) described in section 3.2.2.1 and 3.2.2.2 in Chapter 3. The tests were carried out at 28 days when bond test were also conducted. Geocem 1 and geocem 2 concrete were observed to develop mean compressive strength of 50.5 MPa and 54.5 MPa respectively while for OPC concrete, the mean compressive strength was observed to be 49 MPa. The indirect tensile strengths for OPC, geocem 1 and geocem 2 were found to be 2.67 MPa, 4.68 MPa and 4.94 MPa.

4.2.3 Direct pull-out test

To carry out the direct pull-out test, 500 kN capacity Universal Testing Machine (UTM) was used, where the concrete cube was supported on a steel plate and was placed concentrically to avoid eccentric stress at concrete and reinforcement bar joint. The reinforcement bar was clamped ensuring vertical placement of the sample. The force-controlled pull-out load was enforced on the reinforcement bar. Linear

variable differential transformer (LVDT) attached on top of the concrete sample as seen in Figure 4-2 collected the slip data at the free end of the reinforcement bar. Static monotonically increasing load was applied, as under such loading; concrete strength, yield strength of reinforcement bar, geometry of bar and concrete cover govern the bond behaviour (Gan 2000).

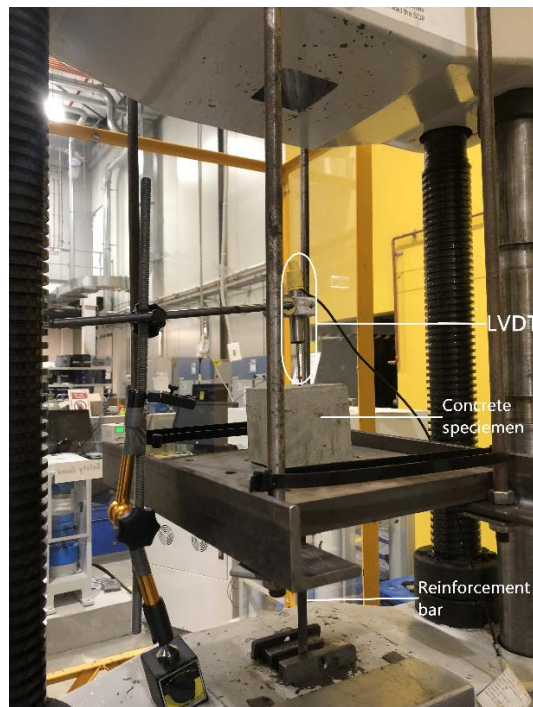


Figure 4-2 Direct pull out test set up

Loading rate for the specimen were calculated as specified in RILEM pull out test:

$$V_p = 5d^2 \text{ (kp/sec)} \quad (4-1)$$

where V_p is the target loading rate and d is reinforcement bar diameter in cm.

Loading rate of 0.07 kN/s was used for 10 mm and 12 mm specimens whereas 0.1 kN/s loading rate was for 16 mm specimen.

4.2.4 Experimental results

4.2.4.1 Failure mode

For geopolymer concrete specimens, the observed failure mode were mostly splitting along the embedded length of the reinforcement bar while few samples failed by rebar pull-out. However, all OPC concrete samples failed by splitting regardless of the reinforcement diameter.

For geopolymer concrete samples, typical rebar pull-out failure was observed for all reinforcement types with an embedment length of 3d. When the embedment length was 7d, all the samples showed splitting failure. In case of 5d embedment length, pull-out failure was observed for both geocem 1 and geocem 2 concrete with 10 mm rebar sample, while samples for 12 mm and 16 mm reinforcement bar failed by splitting. For geopolymer concrete samples with 10mm rebar the c/d ratio was 4.5 while for 12 mm and 16 mm the ratio was 3.6 and 4.2 respectively. Figure 4-3(a) and (b) show the geocem 1 concrete samples that failed on splitting and by pull-out. While pull-out bond failure demonstrates high bond capacity between reinforcement bar and concrete, such failure occurs when the confinement is high causing shear stress to act along the tip of the ribs without any damage occurring to concrete surface and only frictional bond stress is transferred between concrete and reinforcement bar (Abdulrahman et al. 2022; Nurwidayati et al. 2020). However, splitting bond failure occurs due to insufficient concrete cover or confinement (Gan 2000; Mo et al. 2016) resulting in cracking of concrete cover and propagation of crack along the length of the bar as shown in Figure 4-3 (d) and is the most common type of failure in structural members.

Figure 4-3 (c) shows the geocem 1 and OPC concrete sample with 16 mm reinforcement bar and 5d embedment length that failed by splitting. Nonetheless, for both types of geopolymer concretes and OPC concrete, the observed crack pattern for split bond failure was similar as seen in Figure 4-3 (d).

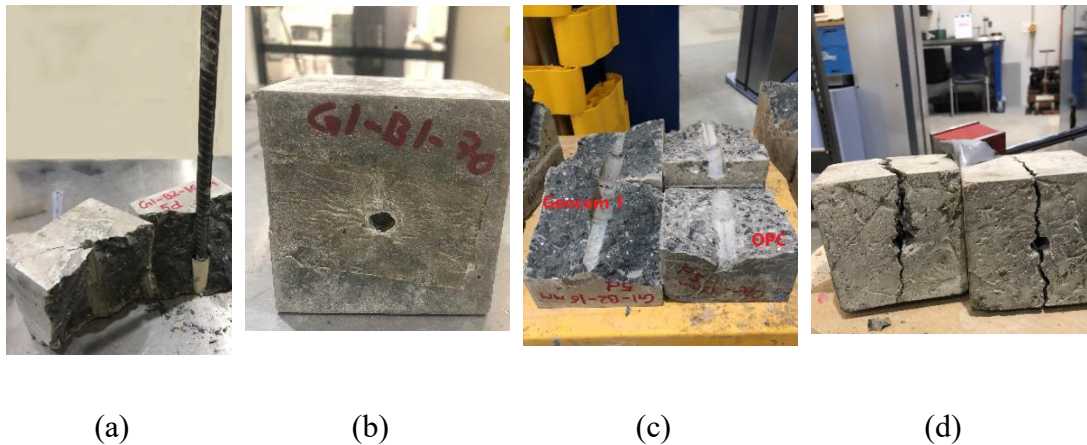


Figure 4-3 Failure of tested specimen (a) split failure of geocem1 sample with 12mm rebar (b) pull-out failure observed in geocem 1 for 10 mm rebar (c) comparison of geocem 1 and OPC sample for 16 mm rebar with 5d embedment length (d) commonly observed split pattern in pull-out test specimen

Majority of the bond test samples for both geopolymer concrete and OPC concrete exhibited splitting bond failure. However, the failure of geopolymer concrete specimen were brittle and destructive in comparison to OPC concrete failure. Similar results of brittle failure of geopolymer concrete were also reported by Sofi et al. (2007a), Sarker (2010) and (Cui 2015). Such higher brittleness of geopolymer concrete compared to OPC concrete has been reported to be due to low fracture energy in geopolymer concrete (Pan, Sanjayan & Rangan 2011). Fracture energy is defined as the energy required to open a unit area of crack surface and is dependent on the

properties of materials. Further, the brittle failure of geopolymer concrete is attributed to the generation of higher radial force in geopolymer sample compared to OPC concrete that is generated due to high pull-out force (Cui 2015) .

4.2.4.2 Ultimate bond strength development in geopolymer concrete

The bond stress in reinforced concrete is usually assumed to be uniformly distributed along the embedded length (Shen et al. 2016), depending on which the bond stress in reinforced concrete is calculated as:

$$\tau = \frac{F}{\pi d L_d} \quad (4-2)$$

where, τ = bond strength, F = applied load, d = nominal diameter of the reinforcement bar and L_d = embedment length.

From the pull-out test, maximum load or the pull-out force before the failure of the specimen was recorded based on which ultimate bond strength (τ_u) was calculated for geopolymer concrete. Table 4-1 summarizes the result for OPC and geopolymer concrete for different reinforcement bars with 5d embedment length.

With the same 5d embedment length, the bond strength of geocem 1 concrete with reinforcement bar was found to be lower than geocem 2 concrete specimen. The high bond strength in geocem 2 compared to geocem 1 can be attributed to high compressive strength development in geocem 2 in comparison to geocem 1. Such increase in bond strength development in relation to increase in compressive strength was also noted by Sarker (2010) for geopolymer concrete.

Table 4-1 Pull-out test result for reinforced OPC and geopolymer concrete samples

Concrete type	Reinforcement bar (d) (mm)	Bond length (l_d) (mm)	Concrete cover (c) (mm)	Concrete cover to diameter ratio (c/d)	Pull-out force (kN)	Ultimate bond strength (MPa)	Failure mode
OPC	10	50	45	4.5	26.31	16.75	Splitting
	12	60	44	3.6	36.59	16.18	Splitting
	16	80	67	4.2	92.88	23.10	Splitting
Geocem 1	10	50	45	4.5	29.03	18.48	Pull-out
	12	60	44	3.6	40.38	17.85	Splitting
	16	80	67	4.2	97.65	24.28	Splitting
Geocem 2	10	50	45	4.5	32.10	20.44	Pull-out
	12	60	44	3.6	44.08	19.49	Splitting
	16	80	67	4.2	103.94	25.85	Splitting

Equating the bond strength of geocem 2 concrete and OPC concrete for 10mm, 12mm and 16mm reinforcement bar individually, around 10 -15% increase in the average bond strength was observed which is similar to the case result reported by Castel & Foster (2015) and (Mathew 2021), while for geocem 1 concrete the increase in comparison to OPC concrete was around 5 -10% only. This comparative increase in bond strength in geopolymer concrete is explained by the higher splitting tensile strength in geopolymer concrete in comparison to OPC concrete (Sarker 2011; Sofi et al. 2007a; Topark-Ngarm, Chindaprasirt & Sata 2015).

Apart from concrete mechanical properties, the development of bond strength is affected by many factors such as geometry of reinforcement bar, concrete cover and embedment length of reinforcement bar. Hence, a parametric study to examine the influence of different reinforcement size and embedment length on bond strength development in geopolymer concrete was carried out.

4.2.4.3 Effect of reinforcement diameter on bond strength development

The effect of reinforcement diameter on bond strength development was explored for three different sized ribbed reinforcement bars with diameter 10 mm, 12 mm and 16 mm. Comparing the bond strength development in different reinforcement bar size, slight decrease in bond strength was observed for all concrete type when reinforcement size increased from 10 mm and 12 mm, while substantial increase in bond strength for all binder type with 16 mm rebar was noticed (Table 4-2). Similar test results for different geopolymer mix and OPC concrete with different size reinforcement bars were also observed in the bond test result by Abdulrahman et al. (2022) and Tang & Cheng (2020). This difference in bond strength development can be due to difference in bar geometry, that is, bar diameter, rib height and rib spacing (Hong & Park 2012). The rib height for 10 mm, 12 mm and 16 mm reinforcement bars were measured to be 0.73 mm, 0.93 mm and 1.59 mm respectively, while the rib spacing were 2.5 mm, 4.9 mm and 6 mm for 10 mm, 12 mm and 16 mm diameter rebar. Consequently, the rib height to diameter ratio was calculated to be 0.073, 0.077 and 0.099 for 10 mm, 12 mm and 16 mm reinforcement bar respectively. The close value of rib height to diameter ratio between 10 mm and 12 mm reinforcement bar signifies the similar bond strength development, while the higher ratio of rib height to

diameter ratio in 16 mm reinforcement bar resulted in higher bond strength development. Investigating the shape parameter of reinforcement bar and height of rib with respect to the bar diameter, Tang & Cheng (2020) also stated that the bond area for larger diameter bar is smaller, resulting in smaller ultimate bond strength. However, the height of rib also significantly affects the bond strength development as it was observed that for specimen with greater rib height to diameter ratio showcased greater ultimate bond strength irrespective of reinforcement bar diameter.

However, comparing the bond strength development for different size reinforcement bar, 12, 16 and 20 mm by Sofi et al. (2007a), 20- 24 mm by (Sarker 2011), and 10, 16 and 25 mm by Kim & Park (2015) based on their bond strength study for geopolymer concrete have stated that while the bond strength in geopolymer concrete is greater than OPC concrete, general decrease in bond strength can be noticed for increase in reinforcement bar size for geopolymer concrete. The parametric study carried out by Khaksefidi, Ghalehnovi & De Brito (2021) using different diameter reinforcement for AIII and AIV patterned reinforcement bars also concluded that the increase in diameter decreases the bond strength value, however the ribbed pattern in the reinforcement also influences the bond strength development for its respective size. Such increase in ultimate bond stress with decreasing deformed bar diameter has also been observed in experimental bond strength study for confined OPC concrete (Soroshian & Choi 1989). Maranan et al. (2015) also based on the study of bond behaviour of glass fibre reinforced polymer (GFRP) reinforced geopolymer concrete reported that the bond strength in geopolymer concrete decreased as the GFRP bar diameter increased. On contrary to these studies, based on the bond test results for geopolymer concrete with 12 mm and 16 mm reinforcement bar provided by Ganesan, Indira & Santhakumar (2015), it was observed that with increase in reinforcement bar

increase in bond strength was observed while for 10 mm geopolymer concrete sample test failed due to yielding. Similarly, Senthil, Bawa & Aswin (2018) reported that increasing the reinforcement bar diameter increases the bond strength characteristics.

Since the results in this study are based on limited number of tests and presence of contrasting conclusions in existing studies, more elaborate study on the influence of reinforcement bar size on bond strength development in geopolymer concrete is necessary to establish the relation between bond strength development and reinforcement bar size and understand the bond behaviour of geopolymer concrete.

Further to this, the value of slip at ultimate bond strength for OPC concrete for 10 mm, 12 mm and 16 mm was recorded to be around 0.4 mm to 0.6 mm, while for geocem 1 the slip value ranged between 0.16 mm to 1.16 mm, with an average of 0.6 mm which was similar to slip value for OPC concrete. For geocem 2, the slip value was recorded between 0.2 mm to 1.8 mm. The average bond-slip behaviour of geopolymer concrete with respect to OPC concrete has been presented in Figure 4-4.

Figure 4-4(a) shows the bond-slip behaviour of geopolymer concrete mapped against OPC concrete with 10mm rebar, difference in the curve can be observed primarily due to failure action of the sample. While both geopolymer concrete specimens showed ductile rebar pull-out failure, OPC sample failed by splitting. For 12 mm rebar and 16 mm rebar (Figure 4-4(b) and (c)), the failure of all the samples occurred by splitting, hence after reaching the peak value, sudden fall in the curve can be observed for all the binder types. This linear fall in the curve correspond to increase in slip value due to applied force on sample. In the bond-slip curve for all the reinforcement type, the bond strength for geocem 2 concrete were observed to be higher than that of geocem 1 concrete, but the slip at failure was smaller.

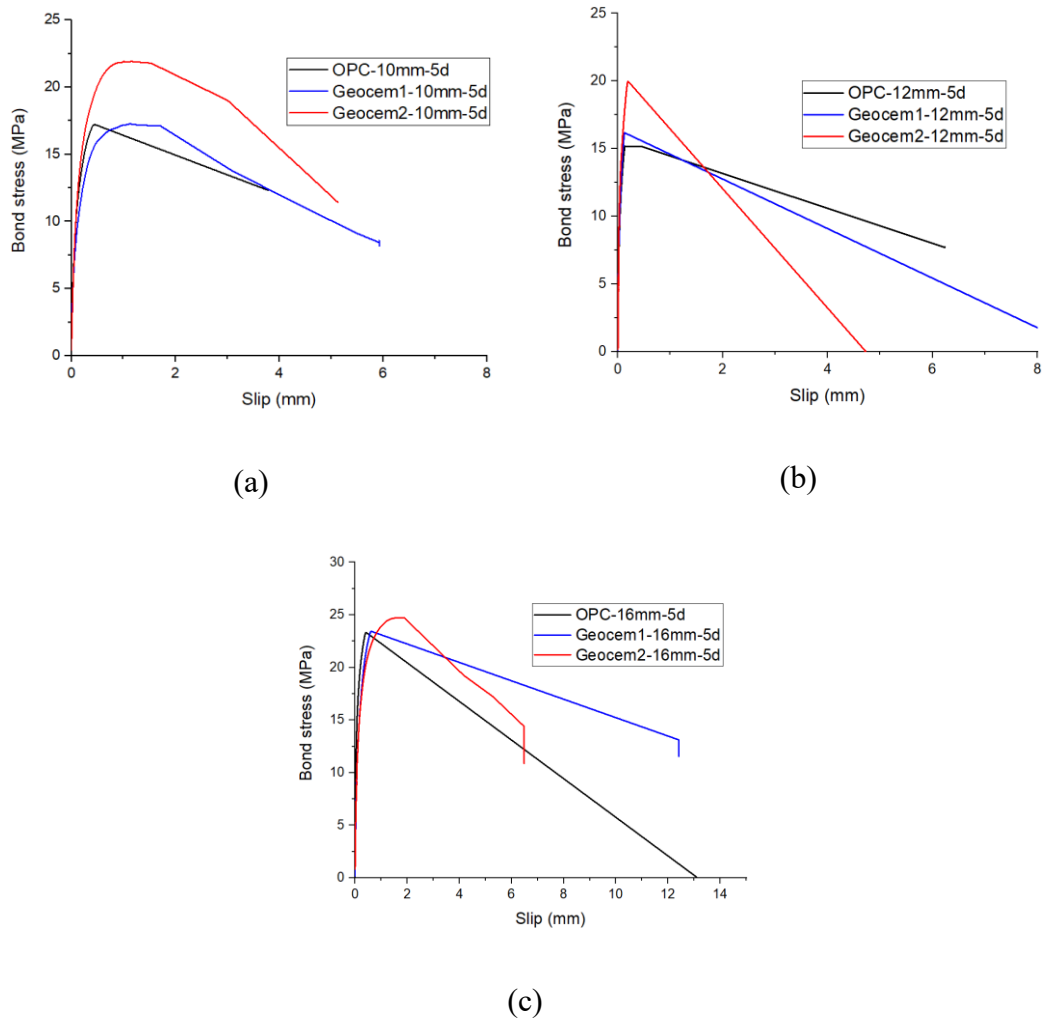


Figure 4-4 Bond-slip curve for geopolymer and OPC concrete for (a) 10 mm (b) 12 mm (c) 16 mm reinforcement bar with 5d embedment length

4.2.4.4 Effect of embedment length on bond strength of geopolymer concrete

While numerous studies have been carried out to explore the bond strength development in geopolymer concrete using direct pull-out test (Castel & Foster 2015; Ganesan, Indira & Santhakumar 2015; Kim & Park 2015), splice test (Chang et al. 2009) and beam-end test (Sarker 2010; Sarker 2011; Sofi et al. 2007a) exploring the influence of compressive strength, reinforcement bar diameter, fibre reinforcement,

curing period, the influence of embedment length on bond strength development in geopolymer concrete has still not been fully explored. Effect of bond length on bond strength development was conducted by Maranan et al. (2015) and Tekle, Khennane & Kayali (2016), but those studies were based on sand-coated glass fibre-reinforced polymer (GFRP). To date very few studies on effect of embedment length on bond strength development in geopolymer concrete have been reported. The study carried out by Vinothini et al. (2015) and Nurwidayati et al. (2020) to investigate the effect of embedment length for 16 mm and 13 mm reinforcement bar respectively, on geopolymer concrete was based on liquid activated geopolymer concrete. Thus, only limited information on the influence of embedment length of reinforcing bar in geopolymer concrete is available. Hence, to explore the influence of embedment length in bond strength development in powder form geopolymer concrete with deformed reinforcement bar, three different embedment lengths (3d, 5d and 7d) for different sized reinforcement bar were considered in this study. Table 4-2 tabulates the test data obtained from the pull-out test for geopolymer concrete with different embedment length cases.

Table 4-2 Pull-out test results for reinforcement bars with different embedment length in geopolymer concrete specimen

Geopolymer concrete type	Embedded length	Geopolymer Concrete Samples	10 mm rebar			12 mm rebar			16 mm rebar		
			Bond stress (MPa)	Slip (mm)	Avg. Bond stress	Bond stress (MPa)	Slip (mm)	Avg. Bond stress	Bond stress (MPa)	Slip (mm)	Avg. Bond stress
Geocem 1	3d	G1-3d-1	22.99	1.14	23.34	21.62	1.31	22.62	21.18	1.15	23.70
		G1-3d-2	23.69	1.19		23.62	0.95		26.22	1.54	
	5d	G1-5d-1	17.58	1.17	18.47	17.76	0.17	17.84	26.15	0.87	24.28
		G1-5d-2	19.36	1.00		17.91	0.26		22.40	0.67	
	7d	G1-7d-1	16.81	0.17	15.44			11.73	16.39	0.22	16.29
		G1-7d-2	14.06	0.08		11.73	0.08		16.18	0.17	
Geocem 2	3d	G2-3d-1	25.65	1.35	25.31	26.99	0.87	24.49	25.68	1.33	26.56
		G2-3d-2	24.98	1.06		21.98	0.95		27.44	1.39	
	5d	G2-5d-1	18.96	1.23	20.44	19.02	0.09	19.49	24.74	1.88	25.85
		G2-5d-2	21.92	1.16		19.96	0.19		26.96	1.09	
	7d	G2-7d-1	15.94	0.36	14.77	10.53	0.10	10.32	18.12	0.18	16.34
		G2-7d-2	13.59	0.21		10.12	0.04		14.56	0.06	

From the collected test results, it can be noted that the maximum bond strength for both geopolymer concrete was achieved for the specimen with 3d embedment length. The decrease in bond strength with increase in embedment length of reinforcing bar was observed. The increase in bond length increases the bond area between geopolymer concrete and reinforcement bar, thereby inversely affecting the bond strength development in concrete specimen. Similar decrease in bond strength development in geopolymer concrete for specimen with 16 mm and 13 mm reinforcement bar and embedment length ranging from 3d to 8d was reported in the study by Vinothini et al. (2015) and Nurwidayati et al. (2020). This decrease in bond stress with increasing embedment length can be observed from Figure 4-5 and Figure 4-6 for geocem 1 and geocem 2 respectively.

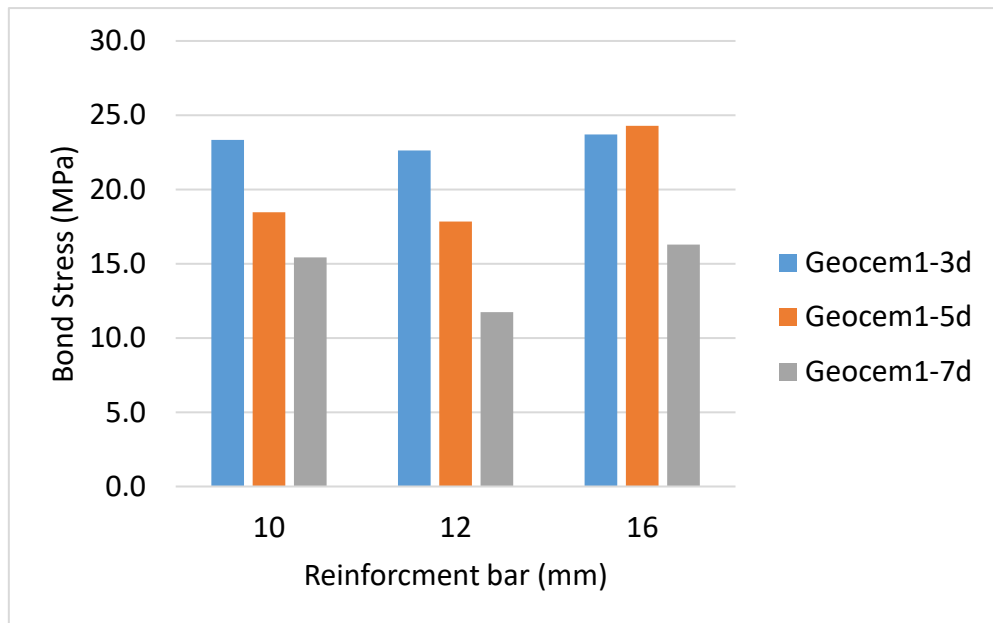


Figure 4-5 Influence of embedment length on bond stress development in Geocem

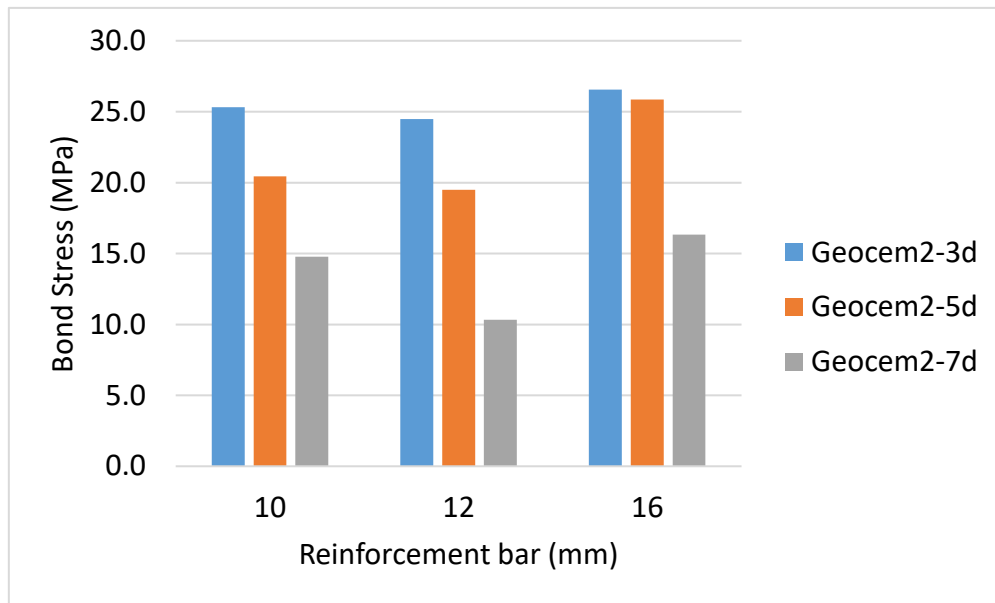


Figure 4-6 Influence of embedment length on bond stress development in Geocem

2

Based on the experimental observation of the pull-out test for both types of geopolymer concrete and OPC, it was noted that for same grade strength of OPC and geopolymer, the latter exhibited higher bond strength, this difference in bond strength development between OPC and geopolymer concrete is due to the high tensile strength capacity of geopolymer concrete. Further, the parametric study for different reinforcement diameter and varying embedment length carried out to explore the influence on bond strength development in geopolymer concrete, it can be observed that the bond strength development in OPC concrete and geopolymer concrete followed similar pattern, where the increase in reinforcement diameter reduces the bond strength and the increase in embedment length causes a decrease in bond strength.

4.3 Model for bond-slip behaviour of geopolymer concrete

To model a realistic structural response of concrete members under load, it is essential to take into account the bond-slip behaviour of reinforced concrete, as such many researches have been carried out proposing several bond-slip relationship for OPC concrete (Abrishami & Mitchell 1996; Harajli, Hamad & Karam 2002; Hong & Park 2012; Khaksefidi, Ghalehnovi & De Brito 2021; Orangun, Jirsa & Breen 1975). The bond-slip model proposed by Eligehausen, Popov & Bertero (1982) as BPE model is widely used for OPC concrete. The BPE model was approved for CEB-FIB (1990) and has been used to model bond-slip behaviour for different failure modes in CEB-FIB (2010). The CEB-FIB model portrays the bond stress development in four parts as shown in Figure 4-7 where the initial development in bond stress is observed due to adhesive bond and mechanical interlocking of the concrete and reinforcement bars which continues till maximum bond stress is reached, where the bond development plateaus. Once the maximum bond stress is reached, the bond stress development is followed by decrease in stress with increasing slip due to increase in radial splitting force causing shearing off of the concrete. This decline in bond stress is finally followed by a constant bond strength value which is attained due to friction between cracked concrete and reinforcement bar, resulting in pull-out failure after the friction bond is lost.

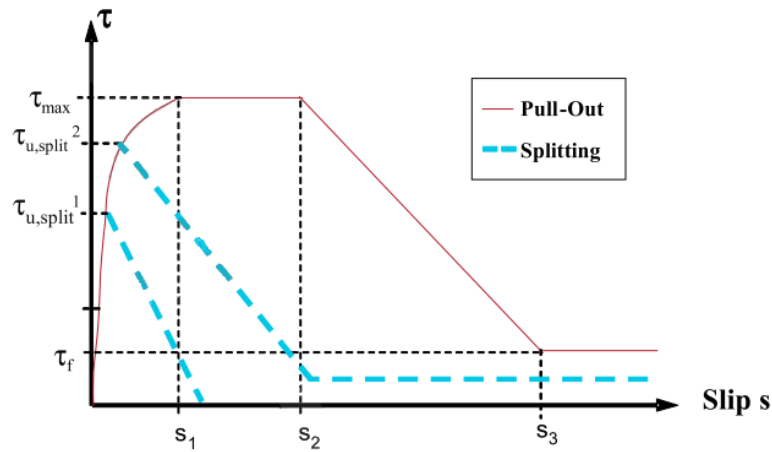


Figure 4-7 Analytical bond-slip relationship in CEB-FIB (2010)

To accommodate to different failure modes, the CEB-FIB model is generally divided into two types: 1) pull out failure mode for well confined concrete that exhibits distinct plateau at maximum bond stress, and 2) splitting failure mode for unconfined concrete that do not show horizontal branch once the maximum bond stress is reached. Based on the failure type and appropriate value relating to failure type, the bond stress-slip behaviour in OPC concrete is described and has been modified in different case studies for fibre reinforced concrete and corroded reinforcement (Harajli, Hamad & Karam 2002; Lin et al. 2019; Sæther & Sand 2012). While efforts to study the bond strength development in geopolymer concrete has been carried out based on which equations to predict the bond strength for geopolymer concrete with embedded reinforcement bar and steel fibre reinforced geopolymer concrete, depending on which suitable embedment length have been proposed (Dahou, Castel & Noushini 2016; Ganesan, Indira & Santhakumar 2015; Kim & Park 2014; Topark-Ngarm, Chindaprasirt & Sata 2015). Few studies have been undertaken that proposed the bond stress-slip equation for liquid activated geopolymer concrete.

Considering the conservative prediction for bond strength based on existing empirical equations for OPC concrete, Cui, Zhang & Bao (2020) conducted the statistical regression analysis and proposed new empirical equations to establish relation between bond stress and slip developed in geopolymer concrete with plain and ribbed reinforcing bar. The proposed equation for bond stress determination for plain reinforced bar and ribbed reinforcement case to be used to model stiffness in finite element model is expressed as equation 4-3 and 4-4 respectively:

$$\tau_b = \frac{1}{0.4809 + 7.55 \times 10^{-5} S_r^2 + \frac{2.3267}{S_r^{1.5}}} \quad (4-3)$$

$$\tau_b = (-0.448 - 4.47 \times 10^{-5} S_r^2 + 3.03 \times 10^{-8} S_r^3 + 0.967 S_r^{0.5}) \sqrt{\frac{f_c}{35}} \quad (4-4)$$

where, τ_b = bond stress in MPa, S_r = slip in μm and f_c = specified compressive strength of concrete.

Albitar et al. (2017b) based on his test study of 102 pull-out samples concluded that though the geopolymer concrete demonstrated high bond capacity than OPC concrete samples, in the absence of standardised model for geopolymer concrete, the available bond-slip model for OPC concrete yield lower bound approximation of bond strength and bond-slip behaviour for geopolymer concrete. The development of bond strength (τ_{max}) in relation to compressive strength (f_c), slip corresponding to maximum bond stress (δ_1), frictional strength (τ_{fric}) and maximum slip (δ_{max}) was described by equation 4-5 to 4-8 respectively.

$$\tau_{\text{max}} = 39.6 f_c^{0.25} - 76.5 \quad (4-5)$$

$$\delta_1 = 0.088 \tau_{\text{max}} - 0.320 \quad (4-6)$$

$$\tau_{\text{fric}} = 0.543 \tau_{\text{max}} - 5.18 \quad (4-7)$$

$$\delta_{\text{max}} = 0.088 \tau_{\text{max}} - 0.320 \quad (4-8)$$

where, τ_{\max} and τ_{fric} is in MPa and δ_1 and δ_{\max} is measured in mm.

However, the equation proposed by Albitar et al. (2017b) has not considered the influence of concrete cover to bar diameter ratio in bond strength development which also affect the bond strength development in geopolymer concrete. Similarly, Abdulrahman et al. (2022) also proposed bond-slip equation based on the experimental test data and the data available from past studies for geopolymer concrete. The equation for maximum bond stress and frictional bond stress with respect to concrete cover and reinforcement diameter was proposed to be followed by the CEB-FIB model as follows:

$$\tau = \tau_{\max} \sqrt{\frac{\delta_r}{\delta_1}} \text{ for } \delta_r < \delta_1 \quad (4-9)$$

$$\tau = \tau_{\max} - (\tau_{\max} - 0.29\tau_{\max}) \left(\frac{\delta_r - \delta_1}{\delta_2 - \delta_1} \right) = \text{ for } \delta_1 < \delta_r < \delta_2 \quad (4-10)$$

$$\tau = 0.33\tau_{\max} \left(\frac{\delta_r}{\delta_2} \right)^{-0.5} \text{ for } \delta_2 < \delta_r < \delta_3 \quad (4-11)$$

$$\tau = \tau_{\text{fr}} \text{ for } \delta_r > \delta_3 \quad (4-12)$$

$$\text{where, } \tau_{\max} = 1.23 \left(\frac{c}{d} \right)^{2/3} \sqrt{f_c} \leq 0.89 \left(\frac{c}{d} \right)^{2/3} \text{ (MPa)}$$

$$\tau_{\text{fr}} = 0.1 \tau_{\max} \leq 0.045 \tau_{\max} \text{ (MPa)}$$

where, τ , τ_{\max} and τ_{fr} are in MPa and δ_1 , δ_2 , δ_3 and δ_r are measured in mm.

But considering the deviation of the bond stress-slip model proposed by Abdulrahman et al. (2022) with the experimental bond stress-slip behaviour of geocem 1 and geocem 2, further investigations have been carried out to propose suitable equations to define bond-slip relation for powder based geopolymer concrete.

4.3.1 Bond stress-slip model for geopolymer concrete

To establish a generic bond stress-slip model for geopolymer concrete, influence of reinforcement diameter and concrete cover, apart from the compressive strength of the concrete, was considered. The experimental bond stress-slip result of samples with different reinforcement diameter and 5d embedment length were selected. As limited number of samples were tested for bond study, the test results for few test samples were not appropriate. Hence, the outlying data set has been ignored. Thus, to define the bond stress-slip model, regression analysis was carried out based on the obtained experimental results, along with available data on bond test of geopolymer concrete under similar condition, to define the main points of the bond-slip plot. The proposed model was then validated against the experimental test results and used to model the interaction between the geopolymer concrete and reinforcement in finite element modelling of geopolymer concrete pipes.

4.3.1.1 Ultimate bond strength

The ultimate bond strength (τ_{\max}) is the maximum bond stress resisted at the interface of reinforcement bar and concrete before failure. For geopolymer concrete, the bond strength has been reported to be higher than that of OPC concrete, and is mainly attributed to the higher tensile strength of the geopolymer concrete (Castel & Foster 2015; Dahou, Castel & Noushini 2016; Topark-Ngarm, Chindaprasirt & Sata 2015). Thus, the analytical equations to determine the ultimate bond strength in geopolymer concrete is simply explained as function of compressive strength in reference to tensile strength.

Figure 4-8 demonstrates the influence of concrete cover to reinforcement diameter (c/d) ratio on ultimate bond strength development on geopolymer concrete. The bond strength value has been normalised by the compressive strength to study the influence of c/d ratio on bond strength. A general increase in ultimate bond strength in relation to increase in c/d ratio can be observed. Such increase in bond strength due to increase in c/d ratio can be credited to the increase in adequate confinement (Chang et al. 2009; Sofi et al. 2007a). A linear regression analysis was carried out based on the experimental data available, a mathematical equation to describe the relationship of maximum bond strength with c/d ratio was derived as:

$$\tau_{\max} = 1.39 * \left(\frac{c}{d}\right)^{1/2} * \sqrt{f_c} \quad (4-13)$$

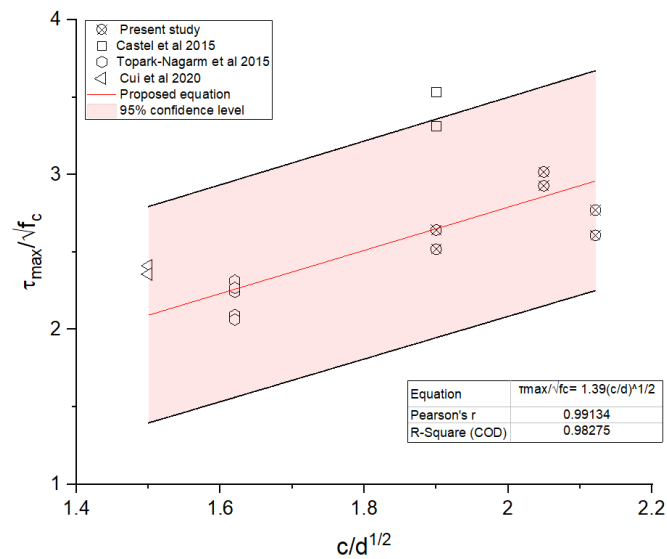


Figure 4-8 Effect of concrete cover to bar diameter (c/d) ratio on ultimate bond strength

Considering the dispersion of the data shown in Figure 4-8, the 95% confidence level of the proposed equation has also been plotted. The 95% confidence level in

regression analysis indicates that there is a 95% probability that the true strength value falls within the interval.

4.3.1.2 Slip at maximum bond stress

To mathematically define the relationship between the slip at maximum stress (S_1) and the corresponding bond strength developed in geopolymer concrete, a regression analysis was carried out based on the obtained experimental results as seen in Figure 4-9. The following expression was derived for the slip at maximum stress:

$$S_1 = 0.07 * \tau_{max} - 0.68 \quad (4-14)$$

In the Figure 4-9, significant scatter in the data can be observed, which can be attributed to different size of reinforcement bar used. Such variation in slip of reinforcement bar has been reported to be highly dependent to the relative rib area (Hong & Park 2012; Mo et al. 2016).

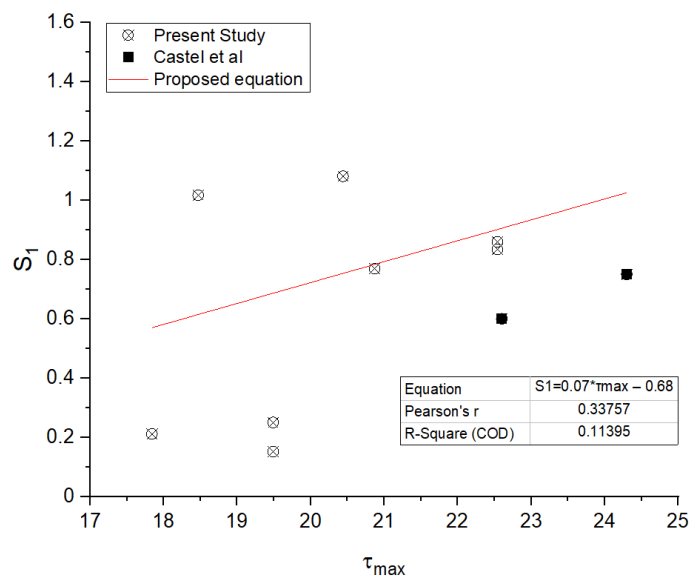


Figure 4-9 Effect of bond strength on S_1

4.3.1.3 Frictional bond strength and maximum slip

During bond failure, the frictional force acting on the interface of reinforcement bar and concrete while the reinforcement bar is being pulled out is termed as frictional bond strength (τ_f), and the maximum slip (S_2) corresponds to this frictional bond strength. Frictional bond strength is dependent on the failure mechanism, as splitting failure causes decrease in confinement around the reinforcement bar causing decrease in frictional force (Albitar et al. 2017b). Figure 4-10 and Figure 4-11 show the relationships of frictional bond strength and maximum slip against maximum bond strength respectively. Carrying out regression analysis based on the test results, the expression for frictional bond strength and maximum slip value was derived as a function of ultimate bond strength as:

$$\tau_f = 0.46 * \tau_{max} \quad (4-15)$$

$$S_2 = 0.28 * \tau_{max} + 0.63 \leq l_r \quad (4-16)$$

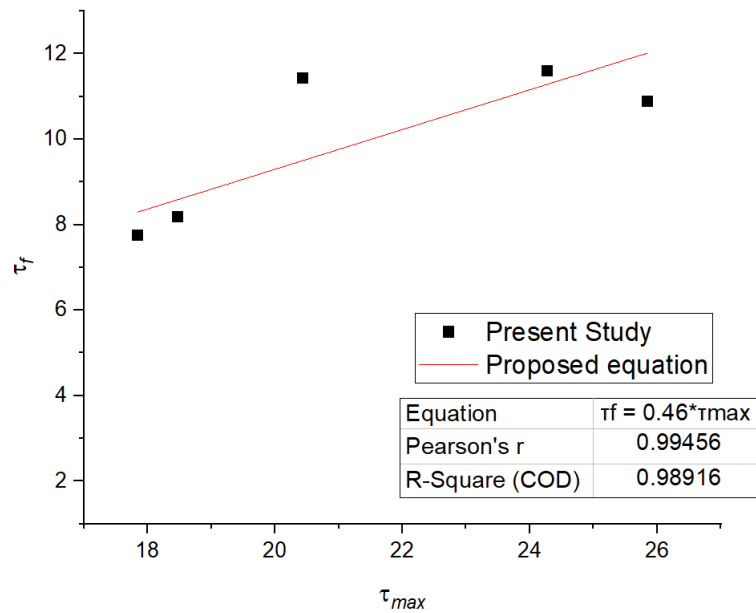


Figure 4-10 Influence of maximum bond strength on frictional bond

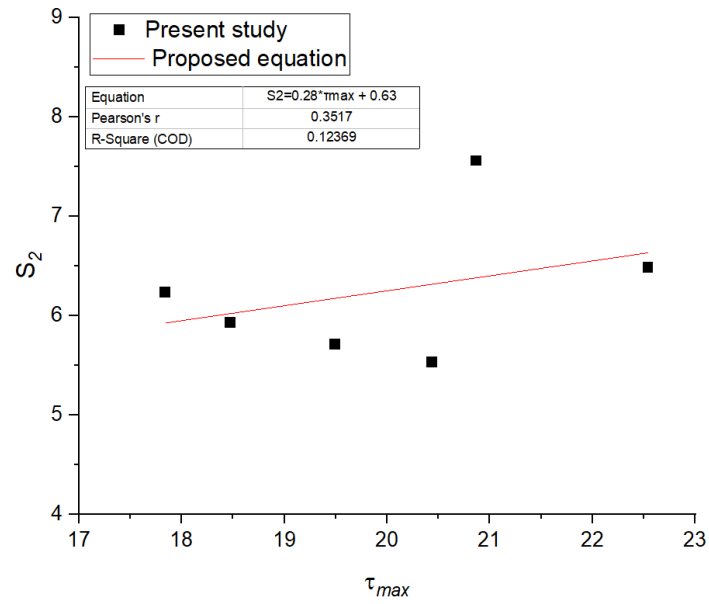


Figure 4-11 Influence of bond strength on S_2

It should be noted that the maximum slip is reliant on the clear distance between the ribs of the reinforcement (l_r), as this defines the point at which shearing of the concrete keys between ribs occur (Albitar et al. 2017b).

4.3.1.4 Comparison of experimental result with bond-slip model

Based on the CEB-FIB (2010) model used to describe the bond-slip relationship and the linear regression analysis performed on the bond properties for geopolymer concrete, the bond stress-slip model was modified to be used for bond-slip analysis for geopolymer concrete and equation 4-17 to 4-19 was proposed.

$$\tau = \tau_{max} \sqrt{\frac{S}{S_1}} \text{ for } S < S_1 \quad (4-17)$$

$$\tau = \tau_{max} - (\tau_{max} - \tau_f) \left(\frac{S - S_1}{S_2 - S_1} \right) \text{ for } S_1 < S < S_2 \quad (4-18)$$

$$\tau = \tau_f \text{ for } S > S_3 \quad (4-19)$$

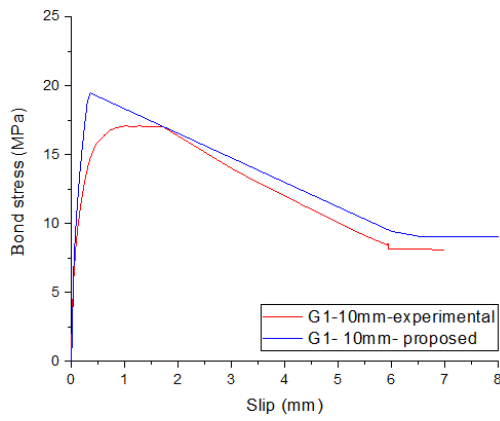
where, $\tau_{max} = 1.23 \left(\frac{c}{d} \right)^{1/2} \sqrt{f_c}$

$$S_1 = 0.07 * \tau_{\max} - 0.68$$

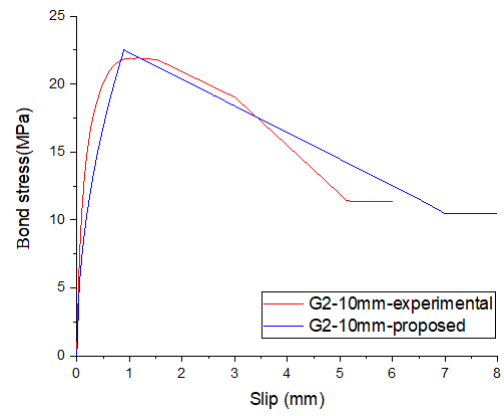
$$\tau_f = 0.46 \tau_{\max}$$

$$S_2 = 0.28 * \tau_{\max} + 0.63$$

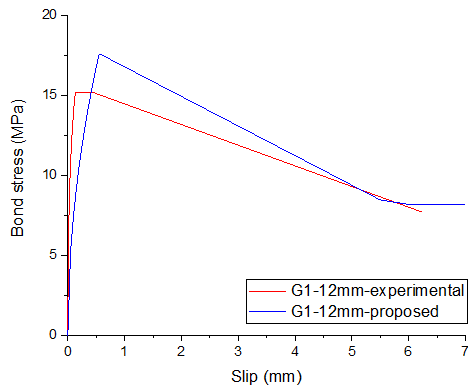
Figure 4-12 demonstrates the bond-slip curve for geopolymer concrete obtained from pull-out tests and compared against the proposed model.



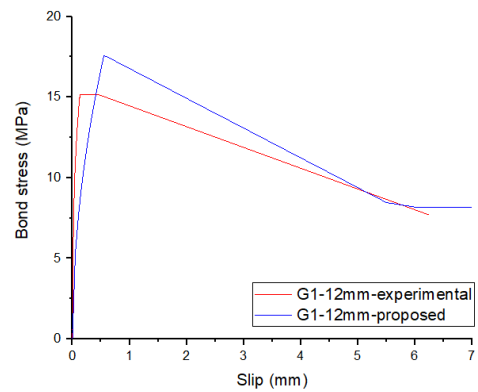
(a)



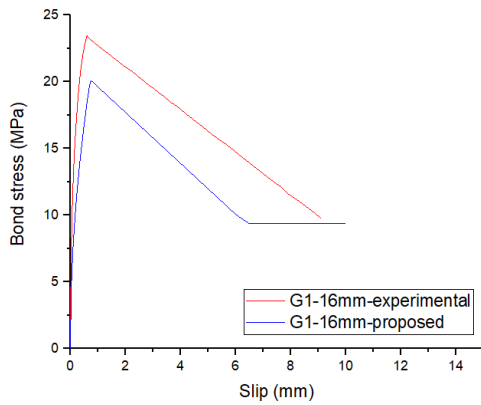
(b)



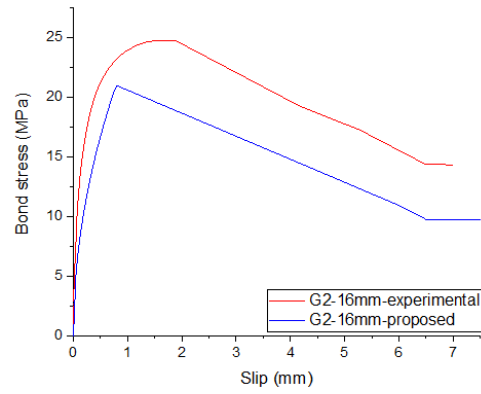
(c)



(d)



(e)



(f)

Figure 4-12 Bond stress-slip model validation for 10 mm, 12 mm and 16 mm reinforcement bar sample for geocem 1 and geocem 2

Referring to Figure 4-12, it can be noted that the proposed bond-slip relation is able to predict reasonably close bond stress-slip behaviour, while for 16mm reinforcement case the bond-slip prediction was relatively on the lower limit of the 95% confidence level of the equation proposed from regression analysis. This bond stress-slip model can thus be used to predict the bond-slip behaviour for reinforcement bar embedded in geopolymer concrete.

4.4 Summary

In this chapter, experimental study of the bond stress-slip behaviour of geopolymer concrete was carried out using pull-out test method. With an objective to establish the bond stress-slip relation to be used in analytical study of geopolymer concrete structure, the bond test was conducted for both geocem 1 and geocem 2 concrete along with OPC concrete. To study the effect on bond strength development due to reinforcement bar size and its embedment length, parametric study was also carried

out. Based on the test results, regression analysis was carried out to propose suitable empirical equations to define the bond stress-slip relation between reinforcement bar and geopolymer concrete to be used in numerical analysis of geopolymer concrete pipe. From the experimental and analytical study carried out, following conclusions were drawn.

- Pull-out failure in bond test sample with 3d embedment length for both geopolymer type concrete was observed, most of the bond test samples for both geopolymer concrete and OPC concrete with 5d and 7d embedment length failed by splitting. The pull-out failure is due to sufficient confinement of reinforcement bar in geopolymer concrete. Further, for splitting failure, failure in geopolymer concrete was observed to be brittle which can be due to the generation of higher radial force in geopolymer concrete corresponding to high pull-out force compared to OPC concrete sample.
- Compared to same grade OPC concrete, development of high compressive and tensile strength in geopolymer concrete contributed towards development of higher bond strength capacity in geopolymer concrete.
- The parametric study carried out to examine the influence of reinforcement diameter on bond strength development showcased increase in reinforcement diameter from 10 mm to 12 mm induced reduction in bond strength while for increase from 12 mm to 16 mm demonstrated increase in bond strength. While the general trend of increase in bond strength with decreasing reinforcement bar is observed, such bond strength development, apart from bar size, is also affected by rib height and clear distance between ribs in reinforcement bar.
- Similarly, for increase in embedment length decrease in bond strength was observed for both geopolymer concrete types and OPC concrete and for all size

of reinforcement bar which is due to increase in bond area between geopolymer concrete and reinforcement bar, thus inversely affecting the bond strength development in concrete specimen.

- The bond stress-slip relation for geopolymer concrete was defined based on CEB-FIB model for concrete, with empirical equations for key points obtained from regression analysis of the test results for geopolymer concrete. The empirical formulas predicted the bond-slip relationship for reinforcement bar embedded in geopolymer concrete within 95% prediction level.

Chapter 5

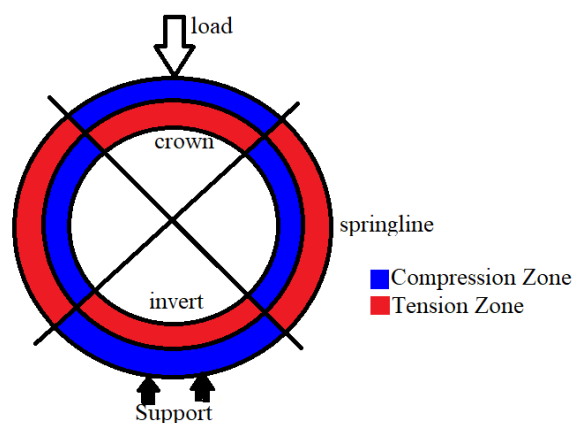
5. Finite element modelling of reinforced concrete pipe

5.1 Background

The reinforced concrete pipes are extensively studied precast concrete structures. Several experimental researches have been conducted to investigate the structural performance of the precast concrete pipes considering different factors like pipe diameter, wall thickness, reinforcement requirement, use of different fibre reinforcement and optimum fibre content (de la Fuente et al. 2011; Haktanir et al. 2007; Hendrickson Jr 1955; Mohamed & Nehdi 2016; Peyvandi, Soroushian & Jahangirnejad 2013; Younis et al. 2021). The structural performance of concrete pipes during experimental analysis are measured against its ultimate load carrying capacity and crack width formation (ASTMC76M 2022; Haktanir et al. 2007). The stress developed in pipe due to loading divides the pipe into two zones: tension and compression zone as shown in Figure 5-1. Concrete behaves strongly in compression and is weak in tension, as such cracks are observed in the tension zone of the pipes as loading increases. During TEB test, when loading is applied to the pipe, cracks begin to develop initially at inner part of crown and invert and subsequent development of crack at outer part of the spring line is observed as loading increases (Davies et al. 2001; Haktanir et al. 2007; Shrestha 2014; Younis 2020; Yu et al. 2016). As the loading further continues in TEB test, ultimate strength failure in pipe can be experienced either due to longitudinal cracks in the crown, invert and springline of the pipe or diagonal and radial tension cracks propagating diagonally through the pipe wall and in radial direction (Hogan 2017; Zamanian 2016). Such longitudinal cracks along the pipe leads to formation of plastic hinge in pipe, thereby causing flexural

failure of the pipe (Figure 5-1b), while the shear or radial failure in pipe (Figure 5-1c) is characterised by diagonal or radial cracks occurring due to radial tension force acting in circular reinforcement bars, causing separation of reinforcement bars from concrete (Heger 1963). After experimenting the single and double cage reinforced concrete pipe under TEB test, Ramadan (2020) reported flexural failure to be principal failure mode in double cage reinforced concrete pipe, while for single cage reinforced concrete pipe radial tension failure governed the failure mode leading to spalling of concrete section. Haktanir et al. (2007), Abolmaali et al. (2012) and Mohamed, Soliman & Nehdi (2015) states for SFRC pipes, flexural failure is commonly observed failure mode.

As carrying out such destructive tests are uneconomical and often inefficient considering the need of human judgement to identify the crack formation with 0.15 mm to 0.3 mm wide during the TEB test. Hence, numerous researchers have relied on numerical modelling of concrete pipes to examine the load bearing capacity and load-deflection behaviour of concrete pipes.



(a) Stress zone in pipe under loading



(b) Flexural cracks in pipe



(c) Radial tension cracks

Figure 5-1 Stress zone in pipe and failure mode in reinforced concrete pipes

de la Fuente et al. (2011) and de Figueiredo et al. (2012) simulated TEB test using MAP (Mechanical Analysis of Pipes) model to study the mechanical behaviour of steel fibre reinforced concrete pipe. The results from the numerical simulation were tallied against experimental results, concluding the efficiency of numerical model to design fibre reinforced concrete pipes since the model gave an average error of 7%, which was within the acceptable contingency range. Similarly, Ferrado, Escalante & Rougier (2018) used ABAQUS software to simulate the steel fibre reinforced concrete (SFRC) pipes. Considering SFRC as homogenous material, the behaviour of SFRC was defined by compression and uniaxial tension curve based on theoretical formulation in existing literature. The load-deflection behaviour and stress distribution for the pipes from experiment matched well with the numerical analysis results. Likewise, a numerical modelling of concrete pipes with different diameter and reinforcement configuration was conducted by Younis et al. (2021), to explore the predictability of service load and ultimate load. Following the concrete damage plasticity (CDP) model equation developed by other authors, the non-linear behaviour

of concrete in compression and tension was defined for the finite element model. Based on the analysis and experimental results, an average prediction error of around 6% for both service load and ultimate load was reported, suggesting the reliability of numerical modelling for design of concrete pipes.

While numerous attempts to study the structural response of OPC concrete pipes for different cases have been noticed, similar contribution towards investigation of structural performance of geopolymer concrete pipes has not been made till date. Hence, based on the validated finite element model for concrete pipes, this study aims to explore the structural behaviour of geopolymer concrete pipes.

In this chapter, development of 3D finite element model of geopolymer concrete pipe to simulate TEB test has been discussed. The model was validated against the experimental load-deflection responses for 450mm OPC concrete pipe. The model was also validated against the experimental data and the finite element analysis results available for OPC concrete pipes in literature. The validated model was updated for geopolymer concretes based on the mechanical properties obtained from experimental tests for grade 50 MPa geopolymer concrete. The empirical equation defining the bond-slip behaviour proposed in previous chapter was assimilated in the finite element model to imitate actual TEB tests on reinforced geopolymer concrete pipes. Subsequently, the numerical model was used to conduct parametric study for reinforcement area, concrete cover and yield strength of steel reinforcement. The results were analysed in comparison to OPC concrete pipe results.

5.2 Experimental program

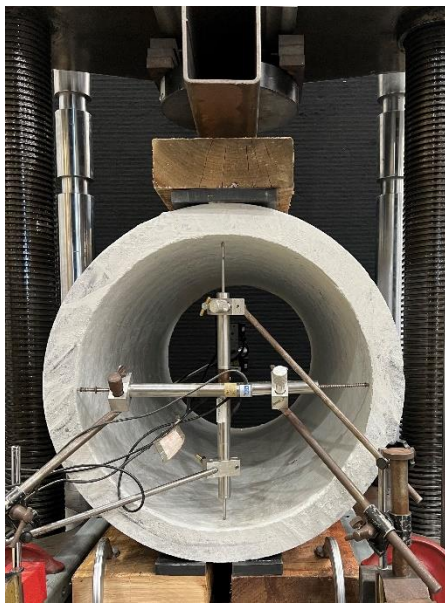
To study the structural response of the reinforced concrete pipe, Three Edge Bearing (TEB) test was performed according to AS/NZS4058 (2007). The TEB test is the standard test developed to assess the structural behaviour of the concrete pipe. The loading condition for the pipe in TEB test is severe and concentrated at the crown of the pipe, unlike the uniformly distributed earth load in underground pipe, however, it is a convenient method commonly used to evaluate the quality of reinforced concrete pipes within the design requirements (AS/NZS4058 2007; ASTM C76M 2022; Tehrani 2016). The main purpose of conducting this test was to determine the load-deflection behaviour of reinforced concrete pipe to be used for validation of FEA model. Table 5-1 provides the detail of the concrete pipe used in the test.

Table 5-1 OPC concrete pipe details

Class	4
Nominal diameter	450 mm
Effective length	900 mm
Wall Thickness	44 mm
Concrete strength	65 MPa
Required Proof load as per AS/NZS 4058	40 kN/m
Required Ultimate load as per AS/NZS 4058	60 kN/m

For the test, a full scale dry precast concrete pipes of class 4 with nominal diameter of 450mm and wall thickness of 45mm manufactured according to

AS/NZS4058 (2007) was evaluated. However, due to the size limitation of the hydraulic Universal Testing Machine (UTM) used for the test, the full-length pipe with effective length of 2.25m was cut to produce pipes of length 900mm. A total of 3 pipes of 900mm length were tested. In TEB test, the pipe is supported on bottom by two wooden bearers with rubber in between the pipe and the bearers, and uniform load is imposed along the length of pipe barrel through a timber bearer at the top of the pipe. The test set up of TEB TEST along with 4 sets of LVDTs mounted to measure the vertical and horizontal deflection in pipe is shown in Figure 5-2a. The UTM was loaded at the rate of 10 kN/min and the data acquisition was carried out through the LVDTs.



a) Three Edge Bearing Test set up



b) Feeler gauge to measure crack

Figure 5-2 Test set up for pipe with LVDTs installed to measure load-deflection behaviour of pipe

As per the specified design load and ultimate load requirement in AS/NZS4058 (2007) for 450 mm diameter pipe, the required design load and ultimate load for 900

mm long pipe is calculated to be 36 kN and 54 kN respectively. The standard further specifies the acceptable crack width for the pipe during testing. The ASTM C76M (2022) also specifies the design requirement for particular class pipe in terms of D-load equivalent to load creating 0.3 mm crack during the test and the ultimate load. As such, pipe performance was also checked for crack width development using feeler gauge (Figure 5-2b) during the loading of the pipe. According to the data obtained for the 3 sample tests carried out on 450mm diameter pipe presented in Figure 5-3 the peak load was observed to be 45 kN on average, while the ultimate load capacity was approximately noted to be 50 kN on average. The average ultimate load was noted to be less due to the difference in casting of the selected sample pipe. The test pipe 3 was casted 15 days before test pipe 1 and 3 which affected the final strength development in the pipe.

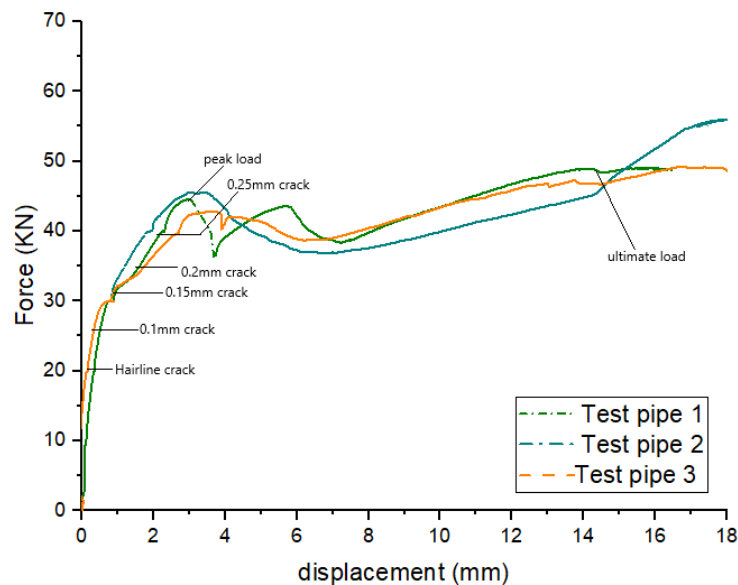


Figure 5-3 Measured load-deflection curves for the reinforced concrete pipes

During the test, for test pipe 1, the first visible hairline crack in the pipe was observed on the inner side of the crown and invert of the pipe for load corresponding to 20 kN. As the loading was applied continuously, the crack of 0.1 mm, 0.15 mm, 0.2

mm and 0.25 mm was measured successively at the load of 26.58 kN, 31.11 kN, 35.74 kN, and 40 kN Figure 5-4(a-e). Longitudinal crack formation was noticed on the outer side of the springline as the loading progressed. Figure 5-4 demonstrates the crack development in the concrete pipe under continuous loading.



1) Hairline crack



2) 0.1 mm crack



3) 0.15mm crack

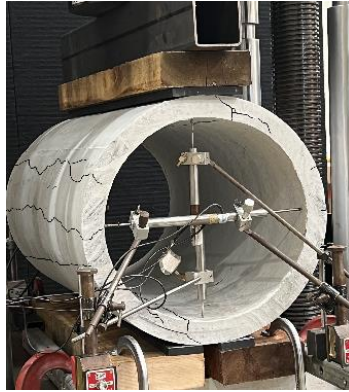


4) 0.2 mm crack



5) 0.25 mm crack

6) Ultimate load



7) Longitudinal crack at springline

Figure 5-4 Crack development in Test pipe 1 at different loading phases

It was observed that with increasing load, longitudinal cracks were developed initially in the inner part of the concrete pipe and as the crack of 0.1 mm was noticed visible cracks in the outer part of the springline was also noticed. During the loading of the pipe, when the concrete loses its stiffness, a sudden drop in the loading capacity was noticed, which was restored as the reinforcement supported the load. This loading behaviour was observed in all three samples until the ultimate load was reached, after which gradual drop in the loading capacity was observed. For all pipe samples, flexure failure was observed.

The experimental results obtained for load-deflection behaviour of reinforced OPC concrete pipe was then used as reference to refine the finite element model of concrete pipe under TEB test.

5.3 Finite element modelling of Three-Edge Bearing test

Most of the researches on finite element modelling of concrete pipes have been carried out for fibre reinforced concrete pipes. In existing literature, limited number of researches on reinforced concrete pipes are based on finite element modelling. Tehrani (2016) and Younis et al. (2021) used ABAQUS software to conduct finite element modelling of concrete pipes, where concrete damaged plasticity (CDP) model was used to define the non-linear behaviour of concrete in compression and tension, while Kataoka et al. (2017) used DIANA software where material characteristics were defined by using total strain model for concrete and Von Mises plasticity model for reinforcement bars. These studies were based on OPC concrete reinforced pipes and validated against the experimental results. This study contributes to the current-state-of-the art by conducting implicit finite element analysis (FEA) of geopolymer concrete pipes using commercially available software ANSYS LS-DYNA. Implicit analysis was performed on the pipe deflection under TEB tests.

5.3.1 Material modelling

5.3.1.1 Concrete model

Considering the complex material behaviour of concrete which includes elastic, non-linear plastic behaviour and material damage, available concrete damage models for numerical modelling of concrete structures are often quite complex as these material models often contain parameters whose values are difficult to obtain from simple tests or whose values have only mathematical meaning and no physical meaning (Kral et al. 2017). To date, there are a lot of material models available to simulate the concrete damage behaviour (Abedini & Zhang 2021; Xu & Wille 2015).

Among them, one simple concrete damage model implemented in LS-DYNA to model concrete behaviour is the Karagozian and Case (K&C) concrete model. A key merit of using K&C concrete model for numerical simulation of concrete behaviour is its reliance on just one main input parameter of unconfined compressive strength. Schwer & Malvar (2005) stated that K&C concrete model can be utilised for analysis involving new concrete materials with no detailed information available to characterise the concrete beside its compressive strength, owing to the fact that the unconfined compressive strength of the concrete not only describes the elastic response, but also accounts for inelastic response including shear failure, compression and tensile failure.

The K&C concrete model is a three-invariant model characterised by three shear failure surfaces: i) yield surface ii) maximum shear failure surface and iii) residual surface. The shear surfaces of K&C concrete model as demonstrated by Malvar et al. (1997) is shown in Figure 5-5.

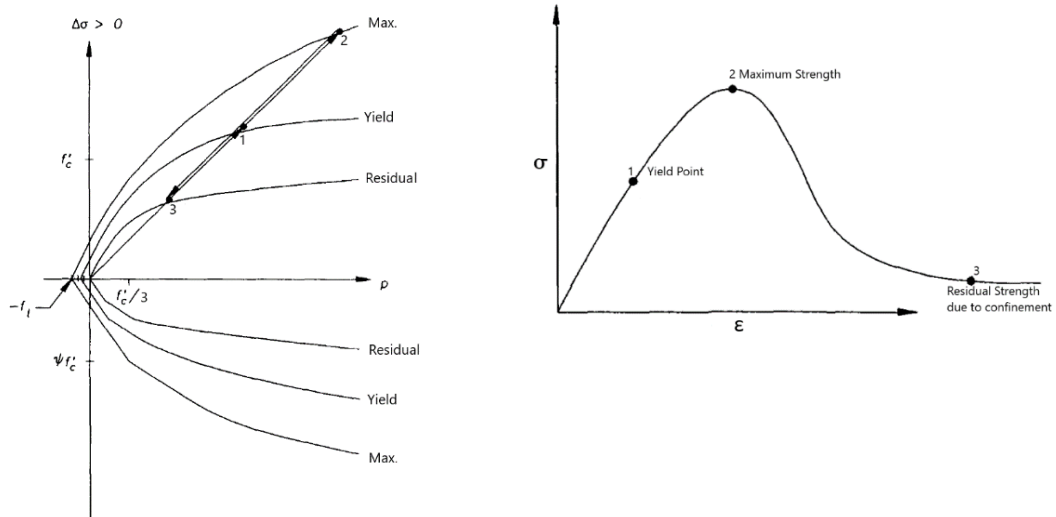


Figure 5-5 Three failure surface of K&C concrete model (Malvar et al. 1997)

The material constitutive behaviour of the K&C concrete model shown in Figure 5-5 can be described into three parts; for initial loading, the deviatoric stresses is elastic

until it reaches the yielding point 1, after which it increases further till the limit surface 2. Following the maximum yield surface, perfectly plastic or softening behaviour up to the residual yield surface 3 can be observed. These shear failure surfaces are mutually independent and can be formulated as (Malvar et al. 1997; Wu, Crawford & Magallanes 2012):

$$F_i(p) = a_{0i} + \frac{p}{a_{1i} + a_{2i}p} \quad (5-1)$$

where, i stands for either yield strength surface (y), maximum strength surface (m) or residual strength surface (r), p is the pressure calculated as $\frac{-I_1}{3}$, I_1 is first invariant of stress tensor and the variables a_{ji} ($j=0,1,2$) are the parameters calibrated from test data.

The resulting failure surface is interpolated between the maximum strength surface and either the yield surface or the residual strength surface as per the following equations:

$$F(I_1, J_2, J_3) = r(J_3) [\eta(\lambda) (F_m(p) - F_y(p) + F_y(p))] \quad \text{for } \lambda \leq \lambda_m \quad (5-2)$$

$$= r(J_3) [\eta(\lambda) (F_m(p) - F_r(p) + F_r(p))] \quad \text{for } \lambda \geq \lambda_m \quad (5-3)$$

where, I_1 is first invariant of stress tensor, J_2 and J_3 are second and third invariants of deviatoric stress tensor, λ is the modified effective plastic strain or the internal damage parameter, $\eta(\lambda)$ is the function of the internal damage parameter λ , with $\eta(0) = 0$, $\eta(\lambda_m) = 1$ and $\eta(\lambda \geq \lambda_m) = 0$, and $r(J_3)$ is the scale factor in the form of the William-Warnke equation (Chen & Han 1988).

The K&C concrete model considers the effect of strain rate, failure and different mechanical-physical properties in compression and tension and hence suitable for concrete modelling (Kral et al. 2017). Based on uniaxial compressive

strength, material parameters are generated, requiring to define only few parameters for the functionality of the material model. In the material model, more parameters can be defined if required. The model requires 49 parameters to be defined along with equation of state, which is complicated as many parameters have only mathematical meaning. Hence, the developers advocate to use parameter generation if the data to define the material is not available. The default parameters in K&C concrete model has been calibrated using the uniaxial, biaxial and triaxial test data that was available for well characterised concrete and using the relationship such as tensile strength and modulus of elastic as function of compressive strength (Schwer & Malvar 2005).

Numerous researches have been undertaken to assess the credibility of the K&C concrete model along with other models. Magallanes (2008) used four material models: Johnson–Cook (HJC) model, Continuous Surface Cap (CSC) model, Karagozian and Case (K&C) concrete model and Brittle Damage Concrete (BDC) model to simulate the damage in reinforced concrete wall and column due to impact loading. It was reported that while HJC and BDC model underestimated the response of the wall and column, the CSC model only favourably predicted the response of reinforced wall while it showed erroneous localised shear failure in column. For both cases of reinforced concrete wall and column, the K&C concrete model appeared to represent the overall deformation favourably, confirming to the suitability of use of K&C concrete model to capture the structural response of reinforced concrete structure with only one parameter. The study carried out by Tu & Lu (2009) to evaluate the concrete model suggested the need to define compressive and tensile strength to capture the concrete behaviour even in the absence of elaborate data to capture all parameter values which are usually generated automatically based on compressive strength value.

Since the experimental test results and past studies on mechanical properties of geopolymer concrete revealed that even though the mechanical performance of geopolymer concrete was better than OPC concrete, the general relationship for determining mechanical properties of OPC can conservatively define geopolymer functioning. Hence, the K&C concrete model was used for both OPC concrete and geopolymer concrete modelling for finite element analysis. For the purpose of the study, 4 parameters were defined as described in Table 5-2.

Table 5-2 Parameters used for material modelling

Parameter	Description	Unit
A0	Uniaxial compressive strength, f_c	MPa
Ft	Uniaxial tensile strength, f_t	MPa
R0	mass density	mg/mm ³
PR	Poisson's ratio	-

5.3.1.2 Reinforcement steel behaviour

The mechanical behaviour of reinforcement bars typically demonstrates same stress-strain behaviour in tension and compression (Kwak & Filippou 1990). The steel reinforcement under uniaxial tensile test typically exhibits the linear elastic stage followed by a yield plateau and a strain hardening range where corresponding increase in stress with respect to strain can be observed until the stress limit drops off to failure. Figure 5-6 showcase the standard stress-strain curve of the reinforcement bar.

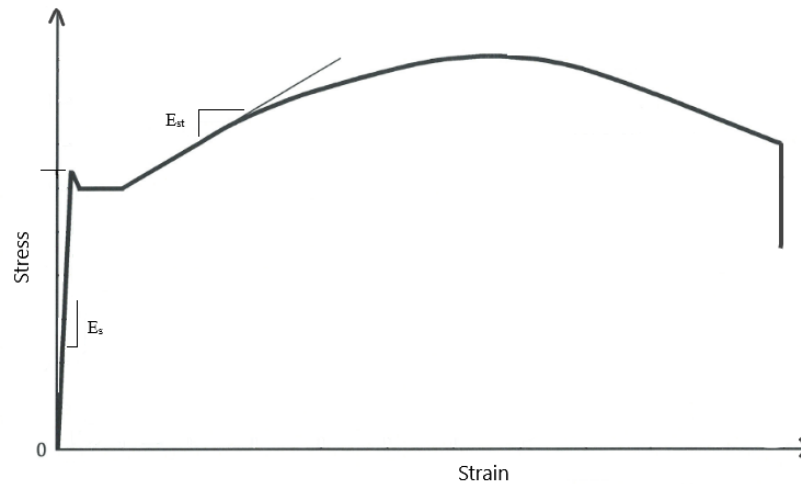


Figure 5-6 Tensile stress-strain curve of steel reinforcement

In numerical study, an elastic-plastic constitutive relationship for reinforcement bar, with or without strain hardening, is commonly adopted for numerical analysis. Figure 5-7 (a) shows the idealised elastic-perfectly plastic model for the steel, which neglects the strength increase due to strain hardening. This model has been used for numerous finite element analysis study (Chen, Teng & Chen 2011; Chen et al. 2008; Obaidat, Heyden & Dahlblom 2010). However, such elastic-perfectly plastic assumption often fails to capture the steel stress at high strain and accurate assessment of the strength of structure at large deformation cannot be made (Supaviriyakit, Pornpongsaroj & Pimanmas 2004). Hence more accurate idealisation of stress-strain curve as shown in Figure 5-7 (b) has been used.

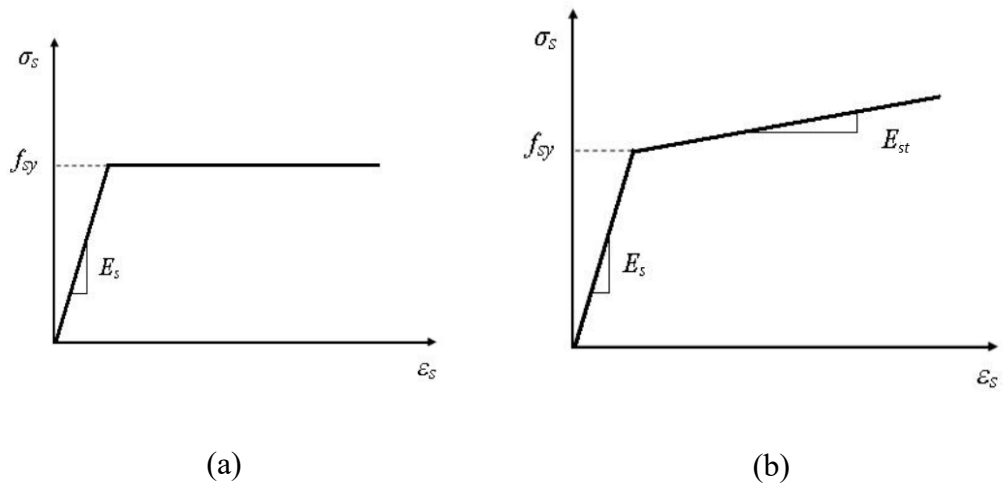


Figure 5-7 Typical stress-strain curve of steel reinforcement representing (a) ideal elastic-perfectly plastic model (b) bilinear elastic-plastic model with linear strain hardening (Du & Jin 2021)

The Piecewise Linear Plasticity model used to represent the steel reinforcement behaviour in LS-DYNA considers the plastic deformation, strain rate effects and failure (Abedini & Zhang 2021). For Piecewise Linear Plasticity model stress-strain curve for the reinforcing steel is treated as bilinear by defining the tangent modulus (LSTC 2014). The steel response is thus, defined by parameters like Young's modulus (E_s), yield strength (f_{sy}) and hardening modulus (E_{st}). The magnitude of hardening modulus E_{st} in the plastic regime is commonly set to 1% of Young's modulus (Elnashai & Izzuddin 1993; Xiao 2015).

5.3.2 Model components

A 3D finite element model to simulate TEB test for the pipe was developed. The finite element model comprised of three components: concrete, reinforcement bars and bearing strips. The pipes of diameter 450 mm, 825 mm and 1200 mm and length

1000 mm were modelled for investigation. The reinforcement bars in the FEM of reinforced concrete is modelled using either smeared or discrete steel formulation (ASCE 1982; Chong 2004). In smeared steel formulation, the steel bar and concrete are represented in the same element and full compatibility between steel and concrete is imposed. In discrete steel formulation, separate element is used to represent the steel bar and are overlayed on the boundary of concrete elements by connecting nodal points. As such, the smeared steel formulation is suitable when the global response of a structure is taken into consideration, and when stresses within specific steel or concrete elements needs to be analysed, discrete formulation should be considered. Hence, in this study, discrete steel formulation was adopted to model the reinforcement bars.

The concrete pipe and bearing strips were modelled using a 3D solid element (SOLID164). Similarly, beam element (BEAM 161) was used to model reinforcing steel bars. The lower bearing strips in pipe were set at $d/12$ mm (where d is the pipe inner diameter) distance apart as suggested in AS/NZS4058 (2007) (Figure 5-8a). As the bearing strips were used to mimic the loading condition in TEB test, the lower bearing strips were fixed to avoid translational and rotational degree of freedom, while the upper bearing strips were restricted in all direction except for vertical displacement movement to allow for displacement controlled loading in the pipe. The interface between the pipe and the bearing strips were defined by an automatic contact in the FE simulation. Modelling of contact surface is crucial for the simulation accuracy. In the present study, the concrete part and boundary part are identified as contact slave and master parts. Contact is defined by identifying the potential penetration of slave node through master segment using a number of different algorithms at every time step (LSTC 2023). Thus, in automatic surface to surface contact, compression loads are

transferred between the slave nodes and the master segments, checking for penetration on both slave and master. If penetration is found, a force proportional to the penetration depth is applied to resist, and ultimately eliminate the penetration. Hence, fine mesh for the rigid body is necessary for contact force to be distributed realistically and to replicate deformable body.

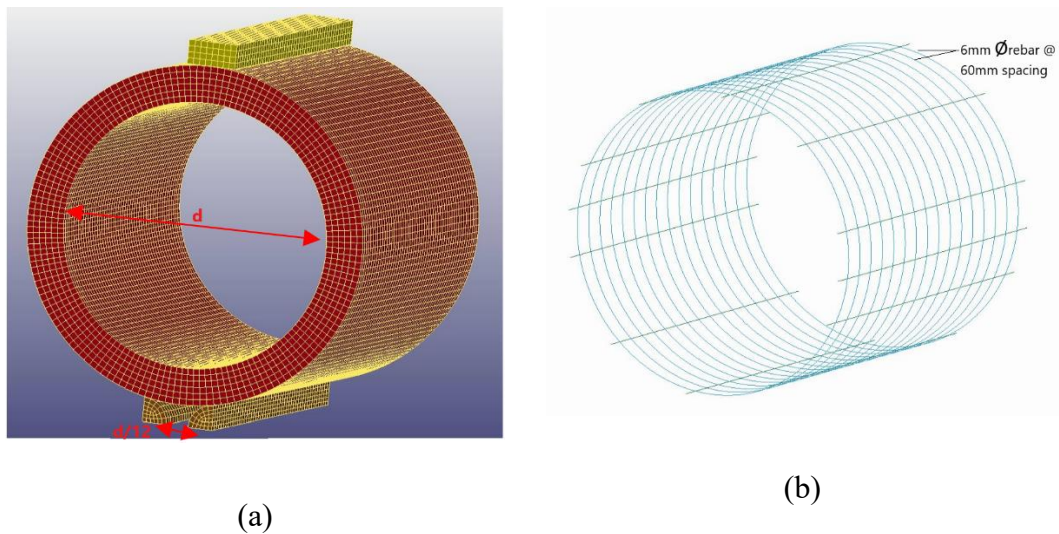


Figure 5-8 3D model of reinforced concrete pipe (a) solid element mesh for concrete material (b) single cage steel reinforcement bar in 825 mm diameter pipe

5.4 Model validation

5.4.1 Material model verification

To verify the material model credibility, the uniaxial compressive test carried out on the OPC concrete was simulated. The model was developed as per the model specification for compressive strength test on OPC concrete cylinder. The bottom supporting plate was fixed, while only translational degree of freedom in vertical direction was allowed for the cylinder and the top supporting plate. For the K&C concrete model, compressive strength of 50 MPa and tensile strength of 2.03 MPa was

defined. The cylinder was subjected to displacement load of 3 mm. Stress developed on the cylinder was obtained by dividing the resultant force acting on the cylinder by the cylinder area. Similarly, the strain was obtained as a ratio of displacement to the total length. Figure 5-9 shows stress development in the cylinder under compressive load.

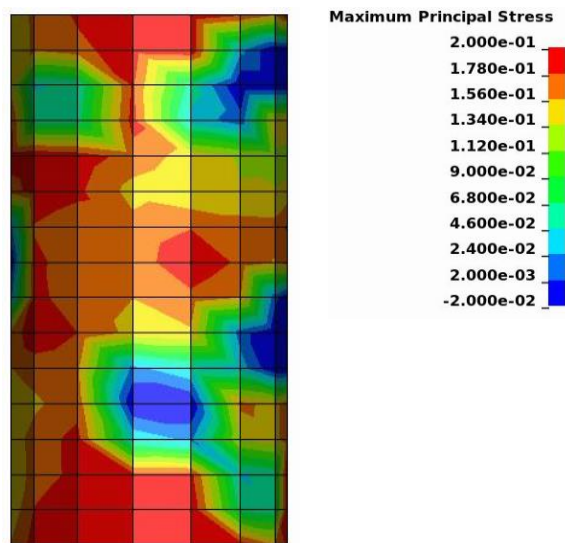


Figure 5-9 Uniaxial Compression test simulation

The compression test analysis was also used for mesh sensitivity analysis. The cylinder was modelled for mesh sizes of 10 mm, 20 mm and 40 mm. Figure 5-10 showcase the stress-strain curve attained from the analysis of compressive strength test on OPC concrete. It was observed that the result obtained for 20 mm and 40 mm mesh size matched more closely than the 10 mm mesh size cylinder. The stress value obtained from the analysis of 20 mm and 40 mm meshed cylinder was approximately 52 MPa, as obtained for the OPC concrete from compressive strength test (Table 5-3), justifying the applicability of K&C concrete model for finite element analysis.

Considering the time required for analysis, 20 mm mesh size was used for further analysis of the concrete pipes to maintain reasonable execution time.

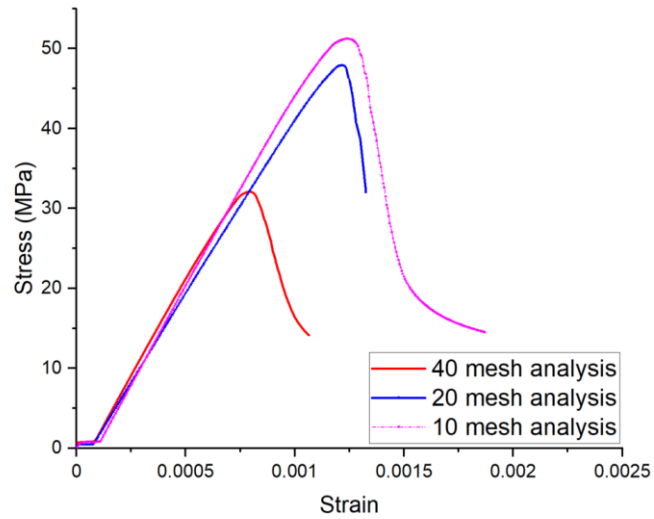


Figure 5-10 Sensitivity analysis of the model

Table 5-3 Compressive strength of OPC concrete obtained from uniaxial compression test

Sample	Failure load (kN)	Area of cylinder (mm ²)	Compressive strength (MPa)
1	411.71	7853.98	52.42
2	381.30	7853.98	48.55
3	445.91	7853.98	56.78
4	411.71	7853.98	52.42
Average Compressive strength			52.54

5.4.2 Validation of finite element model of reinforced concrete pipe

The finite element model to simulate the TEB test in concrete pipe was modelled for 825 mm diameter pipe. Table 5-4 provides details of the pipe geometry used to formulate the model. The 3D model of the pipe and the reinforcement details of the pipe is shown in Figure 5-8.

Table 5-4 Pipe details

Inner diameter	825 mm
Wall thickness	114 mm
Effective length	1000 mm
Area of inner steel (A_{si})	484 mm ² /m
Circular reinforcement	6 mm dia. rebar @ 60 mm spacing

Static non-linear analysis was carried out by applying displacement load to the pipe through upper bearer. Total displacement of 20 mm was defined for the analysis. Load-deflection curve was obtained for the analysed pipe and are presented in terms of design load (kN) and deflection (δ) as a percentage of pipe diameter (shown in Figure 5-11).

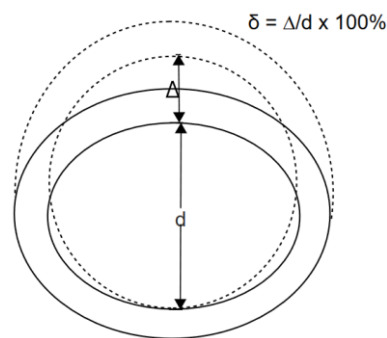


Figure 5-11 Calculation of deflection percentage

For the model generation, concrete compressive strength of 60 MPa was considered to be compared with the experimental data of 60 MPa OPC concrete pipe found in literature, while tensile strength value for OPC concrete was obtained based in relation to compressive strength given in AS3600 (2018). The accuracy of the pipe FEA model was compared against the peak load (D_{peak}), where 0.3 mm crack develops, and ultimate load (D_{ult}). It can be observed from Figure 5-12 that the model overestimated the value of D_{peak} load and D_{ult} by 28% and 18% compared to experimental load data. Since peak load is an indicator of crack load, the overestimated value of peak load showed error with consideration of tensile strength value of the concrete.

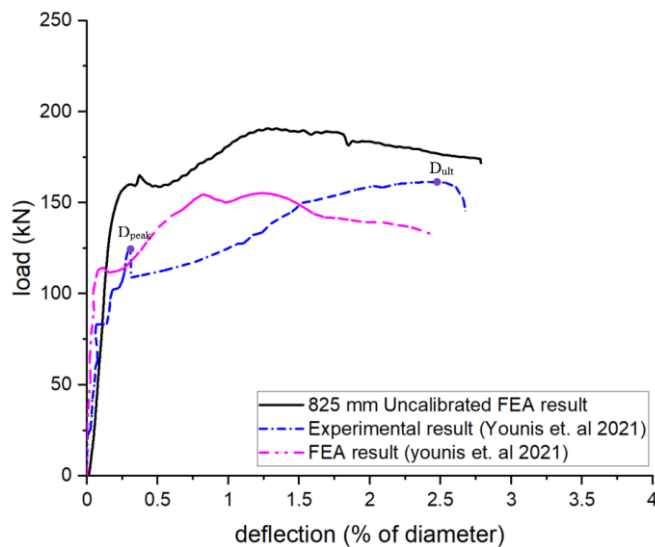


Figure 5-12 Load-deflection plot of un-calibrated FEA model

The numerical model was found to be sensitive to the tensile strength parameter of the concrete model. Depending on design mix of concrete, aggregate type, curing environment and concrete age, the concrete samples generally have different tensile strengths (CEB-FIB 2010). So the FEA model was calibrated for tensile strength parameter for concrete. After calibration, the load- deflection behaviour captured by

the FEA model was close to the experimental result as seen in Figure 5-13. The variation in FEA result with respect to experimental results were found to be 4% and 7% for peak load and ultimate load respectively.

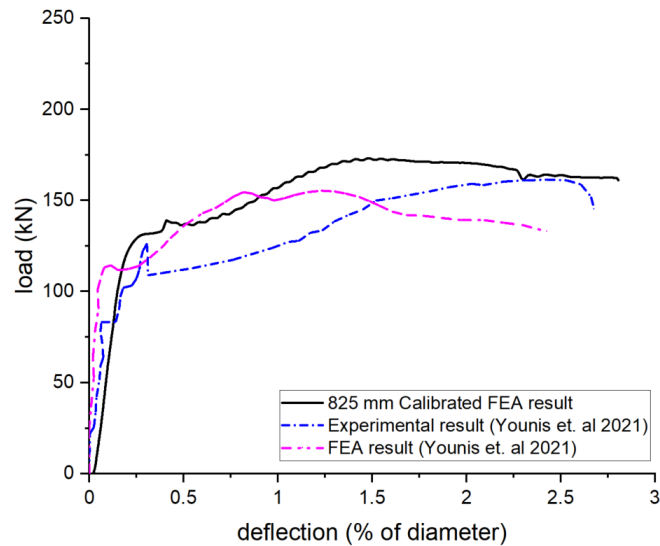


Figure 5-13 Load-deflection plot of 825mm pipe after calibration

The FEA result from LSDYNA was also compared with the FEA plot based on ABAQUS from the literature and it was observed that while FEA model in literature produced conservative result from analysis for ultimate load strength, the FEA model in LS-DYNA more closely represented the experimental results.

Additionally, the validated FEA model was then used to compare with the experimental results for 450mm pipe of 900mm length with wall thickness of 44 mm obtained for experimental test carried out in section 5.2. The developed FEA model well represented the experimental load-deflection behaviour as shown in Figure 5-14, indicating the model to be appropriate for further use in parametric studies.

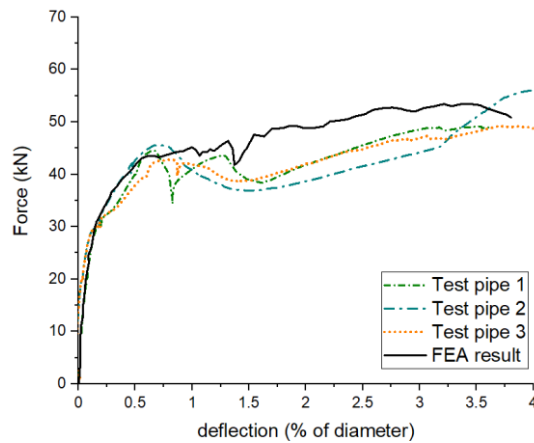
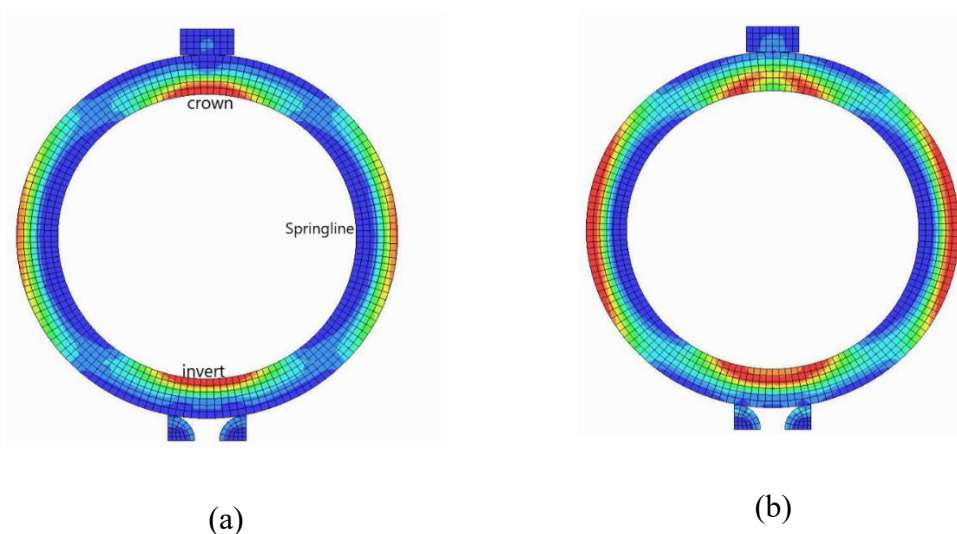
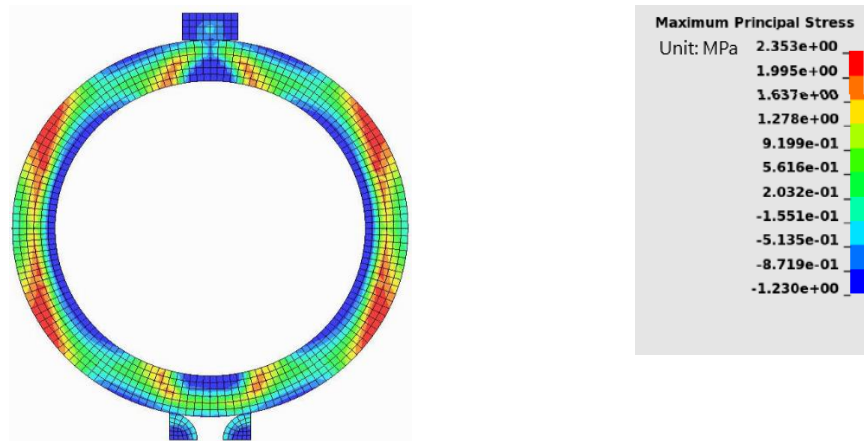


Figure 5-14 Experimental and FEA model results comparison for 450mm pipe

5.4.3 Stress development in concrete pipe

Figure 5-15 shows the propagation of stress along the concrete pipe during TEB test. The simulation shows the stress development in the model to be in agreement with the typical stress development in the pipe during TEB test. It is evident that stress develops initially at the inner face of the crown and invert and on the outer part of the spring-lines (Peyvandi, Soroushian & Jahangirnejad 2014; Ramadan et al. 2020). This initial stress development in elastic phase of loading where about 30% of the total load was applied to the pipe was clearly observed in Figure 5-15(a).





(c)

Figure 5-15 Stress distribution in 825mm OPC concrete pipe when load application is (a) 32% (b) 68% (c) 80% of total applied load

With the increase in the loading, the stress in the concrete continuously increased, and as the loading increased to the peak load, formation of crack in the crown and invert can be realised as the shift in stress from crown and invert towards the bearers was observed as in Figure 5-15b. This diagonal shift in stress is characterised by diagonal shear cracking in experimental test (Ramadan et al. 2020; Younis et al. 2021). Further, as the loading in the pipe increased to ultimate stage, the load resistance capacity in cracked section decreased causing the stress to transfer towards undamaged area in the upper and lower haunches of the pipe which is evident in Figure 5-15c by the development of localised tensile stress in those areas. As the load resistance capacity of the pipe decreased, the stress is carried forward to the steel reinforcement in plastic phase.

5.5 Numerical modelling of geopolymer concrete pipes considering bond-slip behaviour

To carry out the finite element modelling of precast pipes while considering the influence of bond between reinforcement bar and geopolymer concrete, the bond stress-slip model proposed in section 4.3 was used to simulate the bond stress-slip relationship in the finite element analysis. To represent the interfacial behaviour, beam and solid elements used to model discrete reinforcement bar and geopolymer concrete is coupled using `*Constrained_beam_in_solid` (CBIS) constraint, which restrains the beam element in solid such that solid element is defined as “master” while beam element is called “slave” (Chen 2016; Hallquist 2009). The CBIS is capable to provide constraint relaxation along the axial direction as shown in Figure 5-16 (Chen & Do 2019; Kusumaningrum, Prayogo & Tudjono 2021).

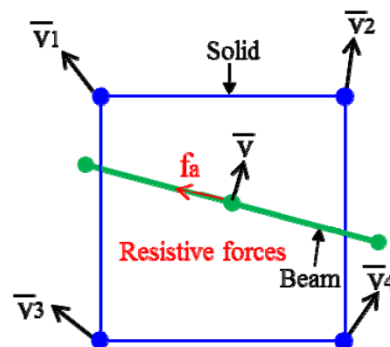


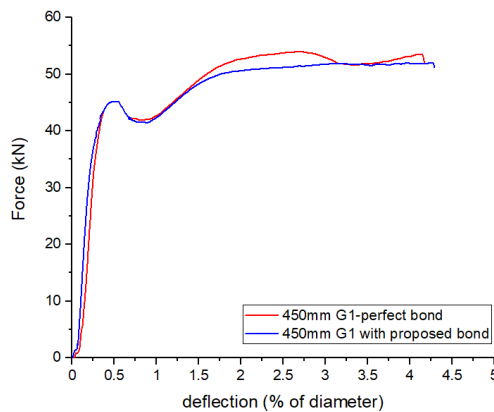
Figure 5-16 Coupling of beam in solid in CBIS (Hayashi, Chen & Hu 2017)

The de-bonding process is then simulated with a user defined function (`*Define_Function`) giving the axial shear force based on the slip between beam nodes and solid elements (Hayashi, Chen & Hu 2017). For implicit analysis, additional output by the function called de-bonding spring stiffness (`*stiff`) is required. Based on

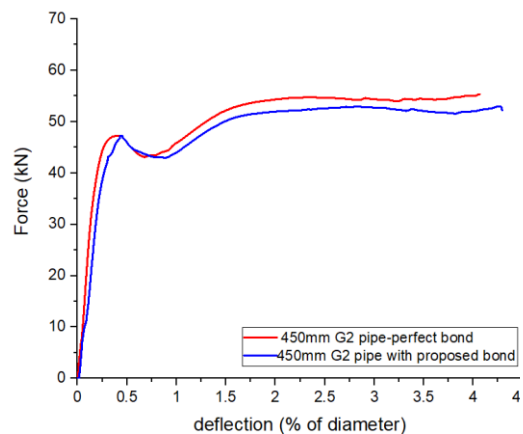
the previously proposed bond-slip relation, the de-bonding process in finite element analysis for geopolymer concrete pipe was defined.

5.5.1 Numerical analysis of geopolymer concrete pipes

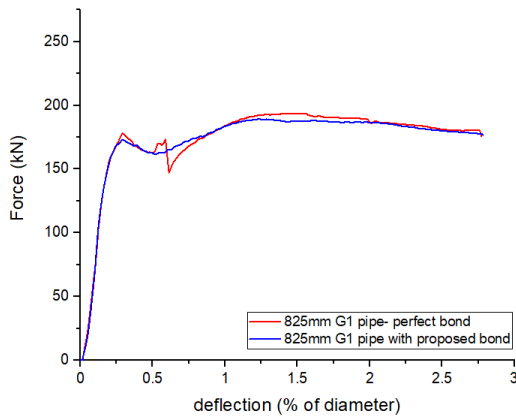
For the numerical investigation, the three dimensional finite element model with bond stress-slip effect was studied for the load-deflection behaviour under displacement load. Based on the proposed equation in section 4.3 from regression analysis, the main points for bond stress-slip behaviour of 4 mm, 6 mm and 7.5 mm reinforcement bar was predicted. In the absence of experimental data for geopolymer concrete pipes in the literature, validation of the predicted value was not done. The results of these numerical investigations were compared with the results of the numerical investigations without bond-slip effect and is shown in Figure 5-17.



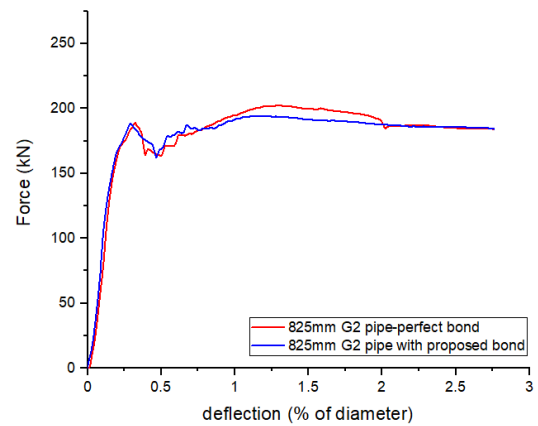
(a) 450 mm diameter Geocem 1 pipe



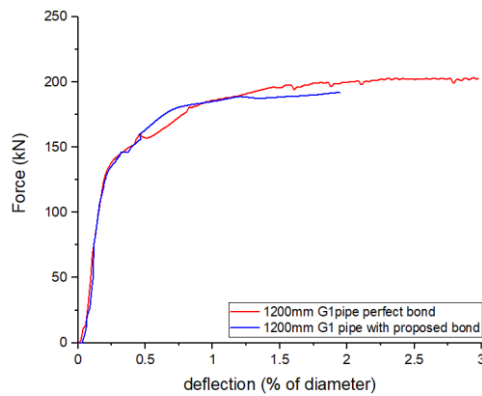
(b) 450 mm diameter Geocem 2 pipe



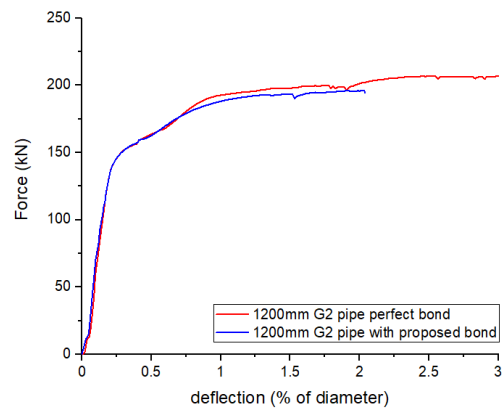
(c) 825 mm diameter Geocem 1 pipe



(d) 825 mm diameter Geocem 2 pipe



(e) 1200 mm diameter Geocem 1 pipe



(f) 1200 mm diameter Geocem 2 pipe

Figure 5-17 Load-deflection comparison for Geocem 1 and Geocem 2 concrete pipes of different diameter with and without bond consideration

The test results in Figure 5-17 indicated that consideration of bond stress-slip relation in finite element analysis affected the post-crack behaviour of the pipe causing decline in the ultimate bond strength. In case of 450 mm G1 and G2 pipe (Figure 5-17 a,b), the variation in ultimate load between the two cases of bond consideration was found to be around 5%. Similarly, for 825 mm (Figure 5-17 c,d) and 1200 mm (Figure 5-17 e,f) geopolymer concrete pipes, the decrease in ultimate load capacity was observed to vary from 5% to 8% for both G1 and G2 pipe cases. The proposed bond-

slip behaviour in geopolymer concrete pipe predicted drop in ultimate load capacity compared to pipe without bond consideration and the amount of reduction depends on the stiffness of the reinforcement bar, rather than the concrete strength (Daud, Cunningham & Wang 2017). Based on the result, it was observed that the perfect bond condition overestimated the result by 5-10%. However, upon considering different bond stress-slip relation in finite element analysis of pull-out test, Kusumaningrum, Prayogo & Tadjono (2021) reported that the perfect bond condition overestimate the bond strength by 60% in comparison to experimental value for OPC concrete pipe, while depending on bond-slip relation used, the variation in bond strength ranged from 44.6% to 1.2%. This suggested that assuming the perfect bond condition in numerical analysis present overestimation of the strength capacity in concrete structure, however the exact detail on the influence was not found to be consistent. Hence, considering the minor variation in numerical result between perfect bond case and bond consideration case for geopolymer concrete, it was deemed suitable to adopt perfect bond condition for parametric study of geopolymer concrete pipes.

5.5.2 Load-deflection behaviour of geopolymer concrete pipes

The load-deflection behaviour of geopolymer concrete pipes in relation to OPC concrete pipes with perfect bond consideration, three different diameter sized pipes were considered for this study. Single cage reinforcement was used in 450 mm and 825 mm pipe while double cage reinforcement was used for 1200 mm pipe based on minimum reinforcement specified in ASTM C76M (2022). All the pipes were modelled to be of effective length 1000 mm. Table 5-5 provides the details for the model development used in this study along with the mechanical properties of the

materials. The compressive strength and tensile strength of concrete adopted in the numerical model was based on the values determined from the experimental tests given in section 3.2.2.

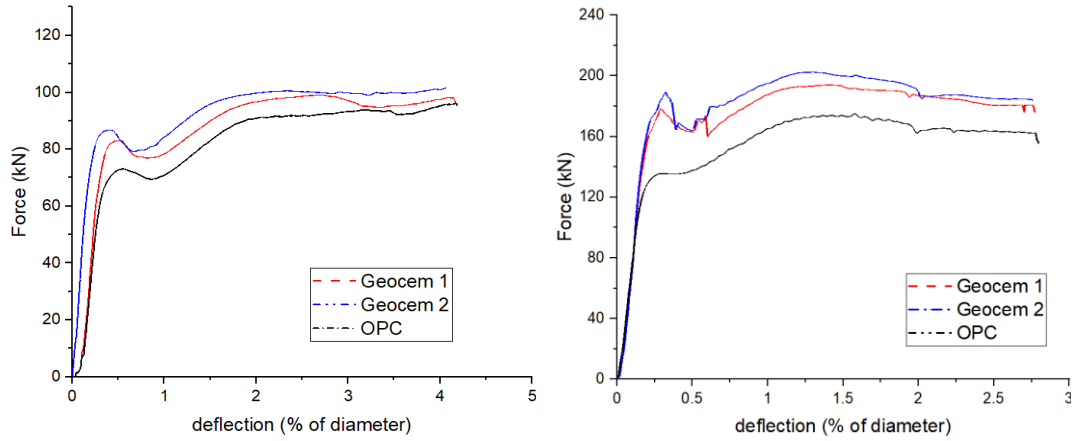
Table 5-5 Physical and Material properties of pipe model

ASTM classification	Inner diameter (mm)	Area of inner steel (A_{si}) (mm^2/m)	Area of outer steel (A_{so}) (mm^2/m)	Wall thickness (mm)
ASTM Class II	450	175	-	42
ASTM Class III	825	484	-	114
ASTM Class IV	1200	565	376	127

Material Properties	Geocem 1	Geocem 2	OPC
Compressive strength (MPa)	56	59	53
Tensile strength (MPa)	3.6	3.8	2.3
Poisson's ratio	0.2	0.2	0.2
Rebar yielding stress (MPa)	500	500	500
Curing date/ Curing period	11 Sept. 2021 / 6 hours	4 Sept. 2021 / 6 hours	1 Sept.2021 / Till test day

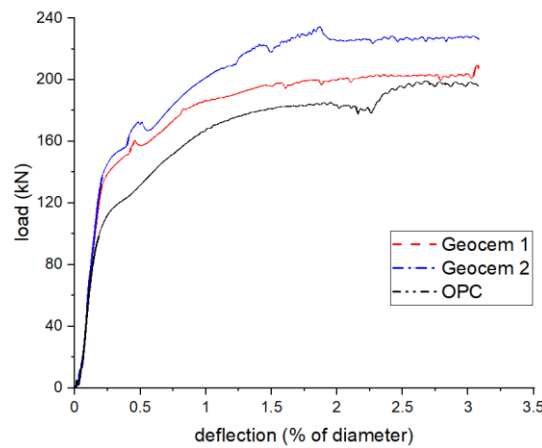
450 mm diameter was used to compare the performance of the geopolymer concrete against OPC concrete in both reinforced and unreinforced cases, while 825 mm diameter and 1200 mm diameter pipes were used for reinforced concrete analysis. The reinforced concrete pipes were also used as control pipe for further parametric

study. Figure 5-18 shows the load-deflection plot of different diameter geopolymer pipe against OPC concrete pipe.



(a) 450 mm pipe

(b) 825 mm pipe



(c) 1200 mm pipe

Figure 5-18 Load- deflection plot for (a) 450 mm pipe (b) 825 mm pipe (c) 1200 mm pipe

The design requirement specified for 450 mm diameter OPC concrete pipe in ASTM C76M (2022) for peak and ultimate loads are 50 N/m/mm and 75 N/m/mm respectively, while for same class AS/NZS 4058 (2007) specifies the design load and ultimate load to be 20 kN/m and 30 kN/m. Between these two standards, apart from

the unit of load measurement, the specified value are same. Thus, comparing the results obtained from numerical analysis of geocem 1 and geocem 2 concrete pipes against the standards requirement, it is evident from Figure 5-18a that the numerical analysis of geopolymer concrete exhibited better load carrying capacity compared to OPC concrete. Since, the geopolymer concrete exhibited higher tensile strength compared to OPC concrete, the load carrying capacity of both geopolymer concrete outperformed the OPC concrete load requirement by approximately 15% for peak load capacity and around 5% for ultimate load capacity by both geopolymer concrete.

Similarly, the 825 mm pipe results showed high load resistance behaviour of geopolymer concrete compared to OPC concrete in the load-deflection plot presented in Figure 5-18b. Peak load capacity of 177.4 kN and 187 kN was observed for geocem 1 and geocem 2 respectively, which was 30 % and 40% higher than that of OPC pipe, while the ultimate load carrying capacity was respectively 12% and 17% higher. The load resistance capacity in geocem 2 was found to be around 5% greater than geocem 1.

From the load-deflection plot for 1200 mm pipe shown in Figure 5-18c, the peak load capacity of geopolymer concrete were observed to be 27% higher than peak load capacity of the same strength OPC concrete pipe and the ultimate load capacity was found to be 14% greater than OPC concrete.

Further comparing the load-deflection plot for single cage pipe and double cage pipe, a dip in the load was noticeable once the pipe reached its peak load capacity, while the drop was not significant for the double cage reinforced pipe. Such difference in the behaviour of single and double cage reinforced pipe was also observed by Tehrani (2016) and Younis et al. (2021). The rise in the load capacity following the

drop after peak load signifies the load stress being carried by the steel reinforcement. Based on this comparative analysis, it was observed that the high tensile strength of geopolymer concrete compared to OPC concrete significantly affects the load bearing capacity of the pipe in TEB test.

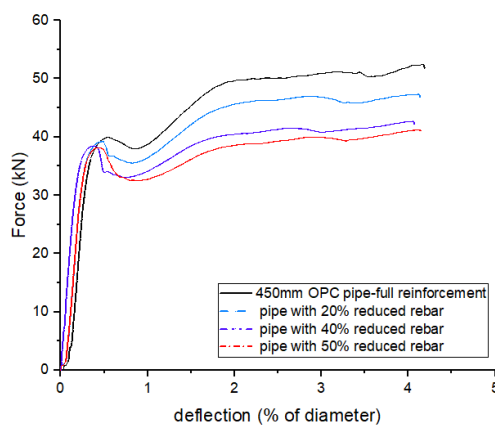
5.6 Parametric study of geopolymer concrete pipes

A parametric study based on varying reinforcement condition was carried out on three different sized pipes with diameter 450 mm, 825 mm and 1200 mm for geocem 1, geocem 2 and OPC respectively. Single cage reinforcement were used for 450 mm and 825 mm pipes and double cage reinforcement was modelled for 1200 mm pipe. The finite element model developed for these 3 sets of pipes were analysed to examine the effect of change in reinforcement area, concrete cover to inner cage and yield strength on load bearing capacity of the pipes. Additionally, the load bearing capacity for unreinforced pipe for 450mm pipe was also analysed. The results obtained from numerical modelling was also compared to design load requirement specified by AS/NZS4058 (2007) and ASTM C76M (2022). The required design load specified by these standards for 450 mm, 825 mm and 1200 mm diameter concrete pipes of length 1 m are 20 kN, 52 kN and 92 kN respectively, while the ultimate test load are quantified as 30 kN, 78 kN and 138 kN respectively. In total 93 FEA models were analysed for the parametric study of the pipes.

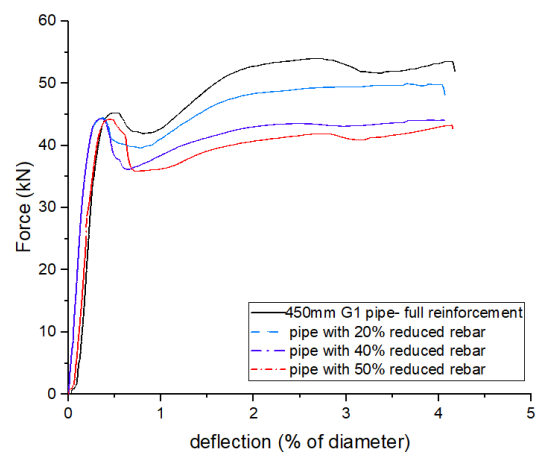
5.6.1 Effect of change in reinforcement area

For concrete structure, steel reinforcement is used to meet the structural performance requirement, as concrete has relatively less tensile strength. To design reinforced concrete pipe, minimum reinforcement criteria for different size and class

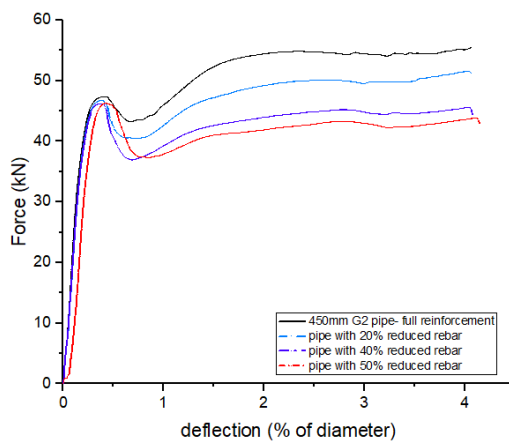
of reinforced concrete pipe has been defined in ASTM C76M (2022) to meet the design load criteria. As such to examine the influence of steel reinforcement area on load-deflection behaviour of reinforced OPC, geocem 1 and geocem 2 concrete pipes, the steel reinforcement was reduced by 20%, 40% and 50% from the total reinforcement as given in Table 5-5. Figure 5-19 shows the load-deflection plot for 450 mm pipe under reduced reinforcement condition.



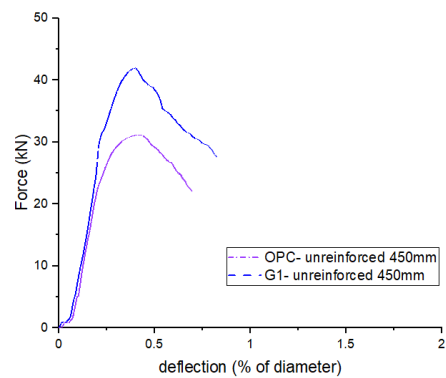
(a) 450mm OPC pipe



(b) 450mm Geocem 1 pipe



(c) 450mm Geocem 2 pipe



(d) 450mm unreinforced pipe

Figure 5-19 Effect on load-deflection behaviour of 450mm pipe due to change in reinforcement steel area

It is obvious for all concrete types (Figure 5-19 a-c), the load bearing capacity of the pipes decreased as the reinforcement area was reduced and the effect is more prominent following the peak load phase where the ultimate loading capacity in the pipe is higher in pipe cases with higher reinforcement area. Since development of crack in concrete structure relies on the tensile strength of concrete, changing the steel reinforcement didn't change the service load capacity of the pipe, hence altering the ultimate load capacity of the pipe in the plastic stage. Furthermore, descent in the loading value was noticed after the peak load before the model regained its load capacity in inelastic phase. Such drop in load capacity was also noted in Tehrani (2016) and Peyvandi, Soroushian & Jahangirnejad (2013) FEA simulation for single cage pipe. When sufficient tensile stress develops in the concrete surface causing concrete to crack, the pipe loses its capacity which is marked by the dip in the load-deflection curve. As the stress in the concrete pipe is transferred to the reinforcement bars, regain in the load capacity is observed until it reaches its ultimate load capacity, after which the pipe fails.

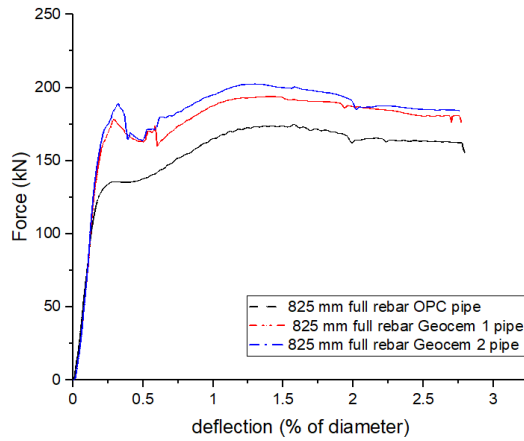
Furthermore, the peak load value of 450 mm OPC concrete pipe was observed to be around 38.25 kN while for geocem 1 and geocem 2 concrete pipes, the peak load value was observed to be around 45 kN and 48 kN respectively. This high service load capacity showcased by geopolymer concrete relates to high tensile strength gain in geopolymer concrete unlike in same grade OPC concrete which observed from the experimental results in section 3.2.2.

To study the service load capacity achievement in the geopolymer concrete pipe with respect to OPC concrete, analysis of 450 mm unreinforced concrete pipe was

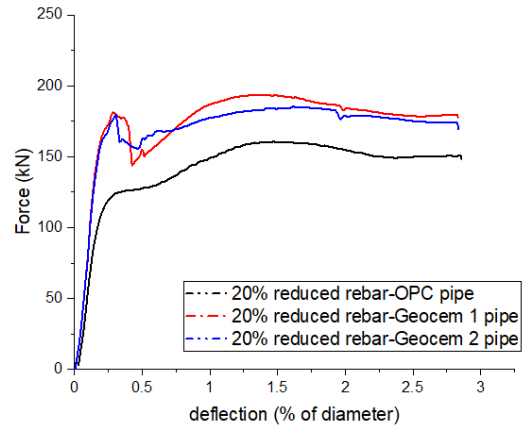
also carried out. AS/NZS4058 (2007) specifies the test load for 450 mm unreinforced concrete pipe as 30 kN. From the comparative plot displayed in Figure 5-19d for load-deformation behaviour of geopolymer concrete against OPC concrete, the service load capacity of the unreinforced OPC concrete pipe was noted to be around 31 kN, while the service load capacity of geocem 1 was 42 kN. The service load capacity in geocem 1 pipe was almost 37% greater than that of the OPC concrete pipe, indicating the use of same grade geopolymer concrete for higher load capacity pipe compared to OPC concrete pipe. Moreover, considering the AS/NZS4058 (2007) requirement of the 30 kN/m as service load and 45 kN/m as ultimate load capacity for class 3 450 mm concrete pipe, unreinforced geopolymer concrete pipe is able to meet the design requirement of the class 3 reinforced concrete pipe.

Similarly, the finite model simulation carried out for 825 mm OPC and geopolymer concrete pipes for the reduced steel reinforcement area has been shown in Figure 5-20 a-d. The dissimilarity in load-deflection behaviour of OPC concrete pipe and geocem 1 and geocem 2 pipe is evident from the plot. The peak load capacity between geocem 1 and geocem 2 concrete for the reduced steel bar case was found to be almost similar, with slight difference in ultimate load capacity. Prominent difference in load-deflection behaviour for geopolymer concrete against OPC concrete was observed with approximately 35% and 43% increase in service load for 20% reduced area of reinforcement bar in geocem 1 and geocem 2 respectively, while 13% and 18% higher ultimate load capacity for the same. For geocem 1 and geocem 2 the service load capacity was observed to be around 186 kN while for OPC it was observed to be 124 kN. Further the rise in load capacity following the drop after surpassing the peak load capacity was still noticed when the reinforcement area in the pipe decreased by 20% (Figure 5-20 a-b), but as the area of reinforcement further decreased by 40%

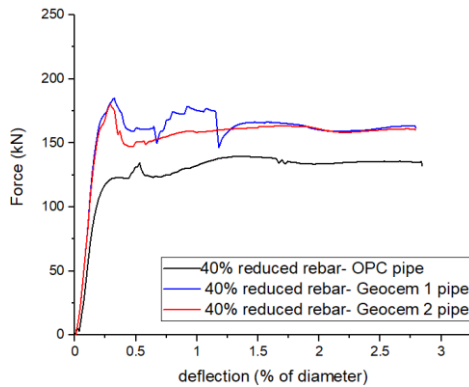
and 50%, rise in the loading capacity was not observed (Figure 5-20 c-d), which suggested the pipes could resist load without failure till the reinforcement area is reduced by 20%.



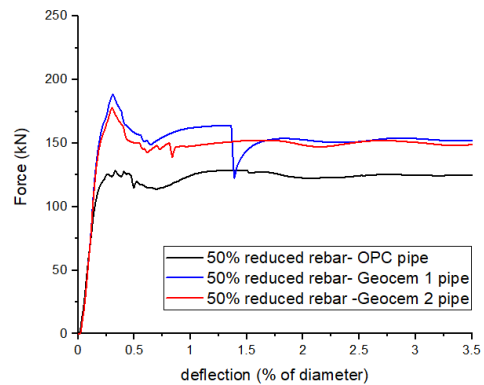
(a) Full rebar case



(b) 20% reduced rebar



(b) 40% reduced rebar

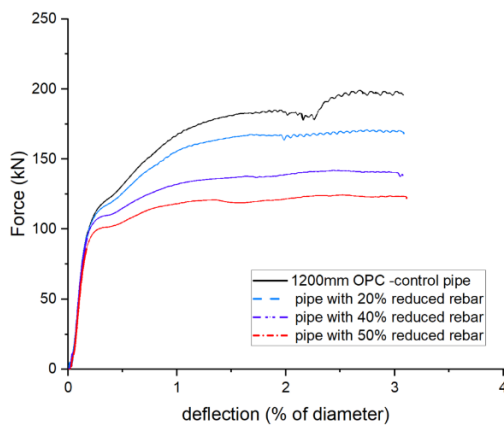


(c) 50% reduced rebar

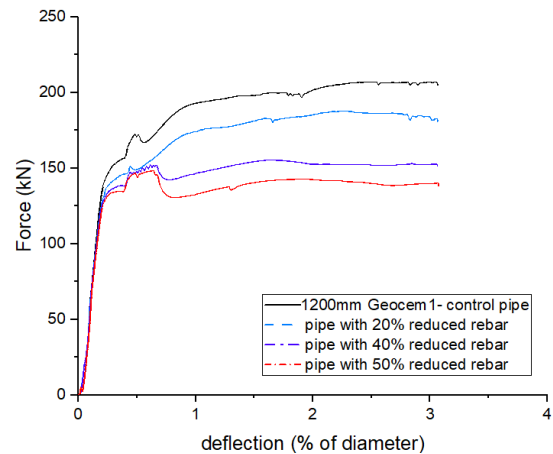
Figure 5-20 Effect on load-deflection behaviour of 825 mm pipe due to change in reinforcement steel area

The case study of finite element model simulated for 1200 mm with double cage steel reinforcement is shown in Figure 5-21 (a-c). Unlike the single cage reinforced concrete pipe of diameter 425 mm and 850, decrease in loading capacity

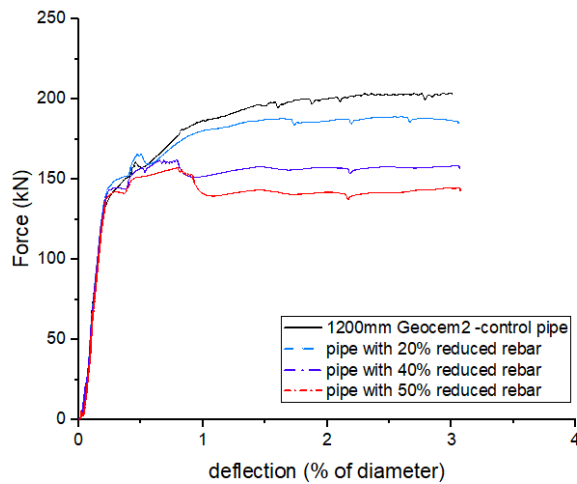
after the peak load was not observed for 1200 mm double cage concrete pipe, rather the rise in loading capacity up to the ultimate loading stage was noticed. Since the steel reinforcement in double cage concrete pipe lie closer to the inner and outer wall of the pipe, the reinforcement steel fell well within the tension block compared to single cage reinforced concrete pipe where the reinforcement bar lies close to the neutral axis of the section. As such, drop due to loss in load capacity in concrete is not observed in the double cage reinforced pipe. Similar to other pipe case, the change in steel reinforcement areas significantly affected the post-crack loading capacity of the pipes with remarkable demonstration of loading capacity in both peak and ultimate load condition by geopolymer concrete compared to OPC concrete.



(a) 1200mm OPC pipe with reduced rebar



(b) 1200mm Geocem 1 pipe with reduced rebar

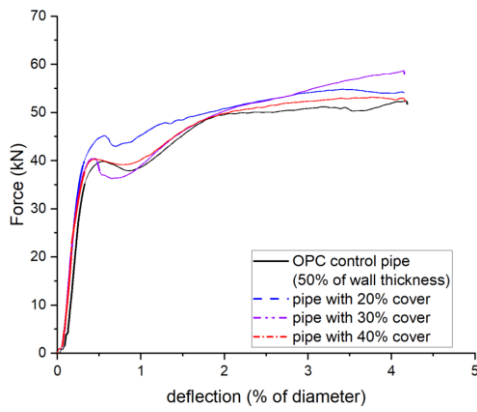


(c) 1200mm Geocem 2 pipe with reduced rebar

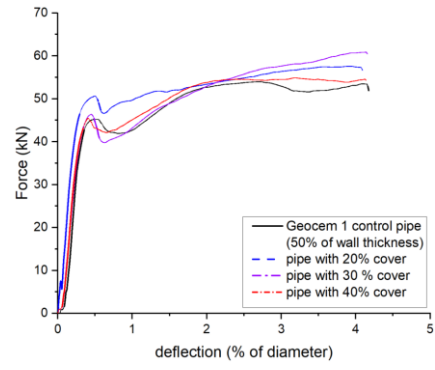
Figure 5-21 Effect on load-deflection behaviour of 1200 mm pipe due to change in reinforcement steel area

5.6.2 Effect of change in concrete cover to inner cage

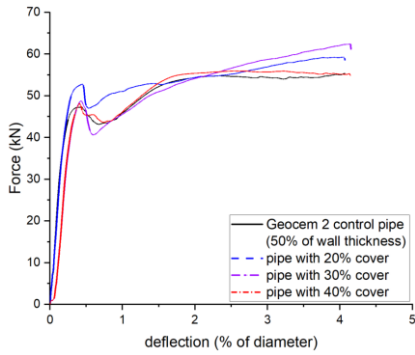
To design reinforced concrete pipe, ASTM C76M (2022) specifies that the concrete cover from inner face of the pipe with single cage reinforcement should be 35% to 50% of wall thickness, while for double cage reinforced concrete pipe, both inner and outer cage should have concrete cover of 25 mm. For the control pipe simulation, 50% of wall thickness was used as concrete cover for 425 mm and 850 mm concrete pipes, while 33% of wall thickness (or 42 mm) was used as concrete cover for 1200 mm concrete pipe. To explore the influence of concrete cover change on the loading capacity of geopolymer concrete compared to OPC concrete, the concrete cover for single cage reinforced concrete pipe was modelled to be 20%, 30% and 40% of wall thickness, while for double cage the concrete cover of 10%, 20% and 30% of the wall thickness was used. This change in concrete cover was adopted to inner wall of the pipe for both single and double reinforced concrete pipes. The load-deflection plot for reduced concrete cover is plotted in Figure 5-22.



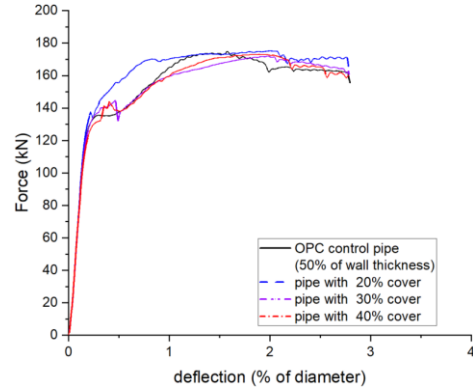
(a) 450 mm OPC pipe



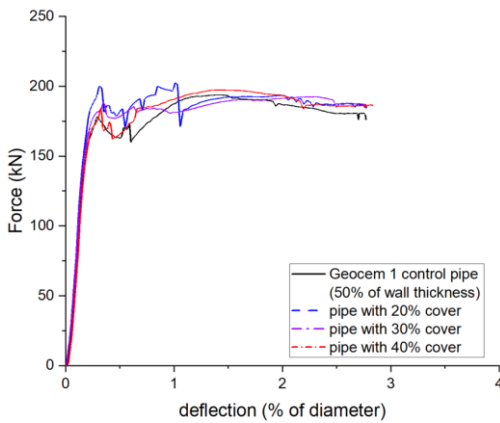
(b) 450 mm Geocem 1 pipe



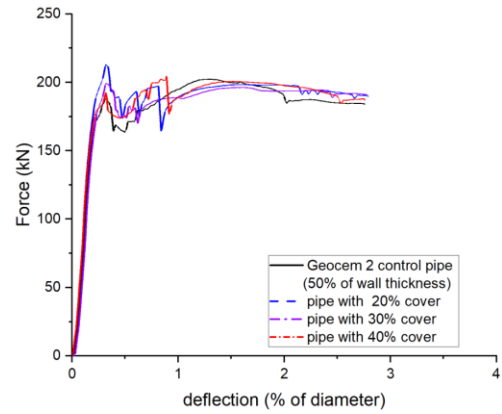
(c) 450 mm Geocem 2 pipe



(d) 825 mm OPC pipe



(e) 825 mm Geocem 1 pipe

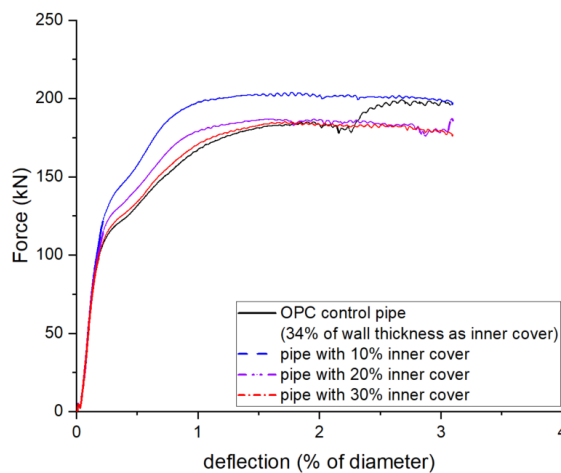


(f) 825 mm Geocem 2 pipe

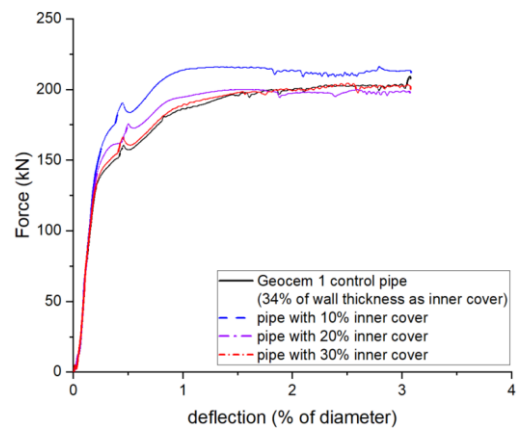
Figure 5-22 Effect on load-deflection behaviour of 450mm and 825 mm pipe due to change in concrete cover

Figure 5-22(a-c) shows the load-deflection plot for 450 mm reinforced concrete pipe with varying concrete cover. For pipe case with 20% of wall thickness as concrete cover, higher peak load and ultimate load capacity have been observed for both geopolymer concrete as well as OPC concrete. However, the load-deflection behaviour of the concrete pipes with 30%, 40% and 50% (control pipe) of wall thickness were found to show load-deflection behaviour with small decrease in loading capacity as the concrete cover increased. For 825 mm concrete pipe shown in Figure 5-22 (d-f), though the pipe with less concrete cover has higher peak load capacity, remarkable change in loading capacity was not identified for change in concrete cover. Younis et al. (2021) accredits such insignificant change in loading behaviour to lower steel content stating that the same diameter pipe models with higher steel reinforcement are more sensitive to change in concrete cover compared to the one with lower steel area.

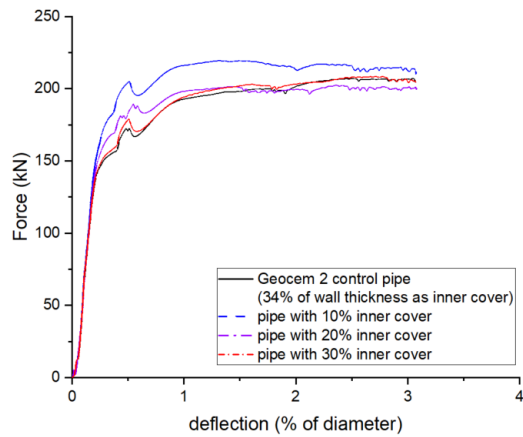
Similarly, for 1200 mm concrete pipe, the load-deflection behaviour for different concrete cover case was plotted in Figure 5-23 (a-c).



(a) 1200 mm- OPC pipe



(b) 1200 mm- Geocem 1 pipe



(c) 1200mm- Geocem 2 pipe

Figure 5-23 Effect on load-deflection behaviour of 1200mm pipe due to change in concrete cover

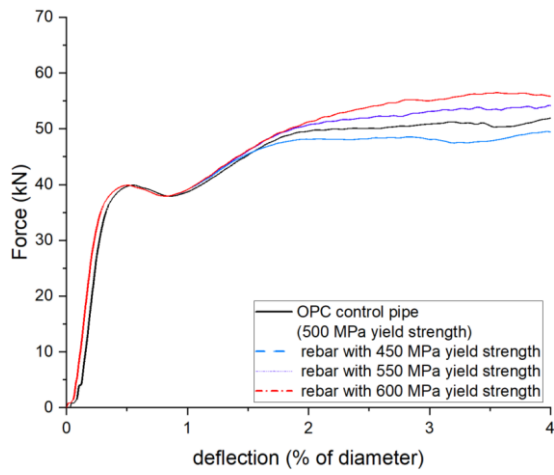
Though the loading capacity of both the geopolymer concretes were greater than OPC concrete pipe, the change in loading behaviour was comparable to OPC concrete pipe, with high peak load and ultimate load resistance demonstrated by pipe with lesser concrete cover.

All finite element simulation for change in concrete cover for both OPC and geopolymer concrete exhibited alteration in peak load and ultimate load capacity considering the change in position of steel cage. It was evident from the load-deflection plot for OPC as well as geopolymer concrete pipes that bearing capacity in pipe increased as the steel cage was closer to the concrete pipe wall. However, reducing the concrete cover for effective load performance could significantly impact the service life of the OPC concrete pipe, as OPC concrete is prone to sulphuric acid attack and chlorination due to the internal and external environment that the concrete pipes are exposed to (Monteny et al. 2000; Wong & Nehdi 2018; Wu, Hu & Liu 2018). However, considering the peak load and ultimate load capacity exhibited by OPC

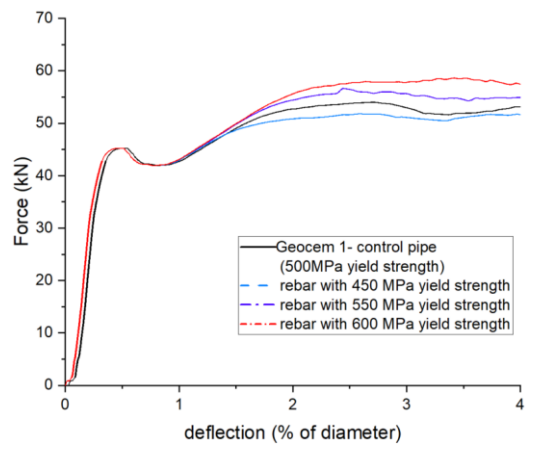
concrete for 20% and 10% cover for single and double cage pipe being comparable to bearing capacity of geopolymer concrete pipe that used 30%-50% of wall thickness as concrete cover, use of geopolymer concrete can be noteworthy for achieving the required loading capacity while practising safe concrete cover guidelines by ASTM C76M (2022).

5.6.3 Effect of change in yield strength

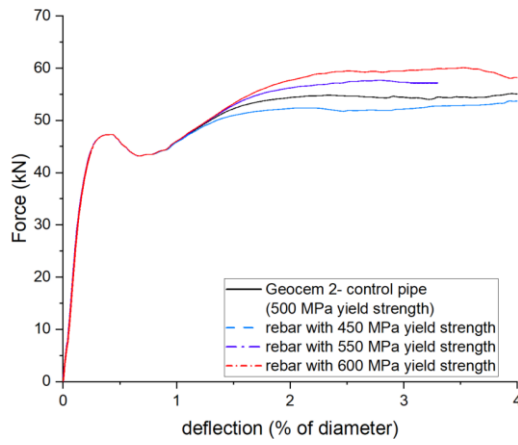
To further carry out the parametric study, the effect of change in yield strength of steel reinforcement bars in the loading behaviour of the geopolymer and OPC concrete pipe was considered. Reinforcement bars with yield strength of 450 MPa, 500 MPa, 550 MPa and 600 MPa was used for parametric study. Since the yield strength of the reinforcement bars contribute towards the post-crack loading response of the pipe, the peak load capacity was not affected by change in yield strength value for all concrete pipes (Figure 5-24 (a-f) and Figure 5-25 (a-c)). However, significant reduction on ultimate loading capacity of the pipe was observed as the yield strength of steel decreased from 600 MPa to 450 MPa. For both 450 mm and 825 mm geopolymer and OPC concrete pipe (Figure 5-24), increase in 2% to 6% in ultimate strength was observed, while for 1200 mm concrete pipe (Figure 5-25) the change in ultimate strength of pipe was observed to be around 6% to 8% for change in yield strength. For all concrete pipe cases with changed yield strength, the ultimate loading capacity in geocem 2 was observed to be 3% higher than geocem 1 and the ultimate loading capacity of geocem 2 was around 4% higher than OPC concrete pipe.



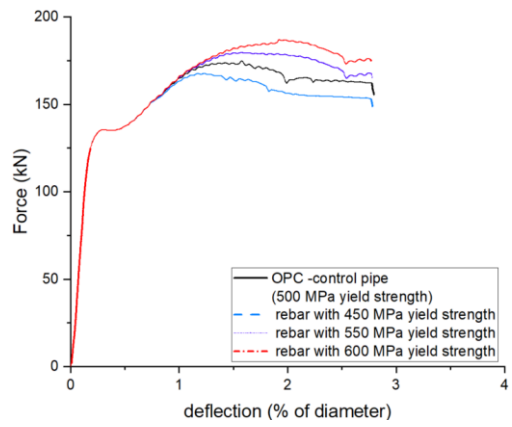
a) 450 mm OPC pipe



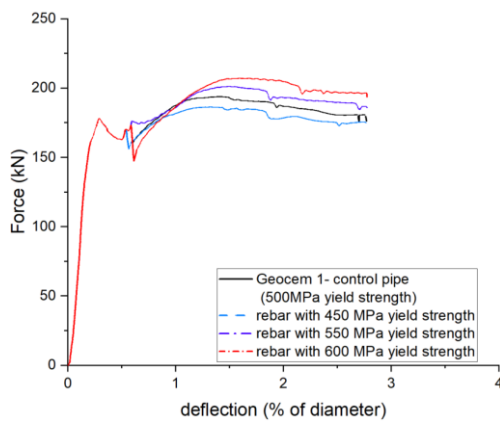
b) 450 mm Geocem 1 pipe



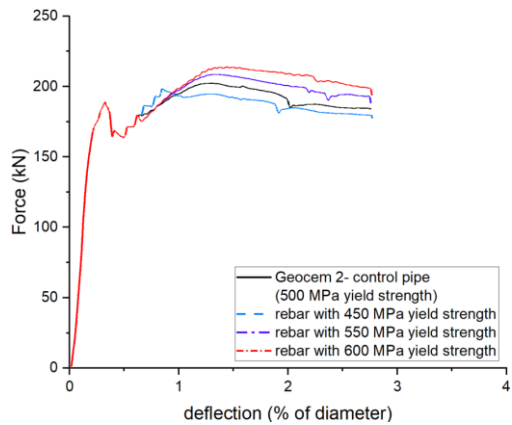
c) 450 mm Geocem 2 pipe



d) 825 mm OPC pipe

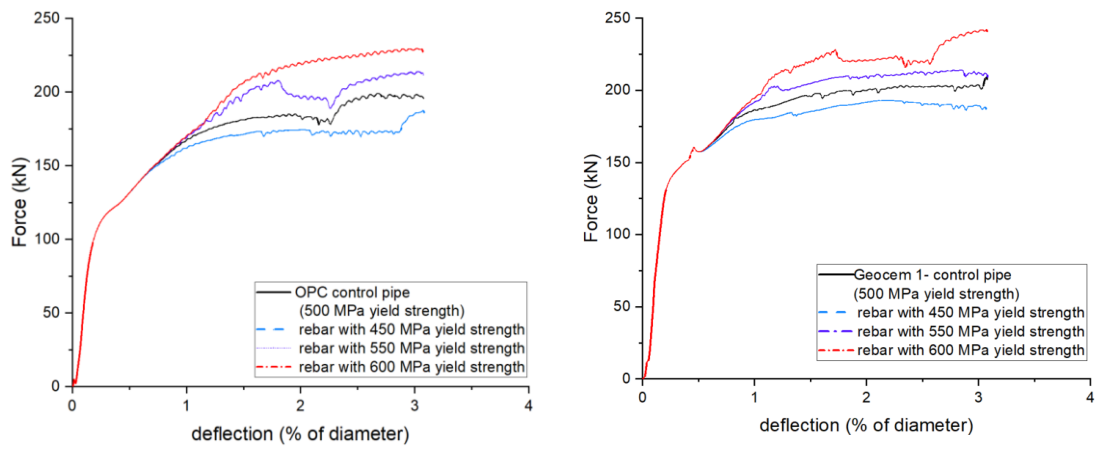


e) 825 mm Geocem 1 pipe



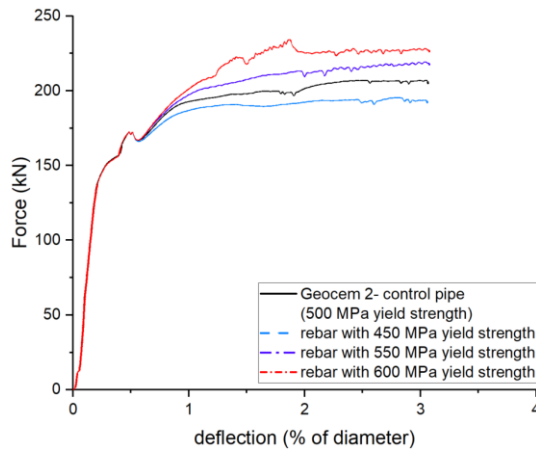
f) 825 mm Geocem 2 pipe

Figure 5-24 Effect on load-deflection behaviour of 450 mm and 825 mm pipe due to change in yield strength of steel



(a) OPC pipe

(b) Geocem 1 pipe



(c) Geocem 2 pipe

Figure 5-25 Effect on load-deflection behaviour of 1200mm pipe due to change in yield strength of steel

5.7 Summary

In this chapter, 3D finite element model of concrete pipe to simulate TEB test was developed in LSDYNA. The K&C concrete model was used to characterize the OPC and geopolymer concrete behaviour, while bilinear elastic-plastic model with linear strain hardening was used to model reinforcement steel in the pipe FE model. The accuracy of concrete model was verified by simulating stress development in concrete cylinder during compression test and was validated against the experimental compression test result. The FE model for 825 mm concrete pipe under TEB test was also validated against the experimental test results provided by Younis et al. (2021). The concrete model was noted to be sensitive to its tensile strength behaviour. Hence, to validate the model against the experimental test result, the model was calibrated for tensile strength parameter of concrete. Validated model was then used to develop 425 mm and 1200 mm concrete pipes which were further used for parametric study of geopolymer and OPC concrete pipes.

Following conclusions were made based on the results obtained from parametric study:

- Change in steel reinforcement area changes the post-crack response of the pipe since reinforcement mostly contributes for strength development in cracked concrete section. Thus, alteration in the ultimate loading capacity of the pipe can be noticed. For all size concrete pipes, notable gain in ultimate load capacity was observed with 20% decrease in steel reinforcement area for both geopolymer concrete types. Meanwhile, with the decrease in steel reinforcement by 40% and 50%, significant gain in loading capacity was not detected after the peak load capacity.

- Considering high tensile strength of both geocem 1 and geocem 2, the peak load and ultimate load capacity exhibited by both geopolymer concrete for all pipe cases were remarkably higher than OPC concrete pipe of same case.
- Comparative study of 450 mm unreinforced geopolymer concrete pipe against OPC concrete pipe revealed that the unreinforced geopolymer concrete pipe can satisfy the load criteria for class 3 450 mm reinforced concrete pipe. Thus, reinforced concrete pipe classified in Class 2 or 3 can be developed without the use of reinforcement by using geopolymer concrete and can still meet the specified design load criteria.
- Similarly, the effect on load-deflection behaviour of pipe due to change in concrete cover was also studied. For all concrete types and all diameter pipes, the load carrying capacity was observed to be high for the pipe case with less concrete cover for inner wall.
- The peak load and ultimate load capacity exhibited by OPC concrete for single and double cage pipe with 20% and 10% of wall thickness as concrete cover was found to be lesser or equivalent to the bearing capacity of geopolymer concrete pipe with 30%-50% concrete cover. Hence, high loading capacity can be obtained for geopolymer concrete pipe while practising safe concrete cover guidelines provided by ASTM C76M (2022).
- Change in yield strength of steel reinforcement affected the post-crack behaviour as yielding stress is transferred in steel reinforcement after cracking of concrete section. It was evident that as the yield strength in reinforcement bars increased, the ultimate strength of the pipe also increased.
- The proposed model was used for bond-slip modelling for numerical analysis of geopolymer concrete pipes which demonstrated overestimation of ultimate bond

capacity of geopolymer concrete pipe by 5% to 10% under perfect bond assumption when compared to analysis result with proposed bond relation.

Chapter 6

6. Structural performance of cracked concrete pipe

6.1 Introduction

Concrete pipeline system is a crucial part of infrastructures designed to convey stormwater and sewerage. Performance of concrete pipes plays a major role in the smooth functioning of the present day cities (Zhang et al. 2018; Zhang et al. 2020). Over the years of use, cracks, corrosion and dislodgment are inevitable in concrete pipes that significantly impact the structural performance. Indeed, cracks in concrete are very common and they can develop due to multiple reasons like normal shrinkage during hardening and drying of concrete, substandard material or even faulty production process, during handling and installation of concrete structures, uneven supporting backfill, external load and degradation due to environmental corrosion (Indiketiya et al. 2019; O'Connell, McNally & Richardson 2010; Peter et al. 2018; Scheperboer et al. 2021; Wong & Nehdi 2018; Zhang et al. 2020). Nonetheless, the structural stability of the concrete pipes are greatly influenced by the external loading factors and the construction features, causing crack formation in pipe (Davies et al. 2001). Millar & Paull (2017) states that the crack formed in concrete during construction affects durability, structural and operational integrity and aesthetics throughout the design life of the structure. Performance of concrete pipes with such cracks can get compromised significantly as such cracks may facilitate ingress of moisture and other destructive environmental substances which may lead to corrosion of reinforcement thus, risking the safety of concrete pipes (Al-lami 2020; Marr 2012; Tran, Setunge & Shi 2018).

As a control measure to address the issue related to cracks, AS/NZS 4058-2007 has specified acceptability criteria of concrete pipes during installation. Depending on the concrete cover provided for the pipes, the crack width ranging from 0.15 mm to 0.25 mm has been specified as conforming pipes, beyond which the pipes are considered non-compliant and can be either used after adopting remedial measures or has to be rejected. In addition to crack width, crack depth of less than 3mm and the length of 300 mm is recommended to be viable for the respective crack width. However, even with these recommended guidelines, the pre-existing cracks on previously load tested pipes may widen marginally after installation and loading (Al-Saleem & Langdon 2014). Often during installation or due to excessive load on the pipes, cracks development aggravate in pipes and can compromise the structural safety of the pipe. Hogan (2017) states that the severity of cracks developed in the pipe depend on the crack pattern, crack location and the size of the crack. Hence, many studies have been carried out to investigate the effect of cracks on structural safety and durability of the pipes.

Studies conducted by Zamanian (2016), Millar & Paull (2017), Wu, Hu & Liu (2018), Al-lami (2020) and Li et al. (2021) explored the effect of crack on pipe performance in relation to cracked pipes subjected to different environmental conditions and acid attack. Attempts to investigate the structural behaviour of concrete pipes due to cracking have also been carried out. Buda-Ozog, Skrzypczak & Kujda (2017) stated that the compliance of theories of concrete cracking with experimental results is less compatible compared to theory of strength limit. This is because cracking issue in concrete pipe is a complex problem that is affected by several poorly controlled factors (Al-Saleem & Langdon 2014; Branco, Arruda & Correia 2013). It was concluded that the tensile strength of the concrete in pipe is higher than tensile

strength of concrete for straight element due to the effect of curvature of pipe, recommending use of appropriate value for concrete tensile strength at failure. Li et al. (2018) carried out a study on damage in concrete pipes due to cracking during installation process, it was concluded that the compressive stress acting on pipe during normal jacking can produce tensile stress resulting in crack formation in the pipe. It was further added such crack formation is intensified if there is a presence of pores in pipe due to poor material used, resulting in concrete tension fracture. In the numerical study carried out by Bentz et al. (2013) and Lehner & Konečný (2017) cracks in concrete was applied as a reduced material parameter, associating to stiffness loss in element. Tabiei & Wu (2003) states that for concrete materials that fails in diffuse manner smeared cracking method can be successfully applied where crack is not represented explicitly.

Though many studies have been carried out to explore the cases of crack development in OPC concrete pipe, one important factor to consider for concrete pipe design is consideration of serviceability performance due to crack development. While studies have been carried out to explore the effect of cracks on OPC concrete pipe, the influence on load-deflection behaviour of the concrete pipes with cracks has not been observed. Further, as a new type of binder, the structural performance of geopolymer precast pipes still have not been studied in detail and it is equally important to explore the effects on pre-existing cracks on performance of geopolymer concrete pipes. Hence, this study focuses on to explore the effect on the load-deflection behaviour due to pre-existing cracks on both OPC concrete pipes and geopolymer concrete pipes.

Experimental study on load-deflection behaviour of OPC concrete pipe due to pre-existing crack at different stages of loading has been explored in this chapter. The

results are used in validation of refined numerical pipe models. Considering crack of different length, depth and on different location, numerical study to investigate load-deflection behaviour of geopolymer concrete pipe is carried out aiming to assist in the decision-making process on maintenance and replacement of geopolymer concrete pipes.

6.2 Experimental program

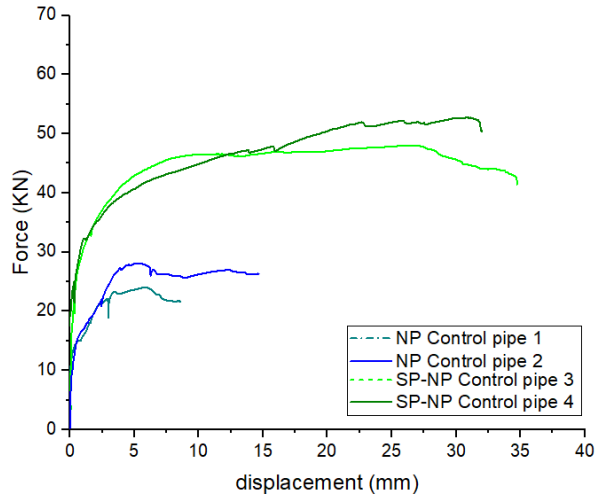
To study the effect on loading capacity of OPC concrete pipes with cracks, standard three-edge bearing tests were carried out on 450 mm internal diameter concrete pipe of class 4 category. Pipes with effective length of 450mm was used for the test. Test set up for the experiment were replicated as described in Chapter 5 with four LVDTs mounted to measure relative displacement in vertical and horizontal direction. Pipes without any cracks (NP) were tested as control pipe for comparison. Additional pipe with spigot pocket (SP-NP) was also tested for non-crack condition. Two uncracked pipes set were used to obtain control pipe test data. The specifications of the pipe tested are provided in Table 6-1.

Table 6-1 Pipe details

Class	4
Nominal diameter	450 mm
Effective length	450 mm
Wall Thickness	44 mm
Concrete strength	65 MPa
Circular reinforcement area	213.63 mm ²
Longitudinal reinforcement	6 nos. of 4 mm rebar
Required Proof load as per AS/NZS 4058	40 kN/m
Required Ultimate load as per AS/NZS 4058	60 kN/m

The control pipes were tracked for crack development starting from hairline crack till 0.25mm wide crack. In Figure 6-1a, the peak load observed in control pipes were 24 kN and 28 kN for NP control pipes 1 and 2 while for pipe sample with spigot pocket (SP-NP), the peak load was observed to be 46.4 kN. It was observed that the spigot pocket in the pipe contributes to load capacity in the pipe when compared to the similar pipe section without spigot pocket. While the hairline crack was observed for control pipe without spigot pocket at around 15 kN, the control pipe with spigot pocket restrained load of 29 kN until first hairline crack. Study carried out by da Silva, El Debs & Kataoka (2018) comparing the strength of spigot pocket pipe with ogee joint

pipe reported that spigot pocket in pipe increased the pipe stiffness influencing the load cracking in spigot pocket pipe compared to ogee joint pipe.



(a)



(b)



(c)

Figure 6-1 (a) Load-deflection curve for control pipe (b) crack development during TEB test in NP control pipe (c) Spigot pocket pipe under TEB test

In the test of NP control pipe 1, the test was ended abruptly due to technical issue in the Universal Testing Machine. As such, for further evaluation of the load-deflection behaviour in cracked pipe, NP control pipe 2 was selected as reference plot.

6.3 Parametric study of concrete pipe with pre-existing cracks

Since development of crack in concrete pipe is random and is difficult to pin the exact location, parametric study was performed to study the load-deflection behaviour of pipe with pre-existing cracks. For the test, 5 mm wide crack with different length and different depth were created on crown and spring-line of the pipes. The cuts were created manually along the axial direction of the pipe using a compact concrete cutting saw. The pipe were tested for the crack cases as shown in Table 6-2. Two samples were tested for each case.

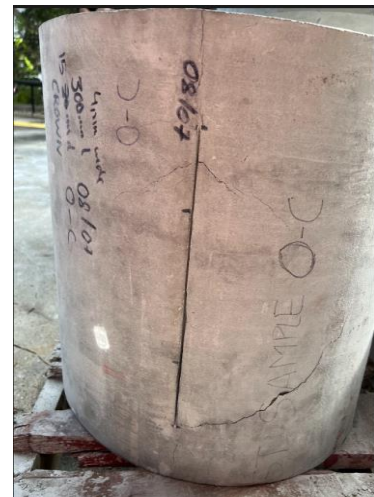
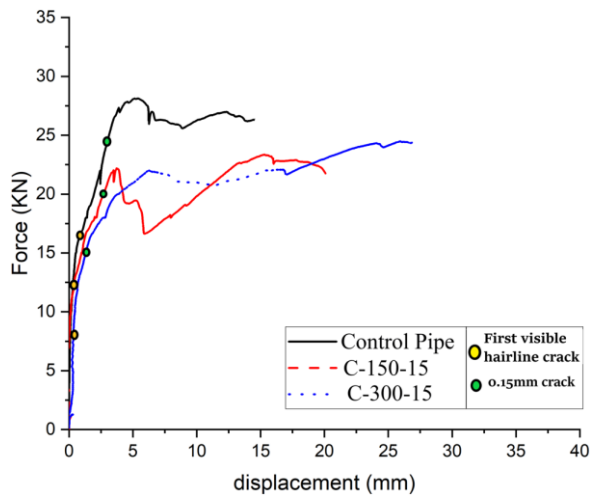
Table 6-2 Cracked pipe tests

Crack Length	Crack Depth	Crack Position	Sample Id
150 mm	15 mm	crown	C-150-15
		Spring-line	S-150-15
300 mm	10 mm	crown	C-300-10
	15 mm	crown	C-300-15
		Spring-line	S-300-15

6.3.1 Effect of change in crack length on pipe performance

Crack length of 300mm and 150mm long crack were tested for crack in outer part of crown and the springline. For crack in crown, reduction in the peak load capacity

was observed to be 21 and 25% for 150mm and 300mm long crack (Figure 6-2a). While gain in strength after the drop due to tensile strength loss in concrete was observed for both crown crack condition, the ultimate strength in the pipe with crown crack with 300 mm length was noticed to be slightly higher than the pipe with crown crack with 150 mm length. Though the loading capacity of pipe with smaller length crack is expected to perform better compared to pipe with longer length as reported by Zhang et al. (2020), the limited number of test carried out on pipe confines the investigation of test results. It was further noticed that though the crack development during the loading initiated in the inner part of crown and invert region which is similar to the control pipe, after the peak load crack propagated in circumferential direction from both corner of the induced cracks. While circumferential cracks do not create structural issue as such cracks only crosses longitudinal reinforcement bar or possibly will expose one circumferential reinforcement and of less structural concern (Al-Saleem & Langdon 2014; CPAA 2006; Hogan 2017). However, depending on the soil condition of the pipe surrounding, such cracks require remediation. The cracks with larger width was developed in pipes with 300 mm long induced cracks compared to pipe with 150 mm long induced cracks. Multiple longitudinal cracks were observed along the springline. The single longitudinal crack developed inside the crown and invert indicates shear failure of the pipe and hence should be assessed for the condition of the pipe CPAA (2006), while such longitudinal at spring-line is attributed to excessive crushing stress in pipe.



(a)

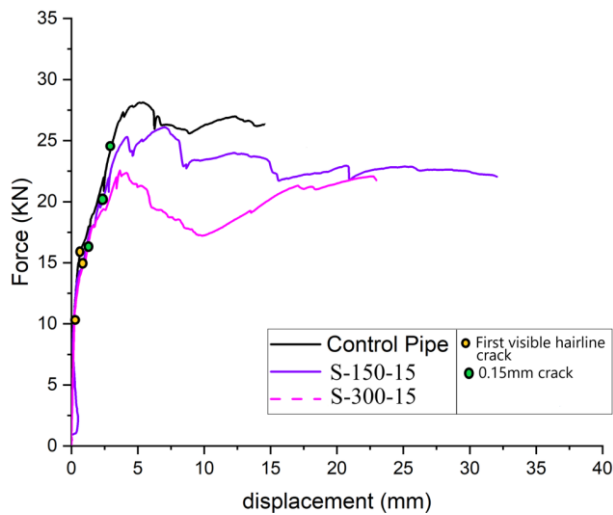
(b)

Figure 6-2 (a) Effect on load-deflection behaviour due to 150mm and 300mm long crack at crown (b) Crack propagation along the radial direction from crack location for 300mm long crown cracked pipe

Table 6-3 Bearing capacity of OPC concrete pipe at different stages of crack development during TEB test

Sample Id	Hairline crack load (kN)	0.15 mm crack load (kN)	Peak load (kN)	Ultimate load (kN)
NP-2	16	24.5	28.2	-
C-150-15	12.5	20	22.1	23.3
S-150-15	14.9	20	26.1	-
C-300-10	13	18	24.3	30
C-300-15	7.5	15	21.8	24.5
S-300-15	10	16	22.1	23

However, for cracks in the springline Figure 6-3 (a), the peak load capacity of the pipe with 150 mm and 300 mm long pre-existing crack was observed to be 10% and 21% lower compared to control pipe. As first observed hairline crack at inner crown propagated to wider crack as it reaches peak load capacity, multiple cracks along the longitudinal direction were also observed at the outer surface of springline for pipe with cracks on springline. With increase in length of crack from 150 mm to 300 mm in the springline of the pipe, the peak load capacity of the pipe decreased by approximately 13%.



(a)



(b)

Figure 6-3(a) Load-deflection behaviour due to 150 mm and 300 mm long crack at springline (b) multiple longitudinal cracks formed in pipe with 150 mm long crack at springline

6.3.2 Effect of change in crack depth on pipe performance

To study the impact of crack depth on the loading capacity of the pipe, cracks in crown of 300 mm long and 5 mm wide with depth of 10 mm and 15 mm was cut into

the outer crown of the pipe. As the loading was applied to the pipe, hairline crack was observed for 15 mm deep cracked pipe at 8 kN load (Figure 6-4) while for pipe with 10mm deep crack, it was observed for load corresponding to 13 kN. With the increasing load, crack width in the inner surface of the crown and invert also increased and many longitudinal cracks at outer surface of springline were formed. The load corresponding to 0.15 mm crack in the pipes with 10 mm and 15 mm deep crack were observed to be 18 kN and 15 kN respectively, while the peak load were observed to be 16% and 22% lesser than the peak load for control pipe. Even though, the peak load capacity of the pipe decreased as the crack depth increased in the crown, gain in load capacity was observed as the load is carried by reinforcement bars before the complete failure of the pipe. However, prominent decrease in ultimate capacity by 17% was observed for change in depth from 10 mm to 15 mm crack.

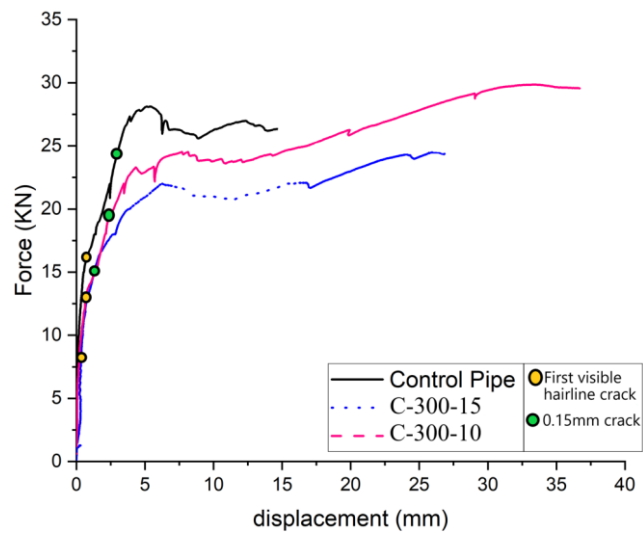
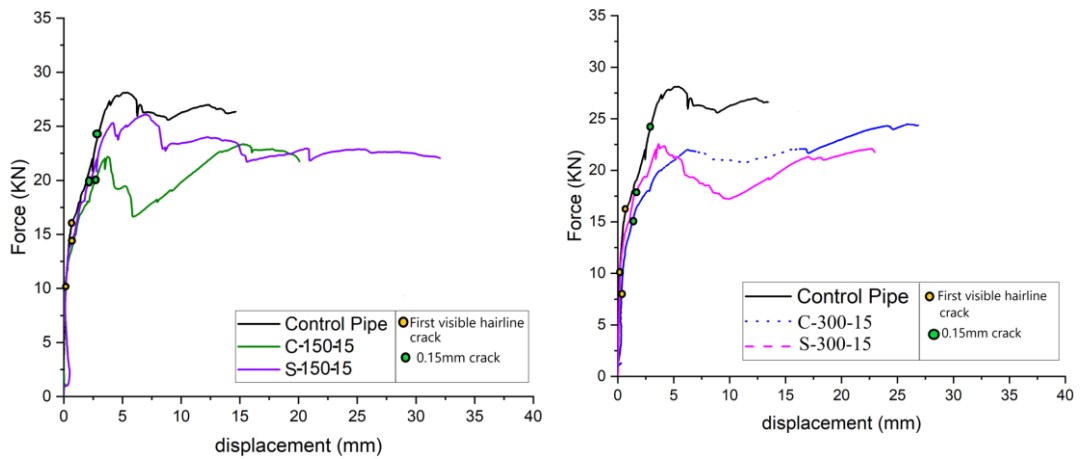


Figure 6-4 Effect on load-deflection behaviour due to 10 mm and 15 mm deep crack at crown

6.3.3 Effect of change in crack location on pipe performance

The influence on load carrying capacity of the pipe due to crack development in different sections of the pipe was also studied by fabricating cracks of length 300 mm and 150 mm long, 15mm deep at the outer part of crown and springline, such that the compression zone in the crown and tension zone in the springline is affected by the cracks. Figure 6-5 shows the load-displacement plot for pipe with 150mm and 300mm long crack.



(a) 150 mm long crack effect

(b) 300 mm long crack effect

Figure 6-5 Load-deflection behaviour of pipe with cracks at different location

For pipe with 150 mm long crack at springline, the peak load capacity was observed to be higher by 12% compared to pipe with crack at crown as seen in Figure 6-5a. For load corresponding to 19.5 kN, crack of 0.15 mm was measured for crown crack of 150 mm long while the same crack was observed for loading capacity of 21.9 kN for 150 mm long crack at springline. When the crack is fabricated in the compressive zone in the concrete section, the tensile stress acting on the inner wall of the crown is the largest (Zhao et al. 2021), conceding the load capacity of the pipe and leading to tensile failure. Though, for 300 mm long cracks at crown and springline, the

peak load capacity was observed to be similar for pipe with crack at springline in comparison to pipe with crown crack (Figure 6-5b). However, on comparing the load-strain curve for the numerical simulation carried out by Zhang et al. (2020) for cracks in crown, springline and invert noted that the pipes with crack on the crown and invert are more easily damaged compared to pipe with springline crack as the strain value was larger for cracks at crown and invert compared to springline.

The experimental analysis on pre-existing crack depth, length and location on concrete pipes performance showcased the load bearing capacity of pipe gets mainly affected in the order of crack depth and length; while comparing the influence of crack location in crown (or compression zone) against springline (or tensile zone), it can be concluded that the crack in crown is more susceptible to failure compared to crack alone at springline. Similar observation for stress development and residual strength in concrete pipes with corroded section was noted by Fang et al. (2019) and Li et al. (2021) stating the residual strength in concrete pipe is greatly affected by corrosion depth rather than corrosion length, while the corrosion width least impacted the residual strength in pipe. While these observations for crack effect on OPC concrete pipe provide basic guideline on pipe vulnerability due to the nature of crack and assist in asset management, influence of pre-existing crack on geopolymer concrete pipe is yet to be carried out.

Thus, considering the development of high compressive and tensile strength in geopolymer concrete compared to OPC concrete, load-deflection behaviour for geopolymer concrete was analysed to explore the bearing capacity of geopolymer concrete pipe with pre-existing crack through numerical modelling.

6.4 Numerical modelling for cracked geopolymer concrete pipe

6.4.1 Pipe model with crack

For numerical modelling of the cracked pipe, the finite element model developed and validated in Chapter 5 was used. A three-dimensional model with its inner diameter of 450 mm, length 500 mm and wall thickness of 45 mm was developed for geopolymer concrete pipe. The K&C concrete model was used to define the non-linear behaviour of geopolymer concrete in ANSYS- LSDYNA. Material properties of geocem 1 was used for the numerical modelling of geopolymer concrete pipe as given in Table 5-5 in Chapter 5. In order to introduce crack in the pipe, the pipe was modelled using mesh size of 5 mm, while the area around the crack was modelled using 1 mm mesh size as seen in Figure 6-6 (a).

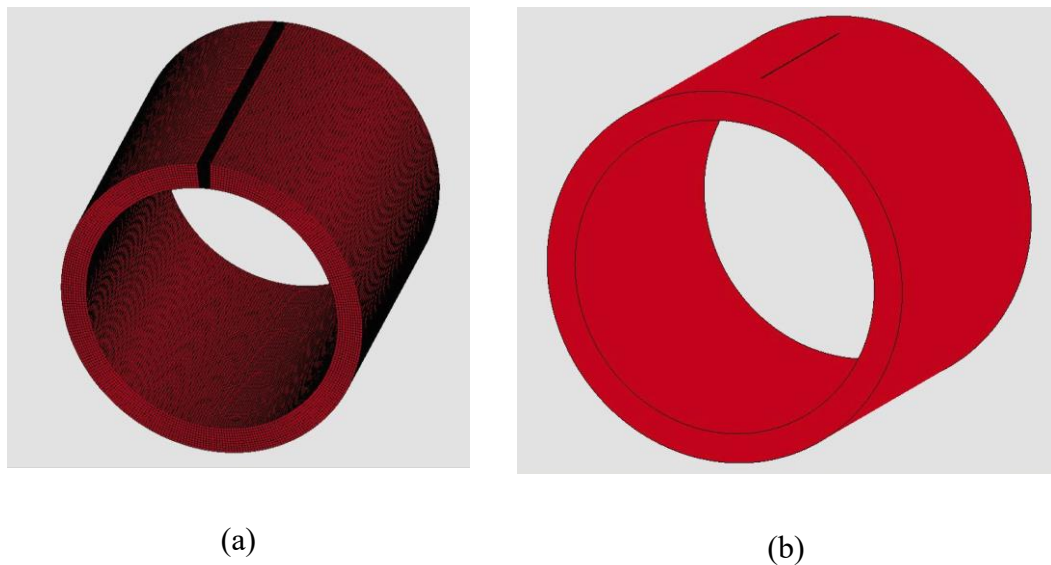


Figure 6-6 (a) Finely meshed geopolymer concrete pipe (b) crack introduced at the crown of pipe model

As the crack in pipe can occur due to multiple reasons, these circumstances can intensify under continuous action of load causing further expansion of crack. However,

it is difficult to predict the location of crack and its dimension. Hence, in an attempt to quantify the crack, a crack of width 1 mm was introduced at the crown of the pipe as shown in Figure 6-6 (b). Thus, by varying the length, depth and position of the crack in the pipe, the effect on the load bearing capacity of the geopolymer concrete pipe is further explored under TEB test. Table 6-4 presents the pipe cases evaluated for the numerical analysis of geopolymer concrete pipes.

Table 6-4 Numerical case study of cracked pipes

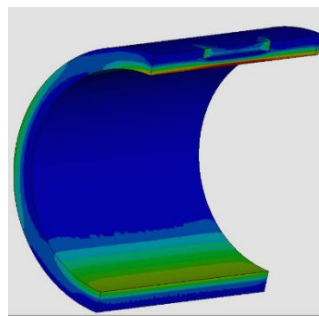
No.	Case Id	Crack length	Crack depth	Crack position
1	G1- no crack	-	-	-
2	G1-200l-25d-C	200	25	Crown
3	G1-300l-25d-C	300		
4	G1-400l-25d-C	400		
5	G1-300l-5d-C	300	5	Crown
6	G1-300l-15d-C		15	
7	G1-300l-15d-Sh	300	15	Shoulder
8	G1-300l-15d-Sp			Springline
9	G1-300l-15d-H			Haunch
10	G1-300l-15d-I			Invert

6.4.2 Effect of crack length on geopolymer concrete pipe

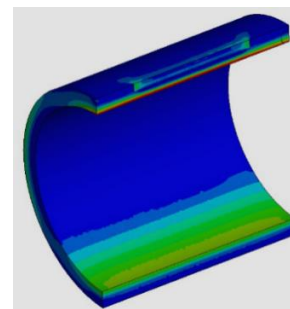
To study the effect of crack length on the geopolymer concrete pipe, crack of 1 mm wide and 25mm deep with varying length of 200 mm, 300 mm and 400 mm was cut

into the crown of the pipe model. The cracked model case was also compared against the numerical analysis result of non-cracked geopolymer concrete pipe.

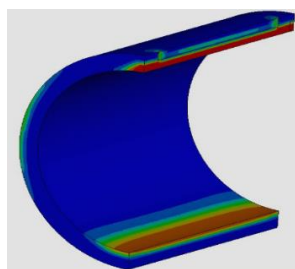
Figure 6-7 shows the stress concentration diagram for geopolymer concrete pipes with pre-existing cracks of length 200 mm, 300 mm and 400 mm. From the figure, it can be interpreted that the length of crack directly affects the stress development in the pipe. As the length of crack increased from 200 mm to 300 mm to 400 mm, continuous increase in stress can be observed indicating the higher risks of damage for geopolymer concrete pipe with respect to increasing crack length. Additionally, Figure 6-8 showcase the numerical analysis result for different crack length on loading behaviour of geopolymer concrete pipe.



(a) 200 mm long crack



(b) 300 mm long crack



(c) 400 mm long crack

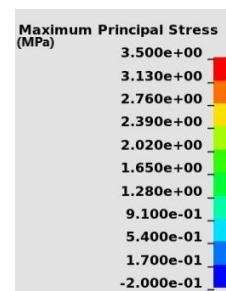


Figure 6-7 Maximum stress distribution in pipe with pre-existing crack of varying length crack

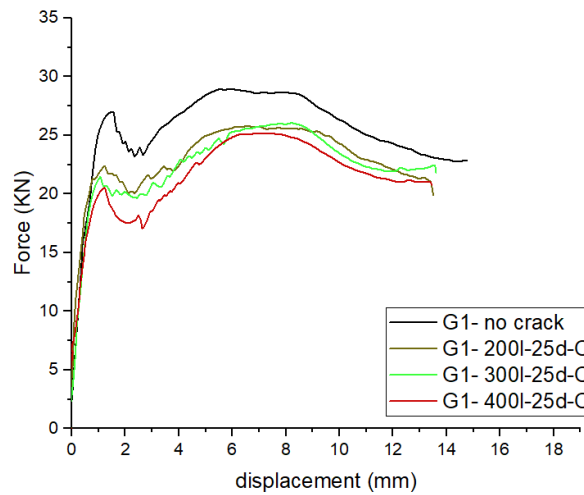


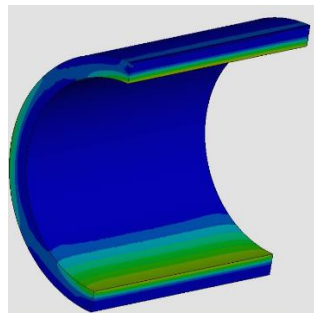
Figure 6-8 Load-displacement curve of geopolymer concrete pipe with pre-existing cracks of varying length on the crown

It was noticed that for increase crack length, the peak load capacity of the geopolymer concrete decreased, while slight decrease in the ultimate load capacity was observed. It is evident from Figure 6-7 where the compressive stress is mainly around the crack while the tensile stress concentration in the pipe can be observed directly underneath the crack location. As the crack length increases, the stress concentration also increased causing stiffness loss in geopolymer concrete, thus decrease in peak load capacity can be noticed as the length of crack increases. For increase in crack length by 100mm, drop in peak load capacity from 200 mm crack to 300 mm crack length and 300 mm to 400 mm crack length was observed to be 4.5%, while the drop in the load capacity in pipe with 200mm long crack compared to perfect condition pipe was found to be 17.5%. The non-cracked pipe with the peak load capacity was noticed to drop from 26.98 kN to 22.28 kN. Comparing the load capacity of 200 mm crack length with 400 mm crack length, the observed drop in peak load is about 9%, which is similar to the drop observed in the experimental analysis for increase in length for OPC concrete.

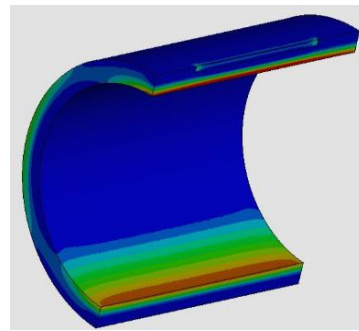
While gain in peak load capacity for geopolymer concrete pipe was affected by the crack length, minor difference in the ultimate load capacity was observed for all geopolymer concrete pipes with pre-existing cracks while the loss in ultimate load capacity was observed to be around 12% compared to non-cracked pipe. This loss in ultimate load capacity compared to non-cracked pipe can be considered due to change in concrete section with reduction of concrete cover for reinforcement bars around the cracked section, while the concrete cover remained the same for pipes with different length crack. This shows the change in crack length significantly impacts the peak load capacity in geopolymer concrete pipes in comparison to ultimate loading capacity, thus influencing the serviceability condition of the pipe.

6.4.3 Effect of crack depth on geopolymer concrete pipe

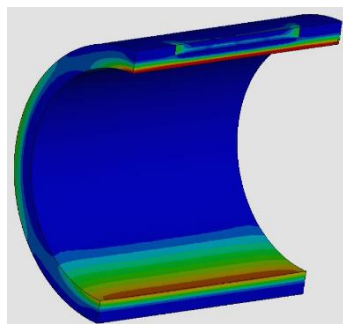
In order to evaluate the bearing capacity change in geopolymer concrete pipe due to change in depth of the crack, 1 mm wide and 300 mm long crack with depth varying from 5 mm, 15 mm to 25 mm was introduced into the crown of the pipe model. Figure 6-9 displays the maximum stress developed in the pipe with crack for a same loading condition while Figure 6-10 shows the graphical plot of the load capacity against the deflection observed.



(a) 5 mm deep crack



(b) 15 mm deep crack



(c) 25 mm deep crack

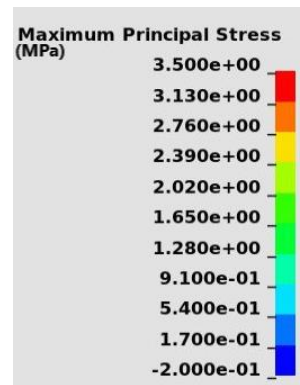


Figure 6-9 Stress development in the pipe with cracks of different depth for same loading condition

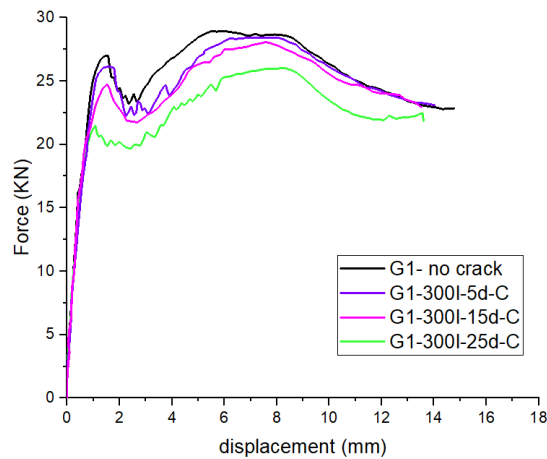


Figure 6-10 Influence on load capacity of geopolymer concrete pipe with crack of different depths

From the stress diagram shown in Figure 6-9, it can be noted that the variation in stress distribution around the crack for same loading condition. The tensile stress acting on the inner wall of the crown and around the crack increases as the crack depth increased. The stress concentration at the end points of the crack can also be seen to intensify as the crack depth increased, resulting in circumferential crack development from the end points of the crack. This aligns with the failure pattern of the tested concrete pipe with pre-existing cracks.

In addition, from the load– deflection curve (Figure 6-10), the difference in the peak load capacity was found to decrease with increase in crack depth, with significant drop noticed for 25 mm deep crack. The peak load capacity for pipe with 5 mm and 15 mm deep crack was observed to be 26 kN and 24.5 kN respectively, while for pipe with 25 mm deep crack was found to be 21 kN. While significant decrease in loading capacity was not observed for pipe with 5 mm deep crack, the loading capacity decreased by 9.3% and 22% for 15 mm and 25 mm deep crack case. Moreover, decrease in ultimate bearing capacity in geopolymer concrete pipes can be noticed for increase in crack depth, indicating the inverse relation between crack depth and ultimate loading capacity. The ultimate bearing capacity in geopolymer concrete pipe decreased by almost 2% and 4% for 5mm and 15 mm deep crack, while the decrease was noted to be 10% for 25 mm deep crack.

Based on the numerical results, it can be confirmed that for geopolymer concrete pipes with pre-existing cracks of varying depth, both peak load capacity and ultimate load capacity decrease with increase in crack depth. Such alteration in loading capacity due to change in crack depth can make pipes susceptible to damage.

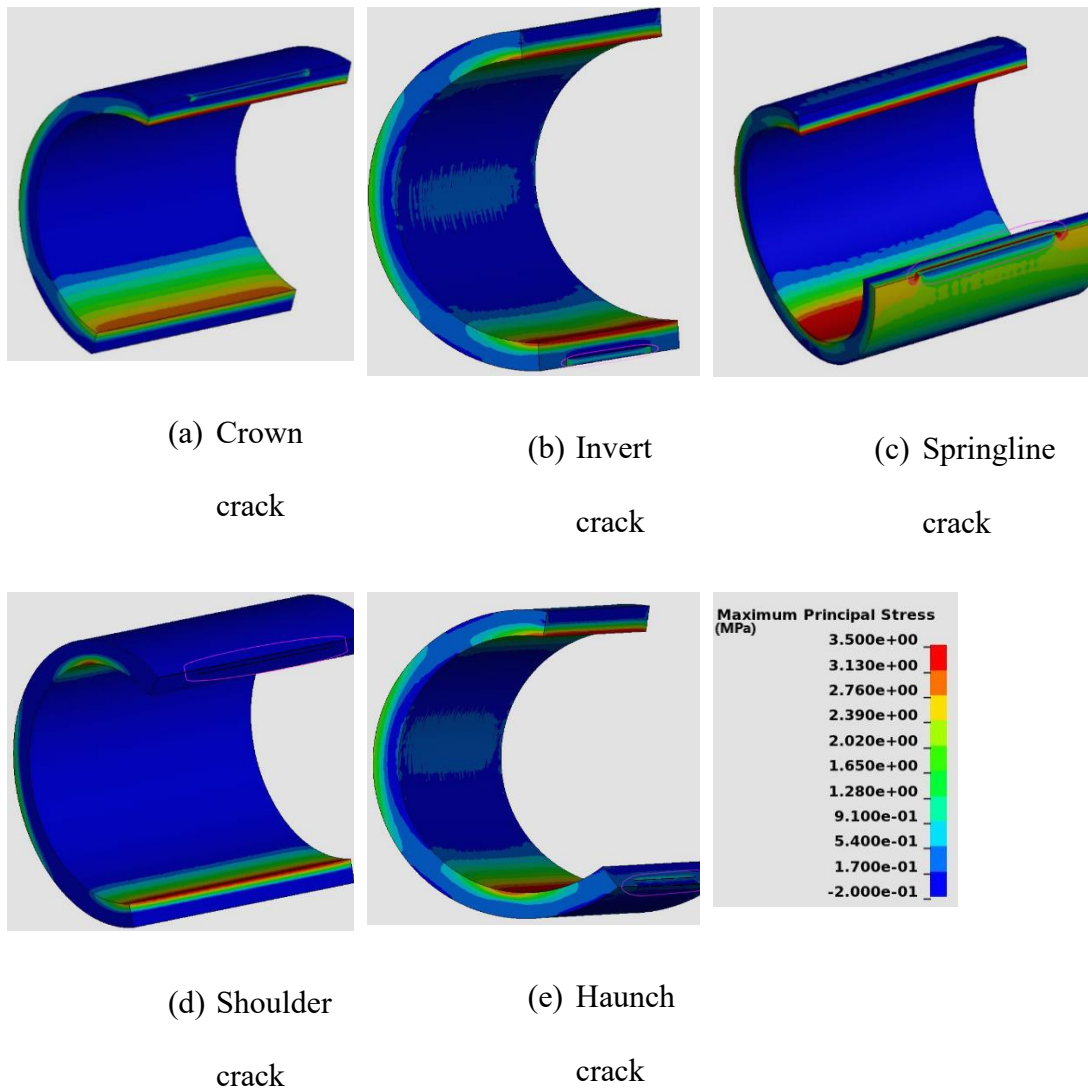


Figure 6-11 Maximum principal stress development in pipe with cracks at different location

6.4.4 Effect of crack location on geopolymer concrete pipe

To further investigate the crack influence on geopolymer concrete pipes, crack of width 1 mm, depth 15 mm and length 300 mm was examined at different positions in the outer wall of the pipes. The cracks were implanted at outer wall of the crown, shoulder, springline, haunch and invert of the pipe. Figure 6-11 shows the maximum

principal stress diagram in geopolymer concrete pipes under the varying crack location.

From the maximum stress diagram, it can be inferred that the stress development is high inside the crown and invert section regardless of the crack location. The intensity of the stress is maximum at the section where the crack is located at the crown and the invert (Figure 6-11a,b), while for crack at springline (Figure 6-11c), the stress concentration is mostly observed around the crack circumference. It should also be noted that the crack in springline lies in tensile zone. The crack at springline thus, acts as plastic hinge, reducing the stress development at the crown and invert (Tran, Setunge & Shi 2018), though the development of stress can be observed to be concentrated around the crack. However, at shoulder, the bottom part of crack is observed to be in compression (Figure 6-11d) without altering the stress development in the pipe, while at haunch (Figure 6-11e) minimum tensile stress development can be observed. As the crack at shoulder and haunch lies in the transition zone (Figure 5-1), it can be concluded that the crack at haunch can impact the pipe greatly compared to crack at shoulder.

Furthermore, Figure 6-12 showcase the loading capacity of the geopolymer concrete pipe for different crack position. Based on the obtained loading capacity data for geopolymer concrete, the peak load capacity were respectively observed to be 24.5 kN, 26.5 kN, 25 kN, 26.1 kN and 24.9 kN for crack at crown, shoulder, springline, haunch and invert in pipe, while slight decrease of about 5% in ultimate load capacity for pipes with crack at crown and invert was observed compared to pipes with crack at shoulder, springline and haunch.

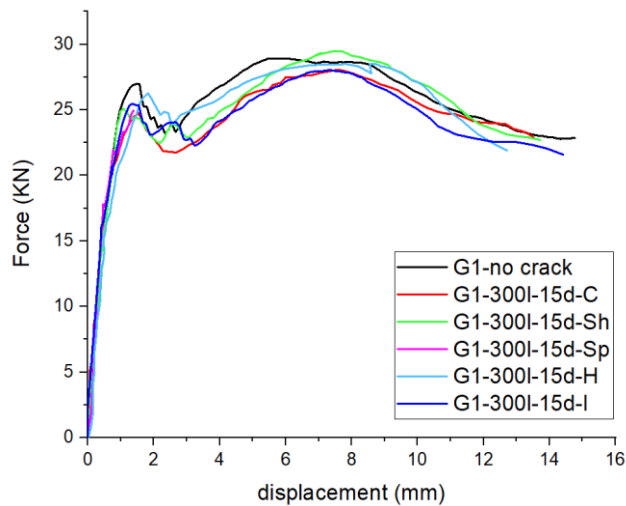


Figure 6-12 Influence on load capacity of geopolymer concrete pipe with crack at different location

Though substantial difference in bearing capacity for different cases of crack location is not observed, the general tendency in load capacity gain is observed to be high for crack located at shoulder, haunch, springline compared to invert and crown. This indicates that the crack located along the loading axis is critical compared to crack located at other locations on the pipe. While cracks in tensile zone affects the bearing capacity in the geopolymer concrete pipe, crack at crown and invert is more inclined to pipe damage compared to crack at springline. Such observation for pipe failure due to crack development at crown, invert, springline and haunch was also marked by CPAA (2006), Hogan (2017) and Tran, Setunge & Shi (2018).

Based on this observation, it can be concluded that loss in bearing capacity in geopolymer concrete pipe with cracks at crown and invert is more compared to crack at springline or haunch, while crack at shoulder presents least risk compared to cracks at other locations. Thus, crack development along the loading axis in pipe is anticipated to cause significant damage in pipe.

6.5 Summary

On conducting the experimental investigation on pipes, it was observed that the spigot pocket section of the pipe provides additional stiffness to the concrete resulting in high load carrying capacity compared to same length pipe without spigot pocket section. Even though limited number of tests and few numerical analysis were carried out in OPC and geopolymer concrete pipes, with and without cracks, following observations were made based on experimental test results.

- In the OPC pipe tests, when the crack length in pipe increases from 200 mm to 400 mm, the peak load capacity in the pipe decreases by 5 to 10% compared to control pipe. Based on numerical analysis carried out on geopolymer concrete pipe, for every increase in crack length by 100 mm, decrease in peak load capacity by 4.5 % was observed.
- For change in crack depth in the OPC pipes, decrease in pipe strength by 4% was observed for every change in depth by 5 mm and reduction in ultimate load capacity by 17% was found.
- The location of crack in concrete pipe also greatly affected the loading capacity of pre-cracked pipes. With crack in crown drop in peak load capacity was observed by 12% compared to crack in springline. With crack in springline, the peak load capacity was observed to be similar for smaller crack compared to larger crack, indicating the crack development in crown as crucial point compared to crack to crack in springline.
- The loss in bearing capacity in geopolymer concrete pipe showcased similar influence of crack length, depth and location as that observed in experimental results for OPC concrete pipes. It was observed that the bearing load capacity of

geopolymer pipe decrease with increase in crack depth and crack length, while the critical position of crack location was found to be along the vertical loading axis.

- The ultimate loading capacity in the geopolymer concrete pipe is greatly impacted by crack depth in compared to the crack length, and the relation between ultimate loading capacity to crack depth is inversely proportional.
- The loss of bearing capacity in geopolymer concrete pipe based on crack location can be classified to be critical for crown and invert, followed by springline and haunch. Crack on shoulder was found to least affect the loading capacity in pipe.

Chapter 7

7. Conclusion and recommendations

7.1 Conclusions

Geopolymer concrete, with its innovative use of industrial by-products, offers a sustainable alternative to OPC concrete with reduced carbon footprint during production. The one-part powder form geopolymer concrete developed by Cement Australia was used in this study that utilizes fly ash and GGBFS as source material along with alkali activator in powder form to overcome the practicality issue raised with liquid activated geopolymer concrete. The mechanical properties of two types of powder form geopolymer concrete: Geocem 1 (general purpose geopolymer) and Geocem 2 (high early strength geopolymer) were investigated for grade 50 MPa geopolymer concrete cured at accelerated temperature. A comparative study carried out to investigate the mechanical properties of geopolymer concrete against OPC concrete showcased early age compressive strength development and improved flexural strength in geopolymer concrete. Such properties of geopolymer concrete can have suitable application in precast concrete pipes where it can benefit not only through rapid production of precast pipe subjected to early age strength gain, but can possibly utilise its high tensile strength capacity in reducing reinforcement requirement. The bond-slip relation between the reinforcement bars and geopolymer concrete were studied, based on which bond-slip relation for powder based geopolymer concrete was proposed and used to further analyse its influence on the performance of reinforced concrete pipe by using finite element model with and without bond consideration.

Hence, to investigate the reliability of geopolymer concrete for precast concrete pipes, load-deflection behaviour of concrete pipe were carried out, along with the development of FE model to simulate TEB test conducted on the pipes. The validated FE model was used to carry out parametric study on geopolymer concrete pipe with changed concrete cover and reinforcement conditions. The ultimate failure load capacity of the geopolymer concrete pipe was further explored considering the bond-slip relation between reinforcement bars and geopolymer concrete. Furthermore, the effect on bearing capacity of concrete pipes with pre-existing cracks was also examined through experimental and numerical study. Hence, based on the outcome from experimental and numerical analysis of geopolymer concrete and pipe structure, following conclusions can be made from this study:

1. The use of powder form of alkali activator in the geopolymer concrete marks the safe handling of geopolymer concrete, unlike the liquid activated geopolymer concrete and can be used in similar manner to that of OPC concrete.
2. The requirement of water/binder ratio for geopolymer concrete to achieve same strength grade concrete is less compared to OPC concrete requirement for water to binder ratio.
3. The gain in compressive strength by both geopolymer concretes in 1 day was higher by around 75% compared to OPC concrete for which the gain in strength was only 10 MPa. This indicates geopolymer concrete to be appropriate for precast concrete pipes. Between geocem 1 and geocem 2, higher amount of GGBFS in geocem 2 resulted in high strength gain in geocem 2 compared to geocem 1.
4. The indirect tensile strength and flexural strength of geopolymer concrete with respect to its compressive strength were found to be higher by 30% and 20% respectively than the values obtained from OPC concrete of same grade, while the

modulus of elasticity and Poisson's ratio of both geopolymer concrete were similar to that of OPC concrete. Therefore, these properties of geopolymer concrete can be capitalised in precast concrete members.

5. The pull-out test carried out to determine the bond strength development in geopolymer concrete compared to OPC concrete revealed higher bond strength capacity in geopolymer concrete. This difference in bond strength development was due to higher compressive strength development in geopolymer concrete compared to same grade OPC concrete.
6. The parametric study carried out to examine the influence of reinforcement diameter on bond strength development showcased increase in reinforcement diameter from 10 mm to 12 mm induced reduction in bond strength while for increase from 12 mm to 16 mm demonstrated increase in bond strength. While the general trend of increase in bond strength with decreasing reinforcement bar is observed, such difference in bond strength development was found to be affected by rib height and clear distance between ribs in reinforcement bar.
7. Similarly, for increase in embedment length decrease in bond strength was observed for both geopolymer concrete type and OPC concrete and for all size of reinforcement bar which is due to increase in bond area between geopolymer concrete and reinforcement bar, thus inversely affecting the bond strength development in concrete specimen.
8. Equation to represent bond-slip relationship for geopolymer concrete was established, based on the pull-out test results.
9. The FE model was developed for concrete pipe and was validated against the experimental test results for concrete pipe. Thus, the FE model can be used in future for design of geopolymer concrete pipes.

10. Consideration of bond-slip modelling for numerical analysis of geopolymer concrete pipes demonstrated overestimation of ultimate bond capacity of geopolymer concrete pipe by 5% to 10% under perfect bond assumption when compared to analysis result with proposed bond relation. Hence, it is recommended to adopt perfect bond condition in numerical analysis of geopolymer concrete pipe design.
11. Parametric study conducted to explore the load-deflection response of geopolymer concrete pipes for change in steel reinforcement area showed that geopolymer concrete pipe can satisfy the specified design load criteria with 20% reduction in reinforcement area for reinforced concrete pipe and increase in pipe diameter in case of unreinforced geopolymer concrete pipe. Thus, use of geopolymer concrete in precast pipe production can result in financial and material savings.
12. For change in concrete cover in geopolymer concrete pipes, concrete pipes with less concrete cover was found to demonstrate higher load carrying capacity. The peak load and ultimate load capacity exhibited by OPC concrete pipe with 20% and 10% of wall thickness as concrete cover was found to be equivalent to geopolymer concrete pipes with concrete cover of 30%-50% of wall thickness, indicating that, with geopolymer concrete pipe high load carrying capacity can be achieved while practising safe concrete cover guidelines provided by ASTM-C76.
13. Change in yield strength of steel reinforcement affected the post-crack behaviour as yielding stress is transferred in steel reinforcement after cracking of concrete section. With increase in the yield strength in steel reinforcement, the ultimate strength of geopolymer concrete pipe also increased.
14. Performance of concrete pipe are greatly affected by the length, depth and position of pre-existing cracks. Based on experimental analysis of OPC concrete pipe

performance with pre-existing crack, it was observed that with increase in crack length, the peak load capacity in the pipe decreases by 5 to 10% compared to control pipe. For change in depth of crack in the pipe, decrease in pipe strength by 4% was observed for change in depth by 5mm, while change in ultimate load capacity by 17% was found. For crack located in crown, drop in peak load capacity was observed by 12% compared to crack in springline, indicating the crack development in crown as crucial point for pipe failure compared to pipe with crack in springline.

15. For geopolymer concrete pipes with pre-existing cracks, the influence of crack length, depth and location on bearing capacity loss were noticed to be similar to experimental results for OPC concrete pipes with crack. It was observed that the load bearing capacity of geopolymer concrete pipe decrease with increase in crack depth and crack length, with crack depth having greater control on failure risk compared to crack length. Additionally, the critical position of crack location was found to be along the vertical loading axis, followed by springline and haunch. Crack on shoulder was found to have least effect on the loading capacity of geopolymer concrete pipe. This finding indicates the damage risk imposed on concrete pipes with pre-existing cracks and can be used as a guideline to evaluate the influence of crack on load bearing capacity and structural integrity of the pipe, in order to take necessary measures for treatment of pipes.

7.2 Recommendations for future studies

This research is based on finite element analysis of geopolymer concrete pipes. The developed model is validated against the OPC concrete pipe test results and appropriate finite element method is followed to attain realistic load-deflection

behaviour of geopolymer concrete pipe, however this research limits in validating the load-deflection response of geopolymer concrete pipe against the test data of geopolymer concrete pipes. Though variation in numerical result between perfect bond case and bond consideration case was observed in the study, however, considering the limited sample study in determining the bond stress-slip relationship which impacts the accuracy of the bond-slip numerical model, further research is required to explore the actual bond stress-slip behaviour for small diameter reinforcement of less than 10mm. In addition to this, comparison of numerical study with bond stress-slip consideration against experimental TEB test of geopolymer concrete pipe is also required to further validate the proposed equation.

As geopolymer concrete poses higher flexural strength compared to OPC concrete, the loading capacity of the geopolymer concrete is shown to improve significantly for use in precast pipes. It is suggested to carry out experimental analysis of geopolymer concrete pipe under TEB test at different age, mainly to explore the early age strength development contribution in loading capacity. It would be interesting to see the loading behaviour of geopolymer concrete pipe under reduced reinforcement area and for unreinforced pipes with greater dimension. Study to examine the load-deflection response and failure of geopolymer concrete pipe under buried condition to emulate the real service condition and can contribute to serviceability based design guides for concrete pipe as the loading criteria under TEB test are more extreme and concentrated, contrast to actual loading condition under buried condition.

Due to constrain in resources, the experimental study carried out on pipes were limited to small length pipes rather than full length pipe. In addition, the limited

samples were tested for OPC concrete pipes with induced cracks, so the best results for the test was not confirmed. Hence, further detail study on full length pipe with pre-existing cracks for geopolymer concrete can provide more profound information on structural performance of geopolymer concrete pipe. Moreover, this study has not covered the repair and strengthening measures for geopolymer concrete pipe with pre-existing cracks. It is thus, beneficial to carry out study investigating the remedial approaches to improve the value of service life cycle of geopolymer concrete pipes. Moreover, it was observed that the serviceability and durability of concrete pipes are greatly affected by the environmental condition, especially the hydrogen sulfate (H_2S) attack on reinforced concrete pipe, it is recommended to investigate on geopolymer concrete durability aspect to develop design practices based on durability.

References

- (FIB), F.I.d.B. 2000, *Bond of Reinforcement in Concrete: State-of-art Report*, International Federation for Structural Concrete.
- Abdulrahman, H., Muhamad, R., Visintin, P. & Shukri, A.A. 2022, 'Mechanical properties and bond stress-slip behaviour of fly ash geopolymer concrete', *Construction and Building Materials*, vol. 327, p. 126909.
- Abedini, M. & Zhang, C. 2021, 'Performance assessment of concrete and steel material models in ls-dyna for enhanced numerical simulation, a state of the art review', *Archives of Computational Methods in Engineering*, vol. 28, no. 4, pp. 2921-42.
- ABNT-NBR8890 2007, *Concrete pipes for circular section for pluvial waters and sanitary sewers- Requirements and test methods*, Associação Brasileira de Normas Técnicas Rio de Janeiro, RJ.
- Abolmaali, A., Mikhaylova, A., Wilson, A. & Lundy, J. 2012, 'Performance of steel fiber-reinforced concrete pipes', *Transportation research record*, vol. 2313, no. 1, pp. 168-77.
- Abrishami, H.H. & Mitchell, D. 1996, 'Analysis of bond stress distributions in pullout specimens', *Journal of Structural Engineering*, vol. 122, no. 3, pp. 255-61.
- ACI211.3R-02 2009, *Guide for Selecting Proportions for No-Slump Concrete*, American Concrete Institute (ACI) Committee 211.
- ACI318 2019, *Building Code Requirements for Structural Concrete*, ACI Committee 318, Farmington Hills, MI, USA.
- ACI363R 1992, *State-of-the-Art Report on High-Strength Concrete*, American Concrete Institute Committee.
- ACI408R-03 2003, *Bond and Development of Straight Reinforcing Bars in Tension*, American Concrete Institute.
- ACPA 1981, *Concrete Pipe Handbook*, American Concrete Pipe Association, Virginia, USA.
- ACPA 2011, 'Concrete pipe design manual', American Concrete Pipe Association Irving, TX, USA.
- ACPA 2016, 'Precast Concrete Pipe Durability', July 2016 edn, American Concrete Pipe Association (ACPA), <<https://www.concretepipe.org/wp-content/uploads/CPInfoDurability072116.pdf>>.

- Al-Chaar, G.K., Alkadi, M. & Asteris, P.G. 2013, 'Natural pozzolan as a partial substitute for cement in concrete', *The Open Construction and Building Technology Journal*, vol. 7, no. 1.
- Al-lami, B.H.K. 2020, 'Performance of Cracked Reinforced Concrete Pipes Subjected to Different Environmental Conditions', The University of Texas at Arlington.
- Al-Saleem, H.I. & Langdon, W. 2014, 'Post Installation Cracking of Reinforced Concrete Pipes- The buried Facts', paper presented to the *Stormwater conference*.
- Albitar, M., Mohamed Ali, M.S., Visintin, P. & Drechsler, M. 2017a, 'Durability evaluation of geopolymer and conventional concretes', *Construction and Building Materials*, vol. 136, pp. 374-85.
- Albitar, M., Visintin, P., Ali, M.S.M., Lavigne, O. & Gamboa, E. 2017b, 'Bond Slip Models for Uncorroded and Corroded Steel Reinforcement in Class-F Fly Ash Geopolymer Concrete', *Journal of Materials in Civil Engineering*, vol. 29, no. 1, p. 04016186.
- Albitar, M., Visintin, P., Mohamed Ali, M.S. & Drechsler, M. 2015, 'Assessing behaviour of fresh and hardened geopolymer concrete mixed with class-F fly ash', *KSCE Journal of Civil Engineering*, vol. 19, no. 5, pp. 1445-55.
- Aldred, J. & Day, J. 2012, 'Is geopolymer concrete a suitable alternative to traditional concrete', *37th Conference on our world in concrete & structures, Singapore*, pp. 29-31.
- Aldred, J.M. 2013, 'Engineering properties of a proprietary premixed geopolymer concrete', *Proceedings Concrete Institute of Australia Biennial Conference, Concrete*.
- Alkhalwaldeh, S. 2019, 'FE modelling of the bond-slip behaviour and its effects on the seismic performance of RC framed structures', Loughborough University.
- American Concrete Pipe Association (ACPA) 1993, *Concrete pipe technology handbook*, American Concrete Pipe Association, Dallas, TX.
- Amran, M., Al-Fakih, A., Chu, S.H., Fediuk, R., Haruna, S., Azevedo, A. & Vatin, N. 2021, 'Long-term durability properties of geopolymer concrete: An in-depth review', *Case Studies in Construction Materials*, vol. 15, p. e00661.
- Amran, M., Debbarma, S. & Ozbakkaloglu, T. 2021, 'Fly ash-based eco-friendly geopolymer concrete: A critical review of the long-term

- durability properties', *Construction and Building Materials*, vol. 270, p. 121857.
- Andrews-Phaedonos, F. 2011, 'Geopolymer “green” concrete: reducing the carbon footprint. The VicRoads experience', *8th Austroads Bridge Conference, Sydney, NSW, Australia*.
- Andrews-Phaedonos, F. 2014, 'Specification and use of geopolymer concrete', *Austroads Bridge Conference, 9th, 2014, Sydney, New South Wales, Australia*.
- Anuradha, R., Sreevidya, V., Venkatasubramani, R. & Rangan, B.V. 2012, 'Modified guidelines for geopolymer concrete mix design using Indian standard'.
- AS1012.8.1 2014, *Methods of testing concrete Method for making and curing concrete - Compression and indirect tensile test specimens*, Standards Australia, Sydney.
- AS1012.8.2 2014, *Methods of testing concrete - Method for making and curing concrete - Flexure test specimens*, Standards Australia, Sydney.
- AS1012.10 2000, *Methods of testing concrete - Determination of indirect tensile strength of concrete cylinders ('Brazil' or splitting test)*, Standards Australia.
- AS1012.11 2000, *Methods of testing concrete, Method 11 – Determination of the modulus of rupture*, Standards Australia, Sydney.
- AS1012.17 1997, *Methods of testing concrete Method 17: Determination of the static chord modulus of elasticity and Poisson's ratio of concrete specimens*, Australian Standard.
- AS3600 2018, *Concrete Structures*, Standards Australia International Ltd, Sydney, NSW.
- AS/NZS1597.1 2010, *Precast reinforced concrete box culverts*, Standard Australia Limited, Sydney, Australia.
- AS/NZS4058 2007, *Precast concrete pipes (pressure and non-pressure)*, Standards Australia Sydney, NSW.
- ASCE 1982, *State-of-the-Art Report on Finite Element Analysis of Reinforced Concrete* ASCE Task Committee, New York.
- ASCE 1998, *Standard Practice for direct design of buried precast concrete pipe using standard installations (SIDD)*, American Society of Civil Engineers.

- ASTM-A944 2022, *Standard Test Method for Comparing Bond Strength of Steel Reinforcing Bars to Concrete Using Beam-End Specimens*, ASTM International, West Conshohocken, PA, United States.
- ASTMC39M 2021, *Standard Test Method for Compressive Strength of Cylindrical Concrete Specimens*, ASTM Committee, West Conshohocken, PA 19428-2959. United States.
- ASTMC76M 2022, *Standard Specification for Reinforced Concrete Culvert, Storm Drain, and Sewer Pipe (Metric)1*.
- Atiş, C., Görür, E., Karahan, O., Bilim, C., Ilkentapar, S. & Luga, E. 2015, 'Very high strength (120 MPa) class F fly ash geopolymer mortar activated at different NaOH amount, heat curing temperature and heat curing duration', *Construction and building materials*, vol. 96, pp. 673-8.
- Atiş, C.D., Bilim, C., Çelik, Ö. & Karahan, O. 2009, 'Influence of activator on the strength and drying shrinkage of alkali-activated slag mortar', *Construction and building materials*, vol. 23, no. 1, pp. 548-55.
- Attal, A., Brigodiot, M., Camacho, P. & Manem, J. 1992, 'Biological mechanisms of H₂S formation in sewer pipes', *Water Science and Technology*, vol. 26, no. 3-4, pp. 907-14.
- Bahraq, A.A., Al-Osta, M.A., Ahmad, S., Al-Zahrani, M.M., Al-Dulaijan, S.O. & Rahman, M.K. 2019, 'Experimental and Numerical Investigation of Shear Behavior of RC Beams Strengthened by Ultra-High Performance Concrete', *International Journal of Concrete Structures and Materials*, vol. 13, no. 1, p. 6.
- Bakria, A.M.M.A., Kamarudin, H., BinHussain, M., Nizar, I.K., Zarina, Y. & Rafiza, A.R. 2011, 'The Effect of Curing Temperature on Physical and Chemical Properties of Geopolymers', *Physics Procedia*, vol. 22, pp. 286-91.
- Barbosa, A., Idelsohn, S., Oñate, E. & Dvorkin, E. 1998, 'Analysis of reinforced concrete structures using ANSYS nonlinear concrete model'.
- Barbosa, V.F., MacKenzie, K.J. & Thaumaturgo, C. 2000, 'Synthesis and characterisation of materials based on inorganic polymers of alumina and silica: sodium polysialate polymers', *International journal of inorganic materials*, vol. 2, no. 4, pp. 309-17.
- Bentz, D.P., Garboczi, E.J., Lu, Y., Martys, N., Sakulich, A.R. & Weiss, W.J. 2013, 'Modeling of the influence of transverse cracking on

- chloride penetration into concrete', *Cement and Concrete Composites*, vol. 38, pp. 65-74.
- Bernal, S.A., de Gutiérrez, R.M., Pedraza, A.L., Provis, J.L., Rodriguez, E.D. & Delvasto, S. 2011, 'Effect of binder content on the performance of alkali-activated slag concretes', *Cement and concrete research*, vol. 41, no. 1, pp. 1-8.
- Binici, H., Durgun, M.Y., Rızaoğlu, T. & Koluçolak, M. 2012, 'Investigation of durability properties of concrete pipes incorporating blast furnace slag and ground basaltic pumice as fine aggregates', *Scientia Iranica*, vol. 19, no. 3, pp. 366-72.
- Binici, H., Durgun, M.Y., Rızaoğlu, T. & Koluçolak, M. 2012, 'Investigation of durability properties of concrete pipes incorporating blast furnace slag and ground basaltic pumice as fine aggregates', *Scientia Iranica*, vol. 19, no. 3, pp. 366-72.
- Bligh, R. & Glasby, T. 2013, 'Development of geopolymer precast floor panels for the Global Change Institute at University of Queensland', *Proceedings Concrete Institute of Australia Biennial Conference, Concrete*.
- Boopalan, C. & Rajamane, N. 2017, 'An investigation of bond strength of reinforcing bars in fly ash and GGBS based geopolymer concrete', *MATEC Web of Conferences*, vol. 97, EDP Sciences, p. 01035.
- Bowker, R., Smith, J., Shah, H. & Flaherty, P. 1991, 'Hydrogen sulfide corrosion in wastewater collection and treatment systems', *United States environmental protection agency, Washington, DC*.
- Branco, F.A.B., Arruda, M.R.T. & Correia, J.P.R.R. 2013, 'Experimental and numerical investigations on the structural response of precast concrete underpasses subjected to live loads', *The Baltic Journal of Road and Bridge Engineering*, vol. 8, no. 1, pp. 48-57.
- Broomfield, J. 2007, *Corrosion of Steel in Concrete: Understanding, Investigation and Repair*, 2nd edn, Taylor & Francis, London.
- Buda-Ozog, L., Skrzypczak, I. & Kujda, J. 2017, 'Cracks analysis in the reinforced concrete pipes', *The Baltic Journal of Road and Bridge Engineering*, vol. 12, no. 2, pp. 88-93.
- Campos, R. 2010, *Comparative analysis of the mechanical performance of polypropylene and steel fibre reinforced concrete pipes*, Projeto FASESP 2009/03982-3. Technical Report. Universidade São Paulo, Sao

- Capozucca, R. 2013, 'Analysis of bond-slip effects in RC beams strengthened with NSM CFRP rods', *Composite Structures*, vol. 102, pp. 110-23.
- Carreira, D.J. & Chu, K.-H. 1985, 'Stress-strain relationship for plain concrete in compression', *Journal Proceedings*, vol. 82, pp. 797-804.
- Castel, A. 2016, 'Bond Between Steel Reinforcement and Geopolymer Concrete' pp. 375-87.
- Castel, A. & Foster, S.J. 2015, 'Bond strength between blended slag and Class F fly ash geopolymer concrete with steel reinforcement', *Cement and Concrete Research*, vol. 72, pp. 48-53.
- CEB-FIB 1990, 'Model Code 90', *Bulletin d'information*, no. 205-206.
- CEB-FIB 2010, 'CEB-FIB model code 2010–Final draft', *Thomas Thelford, Lausanne, Switzerland*.
- Çevik, A., Alzeebaree, R., Humur, G., Niş, A. & Gülşan, M.E. 2018, 'Effect of nano-silica on the chemical durability and mechanical performance of fly ash based geopolymer concrete', *Ceramics International*, vol. 44, no. 11, pp. 12253-64.
- Chang, E.H., Sarker, P., Lloyd, N. & Rangan, B.V. 2009, 'Bond behaviour of reinforced fly ash-based geopolymer concrete beams', *Proceedings of the 24th Biennial Conference of the Concrete Institute Australia*, Concrete Institute of Australia.
- Chen, G., Teng, J. & Chen, J. 2011, 'Finite-element modeling of intermediate crack debonding in FRP-plated RC beams', *Journal of composites for construction*, vol. 15, no. 3, pp. 339-53.
- Chen, G., Teng, J., Chen, J. & Rosenboom, O. 2008, 'Finite element model for intermediate crack debonding in RC beams strengthened with externally bonded FRP reinforcement', *Fourth International Conference FRP Composites in Civil Engineering (CICE2008)*.
- Chen, H. 2016, 'An introduction to* CONstrained_Beam_in_Solid', *FEA Information Engineering Solutions*, vol. 5, no. 10, pp. 79-83.
- Chen, H. & Do, I. 2019, *New Developments in * CONstrained_Beam/Shell/Solid_in_Solid*, LS-DYNA China.
- Chen, W.-F. & Han, D.-J. 1988, *Plasticity for structural engineers*, Springer-Verlag, New York.

- Chi, M. 2012, 'Effects of dosage of alkali-activated solution and curing conditions on the properties and durability of alkali-activated slag concrete', *Construction and Building Materials*, vol. 35, pp. 240-5.
- Chitralla, S., Jadaprolu, G.J. & Chundupalli, S. 2018, 'Study and predicting the stress-strain characteristics of geopolymer concrete under compression', *Case studies in construction materials*, vol. 8, pp. 172-92.
- Chong, K.T. 2004, *Numerical modelling of time-dependent cracking and deformation of reinforced concrete structures*, University of New South Wales.
- Collins, F. & Sanjayan, J. 1999a, 'Workability and mechanical properties of alkali activated slag concrete', *Cement and concrete research*, vol. 29, no. 3, pp. 455-8.
- Collins, F. & Sanjayan, J.G. 1999b, 'Workability and mechanical properties of alkali activated slag concrete', *Cement and concrete research*, vol. 29, no. 3, pp. 455-8.
- Collins, M.P., Mitchell, D. & MacGregor, J.G. 1993, 'Structural design considerations for high-strength concrete', *Concrete international*, vol. 15, no. 5, pp. 27-34.
- Cosenza, E., Manfredi, G. & Realfonzo, R. 1997, 'Behavior and modeling of bond of FRP rebars to concrete', *Journal of composites for construction*, vol. 1, pp. 40-51.
- CPAA, *Concrete pipe facts*, Concrete Pipe Association of Australasia, Australia, viewed 8 April 2019, <<https://www.cpaas.asn.au/General/concrete-pipe-facts.html>>.
- CPAA 2006, *Durability of reinforced concrete pipe – the hard facts!*, Concrete Pipe Association of Australasia.
- CSA-A257 2014, *Standards for concrete pipe and manhole sectiona*, CSA Group, Mississauga, ON.
- Cui, Y. 2015, 'Bond behaviour between reinforcing steel bars and fly-ash based geopolymer concrete', *School of Engineering and Information Technology, University of New South Wales, Canberra*.
- Cui, Y., Zhang, P. & Bao, J. 2020, 'Bond Stress between Steel-Reinforced Bars and Fly Ash-Based Geopolymer Concrete', *Advances in Materials Science and Engineering*, vol. 2020.

- Cullen, N. 1982, 'The sewer dereliction problem—evidence from collapse studies', *Restoration of sewerage systems*, Thomas Telford Publishing, pp. 9-16.
- da Silva, J.L., El Debs, M.K. & Kataoka, M.N. 2018, 'A comparative experimental investigation of reinforced-concrete pipes under three-edge-bearing test: Spigot and Pocket and Ogee Joint pipes', *Acta Scientiarum. Technology*, vol. 40, pp. e30860-e.
- Dahou, Z., Castel, A. & Noushini, A. 2016, 'Prediction of the steel-concrete bond strength from the compressive strength of Portland cement and geopolymer concretes', *Construction and Building Materials*, vol. 119, pp. 329-42.
- Daud, R.A., Cunningham, L.S. & Wang, Y.C. 2017, 'New model for post-fatigue behaviour of CFRP to concrete bond interface in single shear', *Composite Structures*, vol. 163, pp. 63-76.
- Davidovits, J. 1989, 'Geopolymers and geopolymeric materials', *Journal of Thermal Analysis and Calorimetry* vol. 35, no. 2.
- Davidovits, J. 1991, 'Geopolymers: inorganic polymeric new materials', *Journal of Thermal Analysis and calorimetry*, vol. 37, no. 8, pp. 1633-56.
- Davidovits, J. 2005, 'Geopolymer chemistry and sustainable development. The poly (sialate) terminology: a very useful and simple model for the promotion and understanding of green-chemistry', *Proceedings of the world congress Geopolymer*, Saint Quentin, France, pp. 9-15.
- Davidovits, J. 2015, 'False values on CO2 emission for geopolymer cement/concrete published in scientific papers', *Technical Paper*, vol. 24.
- Davies, J.P., Clarke, B.A., Whiter, J.T. & Cunningham, R.J. 2001, 'Factors influencing the structural deterioration and collapse of rigid sewer pipes', *Urban Water*, vol. 3, no. 1, pp. 73-89.
- de Figueiredo, A., Aguado, A., Molins, C. & Chama Neto, P.J. 2012, 'Steel fibre reinforced concrete pipes. Part 2: numerical model to simulate the crushing test', *Revista IBRACON de Estruturas e Materiais*, vol. 5, no. 1, pp. 12-25.
- de la Fuente, A., de Figueiredo, A.D., Aguado, A., Molins, C. & Neto, P.J.C. 2011, 'Experimentation and numerical simulation of steel fibre reinforced concrete pipes', *Materiales de construcción*, vol. 61, no. 302, pp. 275-88.

- de la Fuente, A., Escariz, R.C., de Figueiredo, A.D. & Aguado, A. 2013, 'Design of macro-synthetic fibre reinforced concrete pipes', *Construction and Building Materials*, vol. 43, pp. 523-32.
- Deb, P.S., Nath, P. & Sarker, P.K. 2014, 'The effects of ground granulated blast-furnace slag blending with fly ash and activator content on the workability and strength properties of geopolymer concrete cured at ambient temperature', *Materials & Design (1980-2015)*, vol. 62, pp. 32-9.
- Desayi, P. & Krishnan, S. 1964, 'Equation for the stress-strain curve of concrete', *Journal Proceedings*, vol. 61, pp. 345-50.
- Desnerck, P., De Schutter, G. & Taerwe, L. 2010, 'Bond behaviour of reinforcing bars in self-compacting concrete: experimental determination by using beam tests', *Materials and Structures*, vol. 43, no. 1, pp. 53-62.
- Diaz-Loya, E.I., Allouche, E.N. & Vaidya, S. 2011, 'Mechanical properties of fly-ash-based geopolymer concrete', *ACI materials journal*, vol. 108, no. 3, p. 300.
- Douglas, E., Bilodeau, A. & Malhotra, V. 1992, 'Properties and durability of alkali-activated slag concrete', *Materials Journal*, vol. 89, no. 5, pp. 509-16.
- Du, X. & Jin, L. 2021, 'Methodology: Meso-Scale Simulation Approach', *Size Effect in Concrete Materials and Structures*, Springer, pp. 27-76.
- Duxson, P., Fernández-Jiménez, A., Provis, J.L., Lukey, G.C., Palomo, A. & van Deventer, J.S.J. 2007, 'Geopolymer technology: the current state of the art', *Journal of Materials Science*, vol. 42, no. 9, pp. 2917-33.
- Duxson, P. & Provis, J.L. 2008, 'Designing precursors for geopolymer cements', *Journal of the American Ceramic Society*, vol. 91, no. 12, pp. 3864-9.
- Duxson, P., Provis, J.L., Lukey, G.C., Mallicoat, S.W., Kriven, W.M. & Van Deventer, J.S. 2005, 'Understanding the relationship between geopolymer composition, microstructure and mechanical properties', *Colloids and Surfaces A: Physicochemical and Engineering Aspects*, vol. 269, no. 1-3, pp. 47-58.
- Duxson, P., Provis, J.L., Lukey, G.C. & Van Deventer, J.S. 2007, 'The role of inorganic polymer technology in the development of 'green

- concrete', *Cement and Concrete Research*, vol. 37, no. 12, pp. 1590-7.
- El Naggar, H., Allouche, E. & El Naggar, M. 2007, 'Development of a new class of precast concrete pipes-an experimental evaluation', *Canadian Journal of Civil Engineering*, vol. 34, no. 7.
- Eligehausen, R., Popov, E.P. & Bertero, V.V. 1982, 'Local bond stress-slip relationships of deformed bars under generalized excitations'.
- Elnashai, A.S. & Izzuddin, B.A. 1993, 'Modelling of material nonlinearities in steel structures subjected to transient dynamic loading', *Earthquake engineering & structural dynamics*, vol. 22, no. 6, pp. 509-32.
- EN-1916 2002, *Concrete pipes and fittings, unreinforced, steel fibre and reinforced*, European Committee for Standardization.
- Erdogmus, E., Skourup, B.N. & Tadros, M. 2010, 'Recommendations for design of reinforced concrete pipe', *Journal of Pipeline Systems Engineering and Practice*, vol. 1, no. 1, pp. 25-32.
- Erdogmus, E. & Tadros, M.K. 2006, 'Behavior and Design of Buried Concrete Pipes'.
- Esfahani, M.R. & Rangan, B.V. 1998, 'Bond between normal strength and high-strength concrete (HSC) and reinforcing bars in splices in beams', *Structural Journal*, vol. 95, no. 3, pp. 272-80.
- Fahim Huseien, G., Mirza, J., Ismail, M., Ghoshal, S.K. & Abdulameer Hussein, A. 2017, 'Geopolymer mortars as sustainable repair material: A comprehensive review', *Renewable and Sustainable Energy Reviews*, vol. 80, pp. 54-74.
- Fang, H., Yang, K., Li, B., Tan, P., Wang, F. & Du, X. 2019, 'Experimental and numerical study on mechanical analysis of buried corroded concrete pipes under static traffic loads', *Applied Sciences*, vol. 9, no. 23, p. 5002.
- Farhan, N.A., Sheikh, M.N. & Hadi, M.N. 2019, 'Investigation of engineering properties of normal and high strength fly ash based geopolymer and alkali-activated slag concrete compared to ordinary Portland cement concrete', *Construction and Building Materials*, vol. 196, pp. 26-42.
- Ferdous, W., Manalo, A., Khennane, A. & Kayali, O. 2015, 'Geopolymer concrete-filled pultruded composite beams—concrete mix design and application', *Cement and concrete composites*, vol. 58, pp. 1-13.

- Ferguson, P.M. 1966, 'Bond stress the state of the art', *Journal of the American Concrete Institute*, vol. 63, no. 1, pp. 1161-90.
- Fernández-Jiménez, A., García-Lodeiro, I. & Palomo, A. 2007, 'Durability of alkali-activated fly ash cementitious materials', *Journal of Materials Science*, vol. 42, no. 9, pp. 3055-65.
- Fernández-Jiménez, A., Palomo, J. & Puertas, F. 1999, 'Alkali-activated slag mortars: mechanical strength behaviour', *Cement and concrete research*, vol. 29, no. 8, pp. 1313-21.
- Fernández-Jiménez, A. & Puertas, F. 2002, 'The alkali-silica reaction in alkali-activated granulated slag mortars with reactive aggregate', *Cement and concrete research*, vol. 32, no. 7, pp. 1019-24.
- Fernandez-Jimenez, A.M., Palomo, A. & Lopez-Hombrados, C. 2006, 'Engineering properties of alkali-activated fly ash concrete', *ACI Materials Journal*, vol. 103, no. 2, p. 106.
- Ferrado, F.L., Escalante, M.R. & Rougier, V.C. 2016, 'Numerical simulation of the three edge bearing test of steel fiber reinforced concrete pipes', *Mecánica Computacional*, vol. 34, no. 34, pp. 2329-41.
- Ferrado, F.L., Escalante, M.R. & Rougier, V.C. 2018, 'Simulation of the Three Edge Bearing Test: 3D Model for the Study of the Strength Capacity of SFRC Pipes', *Mecánica Computacional*, vol. 36, no. 6, pp. 195-204.
- Gambarova, P.G. & Rosati, G. 1996, 'Bond and splitting in reinforced concrete: test results on bar pull-out', *Materials and Structures*, vol. 29, no. 5, pp. 267-76.
- Gan, Y. 2000, 'Bond stress and slip modeling in nonlinear finite element analysis of reinforced concrete structures', *University of Toronto*.
- Ganesan, N., Indira, P.V. & Santhakumar, A. 2015, 'Bond behaviour of reinforcing bars embedded in steel fibre reinforced geopolymer concrete', *Magazine of Concrete Research*, vol. 67, no. 1, pp. 9-16.
- Gibbons, P. 1997, 'Pozzolans for lime mortars', *The conservation and repair of Ecclesiastical buildings*.
- Glasby, T., Day, J., Genrich, R. & Aldred, J. 2015, 'EFC geopolymer concrete aircraft pavements at Brisbane West Wellcamp Airport', *Concrete*, vol. 2015, pp. 1-9.
- Gomaa, E., Sargon, S., Kashosi, C., Gheni, A. & ElGawady, M.A. 2020, 'Mechanical properties of high early strength class c fly Ash-Based

- alkali activated concrete', *Transportation Research Record*, vol. 2674, no. 5, pp. 430-43.
- Goto, Y. 1971, 'Cracks formed in concrete around deformed tension bars', *Journal Proceedings*, vol. 68, pp. 244-51.
- Gourley, J.T. 2014, 'Geopolymers in Australia', *Journal of the Australian Ceramics Society*, vol. 50, no. 1, pp. 102-10.
- Gunasekera, C., Setunge, S. & Law, D.W. 2017, 'Correlations between mechanical properties of low-calcium fly ash geopolymer concretes', *Journal of Materials in Civil Engineering*, vol. 29, no. 9, p. 04017111.
- Habert, G., De Lacaillerie, J.D.E. & Roussel, N. 2011, 'An environmental evaluation of geopolymer based concrete production: reviewing current research trends', *Journal of cleaner production*, vol. 19, no. 11, pp. 1229-38.
- Hajimohammadi, A., Provis, J.L. & Van Deventer, J.S. 2008, 'One-part geopolymer mixes from geothermal silica and sodium aluminate', *Industrial & Engineering Chemistry Research*, vol. 47, no. 23, pp. 9396-405.
- Haktanir, T., Ari, K., Altun, F. & Karahan, O. 2007, 'A comparative experimental investigation of concrete, reinforced-concrete and steel-fibre concrete pipes under three-edge-bearing test', *Construction and Building Materials*, vol. 21, no. 8, pp. 1702-8.
- Hallquist, J.O. 2009, 'LS-DYNA® Keyword User's Manual Volume I', *Livermore Software Technology Corporation*.
- Hammaty, Y., DeRoeck, G. & Vandewalle, L. 1991, 'Finite element modeling of reinforced concrete taking into consideration bond-slip', *5th ANSYS Int. Conf.*
- Harajli, M., Hamad, B. & Karam, K. 2002, 'Bond-slip response of reinforcing bars embedded in plain and fiber concrete', *Journal of Materials in Civil Engineering*, vol. 14, no. 6, pp. 503-11.
- Hardjito, D. & Rangan, B.V. 2005, 'Development and properties of low-calcium fly ash-based geopolymer concrete'.
- Hardjito, D., Wallah, S., Sumajouw, D. & Rangan, B. 2004a, 'Brief review of development of geopolymer concrete', *Invited Paper, George Hoff Symposium, American Concrete Institute. Las Vegas, USA*.
- Hardjito, D., Wallah, S., Sumajouw, D. & Rangan, B. 2005, 'Introducing fly ash-based geopolymer concrete: manufacture and engineering

- properties', *30th conference on our world in concrete & structures*, vol. 24.
- Hardjito, D., Wallah, S.E., Sumajouw, D.M. & Rangan, B.V. 2004b, 'On the development of fly ash-based geopolymer concrete', *Materials Journal*, vol. 101, no. 6, pp. 467-72.
- Hassan, A., Arif, M. & Shariq, M. 2019, 'Use of geopolymer concrete for a cleaner and sustainable environment—A review of mechanical properties and microstructure', *Journal of cleaner production*, vol. 223, pp. 704-28.
- Hayashi, S., Chen, H. & Hu, W. 2017, 'Compression Molding Analysis of Long Fiber Reinforced Plastics using Coupled Method of Beam and 3D Adaptive EFG in LS-DYNA', *11th European LS-DYNA Conference*.
- Heah, C., Kamarudin, H., Al Bakri, A.M., Binhussain, M., Luqman, M., Nizar, I.K., Ruzaidi, C. & Liew, Y. 2011, 'Effect of curing profile on kaolin-based geopolymers', *Physics Procedia*, vol. 22, pp. 305-11.
- Heath, A., Paine, K., Goodhew, S., Ramage, M. & Lawrence, M. 2013, 'The potential for using geopolymer concrete in the UK', *Proceedings of the Institution of Civil Engineers-Construction Materials*, vol. 166, no. 4, pp. 195-203.
- Heath, A., Paine, K. & McManus, M. 2014, 'Minimising the global warming potential of clay based geopolymers', *Journal of Cleaner Production*, vol. 78, pp. 75-83.
- Heger, F.J. 1963, 'Structural behavior of circular reinforced concrete pipe-Development of Theory', *Journal Proceedings*, vol. 60, pp. 1567-614.
- Heger, F.J. 1982, 'Structural design method for precast reinforced concrete pipe', *Transportation Research Record*, vol. 878, pp. 93-100.
- Hendrickson Jr, J.G. 1955, 'TESTS OF LARGE-DIAMETER REINFORCED-CONCRETE PIPE', *Highway Research Board Bulletin*, no. 102.
- Hodges, S.M. & Enyart, J.I. 1993, 'Standard Installations: A Synopsis of the ASCE Standard Practice for Direct Design of Buried Precast Concrete Pipe', *Pipeline Infrastructure II*, ASCE, New York, pp. 595-609.
- Hogan, A. 2017, 'Effects of Cracks in Reinforced Concrete Pipe'.

- Hognestad, E., Hanson, N.W. & McHenry, D. 1955, 'Concrete stress distribution in ultimate strength design', *Journal Proceedings*, vol. 52, pp. 455-80.
- Hong, S. & Park, S.-K. 2012, 'Uniaxial bond stress-slip relationship of reinforcing bars in concrete', *Advances in Materials Science and Engineering*, vol. 2012.
- Hu, S. & Liu, X. 2012, 'Overload test and failure mechanism analysis of prestressed concrete cylinder pipe', *J. Hydroelectr. Eng.*, vol. 31, no. 1, pp. 103-7.
- Hu, S., Shen, J., Wang, D. & Cai, X. 2010, 'Experiment and numerical analysis on super caliber prestressed concrete cylinder pipes with cracks', *Journal of Hydraulic Engineering*, vol. 41, no. 7, pp. 876-82.
- Huntzinger, D.N. & Eatmon, T.D. 2009, 'A life-cycle assessment of Portland cement manufacturing: comparing the traditional process with alternative technologies', *Journal of Cleaner Production*, vol. 17, no. 7, pp. 668-75.
- Imtiaz, L., Rehman, S.K.U., Ali Memon, S., Khizar Khan, M. & Faisal Javed, M. 2020, 'A review of recent developments and advances in eco-friendly geopolymers concrete', *Applied Sciences*, vol. 10, no. 21, p. 7838.
- Indiketiya, S., Jegatheesan, P., Rajeev, P. & Kuwano, R. 2019, 'The influence of pipe embedment material on sinkhole formation due to erosion around defective sewers', *Transportation Geotechnics*, vol. 19, pp. 110-25.
- Isgor, O.B. 2001, 'A Durability Model for Chloride and Carbonation Induced Steel Corrosion in Reinforced Concrete Members'.
- Islam, A., Alengaram, U.J., Jumaat, M.Z., Bashar, I.I. & Kabir, S.A. 2015, 'Engineering properties and carbon footprint of ground granulated blast-furnace slag-palm oil fuel ash-based structural geopolymers concrete', *Construction and building materials*, vol. 101, pp. 503-21.
- Jayadevan, K., Østby, E. & Thaulow, C. 2004, 'Fracture response of pipelines subjected to large plastic deformation under tension', *International Journal of Pressure Vessels and Piping*, vol. 81, no. 9, pp. 771-83.

- Joorabchian, S.M. 2010, 'Durability of concrete exposed to sulfuric acid attack', *Theses and dissertations. Presented to Ryerson University, Toronto, Ontario, Canada.*
- Junaid, M.T., Karzad, A.S. & Altoubat, S. 2020, 'Stress-strain behaviour and strength properties of ambient cured geo-polymer concrete', *IOP Conference Series: Materials Science and Engineering*, vol. 839, IOP Publishing, p. 012005.
- Junaid, M.T., Kayali, O., Khennane, A. & Black, J. 2015, 'A mix design procedure for low calcium alkali activated fly ash-based concretes', *Construction and Building Materials*, vol. 79, pp. 301-10.
- Kabir, M., Islam, M. & Chowdhury, M. 2015, 'Bond stress-slip behaviour between concrete and steel rebar via pullout test: experimental and finite element analysis', paper presented to the *First International Conference on Advances in Civil Infrastructure and Construction Materials*, Dhaka, Bangladesh.
- Kataoka, M.N., da Silva, J.L., de Oliveira, L.M.F. & El Debs, M.K. 2017, 'FE analysis of RC pipes under three-edge-bearing test: Pocket and diameter influence', *Computers and Concrete*, vol. 20, no. 4, pp. 483-90.
- Kathirvel, P., Thangavelu, M., Gopalan, R. & Kaliyaperumal, S.R.M. 2017, 'Bond characteristics of reinforcing steel embedded in geopolymer concrete', *IOP Conference Series: Earth and Environmental Science*, vol. 80, IOP Publishing, p. 012001.
- Khaksefidi, S., Ghalehnovi, M. & De Brito, J. 2021, 'Bond behaviour of high-strength steel rebars in normal (NSC) and ultra-high performance concrete (UHPC)', *Journal of Building Engineering*, vol. 33, p. 101592.
- Khale, D. & Chaudhary, R. 2007, 'Mechanism of geopolymerization and factors influencing its development: a review', *Journal of materials science*, vol. 42, no. 3, pp. 729-46.
- Kidd, P. 2009, 'One-Part Dry Mix Geopolymer Binder', *Ambient Cured Geopolymer Program.*
- Kim, J.-S. & Park, J.H. 2015, 'An experimental investigation of bond properties of reinforcements embedded in geopolymer concrete', *Int. J. Civ. Struct. Constr. Archit. Eng.*, vol. 9, no. 2, pp. 92-5.
- Kim, J.S. & Park, J. 2014, 'An experimental evaluation of development length of reinforcements embedded in geopolymer concrete',

- Applied Mechanics and Materials*, vol. 578, Trans Tech Publ, pp. 441-4.
- Koenke, C., Harte, R., Krätzig, W. & Rosenstein, O. 1998, 'On adaptive remeshing techniques for crack simulation problems', *Engineering Computations*.
- Kral, P., Hradil, P., Kala, J., Hokes, F. & Husek, M. 2017, 'Identification of the parameters of a concrete damage material model', *Procedia Engineering*, vol. 172, pp. 578-85.
- Kumar, S., Kumar, R. & Mehrotra, S. 2010, 'Influence of granulated blast furnace slag on the reaction, structure and properties of fly ash based geopolymer', *Journal of materials science*, vol. 45, no. 3, pp. 607-15.
- Kumbar, P., Sheelavant, S., Sanni, S.H. & Kerur, S.B. 2013, 'Experimental Validation of geopolymer Concrete Beams using Finite Element analysis', *Int. J. Eng. Res. Technol.*, vol. 2, no. 12, pp. 3806-11.
- Kupwade-Patil, K. & Allouche, E.N. 2013, 'Examination of chloride-induced corrosion in reinforced geopolymer concretes', *Journal of Materials in Civil Engineering*, vol. 25, no. 10, pp. 1465-76.
- Kurtoglu, A.E., Alzebaree, R., Aljumaili, O., Nis, A., Gulsan, M.E., Humur, G. & Cevik, A. 2018, 'Mechanical and durability properties of fly ash and slag based geopolymer concrete', *Advances in concrete construction*, vol. 6, no. 4, p. 345.
- Kusumaningrum, P., Prayogo, G.M. & Tadjono, S. 2021, 'Finite element modelling of monotonic pull-out test of deformed steel rebar embedded in well-confined concrete', *E3S Web of Conferences*, vol. 331, EDP Sciences, p. 05012.
- Kwak, H.-G. & Filippou, F.C. 1990, *Finite element analysis of reinforced concrete structures under monotonic loads*, Citeseer.
- Langan, B.W., Weng, K. & Ward, M.A. 2002, 'Effect of silica fume and fly ash on heat of hydration of Portland cement', *Cement and Concrete Research*, vol. 32, no. 7, pp. 1045-51.
- Lavanya, G. & Jegan, J. 2015, 'Evaluation of relationship between split tensile strength and compressive strength for geopolymer concrete of varying grades and molarity', *Int. J. Appl. Eng. Res.*, vol. 10, no. 15, pp. 35523-7.
- Law, D.W., Adam, A.A., Molyneaux, T.K., Patnaikuni, I. & Wardhono, A. 2015, 'Long term durability properties of class F fly ash

- geopolymer concrete', *Materials and Structures*, vol. 48, no. 3, pp. 721-31.
- Lee, D.T.C. & Lee, T.S. 2017, 'The effect of aggregate condition during mixing on the mechanical properties of oil palm shell (OPS) concrete', *MATEC Web of Conferences*, vol. 87, EDP Sciences, p. 01019.
- Lee, N. & Lee, H.-K. 2013, 'Setting and mechanical properties of alkali-activated fly ash/slag concrete manufactured at room temperature', *Construction and Building Materials*, vol. 47, pp. 1201-9.
- Lee, W. & Van Deventer, J. 2004, 'The interface between natural siliceous aggregates and geopolymers', *Cement and Concrete Research*, vol. 34, no. 2, pp. 195-206.
- Lehner, P. & Konečný, P. 2017, 'Numerical Validation of Concrete Corrosion Initiation Model Considering Crack Effect Model and Aging Effect', *Procedia engineering*, vol. 190, pp. 154-61.
- Li, C., Gong, X.Z., Cui, S.P., Wang, Z.H., Zheng, Y. & Chi, B.C. 2011, 'CO₂ emissions due to cement manufacture', *Materials Science Forum*, vol. 685, Trans Tech Publ, pp. 181-7.
- Li, C., Zhong, Z., Bie, C. & Liu, X. 2018, 'Field performance of large section concrete pipes cracking during jacking in Chongqing—A case study', *Tunnelling and Underground Space Technology*, vol. 82, pp. 568-83.
- Li, N., Shi, C., Zhang, Z., Wang, H. & Liu, Y. 2019, 'A review on mixture design methods for geopolymer concrete', *Composites Part B: Engineering*, p. 107490.
- Li, X., Chen, G., Liu, X., Ji, J. & Han, L. 2021, 'Analysis and Evaluation on Residual Strength of Pipelines with Internal Corrosion Defects in Seasonal Frozen Soil Region', *Applied Sciences*, vol. 11, no. 24, p. 12141.
- Li, Z. 2011, *Advanced concrete technology*, John Wiley & Sons.
- Liang, X. & Ji, Y. 2021, 'Mechanical properties and permeability of red mud-blast furnace slag-based geopolymer concrete', *SN Applied Sciences*, vol. 3, no. 1, p. 23.
- Liao, W.-C., Chen, P.-S., Hung, C.-W. & Wagh, S.K. 2020, 'An innovative test method for tensile strength of concrete by applying the strut-and-tie methodology', *Materials*, vol. 13, no. 12, p. 2776.
- Lin, H., Zhao, Y., Ozbolt, J., Feng, P., Jiang, C. & Eligehausen, R. 2019, 'Analytical model for the bond stress-slip relationship of deformed

- bars in normal strength concrete', *Construction and Building Materials*, vol. 198, pp. 570-86.
- Lingyu, T., Dongpo, H., Jianing, Z. & Hongguang, W. 2021, 'Durability of geopolymers and geopolymer concretes: A review', *REVIEWS ON ADVANCED MATERIALS SCIENCE*, vol. 60, no. 1, pp. 1-14.
- Long, X., Tan, K.H. & Lee, C.K. 2014, 'Bond stress-slip prediction under pullout and dowel action in reinforced concrete joints', *ACI Struct. J.*, vol. 111, no. 4, pp. 977-87.
- Lowes, L.N., Moehle, J.P. & Govindjee, S. 2004, 'Concrete-steel bond model for use in finite element modeling of reinforced concrete structures', *Structural Journal*, vol. 101, no. 4, pp. 501-11.
- LSTC 2014, 'LS-DYNA keyword user's manual: Material Models', LS-DYNA R7.1 edn, vol. II, Livermore Software Technology Corporation, Livermore, CA.
- LSTC 2023, *Contact modeling in LS-DYNA*, Livermore Software Technology Corporation Livermore, California,, viewed 06 March 2023, <<https://www.dynasupport.com/tutorial/ls-dyna-users-guide/contact-modeling-in-ls-dyna>>.
- Lutz, L.A. & Gergely, P. 1967, 'Mechanics of bond and slip of deformed bars in concrete', *Journal Proceedings*, vol. 64, pp. 711-21.
- Magallanes, J.M. 2008, 'Importance of concrete material characterization and modelling to predicting the response of structures to shock and impact loading', *Structures under shock and impact X*, vol. 98, pp. 241-50.
- Malvar, L.J. 1994, *Bond stress-slip characteristics of FRP rebars*, Naval Facilities Engineering Service Center Port Hueneme CA.
- Malvar, L.J., Crawford, J.E., Wesevich, J.W. & Simons, D. 1997, 'A plasticity concrete material model for DYNA3D', *International journal of impact engineering*, vol. 19, no. 9-10, pp. 847-73.
- Maranan, G., Manalo, A., Karunasena, K. & Benmokrane, B. 2015, 'Bond stress-slip behavior: case of GFRP bars in geopolymer concrete', *Journal of Materials in Civil Engineering*, vol. 27, no. 1, p. 04014116.
- Marr, J. 2012, 'A Research Plan and Report on Factors Affecting Culvert Pipe Service Life in Minnesota', *Minnesota Department of Transportation: Saint Paul, MN, USA*.

- Mathew, G. 2021, 'Bond-slip Behavior Of Geopolymer Concrete After Exposure To Elevated Temperatures', *Jordan Journal of Civil Engineering*, vol. 15, no. 4.
- Mehta, A. & Siddique, R. 2018, 'Sustainable geopolymer concrete using ground granulated blast furnace slag and rice husk ash: Strength and permeability properties', *Journal of Cleaner Production*, vol. 205, pp. 49-57.
- Millar, D. & Paull, R. 2017, 'New recommended practices in concrete durability', *Journal of Asian Concrete Federation*, vol. 3, no. 1, pp. 1-11.
- Min, H. & Song, Z. 2018, 'Investigation on the Sulfuric Acid Corrosion Mechanism for Concrete in Soaking Environment', *Advances in Materials Science and Engineering*, vol. 2018.
- Mirza, S.M. & Houde, J. 1979, 'Study of bond stress-slip relationships in reinforced concrete', *Journal proceedings*, vol. 76, pp. 19-46.
- Mo, K.H., Alengaram, U.J. & Jumaat, M.Z. 2016, 'Structural performance of reinforced geopolymer concrete members: A review', *Construction and Building Materials*, vol. 120, pp. 251-64.
- Mo, K.H., Visintin, P., Alengaram, U.J. & Jumaat, M.Z. 2016, 'Bond stress-slip relationship of oil palm shell lightweight concrete', *Engineering Structures*, vol. 127, pp. 319-30.
- Mohamad Ali, A., Farid, B. & Al-Janabi, A. 1990, 'Stress - Strain Relationship For Concrete in Compression Made of Local Materials', *Journal of King Abdulaziz University-Engineering Sciences*, vol. 2.
- Mohamed, N. 2015, 'Experimental and Numerical Study on Full-Scale Precast Steel Fibre-Reinforced Concrete Pipes'.
- Mohamed, N. & Nehdi, M.L. 2016, 'Rational finite element assisted design of precast steel fibre reinforced concrete pipes', *Engineering Structures*, vol. 124, pp. 196-206.
- Mohamed, N., Soliman, A.M. & Nehdi, M.L. 2014, 'Full-scale pipes using dry-cast steel fibre-reinforced concrete', *Construction and Building Materials*, vol. 72, pp. 411-22.
- Mohamed, N., Soliman, A.M. & Nehdi, M.L. 2015, 'Mechanical performance of full-scale precast steel fibre-reinforced concrete pipes', *Engineering Structures*, vol. 84, pp. 287-99.

- Mohammed, A.A., Ahmed, H.U. & Mosavi, A. 2021, 'Survey of Mechanical Properties of Geopolymer Concrete: A Comprehensive Review and Data Analysis', *Materials*, vol. 14, no. 16, p. 4690.
- Monteny, J., Vincke, E., Beeldens, A., De Belie, N., Taerwe, L., Van Gemert, D. & Verstraete, W. 2000, 'Chemical, microbiological, and in situ test methods for biogenic sulfuric acid corrosion of concrete', *Cement and Concrete Research*, vol. 30, no. 4, pp. 623-34.
- Motorwala, A., Shah, V., Kammula, R., Nannapaneni, P. & Raijiwala, D. 2013, 'Alkali activated fly-ash based geopolymer concrete', *International journal of emerging technology and advanced engineering*, vol. 3, no. 1, pp. 159-66.
- Naggar, H.E., Allouche, E. & Naggar, M.H.E. 2007, 'Development of a new class of precast concrete pipes-a numerical evaluation', *Canadian Journal of Civil Engineering*, vol. 34, no. 7, pp. 870-84.
- Nath, P. & Sarker, P.K. 2012, 'Geopolymer concrete for ambient curing condition', *Australasian Structural Engineering Conference 2012: The past, present and future of Structural Engineering*, Engineers Australia, p. 225.
- Nath, P. & Sarker, P.K. 2014, 'Effect of GGBFS on setting, workability and early strength properties of fly ash geopolymer concrete cured in ambient condition', *Construction and Building materials*, vol. 66, pp. 163-71.
- Nath, P. & Sarker, P.K. 2017, 'Flexural strength and elastic modulus of ambient-cured blended low-calcium fly ash geopolymer concrete', *Construction and Building Materials*, vol. 130, pp. 22-31.
- Nath, P., Sarker, P.K. & Rangan, V.B. 2015, 'Early age properties of low-calcium fly ash geopolymer concrete suitable for ambient curing', *Procedia Engineering*, vol. 125, pp. 601-7.
- NBR-6118 2003, *Design of concrete structures*, Brazilian Association Standards, Rio de Janeiro, Brazil.
- Neupane, K. 2015, 'Evaluation of early age and mechanical properties of geopolymer concrete'.
- Neupane, K. 2016, 'Investigation on modulus of elasticity of powder-activated geopolymer concrete', *International Journal of Structural Engineering*, vol. 7, no. 3, pp. 262-78.
- Neupane, K., Baweja, D., Shrestha, R., Chalmers, D. & Sleep, P. 2014, 'Mechanical properties of geopolymer concrete: Applicability of

- relationships defined by AS 3600', *Concrete in Australia*, vol. 40, no. 1, pp. 50-6.
- Neupane, K., Chalmers, D. & Kidd, P. 2018, 'High-Strength Geopolymer Concrete—Properties, Advantages and Challenges', *Adv. Mater.*, vol. 7, pp. 15-25.
- Neupane, K., Hadigheh, S. & Dias-da-Costa, D. 2019, 'Numerical Study on the Structural Behaviour of a Geopolymer Prestressed Concrete Beam'.
- Neupane, K., Kidd, P., Chalmers, D., Baweja, D. & Shrestha, R. 2016, 'Investigation on compressive strength development and drying shrinkage of ambient cured powder-activated geopolymer concretes', *Australian Journal of Civil Engineering*, vol. 14, no. 1, pp. 72-83.
- Neville, A. 2004, 'The confused world of sulfate attack on concrete', *Cement and Concrete research*, vol. 34, no. 8, pp. 1275-96.
- Neville, A.M. 1995, *Properties of concrete*, vol. 4, Longman London.
- Ngo, D. & Scordelis, A.C. 1967, 'Finite element analysis of reinforced concrete beams', *Journal Proceedings*, vol. 64, pp. 152-63.
- Nguyen, K.T., Ahn, N., Le, T.A. & Lee, K. 2016, 'Theoretical and experimental study on mechanical properties and flexural strength of fly ash-geopolymer concrete', *Construction and Building Materials*, vol. 106, pp. 65-77.
- Nilson, A.H. 1968, 'Nonlinear analysis of reinforced concrete by the finite element method', *Journal Proceedings*, vol. 65, pp. 757-66.
- Nilson, A.H. 1971, *Bond stress-slip relations in reinforced concrete*.
- Nilson, A.H. 1972, 'Internal measurement of bond slip', *Journal proceedings*, vol. 69, pp. 439-41.
- Nourpanah, N. & Taheri, F. 2011, 'Ductile crack growth and constraint in pipelines subject to combined loadings', *Engineering Fracture Mechanics*, vol. 78, no. 9, pp. 2010-28.
- Noushini, A., Aslani, F., Castel, A., Gilbert, R.I., Uy, B. & Foster, S. 2016, 'Compressive stress-strain model for low-calcium fly ash-based geopolymer and heat-cured Portland cement concrete', *Cement and Concrete Composites*, vol. 73, pp. 136-46.
- Nurrudin, M.F., Haruna, S., Mohammed, B.S. & Sha'aban, I.G. 2018, 'Methods of curing geopolymer concrete: A review', *International Journal of Advanced and Applied Sciences*, vol. 5, no. 1, pp. 31-6.

- Nuruddin, M.N., Kusbiantoro, A.K., Qazi, S.Q., Darmawan, M.D. & Husin, N.H. 2011, 'Development of geopolymer concrete with different curing conditions', *IPTEK The Journal for Technology and Science*, vol. 22, no. 1.
- Nurwidayati, R., Ekaputri, J., Triwulan & Suprobo, P. 2020, 'Effect of embedment length on bond strength of geopolymer concrete', *AIP Conference Proceedings*, vol. 2291, AIP Publishing LLC, p. 020022.
- Nyale, S.M., Babajide, O.O., Birch, G.D., Böke, N. & Petrik, L.F. 2013, 'Synthesis and Characterization of Coal Fly Ash-based Foamed Geopolymer', *Procedia Environmental Sciences*, vol. 18, pp. 722-30.
- O'Connell, M., McNally, C. & Richardson, M.G. 2010, 'Biochemical attack on concrete in wastewater applications: A state of the art review', *Cement and Concrete Composites*, vol. 32, no. 7, pp. 479-85.
- Obaidat, Y.T., Heyden, S. & Dahlblom, O. 2010, 'The effect of CFRP and CFRP/concrete interface models when modelling retrofitted RC beams with FEM', *Composite Structures*, vol. 92, no. 6, pp. 1391-8.
- Orangun, C., Jirsa, J.O. & Breen, J.E. 1975, *The strength of anchored bars: a reevaluation of test data on development length and splices*, Center for Highway Research, University of Texas at Austin.
- Palomo, A., Blanco-Varela, M.T., Granizo, M., Puertas, F., Vazquez, T. & Grutzeck, M. 1999, 'Chemical stability of cementitious materials based on metakaolin', *Cement and Concrete Research*, vol. 29, no. 7, pp. 997-1004.
- Palomo, A., Grutzeck, M. & Blanco, M. 1999, 'Alkali-activated fly ashes: A cement for the future', *Cement and concrete research*, vol. 29, no. 8, pp. 1323-9.
- Pan, Z., Sanjayan, J.G. & Rangan, B.V. 2011, 'Fracture properties of geopolymer paste and concrete', *Magazine of concrete research*, vol. 63, no. 10, pp. 763-71.
- Parthiban, K., Saravananarajamohan, K., Shobana, S. & Bhaskar, A.A. 2013, 'Effect of replacement of slag on the mechanical properties of fly ash based geopolymer concrete', *Int. J. Eng. Technol*, vol. 5, no. 3, pp. 2555-9.

- Pasupathy, K., Berndt, M., Sanjayan, J., Rajeev, P. & Cheema, D.S. 2017, 'Durability of low-calcium fly ash based geopolymer concrete culvert in a saline environment', *Cement and Concrete Research*, vol. 100, pp. 297-310.
- Patankar, S.V., Ghugal, Y.M. & Jamkar, S.S. 2015, 'Mix design of fly ash based geopolymer concrete', *Advances in structural engineering*, Springer, pp. 1619-34.
- Pauw, A. 1960, *Static modulus of elasticity of concrete as affected by density*, University of Missouri.
- Peckworth, H.F. & Hendrickson, J.G. 1964, 'Gravity flow reinforced concrete pipe design', *Journal of the Pipeline Division*, vol. 90, no. 1, pp. 33-48.
- Peter, J.M., Chapman, D., Moore, I.D. & Hault, N. 2018, 'Impact of soil erosion voids on reinforced concrete pipe responses to surface loads', *Tunnelling and Underground Space Technology*, vol. 82, pp. 111-24.
- Peyvandi, A., Soroushian, P. & Jahangirnejad, S. 2013, 'Enhancement of the structural efficiency and performance of concrete pipes through fiber reinforcement', *Construction and Building Materials*, vol. 45, pp. 36-44.
- Peyvandi, A., Soroushian, P. & Jahangirnejad, S. 2014, 'Structural Design Methodologies for Concrete Pipes with Steel and Synthetic Fiber Reinforcement', *ACI Structural Journal*, vol. 111, no. 1, pp. 83-91.
- Pham, D.Q., Nguyen, T.N., Le, S.T., Pham, T.T. & Ngo, T.D. 2021, 'The structural behaviours of steel reinforced geopolymer concrete beams: An experimental and numerical investigation', *Structures*, vol. 33, Elsevier, pp. 567-80.
- Pop, I., De Schutter, G., Desnerck, P. & Onet, T. 2013, 'Bond between powder type self-compacting concrete and steel reinforcement', *Construction and Building Materials*, vol. 41, pp. 824-33.
- Popovics, S. 1973, 'A numerical approach to the complete stress-strain curve of concrete', *Cement and concrete research*, vol. 3, no. 5, pp. 583-99.
- Provis, J.L. & Deventer, J.S.J.v. 2014, *Alkali Activated Materials*, Springer, Dordrecht.
- Provis, J.L. & Van Deventer, J.S.J. 2009, *Geopolymers: structures, processing, properties and industrial applications*, Elsevier.

- Puertas, F., Martínez-Ramírez, S., Alonso, S. & Vázquez, T. 2000, 'Alkali-activated fly ash/slag cements: strength behaviour and hydration products', *Cement and concrete research*, vol. 30, no. 10, pp. 1625-32.
- Puertas, F., Martínez-Ramírez, S., Alonso, S. & Vázquez, T. 2000, 'Alkali-activated fly ash/slag cements: strength behaviour and hydration products', *Cement and concrete research*, vol. 30, no. 10, pp. 1625-32.
- Purdon, A.O. 1940, 'The action of alkalis on blast-furnace slag', *J Soc Chem Ind*, vol. 59, no. 9, pp. 191-202.
- Qiu, J., Zhao, Y., Xing, J. & Sun, X. 2019, 'Fly ash/blast furnace slag-based geopolymer as a potential binder for mine backfilling: effect of binder type and activator concentration', *Advances in Materials Science and Engineering*, vol. 2019.
- Raijiwala, D. & Patil, H. 2011, 'Geopolymer concrete: A concrete of the next decade', *Concrete Solutions*, vol. 287.
- Ramadan, A., Shehata, A., Younis, A.-A., Wong, L.S. & Nehdi, M.L. 2020, 'Modeling structural behavior of precast concrete pipe with single elliptical steel cage reinforcement', *Structures*, vol. 27, Elsevier, pp. 903-16.
- Ramadan, A., Shehata, A., Younis, A.-A., Wong, L.S. & Nehdi, M.L. 2020b, 'Modeling structural behavior of precast concrete pipe with single elliptical steel cage reinforcement', *Structures*, vol. 27, pp. 903-16.
- Ramadan, A., Younis, A.-A., Wong, L.S. & Nehdi, M.L. 2020a, 'Investigation of structural behavior of precast concrete pipe with single elliptical steel cage reinforcement', *Engineering Structures*, vol. 219, p. 110881.
- Ramadan, A.S. 2020, 'Experimental and Numerical Study of Precast Concrete Pipe with Single Elliptical Steel Cage Reinforcement', The University of Western Ontario.
- Ramujee, K. & PothaRaju, M. 2017, 'Mechanical Properties of Geopolymer Concrete Composites', *Materials Today: Proceedings*, vol. 4, no. 2, Part A, pp. 2937-45.
- Rangan, B.V. 1990, 'Strength of reinforced concrete slender columns', *Structural Journal*, vol. 87, no. 1, pp. 32-8.
- Rangan, B.V. 2008, 'Fly ash-based geopolymer concrete'.

- Redox 2017, 'Safety Data Sheet: Soda Ash Dense', Redox Pty. Ltd., Minto, NSW, Australia, 03 Aug 2017.
- Rehm, G. 1957, 'The fundamental law of bond', *Proceedings of the Symposium on Bond and Crack Formation in Reinforced Concrete, Stockholm*, vol. 2, pp. 491-8.
- RILEM, T. 1970, 'Bond test for reinforcing steel: 2. Pull-out test', *Mater. Struct*, vol. 3, no. 15, pp. 175-8.
- Roa-Rodríguez, G., Aperador, W. & Delgado, A. 2014, 'Resistance to chlorides of the alkali-activated slag concrete', *International Journal of Electrochemical Science*, vol. 9, no. 1, pp. 282-91.
- Rostami, V., Shao, Y. & Boyd, A.J. 2011, 'Durability of concrete pipes subjected to combined steam and carbonation curing', *Construction and Building Materials*, vol. 25, no. 8, pp. 3345-55.
- Rovnaník, P. 2010, 'Effect of curing temperature on the development of hard structure of metakaolin-based geopolymer', *Construction and Building Materials*, vol. 24, no. 7, pp. 1176-83.
- Roy, D.M. 1999, 'Alkali-activated cements opportunities and challenges', *Cement and Concrete Research*, vol. 29, no. 2, pp. 249-54.
- Ryu, G.S., Lee, Y.B., Koh, K.T. & Chung, Y.S. 2013, 'The mechanical properties of fly ash-based geopolymer concrete with alkaline activators', *Construction and building materials*, vol. 47, pp. 409-18.
- Sæther, I. & Sand, B. 2012, 'FEM simulations of reinforced concrete beams attacked by corrosion', *ACI Structural Journal*, vol. 109, no. 2, pp. 15-31.
- Sakulich, A.R., Anderson, E., Schauer, C.L. & Barsoum, M.W. 2010, 'Influence of Si: Al ratio on the microstructural and mechanical properties of a fine-limestone aggregate alkali-activated slag concrete', *Materials and Structures*, vol. 43, no. 7, pp. 1025-35.
- Sani, M.A. & Muhamad, R. 2020, 'Bond behaviour of geopolymer concrete in structural application: A review', *IOP Conference Series: Earth and Environmental Science*, vol. 476, IOP Publishing, p. 012017.
- Sarker, P. 2010, 'Bond strengths of geopolymer and cement concretes', *Advances in Science and Technology*, vol. 69, Trans Tech Publ, pp. 143-51.
- Sarker, P.K. 2009, 'Analysis of geopolymer concrete columns', *Materials and structures*, vol. 42, no. 6, pp. 715-24.

- Sarker, P.K. 2011, 'Bond strength of reinforcing steel embedded in fly ash-based geopolymer concrete', *Materials and structures*, vol. 44, no. 5, pp. 1021-30.
- Scheperboer, I.C., Luimes, R.A., Suiker, A.S., Bosco, E. & Clemens, F. 2021, 'Experimental-numerical study on the structural failure of concrete sewer pipes', *Tunnelling and Underground Space Technology*, vol. 116, p. 104075.
- Schwer, L.E. & Malvar, L.J. 2005, 'Simplified concrete modeling with* MAT_CONCRETE_DAMAGE_REL3', *JRI LS-Dyna User Week*, pp. 49-60.
- Selby, D.R. 2012, 'An investigation into the bond of steel reinforcement in geopolymer and ordinary portland cement concrete', *The UNSW Canberra at ADFA Journal of Undergraduate Engineering Research*, vol. 4, no. 1.
- Senthil, K., Bawa, S. & Aswin, C. 2018, 'Influence of concrete strength and diameter of reinforcing bar on pullout tests using finite element analysis', *Journal of Structural Engineering*, vol. 1, no. 3, pp. 105-16.
- Shafaie, J., Hosseini, A. & Marefat, M. 2009, '3D finite element modelling of bond-slip between rebar and concrete in pullout test', *3rd International Conference on Concrete & Development, Iran*.
- Shen, D., Shi, X., Zhang, H., Duan, X. & Jiang, G. 2016, 'Experimental study of early-age bond behavior between high strength concrete and steel bars using a pull-out test', *Construction and Building materials*, vol. 113, pp. 653-63.
- Shook, W.E. & Bell, L.W. 1998, 'Corrosion control in concrete pipe and manholes', *Technical Presentation, Water Environmental Federation, Florida*.
- Shrestha, P. 2014, 'Development of geopolymer concrete for precast structures'.
- Siddika, A., Amin, M., Rayhan, M., Islam, M., Mamun, M., Alyousef, R. & Amran, M. 2021, 'Performance of sustainable green concrete incorporated with fly ash, rice husk ash, and stone dust', *Acta Polytechnica*, vol. 61, pp. 279-91.
- Silmaco 2016, *Sodium Metasilicate: Green and Efficient*, vol. 2, S:ILMACO Silicates Manufacturing Company.

- Silmaco 2018, 'SAFETY DATA SHEET: SODIUM METASILICATE ANHYDROUS', SILMACO Silicates Manufacturing Company, Lanaken, Belgium, 10 Feb 2018.
- Silva, J.d., El Debs, M.K. & Beck, A.T. 2008, 'Reliability evaluation of reinforced concrete pipes in crack opening limit state', *Revista IBRACON de Estruturas e Materiais*, vol. 1, pp. 314-30.
- Sindhunata, Van Deventer, J., Lukey, G. & Xu, H. 2006, 'Effect of curing temperature and silicate concentration on fly-ash-based geopolymerization', *Industrial & Engineering Chemistry Research*, vol. 45, no. 10, pp. 3559-68.
- Singh, B., Ishwarya, G., Gupta, M. & Bhattacharyya, S. 2015, 'Geopolymer concrete: A review of some recent developments', *Construction and building materials*, vol. 85, pp. 78-90.
- Sofi, M., Van Deventer, J., Mendis, P. & Lukey, G. 2007a, 'Bond performance of reinforcing bars in inorganic polymer concrete (IPC)', *Journal of Materials Science*, vol. 42, no. 9, pp. 3107-16.
- Sofi, M., van Deventer, J.S.J., Mendis, P.A. & Lukey, G.C. 2007b, 'Engineering properties of inorganic polymer concretes (IPCs)', *Cement and Concrete Research*, vol. 37, no. 2, pp. 251-7.
- Songpiriyakij, S., Pungern, T., Pungpretrakul, P. & Jaturapitakkul, C. 2011, 'Anchorage of steel bars in concrete by geopolymer paste', *Materials & Design*, vol. 32, no. 5, pp. 3021-8.
- Soroushian, P. & Choi, K.-B. 1989, 'Local Bond of Deformed Bars with Different Diameters in Confined Concrete', *ACI Structural Journal*, vol. 86, no. 2, pp. 217-22.
- Spangler, M. 1967, *The Case Against the Ultimate Load Test for Reinforced Concrete Pipe*.
- Spangler, M.G. 1933, *The supporting strength of rigid pipe culverts*, Iowa State College.
- Strukar, K., Kalman Šipoš, T., Dokšanović, T. & Rodrigues, H. 2018, 'Experimental Study of Rubberized Concrete Stress-Strain Behavior for Improving Constitutive Models', *Materials (Basel)*, vol. 11, no. 11.
- Sumajouw, D., Hardjito, D., Wallah, S. & Rangan, B. 2007, 'Fly ash-based geopolymer concrete: study of slender reinforced columns', *Journal of materials science*, vol. 42, no. 9, pp. 3124-30.
- Sumajouw, M. & Rangan, B.V. 2006, 'Low-calcium fly ash-based geopolymer concrete: reinforced beams and columns'.

- Supaviriyakit, T., Pornpongsaroj, P. & Pimanmas, A. 2004, 'Finite element analysis of FRP-strengthened RC beams', *Songklanakarin Journal of science and technology*, vol. 26, no. 4, pp. 497-507.
- Swamy, R.N. 2002, 'Role and effectiveness of mineral admixtures in relation to alkali-silica reaction', *The Alkali-Silica Reaction in Concrete*, CRC Press, pp. 112-37.
- Tabiei, A. & Wu, J. 2003, 'Development of the DYNA3D simulation code with automated fracture procedure for brick elements', *International Journal for Numerical Methods in Engineering*, vol. 57, no. 14, pp. 1979-2006.
- Tabiei, A. & Zhang, W. 2016, 'Evaluation of various numerical methods in LS-DYNA® for 3D Crack Propagation', *Proceedings of the Conference Proceedings 14th International LS-DYNA Users Conference*, Royal Dearborn Hotel and Convention Center Detroit, MI, USA.
- Talha Junaid, M., Kayali, O. & Khennane, A. 2017, 'Response of alkali activated low calcium fly-ash based geopolymer concrete under compressive load at elevated temperatures', *Materials and Structures*, vol. 50, no. 1, pp. 1-10.
- Tang, C.-W. & Cheng, C.-K. 2020, 'Modeling Local Bond Stress–Slip Relationships of Reinforcing Bars Embedded in Concrete with Different Strengths', *Materials*, vol. 13, no. 17, p. 3701.
- Tehrani, A.D. 2016, 'Finite element analysis for ASTM C-76 reinforced concrete pipes with reduced steel cage'.
- Tekle, B.H., Khennane, A. & Kayali, O. 2016, 'Bond properties of sand-coated GFRP bars with fly ash–based geopolymer concrete', *Journal of Composites for Construction*, vol. 20, no. 5, p. 04016025.
- Tempest, B. 2010, 'Engineering characterization of waste derived geopolymer cement concrete for structural applications', vol. 71, no 08.
- Tepfers, R. 1979, 'Cracking of concrete cover along anchored deformed reinforcing bars', *Magazine of concrete research*, vol. 31, no. 106, pp. 3-12.
- Thokchom, S., Ghosh, P. & Ghosh, S. 2009, 'Resistance of fly ash based geopolymer mortars in sulfuric acid', *ARPJ. Eng. Appl. Sci.*, vol. 4, no. 1, pp. 65-70.

- Thomas, R.J. & Peethamparan, S. 2015, 'Alkali-activated concrete: Engineering properties and stress-strain behavior', *Construction and building materials*, vol. 93, pp. 49-56.
- Topark-Ngarm, P., Chindaprasirt, P. & Sata, V. 2015, 'Setting time, strength, and bond of high-calcium fly ash geopolymer concrete', *Journal of materials in civil engineering*, vol. 27, no. 7, p. 04014198.
- Tran, H., Setunge, S. & Shi, L. 2018, 'A CASE STUDY ON THE REMAINING STRENGTH OF STORMWATER DRAINAGE PIPES'.
- Tu, Z. & Lu, Y. 2009, 'Evaluation of typical concrete material models used in hydrocodes for high dynamic response simulations', *International Journal of Impact Engineering*, vol. 36, no. 1, pp. 132-46.
- Turner, L.K. & Collins, F.G. 2013, 'Carbon dioxide equivalent (CO₂-e) emissions: A comparison between geopolymer and OPC cement concrete', *Construction and Building Materials*, vol. 43, pp. 125-30.
- Uma, K., Anuradha, R. & Venkatasubramani, R. 2012, 'Experimental investigation and analytical modeling of reinforced geopolymer concrete beam', *International Journal of Civil & Structural Engineering*, vol. 2, no. 3, pp. 817-27.
- Valencia-Saavedra, W.G., de Gutiérrez, R.M. & Puertas, F. 2020, 'Performance of FA-based geopolymer concretes exposed to acetic and sulfuric acids', *Construction and Building Materials*, vol. 257, p. 119503.
- Valiente, A. 2001, 'Stress corrosion failure of large diameter pressure pipelines of prestressed concrete', *Engineering Failure Analysis*, vol. 8, no. 3, pp. 245-61.
- Valliappan, S. & Doolan, T.F. 1972, 'Nonlinear stress analysis of reinforced concrete', *Journal of the Structural Division*, vol. 98, no. 4, pp. 885-98.
- van Jaarsveld, J. & Van Deventer, J. 1999, 'Effect of the alkali metal activator on the properties of fly ash-based geopolymers', *Industrial & engineering chemistry research*, vol. 38, no. 10, pp. 3932-41.
- Van Jaarsveld, J., Van Deventer, J. & Lukey, G. 2003, 'The characterisation of source materials in fly ash-based geopolymers', *Materials Letters*, vol. 57, no. 7, pp. 1272-80.

- Van Jaarsveld, J., Van Deventer, J.S. & Lukey, G. 2002, 'The effect of composition and temperature on the properties of fly ash-and kaolinite-based geopolymers', *Chemical Engineering Journal*, vol. 89, no. 1-3, pp. 63-73.
- Venu, M. & Rao, T.G. 2018, 'An Experimental Investigation of the Stress-Strain Behaviour of Geopolymer Concrete', *Slovak Journal of Civil Engineering*, vol. 26, no. 2, pp. 30-4.
- Vijai, K., Kumutha, R. & Vishnuram, B. 2010, 'Effect of types of curing on strength of geopolymer concrete', *International journal of physical sciences*, vol. 5, no. 9, pp. 1419-23.
- Vinothini, M., Mallikarjun, G., Gunneswararao, T.D. & Rama Seshu, D. 2015, 'Bond Strength Behaviour of Geopolymer Concrete', *Malaysian Journal Of Civil Engineering*, vol. 27, no. 3, pp. 371-81.
- Vora, P.R. & Dave, U.V. 2013, 'Parametric studies on compressive strength of geopolymer concrete', *Procedia Engineering*, vol. 51, pp. 210-9.
- Vu, T.H., Gowripalan, N., Sirivivatnanon, V., De Silva, P. & Kidd, P. 2019, 'Assessing Corrosion Resistance of Powder Form of Geopolymer Concrete', *29 Biennial Conference of the Concrete Institute of Australia*.
- Wallah, S. & Rangan, B.V. 2006, 'Low-calcium fly ash-based geopolymer concrete: long-term properties'.
- Wang, Y. & Wang, F. 2006, 'Simulation of bond-slip relationship between concrete and reinforcing bar in ANSYS', *Journal of Tianjin University*, vol. 39, no. 2, pp. 209-13.
- Wight, J.K. & Macgregor, J.G. 2012, 'Reinforced Concrete Mechanics and Design, 2012', Pearson Education, Inc., Upper Saddle River, New Jersey.
- Wong, L. & Nehdi, M. 2018, 'Critical Analysis of International Precast Concrete Pipe Standards', *Infrastructures*, vol. 3, no. 3, p. 18.
- Wongpa, J., Kiattikomol, K., Jaturapitakkul, C. & Chindaprasirt, P. 2010, 'Compressive strength, modulus of elasticity, and water permeability of inorganic polymer concrete', *Materials & Design*, vol. 31, no. 10, pp. 4748-54.
- Wu, L., Hu, C. & Liu, W.V. 2018, 'The Sustainability of Concrete in Sewer Tunnel—A Narrative Review of Acid Corrosion in the City of Edmonton, Canada', *Sustainability*, vol. 10, no. 2, p. 517.

- Wu, Y., Crawford, J.E. & Magallanes, J.M. 2012, 'Performance of LS-DYNA concrete constitutive models', *12th International LS-DYNA users conference*, vol. 1, pp. 1-14.
- Xiao, S. 2015, 'Numerical study of dynamic behaviour of RC beams under cyclic loading with different loading rates', *Magazine of Concrete Research*, vol. 67, no. 7, pp. 325-34.
- Xie, Z. & Xi, Y. 2001, 'Hardening mechanisms of an alkaline-activated class F fly ash', *Cement and Concrete Research*, vol. 31, no. 9, pp. 1245-9.
- Xing, G., Zhou, C., Wu, T. & Liu, B. 2015, 'Experimental study on bond behavior between plain reinforcing bars and concrete', *Advances in Materials Science and Engineering*, vol. 2015.
- Xu, M. & Wille, K. 2015, 'Calibration of K&C concrete model for UHPC in LS-DYNA', *Advanced materials research*, vol. 1081, Trans Tech Publ, pp. 254-9.
- Yewale, V.V., Shirsath, M. & Hake, S. 2016, 'Evaluation of efficient type of curing for geopolymer concrete', *Evaluation*, vol. 3, no. 8.
- Yifei, C. 2015, 'Bond behaviour between reinforcing steel bars and fly-ash based geopolymer concrete', *School of Engineering and Information Technology, University of New South Wales, Canberra*.
- Yip, C.K.-B. 2004, 'The role of calcium in geopolymerisation'.
- Yip, C.K., Lukey, G.C., Provis, J.L. & Van Deventer, J.S. 2008, 'Effect of calcium silicate sources on geopolymerisation', *Cement and Concrete Research*, vol. 38, no. 4, pp. 554-64.
- Younis, A.-A. 2020, 'Experimental and Numerical Study on Three-Edge Bearing Test for Reinforced Concrete Pipe'.
- Younis, A.-A., Shehata, A., Ramadan, A., Wong, L.S. & Nehdi, M.L. 2021, 'Modeling structural behavior of reinforced-concrete pipe with single, double and triple cage reinforcement', *Engineering Structures*, vol. 240, p. 112374.
- Yu, X., Riahi, E., Entezarmahdi, A., Najafi, M. & Sever, V.F. 2016, 'Experimental and numerical analyses of strength of epoxy-coated concrete under different load configurations', *Journal of Pipeline Systems Engineering and Practice*, vol. 7, no. 2, p. 04015024.
- Zamanian, S. 2016, 'Probabilistic performance assessment of deteriorating buried concrete sewer pipes', The Ohio State University.

- Zhang, Y., Yan, Z.-g., Zhu, H.-h. & Ju, J.W. 2018, 'Experimental study on the structural behaviors of jacking prestressed concrete cylinder pipe', *Tunnelling and Underground Space Technology*, vol. 73, pp. 60-70.
- Zhang, Z., Fang, H., Li, B. & Wang, F. 2020, 'Mechanical Properties of Concrete Pipes with Pre-Existing Cracks', *Applied Sciences*, vol. 10, no. 4, p. 1545.
- Zhang, Z., Wang, H., Provis, J.L. & Reid, A. 2013, 'Efflorescence: a critical challenge for geopolymer applications?', *Concrete Institute of Australia's Biennial National Conference 2013*, Concrete Institute of Australia, pp. 1-10.
- Zhao, L., Zheng, L., Qin, H., Geng, T., Tan, Y. & Zhang, Z. 2021, 'Research on Failure Characteristics of Concrete Three-Point Bending Beams with Preexisting Cracks in Different Positions Based on Numerical Simulation', *Geofluids*, vol. 2021.
- Zhuge, Y., Fan, W., Duan, W. & Liu, Y. 2021, 'The durability and rehabilitation technologies of concrete sewerage pipes: A state-of-the-art review', *Journal of Asian Concrete Federation*, vol. 7, no. 2, pp. 1-16.

Appendix A

Sample	Compressive strength (MPa)- Geocem 1				
	Day 1	Day 7	Day 14	Day 28	Day 90
1	37.7	44.4	51.64	55.1	61.2
2	35.3	42.6	48.83	49.5	58.6
3	39.8	49.8	51.36	59	64.8
4	-	-	-	56.6	-
Average strength	37.6	46.6	50.6	55.1	61.5

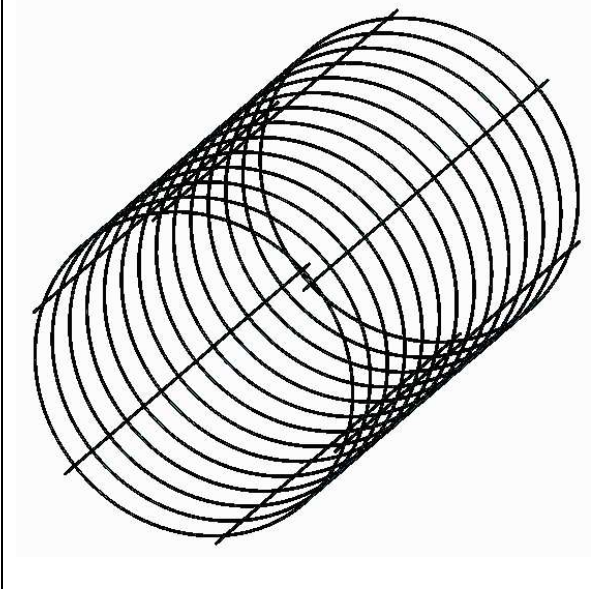
Sample	Compressive strength (MPa)- Geocem 2				
	Day 1	Day 7	Day 14	Day 28	Day 90
1	47.65	51.6	54.46	59	60.2
2	46.07	56.8	53.37	58.2	59.8
3	48.04	50	54.46	59.8	65.1
4	-	-	55.95	58	65.2
Average strength	47.3	51.6	54.6	58.8	62.5

Sample	Compressive strength (MPa)- OPC				
	Day 1	Day 7	Day 14	Day 28	Day 90
1	9.8	30.6	48.5	52.4	61.5
2	10.5	34.2	43.8	56.5	62.3
3	-	31.3	45.1	52.4	57.9
4	-	-	-	48.5	54.6
Average strength	10.2	32.5	46.3	52.5	59.1

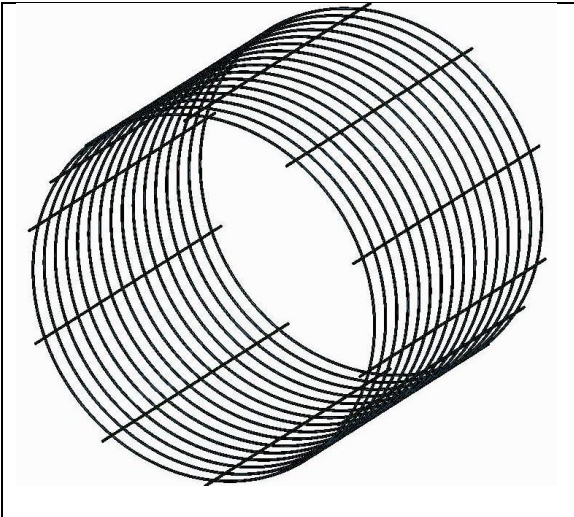
Appendix B

Reinforcement bar details of the pipe model:

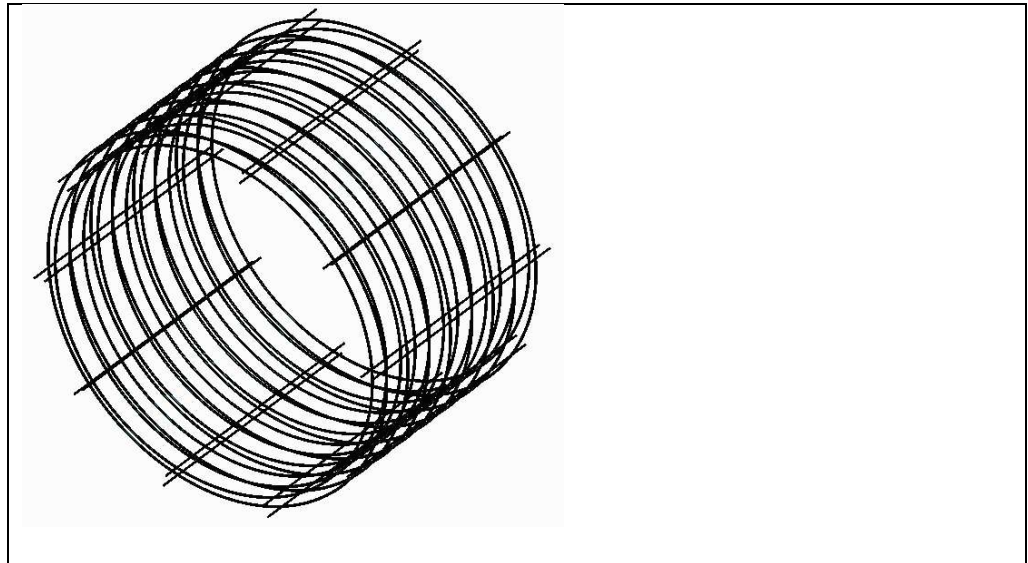
(a) 450 mm Single cage reinforced geopolymer pipe

	Area of reinforcement bar per m length = $175 \text{ mm}^2/\text{m}$
	Inner Cage= 4 mm dia. rebar @ 71 mm spacing
	Longitudinal bars= 6 nos. of 4 mm dia rebar

(b) 825mm Single cage reinforced concrete pipe

	Area of reinforcement bar per m length = $484 \text{ mm}^2/\text{m}$
	Inner Cage= 6 mm dia. rebar @ 60 mm spacing
	Longitudinal bars= 6 nos. of 4 mm dia rebar

(c) 1200 mm Double cage reinforced concrete pipe



Area of inner reinforcement bar per m length = $565 \text{ mm}^2/\text{m}$

Area of outer reinforcement bar per m length = $376 \text{ mm}^2/\text{m}$

Inner Cage= 7.5 mm dia. rebar @ 80 mm spacing

Outer Cage= 7.5 mm dia. rebar @ 120 mm spacing

Longitudinal bars= 6 nos. of 4 mm dia rebar